# Design, Synthesis, Characterization and Functional Properties of Metal Coordination Complexes of New Derivatives of Quinoxaline-*o*-dithiol Ligands: Towards Modeling the Active Sites of [FeFe]-Hydrogenase

A Thesis
Submitted for the degree of
**DOCTOR OF PHILOSOPHY**

By

**Gummadi Durgaprasad**


**School of Chemistry**
**University of Hyderabad**
**Hyderabad 500 046**
**Andhra Pradesh**
**India**

**June, 2012**

అమ్మ, నాన్న
అమ్మమ్మ, తాతయ్య
మరియు
గురువులకి అంకితం.....

## STATEMENT

I hereby declare that the matter embodied in the thesis is the result of investigation carried out by me in the School of Chemistry, University of Hyderabad, Hyderabad, India, under the supervision of **Prof. Samar K. Das**.

In keeping with the general practice of reporting scientific observations, due acknowledgements have been made wherever the work described is based on the findings of other investigators. Any omission, which might have occurred by oversight or error, is regretted.

**Gummadi Durgaprasad**

University of Hyderabad
June, 2012

**Prof. Samar Kumar Das, F.A.Sc**
**School of chemistry**
**University of Hyderabad**
**Gachibowli, Hyderabad-500046, India**
**Work: +91-40-23011007**
**Residence: +91-40-23010536**
**Fax: +91-40-2301246**
**E-mail: skdsc@uohyd.ernet.in**

# CERTIFICATE

Certified that the work contained in the thesis entitled "**Design, Synthesis, Characterization and Functional Properties of Metal Coordination Complexes of New Derivatives of Quinoxaline-*o*-dithiol Ligands: Towards Modeling the Active Sites of [FeFe]-Hydrogenase"** has been carried out by Mr. Gummadi. Durgaprasad under my supervision and the same has not been submitted elsewhere for a degree.

**Prof. Samar K. Das**

**(Supervisor)**

**Dean**

**School of Chemistry**

# Acknowledgements

I express my deep sense of gratitude and profound thanks to my supervisor **Prof. Samar K. Das** for his valuable guidance, patience, encouragement, and for the freedom he gave me in carrying out research. His optimistic approach towards every aspect was admirable and inspiring. Throughout my Ph.D tenure, he is always approachable, helpful, friendly and extremely tolerant. I consider my association with him as a cherishable memory in my life.

I take this opportunity to thank Prof. M. V. Rajasekharan, Dean, School of Chemistry for providing us the facilities needed for our research. I extend my sincere thank to former Deans Prof. D. Basavaiah and Prof. M. Periasamy, and all the faculty members, School of Chemistry for their co-operation on various aspects.

I am deeply indebted to Prof. S. Pal for his suggestions and allowing me to perform studies using the electrochemical facilities for my doctoral work.

It is great pleasure to thank my lab seniors Dr. V. Shivaiah, Dr. S. Supriya, Dr. V. Madhu (for initiating my work and valuable suggestions), Dr. Raghavaiah, Dr. C. H. Pradeep, Dr. Prabhakar, Dr. Arumuganathan, and Dr. Tanmay for their help, pleasant company, and cooperation during my Ph.D. tenure. From the bottom of my heart I thank to my friends and labmates Dr. Rambabu, Dr. Srinivas, Bharat (babi), Kishore (bangaram) for their support throughout the tenure. Without their help and encouragement it is not possible to complete the work. I wish to thank my juniors Mrs. Monima, Mrs. Sridevi garu, Mr. Veeranna, Chinnabbai and Ms. Paulami, Praveen, Krishna, Ms. Olivia for their cooperation, help, and creating cheerful work atmosphere. I thank to M.Sc and UGC networking project students Shivaiah, Ashok, Siva (iict), Sreenivas (ugc), Lavanya, Dr. Pratap, Sunitha, Pal, Raju and Y. Mahesh to work with me and helping to complete my thesis work. A special note of thank to Ms. Arti, for helping me at various occasions during my stay here.

I also thank all the non-teaching staff of the School of Chemistry and COSIST for their assistance on various occasions. It's my privilege to acknowledge Mr. Shetty and Mr. A. R. Shetty for timely supply of chemicals, Mr. Vara Prasad for all his art with glass blowing, Mr. Satyanarayana, Mr. Turab, Mrs. Vijayalaxmi and Mr. Bhaskar Rao for their excellent job with NMR spectra and LC-MS spectra, Mr. Ramana helping in XRD room,

and Ms. Asia Parwez and Gomathi for her tireless effort for collecting IR spectra. I would like to thank office staff Durgesh, Jayaram, Sharma, Sai, lab assistant Venky (NMR) and Krishna Rao (security guard) for helping me at various occasions. The assistance of Dr. Manjunath and Mr. Suresh (EPR) are gratefully appreciated. A special note of thank to Dr. P. Raghavaiah, for teaching me the fundamentals of X-ray crystallography and helping me to solve the various crystallography problems.

I would like to acknowledge Prof. Dindi Satyanayana, Dr. Umabala, Prof. A.V. Prasada Rao, Prof. GNR, Prof. ASN, Prof. Sivarao and Prof. Vani, and all my teachers during my Post graduation at Andhra University, Visakhapatnam, and also thankful to all my teachers in graduation especially Mr. Phanidra garu, Mr. V. Raju garu, Bose garu, Mr. Ramakrishna garu.

I take this opportunity to thank all my school teachers, especially Sreedhar garu, Vijay kumar sir for their wonderful teaching, encouragement, kindness, and affection and very much thankful to Dr. Suneel for his encouragement.

I feel fortunate to have friends Sathish, Satish (Akiri), Ravi who have been good friends over the years, for keeping me sane, giving me perspective and who have made the time more enjoyable.

I am lucky enough to have the support of many School of Chemistry friends and colleagues Dr. DK, Dr. Krishna kishore, Nagaraju, Mallesh, NagaRaju (MP lab), Chaitanya, Dr. M. Ramu, Dr. Phani Pavan, Anjaneyalu, Dr. Ram Suresh, Dr. Venu Srinivas, Dr. Sanjeev, Dr. Ravi, Dr. Vikram, Vijji, P. Kishore, Anand, Kalyan, Santhosh, Balu, Narayana, Chandrsekhar, Ajay, Nagarjuna(VB lab), Gupta, Hari, Karunakar, Srinu (LGP), Ramu yadav, Mallesh, Bhanu, Nagarjuna, Srinivas, Seshu, Sudharani, Rama Krishna, Venu, Dr. Suresh, Madhu, Ramaraju, Ramkumar, Prakash, Ramesh, Haneesh, Sekhar Reddy, Ganesh, Vigensh, Praveen, S. Naidu, Dr. Arindam, Dr. Arun Babu, Malakappa, Swamy, Krishna charry, Dr. Bijju, Dr. Bhargavi, Dr. Jagadeesh, Dr.Bipul, Dr. Ranjith, Dr. Naba, Palash, Suryanarayana, Rajesh, Ashok, Chandu, Dr. Raji, Dr. Anindita, Tulika, Mousami, Dr. J. P. anna, Dr. Abijit, Dr. Rajesh, Balaswamy, Dr. Narahari anna, Tirupathi Reddy, Pavan, Yaseen, Sasi, Dr. Bhuvan anna, Dr. Sajna, Ramesh, Gangadhar, Srinu, Nagarjuna reddy, Dr. Ramesh Reddy anna, Dr. Aravind, Sekhar Reddy, Satpal, Santosh, Mallikarjun, lee, Dr. Lenin babu, Guru Braham, Laxaman, Dr. Satish, Dr. Sivaranjan Reddy, Rajgopal Sr., Rajgopal Jr., Dr. Kishore, Dr. Ramkumar, Dr. Narayana, Dr. Rumpa, Dr. Vijendhra Reddy, Chary, Bharani, Shivaprasad, Srinivas Reddy, Ganesh,

Srinivas(RB lab), Raveendra Babu, Vanaja, Naveen, Ramana, Sandeep, Tridib, Obaiah, Satish (PKP), Vikranth, Bashak, Pramithi, Narayana, Ajay, N. Ghosh, exceptionally generous in helping me at various occasions.

I would like to acknowledge the NRS hostelmates chairman (phalgun), Sudhakar garu, Sanjeev, Anil, GK, Durgarao, Balu, Ravi, Rajesh, Venkat, for making the hostel life more memorable.

I specially thank my M.Sc. classmates Dr. Ramesh (boku), Dr. Ramu, Dr. Johnpal, Dr. Asiri naidu, Dr. Charan, Dr. Harikrishna, GR, Sunil, Dr. Phaneendra Sai, and AU juniors Dr. Rajesh, Dr. Yedukondalu, Dr. Suresh, Malayadri, Subbarao, Pardhasardhi, Anji for the memorable moments which I have shared with them.

I would like to thank my school friends Murali(Apsara), Ganapathi, Somaraju, M.S. Rao, Siva, Katta siva, Murali, Ayyappa, Balaji, Jella, Bandi, Satyasri. I should also thank B.Sc. friends Pardhu, Hari, Vishnu, Ramakrishna, Madhu, Ramesh, Ganesh, Narayana. I also like to thank to my M.Sc. friends Padmalatha, Sridevi, Kalpana, karimulla, Prasad, Naidu and Messaiah for their memorable presence in my life and also thankful to my students Ramakrishna, Bt, suneel.

It is great pleasure to thank my family members Tatayya, Amamma, Nanna, Amma and my lovable brother Ganesh for their support and affection throughout my life. The knowledge that they will always be there to pick up the pieces is what allows me to repeatedly risk getting shattered. All my achievements are the outcome of my parent's encouragements and blessings.

I would take this opportunity to thank my Peddananna-Apparao, Paparao, Peddamma-Narsa, Papa, Sisters- Parvathi, Bullaka, Durga, Naga, Kumari, Brothers- Satyanarayana, Vasu, Srinu, simhachalam, Ravi. Siva, Venkataraobabai, Ravudumama, Venkateswaraotata, Seshu tata, Ramalakshmi mama, Srinu maya, Anu atta, Prbha, Sankarbabai, Chellama, Nageswaraobabai, Nani babai, Chinni, Chinna Nani, Kanaka mama, Padma atta, Venkat and their families for their love and support.

***Gummadi Durgaprasad…***

University of Hyderabad

June, 2012

# SYNOPSIS

The thesis work entitled with **"Design, Synthesis, Characterization and Functional Properties of Metal Coordination Complexes of New Derivatives of Quinoxaline-*o*-dithiol Ligands: Towards Modeling the Active Sites of [FeFe]-Hydrogenase",** consists of five chapters: (**1**) A General Overview on Metal-*o*-dithiolene Chemistry: Introduction and Motivation of the Present Work, (**2**) Synthesis, Structural Characterization and Electrochemical Studies of $[Fe_2(\mu\text{-L})(CO)_6]$ and $[Fe_2(\mu\text{-L})(CO)_5(PPh_3)]$ (L = pyrazine-2,3-dithiolate, quinoxaline-2,3-dithiolate and pyrido[2,3-*b*]pyrazine-2,3-dithiolate): Towards Modeling the Active Sites of [FeFe]–Hydrogenase, **(3)** 1,2-ene Dithiolate Bridged Diiron Carbonyl-Phosphine and -Phosphite Complexes in Relevance to the Active Site of [FeFe]-hydrogenases: Synthesis, Characterization and Electrocatalysis, **(4)** Influence of Coordinated Crystallizing Solvents and Bulkiness of Ligands in Tuning the Structural Diversity and Dimensionality of Alkali Metal Based Coordination Polymers of Metal Bis(dithiolene) Complexes and **(5)** Design, Synthesis and Characterization of New Derivates of Mono- and Bis Quinoxaline-*o*-dithiol Ligands: Their Coordination Complexes with Transition Metals.

Apart from the first chapter (introduction), each chapter is subdivided into three parts: (a) Introduction (literature survey), (b) Results and Discussion and (c) Experimental Section. The compounds obtained in the present study are, in general, characterized by IR and NMR ($^{1}H$, $^{13}C$ & $^{31}P$) techniques followed by elemental analyses and mass spectra (LC-MS). Wherever feasible, X-ray structure determination is undertaken. Summary as well as references are compiled at the end of each part.

## Chapter 1

## A General Overview on Metal-*o*-dithiolene Chemistry: Introduction and Motivation of the Present Work

This chapter begins with more basic knowledge about dithiolene ligands and their metal complexes. It also reveals brief discussion about their syntheses, characterizations and properties. Applications of metal dithiolene complexes are mainly divided into three categories, (1) Enzyme active site model complexes (2) coordination polymers, conducting materials and (3) in

coordination chemistry. Some of the important transition metal 1,2–dithiolene complexes are picked up to describe their solid state properties, such as, magnetic, conducting, superconducting, and optical properties (NLO, emission properties). The discussions on structural, spectroscopic, bonding, reactivity, and electrochemistry of transition metal 1,2–dithiolene complexes are also briefed.

## Chapter 2

## Synthesis, Structural Characterization and Electrochemical Studies of $[Fe_2(\mu\text{-}L)(CO)_6]$ and $[Fe_2(\mu\text{-}L)(CO)_5(PPh_3)]$ (L = pyrazine-2,3-dithiolate, quinoxaline-2,3-dithiolate and pyrido[2,3-*b*]pyrazine-2,3-dithiolate): Towards Modeling the Active Sites of [FeFe]–Hydrogenase

The second chapter describes the reaction of heterocyclic 1,2-ene-dithiol ligands, namely, pyrazine-2,3-dithiol ($H_2$pydt), quinoxaline-2,3-dithiol ($H_2$qdt) and pyrido[2,3-*b*]pyrazine-2,3-dithiol ($H_2$ppdt) with $Fe_2(CO)_9$ yielding the '[FeFe]–hydrogenase' model complexes $[Fe_2\{\mu\text{-pydt}\}(CO)_6]$ **(1)**, $[Fe_2\{\mu\text{-qdt}\}(CO)_6]$ **(2)** and $[Fe_2\{\mu\text{-ppdt}\}(CO)_6]$ **(3),** respectively. A further reaction of complexes **1**, **2** and **3** with $PPh_3$ in the presence of equimolar amount of decarbonylating agent $Me_3NO$ in $CH_3CN$ at room temperature resulted in the formation of unsymmetrical mono-$PPh_3$-substituted model complexes $[Fe_2\{\mu\text{-pydt}\}(CO)_5PPh_3]$ **(4)**, $[Fe_2\{\mu\text{-qdt}\}(CO)_5PPh_3]$ **(5)** and $[Fe_2\{\mu\text{-ppdt}\}(CO)_5PPh_3]$ **(6),** respectively. The complexes **1**–**6** were well characterized by routine elemental analysis, IR, $^1$H NMR, $^{13}$C NMR spectroscopy and unambiguously characterized by X–ray crystallographic analysis. IR spectroscopy and electrochemical analysis show that an increase of the electron–withdrawing character of the bridging ligands (where electron–withdrawing character is in the order of $pydt^{2-} > ppdt^{2-} \geq qdt^{2-}$) leads to a decreased electron density at the iron centers, which yield a milder reduction potential and higher CO stretching frequencies. Electronic properties of the diiron site can be modified by choosing the suitable aromatic dithiol ligand. The electrocatalytic proton reduction of compound **1** was studied by cyclic voltammograms in the presence of a strong acid, such as, *p*-toluenesulfonic acid (*p*-HOTs, p$K_a$ = 8.7) in $CH_3CN$. Complex **1** shows a significant electrocatalytic response by following CECE (chemical–electrochemical–chemical–

electrochemical) mechanism. All the compounds **1–6** are further characterized by electrochemical studies.

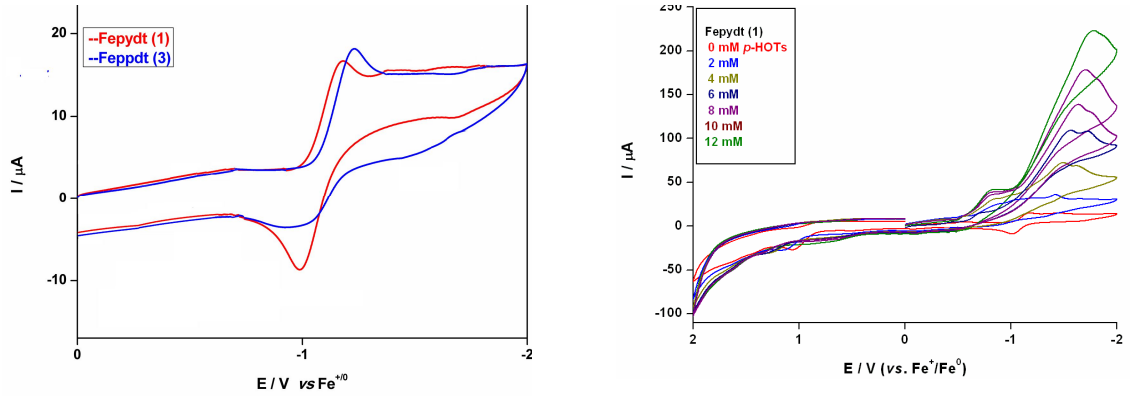


**(a)** **(b)**

**Fig. 1.** (a) Cyclic voltammograms of complexes **1** (red) and **3** (blue) (1.0 mM) in 0.1 M *n*-$Bu_4NClO_4$/MeCN at a scan rate of 100 $mVs^{-1}$. Potential are *vs.* $Fc^{+/0}$. (b) Cyclic voltammogram of complex **1** with 1.0 mM complex and 0–8 mM *p*-HOTs in $CH_3CN$ solution (0.1 M *n*-$Bu_4NClO_4$) at a scan rate of 100 mV $s^{-1}$.

## Chapter 3

## 1,2-ene Dithiolate Bridged Diiron Carbonyl-Phosphine and -Phosphite Complexes in Relevance to the Active Site of [FeFe]-hydrogenases: Synthesis, Characterization and Electrocatalysis

The third chapter describes a series of binuclear $Fe^IFe^I$ complexes, that have been prepared by the treatment of *N*–heterocyclic 1,2-dithiols, such as, quinoxaline-6,7-dithiol ($H_2$6,7-qdt), 2,3-diphenyl-6,7-quinoxaline dithiol ($H_2$diph-6,7-qdt) and 2,1,3-benzothiadiazole-5,6-dithiol ($H_2$btdt) with $Fe_2(CO)_9$ resulting in the formation of $[Fe_2\{\mu$-6,7-qdt$\}(CO)_6]$ (**1**), $[Fe_2\{\mu$-diph-6,7-qdt$\}(CO)_6]$ (**2**) and $[Fe_2\{\mu$-btdt$\}(CO)_6]$ (**9**) respectively. These complexes have been examined to explore structural, electronic and electrochemical effects on substituting one or two CO group(s) with other good donor ligands, e.g., phosphine and phosphite ligands. Mono-phosphine substituted compounds $[Fe_2\{\mu$-6,7-qdt$\}(CO)_5PPh_3]$ **(3)**, $[Fe_2\{\mu$-diph-6,7-qdt$\}(CO)_5PPh_3]$ **(4)** and $[Fe_2\{\mu$-btdt$\}(CO)_5PPh_3]$ **(10)** are synthesized by the reactions of **1**, **2** and **3**, respectively with $PPh_3$ in the presence of $Me_3NO$. Interestingly, treatment of **1**, **2** and **3** with controlled amount of $P(OEt)_3$ affords the mono-substituted phosphite derivatives $[Fe_2\{\mu$-6,7-qdt$\}(CO)_5P(OEt)_3]$ **(5),** $[Fe_2\{\mu$-diph-6,7-qdt$\}(CO)_5P(OEt)_3]$ **(6),** $[Fe_2\{\mu$-btdt$\}(CO)_5$ $P(OEt)_3]$

**(11)** respectively. The same reaction with an excess amount of $P(OEt)_3$ affords the di-substituted phosphite derivatives $[Fe_2\{\mu\text{-}6,7\text{-qdt}\}(CO)_4\{P(OEt)_3\}_2]$ **(7)**, $[Fe_2\{\mu\text{-diph-}6,7\text{-qdt}\}(CO)_4\{P(OEt)_3\}_2]$ **(8)** and $[Fe_2\{\mu\text{-btdt}\}(CO)_4\{P(OEt)_3\}_2]$ **(12)** correspondingly. These new complexes **1–12** have been characterized by IR, $^1H$, $^{13}C$, and $^{31}P\{^1H\}$ NMR and mass spectroscopy including elemental analysis.

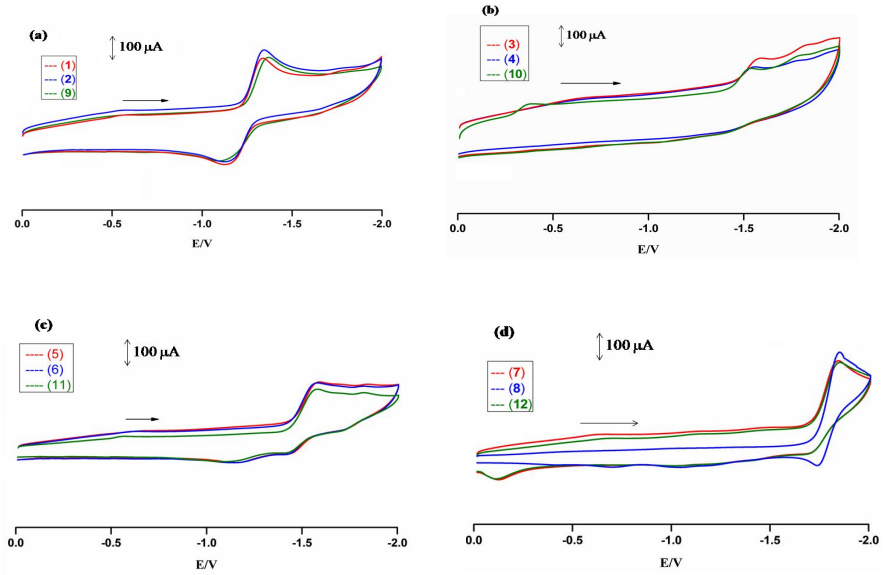


**Fig. 2.** Cyclic voltammograms of complexes (a)**1** (red), **2** (blue) and **9** (olive); (b) **3** (red), **4** (blue) and **10** (olive); (c) **5** (red), **6** (blue) and **11** (olive); (d) **7** (red), **8** (blue) and **12** (olive) (1.0 mM) in 0.1 M *n*-$Bu_4NClO_4$/MeCN at a scan rate of 100 $mVs^{-1}$. Potential are *vs.* $Fc^{0/+}$.

The solid state structures for all compounds have been determined by single-crystal X-ray structure analyses. Interestingly, complex **9** shows non-covalent interactions, such as, weak S···N and S···S supramolecular contacts. The S···N contact distance is 3.0701(1) and S···S interactions are described by a distance of 3.641(1) Å. These combined weak S···N and S···S non-covalent interactions result in the formation of an one-dimensional chainlike arrangement. The electrochemistry of **1**–**12** was performed by cyclic voltammetry to evaluate the effects of phosphine and phosphite ligands on the reduction potentials of the iron atoms of the all carbonyl model complexes. The electrocatalytic activities of model complexes **2**, **9** and **10**–**12** toward proton reduction of a strong acid *p*–HOTs have been described. For the electro-catalytic proton reduction by the all carbonyl compound $[Fe_2\{\mu\text{-diph-}6,7\text{-qdt}\}(CO)_6]$ (**2**), we have proposed

CEEC mechanism. The hexa carbonyl compound $[Fe_2\{\mu\text{-btdt}\}(CO)_6]$ (**9**) does not undergo protonation with *p*-toluenesulfonic acid in its $\{Fe^IFe^I\}$ oxidation state, probably due to the involvement / delocalization of lone pair of electrons of ring nitrogen with ring sulfur pi-electrons. Accordingly an EC electrocatalytic reduction mechanism is proposed for compound **3**.

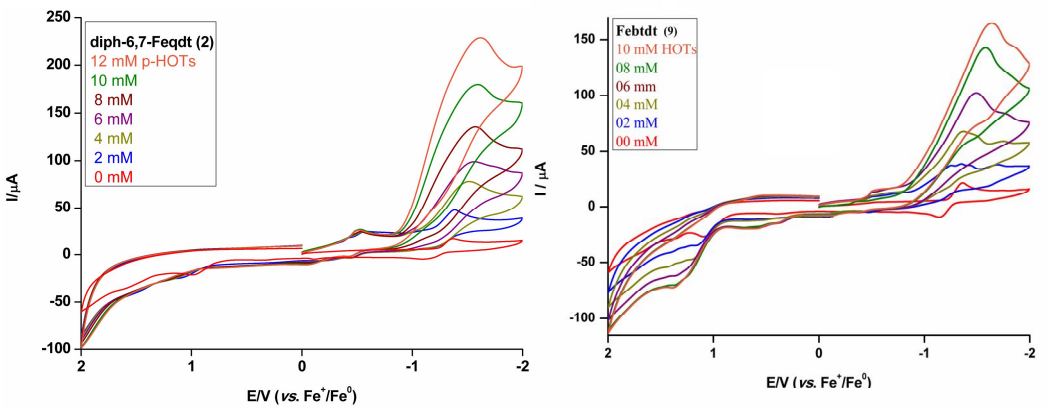


**Fig. 3.** Cyclic voltammogram of complexes **2** and **9** with 1.0 mM complex and 0–12 mM *p*-HOTs in $CH_3CN$ solution (0.1 M *n*-$Bu_4NClO_4$) at a scan rate of 100 mV $s^{-1}$.

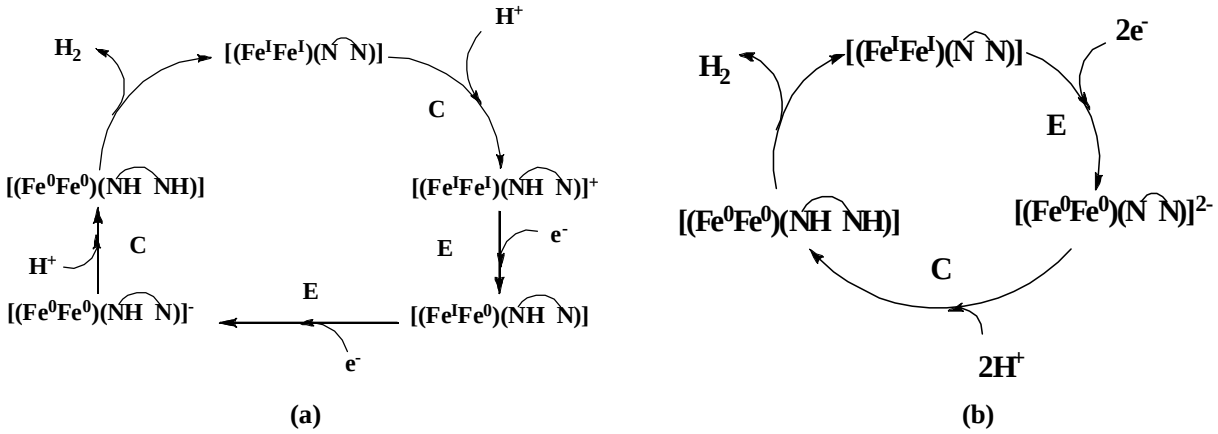


**Fig. 4.** A schematic representation of plausible (a) CEEC and (b) EC mechanisms for electrocatalytic proton reduction in the presence of *p*–HOTs for compounds **2** and **9** respectively**.**

## Chapter 4

## Influence of Coordinated Crystallizing Solvents and Bulkiness of Ligands in Tuning the Structural Diversity and Dimensionality of Alkali Metal Based Coordination Polymers of Metal Bis(dithiolene) Complexes

The fourth chapter describes the self assembly of coordination networks based on metal bis(dithiolene) complexes $[M(diph\text{-}6,7\text{-}qdt)_2]^{1-}$ (M = Cu(III) and Au(III); diph-6,7-$qdt^{2-}$ = 2,3-diphenylquinoxaline-6,7-dithiolate), where self assembly is influenced by the coordinating solvents through the coordination with sodium metal ion. In order to investigate the effect of coordinating solvent and bulkiness of the dithiol ligand on the dimensionality of the coordination networks, we have synthesized six coordination complexes $[Na(CH_3OH)_3][Cu(diPh\text{-}6,7\text{-}qdt)_2]\cdot MeOH$ (**1**), $[Na(THF)_2(OH_2)_2(C_2H_5OC_2H_5)][Cu(diPh\text{-}6,7\text{-}qdt)_2]$ (**2**), $[Na(CH_3COCH_3)_2(OH_2)][Cu(diPh\text{-}6,7\text{-}qdt)_2]$ (**3**), $\{[Na(CH_3CN)][Cu(diPh\text{-}6,7\text{-}qdt)_2]\}_n$ (**4**), $[Na(THF)_2(OH_2)_2(C_2H_5OC_2H_5)][Au(diPh\text{-}6,7\text{-}qdt)_2]$ (**5**) and $[Na(CH_3COCH_3)_2(OH_2)][Au(diPh\text{-}6,7\text{-}qdt)_2]$ (**6**).

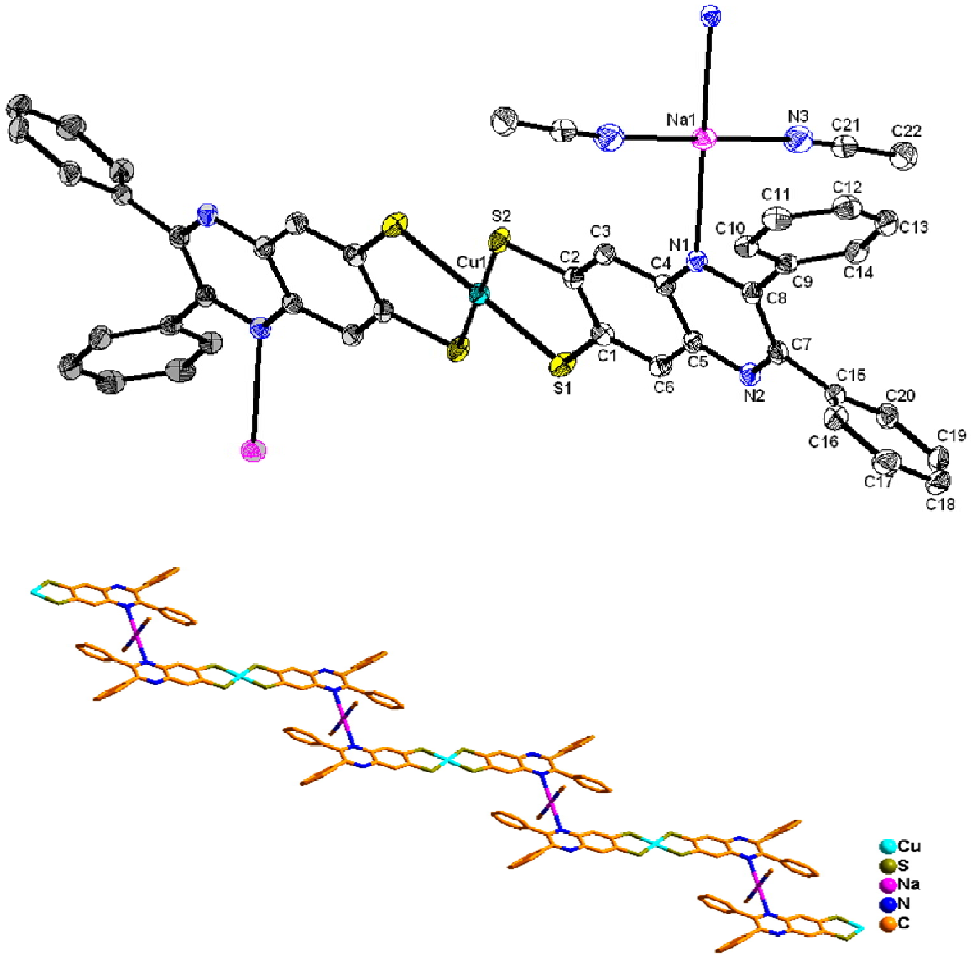


**Fig. 5.** Thermal ellipsoid plots of: (a) compound **4** (40% probability); (b) extended 1D network in the crystal structure of the compound **4.** Hydrogen atoms omitted for clarity.

Copper complexes **1**–**4** were obtained from different solvent recrystallization of dark green colored solid which was obtained from the reaction of one mole equivalent of $CuCl_2$ with two mole equivalents of $H_2$diph-6,7-qdt in MeOH treated with excess amount of NaOH in presence of open atmosphere. Recrystallization from the acetonitrile / ether diffusion leads to the formation of 1D coordination polymer containing compound, whereas MeOH/ether, THF/ether and acetone/ether diffusion leads to formation of discrete molecule instead of forming coordination polymers. In the self-assembly process, the dimensionality of the networks of coordination complexes/polymers **1**–**6** is greatly influenced by the hybridization of central carbon atom attached to the coordinating solvent atom ('N' or 'O') of the recrystallizing solvents. To understand the influence of solvent, bulkiness of dithiol ligand and the counter cation on the structural diversity and dimensionality of complexes **1**-**4**, we have done comparative studies with sodium-based [M(btdt)] (M = Cu and Au) ($btdt^{2-}$ = 2,1,3-benzenethiadiazole-5,6-dithiolate) coordination polymers reported by our group. All these compounds have been structurally characterized unambiguously by single crystal X-ray crystallography. Interestingly, copper compounds **1**–**4** show one quasi-reversible reduction response at $E_{1/2}$ = –0.187 V *vs* Ag/AgCl in DMF solutions.

## Chapter 5

## Design, Synthesis and Characterization of New Derivatives of Quinoxaline-*o*-dithiol Ligands: Their Coordination Complexes with Transition Metals

In the fifth chapter we have designed and synthesized a new class of *N*-Heterocyclic mono and bis(quinoxaline-*o*-dithiol) ligands and their transition metal complexes. All the compounds **2a**–**i**, **3a**–**i**, **4a**–**i** and **5a**–**i** (see Schemes 1 and 2 shown below) have been characterized by IR, $^{1}H$, $^{13}C\{^{1}H\}$ NMR, mass spectroscopy, elemental analysis and the compounds **2d**, **2g** are unambiguously characterized by X–ray crystallographic analysis. The present synthetic route offers us an excellent pathway to synthesize the quinoxaline-*o*-dithiol ligands starting from the 3,4-diamino benzoic acid. The corresponding metal complex of the ligand **5a** have been synthesized and characterized by single crystal X-ray analysis. This complex shows strong charge transfer (CT) band at 575 nm in solid-state electronic absorption

and electrochemical properties of complex **6** (Scheme 3) was performed by cyclic voltammetry, which shows a quasi-reversible one electron-oxidation process at $E_{1/2}$ = +0.44 V *vs* Ag/AgCl.

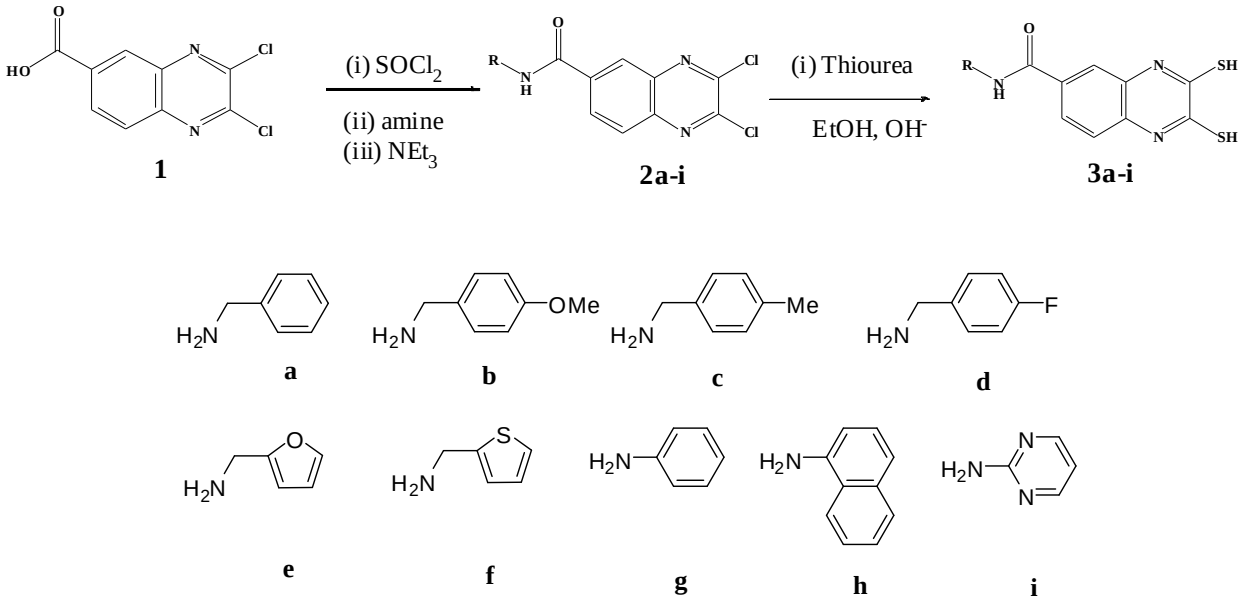


**Scheme 1.** Synthetic route for mono quinoxaline-*o*-dithiols

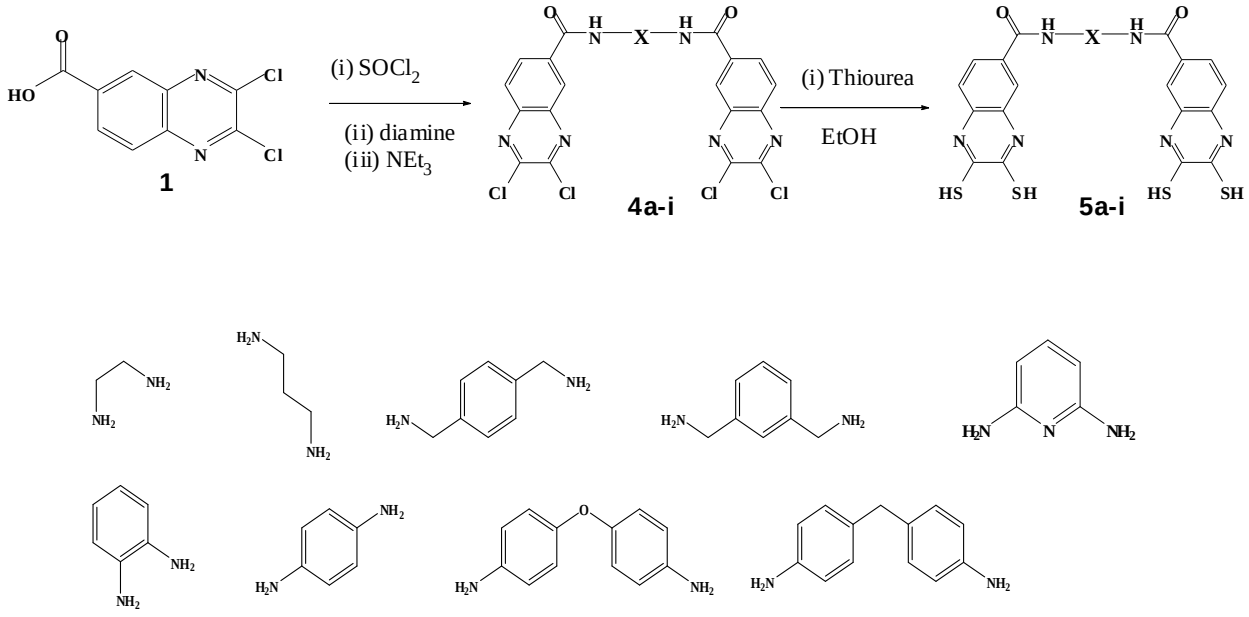


**Scheme 2.** Synthetic route for bis quinoxaline-*o*-dithiols.

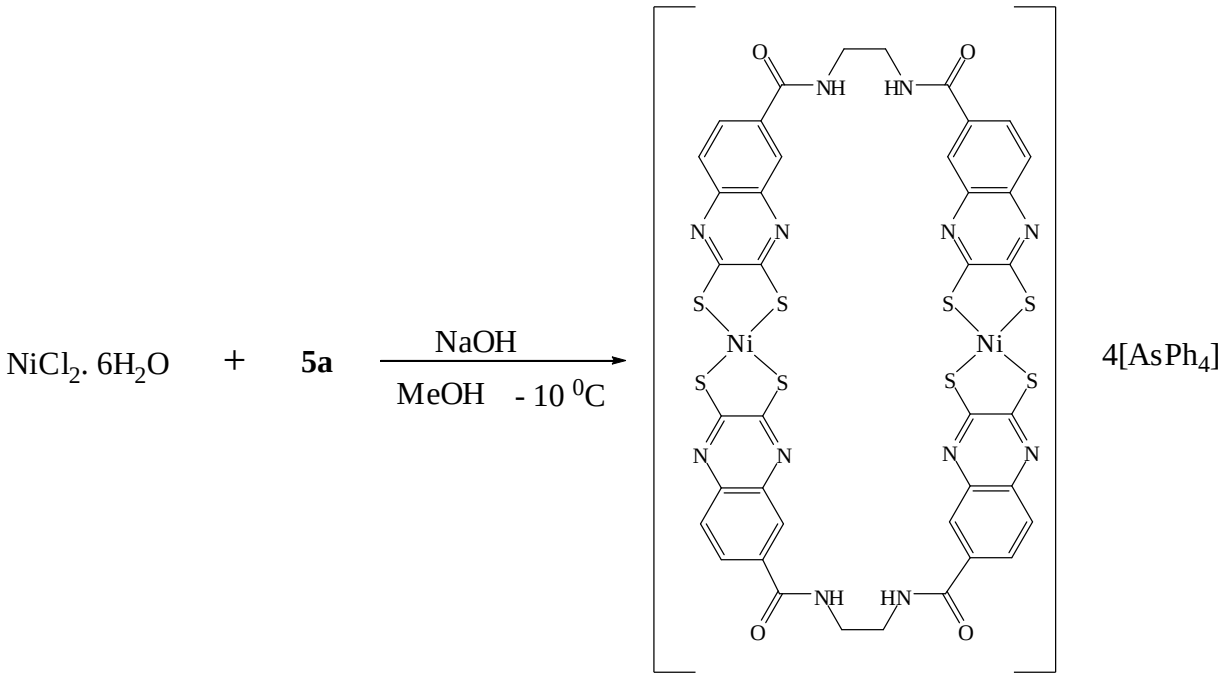


**Scheme 3.** Synthesis of complex $(PhAs)_4[Ni_2(\mathbf{5a})_2]$ (**6**).

# CONTENTS

# A general overview on metal *o*-dithiolene chemistry: Introduction and motivation of the present work

1 Chapter

## 1.1. Dithiolene Ligands and its Electronic Structure

Dithiolene ligands are unsaturated bidentate ligands, in which the two donor atoms are sulfur. Dithiolene ligands can exist in three different forms (depending upon their oxidation states). They are the dianionic "ene-1,2-dithiolate", the neutral "1,2-dithioketone or 1,2-dithione" and a monoanionic radical intermediate "1,2-ene-dithiete" between the dianionic and neutral forms as shown in Scheme 1.1. Dithiolene ligands are referred as non-innocent ligands. This is because, when a dithiolene ligand is complexed with a metal atom, the oxidation state of the ligand (and therefore the metal center) cannot be easily defined. In reality, 1,2-dithiones have not been characterized crystallographically.

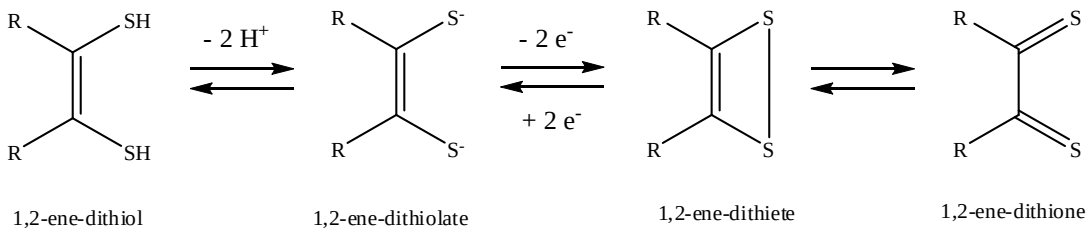


**Scheme 1.1.** The resonance forms of dithiolene ligand.

Thus, the electronic structures of 1,2-dithiolene ligands are generally viewed as dianionic form (1,2-ene-dithiolate) or neutral form (1,2-ene-dithione). The neutral form has four π–electrons and the dianionic form has six π–electrons as described in Scheme 1.1. This shows that two-electron oxidation of the dianionic form, ene–1,2–dithiolate results in the formation of the 1,2–diketone form. Moreover, these resonance forms decide the oxidation state of the concerned metal coordinating 1,2-dithiolene ligands.

## 1.2. Nomenclature

In the naming of "dithiolene" there is considerable unpredictability, within in the literature, which is generally decided by the substituent(s) on dithiolene and the oxidation

state of the concerned metal [1,2]. The term dithiolene was initially introduced by McCleverty and co-workers [3-8] and Balch *et al.* [9] to give a general name for the ligand that does not specify a particular oxidation state. The general formula of 1,2-dithiolate dianion is $R_2C_2S_2^{2-}$. Nomenclature, such as, 1,2-ethenedithiolate or 1,2-benzenedithiolate as base terminology is useful as a reliable naming practice for the free ligands. However, the term dithiolate does not specify that dithiolenes are different from saturated 1,2-dithiolate ligands and does not group structures that have related electronic configurations and bonding tendencies. This 1,2-dithiolene can also be described by different nomenclatures such as 1,2-alkenedithiol or 1,2-dithiete or 1,2-dithione depending on the oxidation states. This concept can be expressed by the Scheme 1.1.

## 1.3. Classification of Dithiolenes

The unsaturated dithiolato ligands have been divided into groups of having odd and even numbers of π–orbitals, respectively.

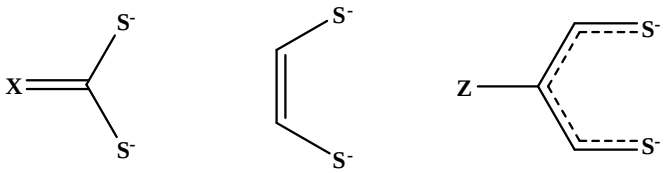


odd even odd

This classification results in the recognition of three unique classes: 1,2–dithiolates (even), 1,1'–dithiolate (odd) and 1,3–dithiolates (odd).

**1,1'–dithiolates**

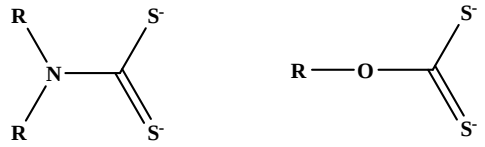


Alkyl dithiocarbamate Alkyl Xanthate

**1,3–dithiolates**

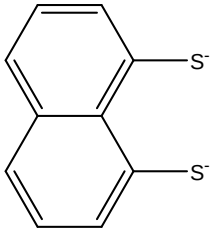


1,8-Napthalene-dithiolate

**1,2-dithiolates**

There is a considerable interest in the 1,2-dithiolate ligands and more number of 1,2-dithiolate ligands are reported in the literature [1]. Due to the broad range of 1,2-dithiolene in the literature, these can be further classified into following categories.

**Arene-1,2-dithiolates**

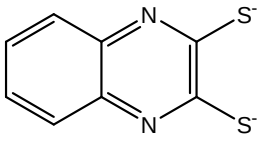


$\{qdt\}^{2-}$

Quinoxaline-2,3-dithiolate

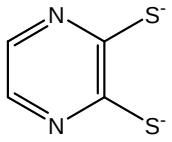


$\{pydt\}^{2-}$

Pyrazine-2,3-dithiolate

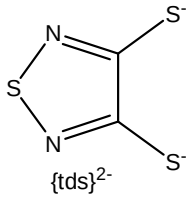


$\{tds\}^{2-}$

2,1,3-Thiadiazole-4,5-dithiolate

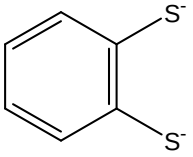


$\{bdt\}^{2-}$

Benzene-1,2-dithiolate

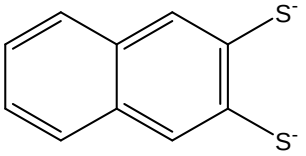


Napthalene-2,3-dithiolate

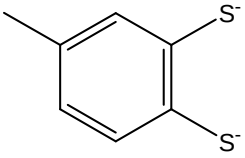


$\{tdt\}^{2-}$

Toluene-3,4-dithiolate

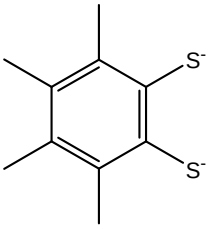


Toluene-3,4-dithiolate

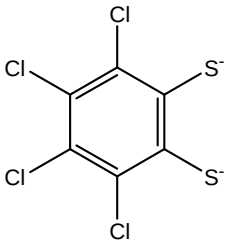


Toluene-3,4-dithiolate

**Alkene-1,2-dithiolates**

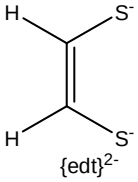


$\{edt\}^{2-}$

Ethene-1,2-dithiolate

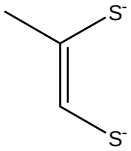


Propene-1,2-dithiolate

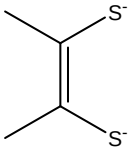


But-2-ene-2,3-dithiolate

**Inorganic-1,2-dithiolates**

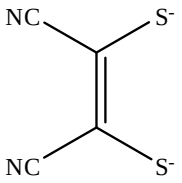


{mnt}$^{2-}$

1,2-Malonitrile-1,2-dithiolate

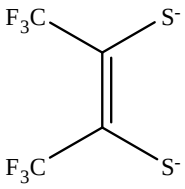


{tfd}$^{2-}$

1,2-Bis(trifluormethyl)ethylenedithiolate

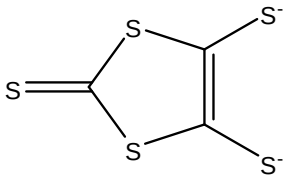


{dmit}$^{2-}$

1,3-Dithiole-2-thione-4,5-dithiolate

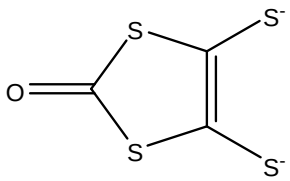


{dmio}$^{2-}$

1,3-Dithiole-2-one-4,5-dithiolate

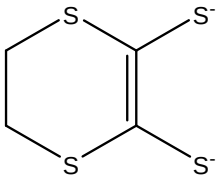


{dddt}$^{2-}$

5,6-Dihydro-1,4-dithiine-2,3-dithiolate

## 1.4. Metal *o*–dithiolene Complexes and its classification

Metal dithiolene complexes are known to exhibit a non-innocent character originating from these quasi-aromaticity and strong π–electron donor ability due to the involvement of sulfur atoms. Consequently, the rational development of 1,2–dithiolene based transition metal complexes are of current interest. However, the work had been done before 1960s to determine the metal quantification in the quantative analysis. The modern era of dithiolene research was started in the early of 1960's with contributions from three research groups, namely, Schrauzer and co–workers [10,11], Gray and co-workers [12,13] and Davison-Holm and co–workers [14]. First they established that the square–planar nature, redox activity, and broad scope of the highly colored bis(dithiolene) complexes of late transition metals, such as Fe, Co, Rh, Ir, Ni, Pd, Pt, Cu, Au and Zn. Later on, this area became further interested in the synthesis and structural characterization of tris and

tetrakis(dithiolene) complexes, whereby, their geometries were established by Eisenberg and Ibers [15,16]. In the last three decades, remarkable progress in this research area arose because of their immense contributions in the areas of materials science, enzymology, analytical science and reactivity, which broadened the impact and importance of dithiolene chemistry. Metal dithiolene complexes often exist in numerous oxidation states. This is due to the more delocalized nature of dithiolene ligands. The oxidized dithiolene complexes have relatively more 1,2-dithioketone character. In reduced complexes, the ligand assumes more ene-1,2-dithiolate character. These descriptions are evaluated by examination of differences in C–C and C–S bond distances.

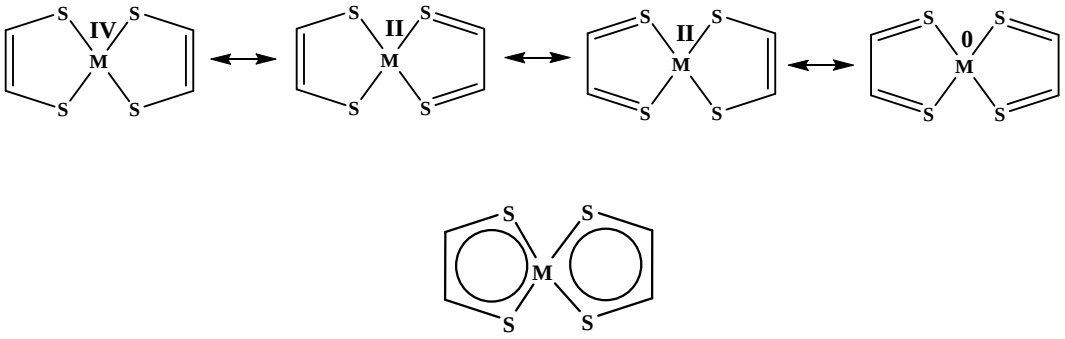


**Scheme 1.2.** Various bonding description of M(dithiolene)$_2$ complexes.

Many characteristics of dithiolene compounds can be rationalized in terms of the structure and bonding of the bidentate S-chelate of the dithiolene ligand. Distinct from saturated 1,2–dithiolate ligands, dithiolene ligands form relatively rigid and roughly planar five membered rings with considerable electronic flexibility in the relevant complexes. The Scheme 1.2 represents various bonding descriptions of a representative complex, in which the formal oxidation states of the metal and ligand vary. Such electronic versatility may make it difficult to establish a bonding description of a dithiolene complex. However, bond distances, such as the S−C lengths, have been used as indicator of the electronic configuration of a dithiolene complex [6]. The long S−C distances of ~1.77 Å are characteristic of ligand bonding in the dithiolate form; and the short S−C distances, as low as ~1.64 Å, are more characteristic of dithione bonding. The dithiolene ligand π orbitals interact with the dπ orbitals of metal to give frontier orbitals of mixed–ligand and –metal character. Both bis- and tris-dithiolene complexes exhibit a certain degree of aromaticity.

**Classification**

Although various dithiolene complexes have been developed so far, to our knowledge, they are classified into three main categories:

**(a) Homoleptic dithiolene complexes:** In this case, the coordinating ligand is 1,2-dithiolene [17,18]. These are further classified into metal bis(1,2-ditiolene) with square-planar (M = 8–10 metals) or tetrahedral geometries (M = 10–11 metals), and metal tris(dithiolene) complexes with trigonal prismatic geometries (M = 5–7 metals) or octahedral geometries (M = 4, 7–9 metals). New tetrakisdithiolene complexes (M = Ce, U) have recently been prepared by Fourmigue's and Duval's groups [19,20].

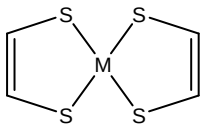


Metal bis(dithiolene)

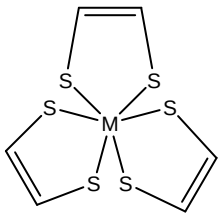


Metal tris(dithiolene)

(**b**) **Heteroleptic dithiolene complexes**: It has a dithiolene and other inorganic ligands. The typical examples are the square-planar luminescent [(N∧N)M(dithiolene)] (M = Pt, N∧N = diimine) [21,22], [(P∧P)M(dithiolene)] (M = Pt, P∧P = diphosphine) [23,24] and [oxo-M(dithiolene)$_2$] (M = Mo, W) complexes [25-27].

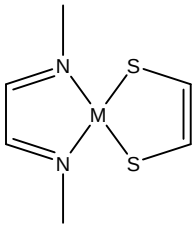


Metal(dithiolene)(diimine)

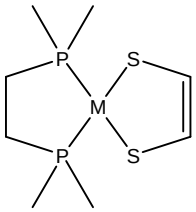


Metal(dithiolene)(diphosphine)

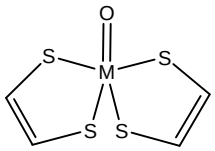


Metal-oxo(dithiolene)$_2$

**(c) Organometallic dithiolene complexes**: This incorporates the dithiolene ligand and some organic ligands for metal–carbon bond. Relevant examples include [(ppy)Au(dithiolene)] (ppy = 2-phenylpyridyl) [28] and [(cod)Pt(dithiolene)] (cod = 1,5-cyclooctadiene) [29] complexes.

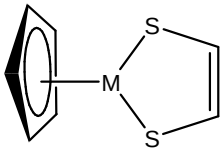


Metal(dithiolene)(cyclopentadienyl)

## 1.5. Applications of Metal *o*-dithiolene Complexes

Metal bis(*o*-dithiolene) complexes have been extensively studied since last five decades due to their novel properties and application in diverse areas of research, such as, conducting and magnetic materials, non-linear optics, dyes, catalysis and bioinorganic chemistry among others. These properties and applications arise due to their combination of functional properties, *vivid* redox behavior, and diversity of molecular geometries, magnetic moments and specific intermolecular interactions (such as coordination polymers).

### 1.5.1. Metal Dithiolenes in Biology

In contrast to their long history of dithiolene complexes and the studies of their properties towards material science with respect to photonics and electronic conductors, only last three decades receive considerable interest to those scientists studying biological systems. This is because dithiolene-chelate is involved / present in the active site of certain metalloenzymes, especially Mo- and W- containing enzymes. Depending upon the active-site of the structure, dithiolene-containing molybdenum and tungsten enzymes are classified into four families as shown in Scheme 1.3 [30-32].

Dithiolenes play an important role in natural systems. Thus, a dithiolene group is present an integral component of molybdopterin (MPT), the moiety that binds the molybdenum (or tungsten) at the catalytic centre of enzymes that transfer an oxygen atom to or from the substrate. A wide range of reactions are present in virtually all living systems and many of these enzymes are structurally characterized. Each catalytic centre contains a single metal atom, which bound to one or two MPT groups and with other donor atoms also. Spectroscopic information indicates that the oxygen atom transfer reaction takes place at the metal centre, which indicates that there is a change in oxidation state of metal from M(VI) to M(IV) (or vice-versa). This chemistry has been replicated by low molecular weight analogues of these centers.

More significantly, the complexes $[MO_2(bdt)_2]^{2-}$and $[MO_2(mnt)_2]^{2-}$ (M = Mo or W) constitute reasonable structural models for oxotransferase enzymes [33]. The Mo containing enzyme is called molybdopterin and the crystal structure of one molybdenum-pterin cofactor enzyme, shows coordination of two pterin units to one molybdenum center [34]. Some schematic representations of the 1,2-dithiolene containing molybdenum and

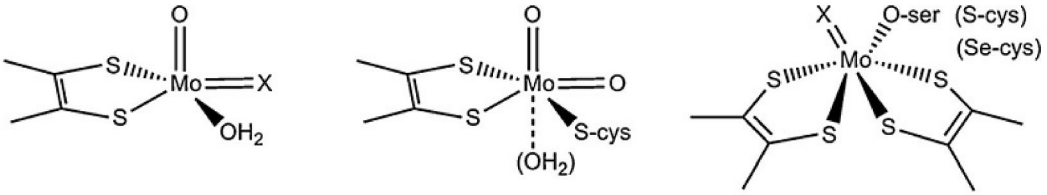


Xanthine dehydrogenase / Xanthine oxidase (XDH/XO) family (X= S or O)

Sulfite oxidase (SO) family

DMSO reductase (DMSOR) family

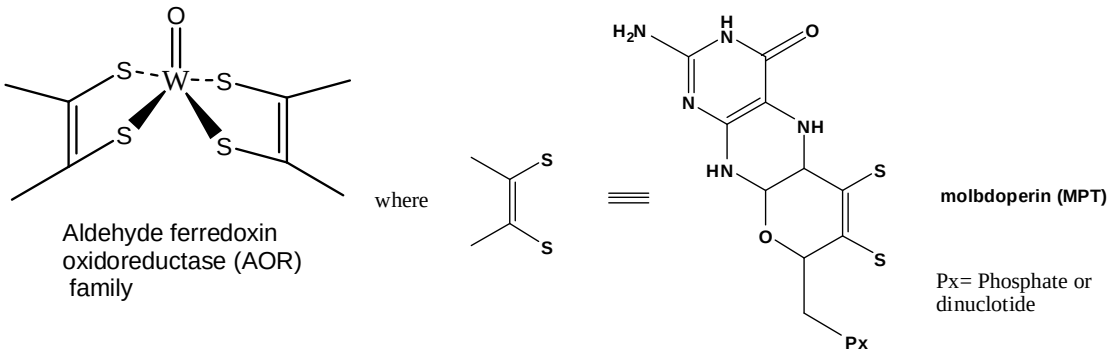


Aldehyde ferredoxin oxidoreductase (AOR) family

**Scheme 1.3.** The four families of dithiolene-containing molybdenum and tungsten enzymes based on structure of the catalytic reaction centers.

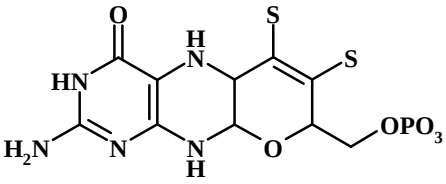


Molybdopterin (MPT)

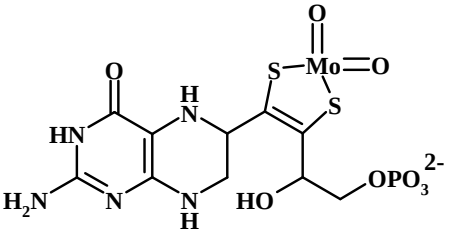


Molybdenum cofactor

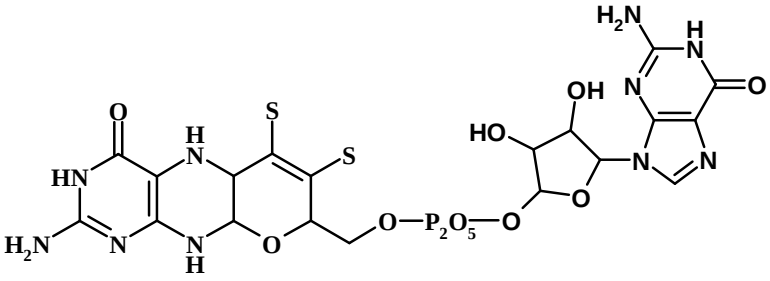


Molybdopterin guanine dinucleotide (MGD)

**Scheme 1.4.** Schematic representations of some of 1,2-dithiolene containing molybdenum and tungsten cofactors in relevant metalloenzymes.

tungsten enzymes are depicted in Scheme 1.4. Rajagopalan and co-workers [35-38] have proposed a structure for the molybdenum cofactor from the various spectroscopic measurements. The proposed structure for the molybdenum cofactor depicts it as a complex of molybdopterin and Mo, with the metal linked to the dithiolene sulfurs. They have suggested that, the molybdopterin is not a unique molecule, since it is found in several forms that differ in the phosphate terminus of the side chain.

*Enzyme active sites and model complexes*

These metal (*o*-dithiolene) complexes also serves as the model compounds for the active sites of natural enzymes, such as, hydrogenases enzymes. The natural energy resources predominantly used today are diminishing and their continued use has become more harmful for the environment. Efforts to develop alternative energy sources and fuels have become the major goals for science community. Dihydrogen is one of the future fuels that cause no deleterious products for the environment. So an efficient production of $H_2$ in good yield has become a challenge. Hydrogen evolution and uptake in the biological energy cycle is mostly catalyzed by three type of metalloenzymes based on metal atom present in that.

1. [FeFe]-hydrogenase,
2. Fe-Only hydrogenase and
3. [NiFe]-hydrgenase

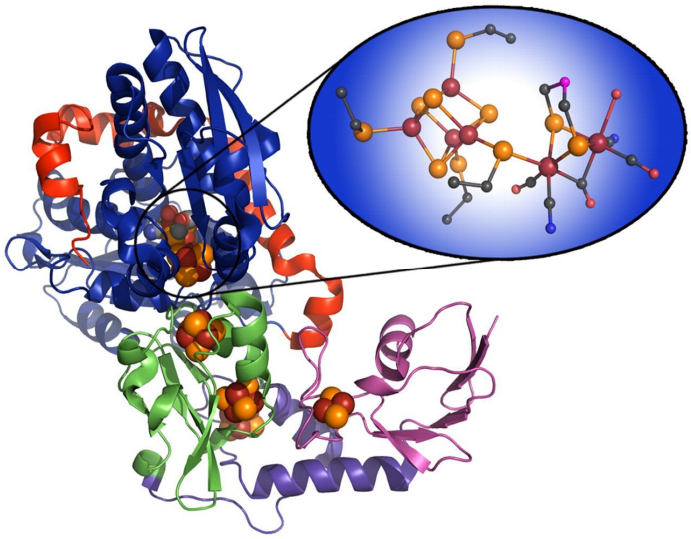

**Fig. 1.1.** Ribbon representation of Clostridium pasteurianum (CpI) [FeFe] hydrogenase (Protein Data Bank ID code: 3C8Y) with the FeS clusters and H cluster shown as space filling models, and zoom of the H cluster as ball and stick representation.

Out of these three, [FeFe]-hydrogenase is more predominant because it can produce 9000 molecules of $H_2$/S per enzyme molecule at 30 ºC [39-42], which is 10-100 times more active than its [NiFe] counterpart [39]. X-ray crystal structure of [FeFe]-hydrogenase is isolated from microorganisms such as *Desulfovibrio desulfuricans* [43] and *Clostridium pasteurianum* (CpI) [44]. The main function of this enzyme is to catalyze the two-electron reduction of two protons to yield dihydrogen as shown in eq. 1.

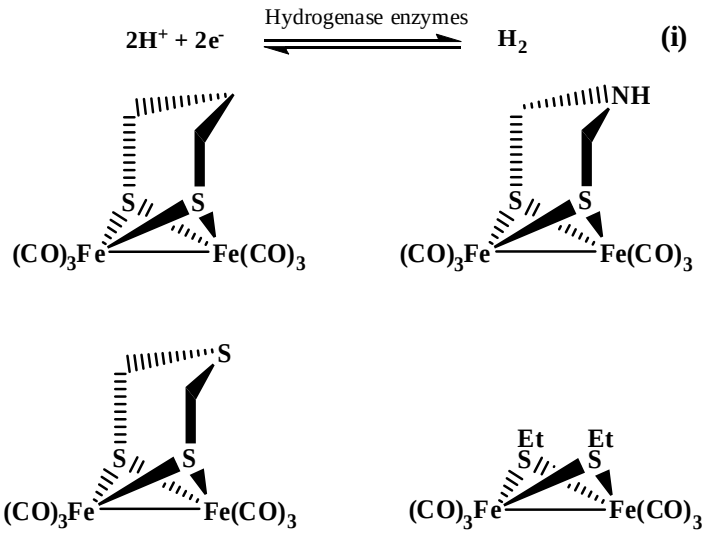


**Scheme 1.5.** Aliphatic dithiol bridged $Fe^{I}Fe^{I}$ complexes serves as [FeFe]-hydrogenase active site model complexes.

It consists of a 4Fe-4S cubane structure, bridged by cysteinyl-S to a novel 2Fe2S subunit. The 4Fe-4S unit probably mediates electron transfer while the 2Fe2S subunit is responsible for the formation and activation of hydrogen. Both iron atoms of the [2Fe] subsite exist with octahedral coordination geometry and 2Fe2S subunit is in butterfly conformation as shown in Fig. 1.1. Because of the significance of hydrogen as a potential energy source of the future, [45,46] the synthetic organometallic chemists have skillfully synthesized and characterized numerous bioinspired synthetic analogues of the active sites of [FeFe]-hydrogenases as shown in Scheme 1.5 [47–58]. Capon and co-workers first reported the benzene-1,2-dithiol (bdt) bridged diiron complex as [FeFe]-hydrogenase active site model [59] and it has been further used by Lichtenberger, Evans, Glass and co-workers to demonstrate electro

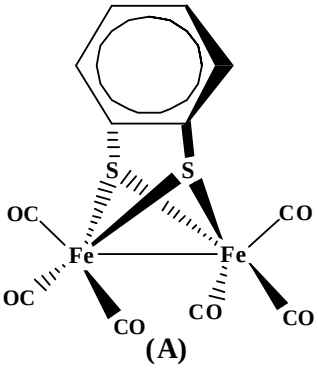

**(A)**

catalytic hydrogen generation from weak acids [60,61]. They have described a novel mechanism deduced from both electrochemical and theoretical studies on compound **A** as shown in Scheme 1.6. For the system **A**, the ene-1,2-dithiolate ($bdt^{2-}$) ligand coordination

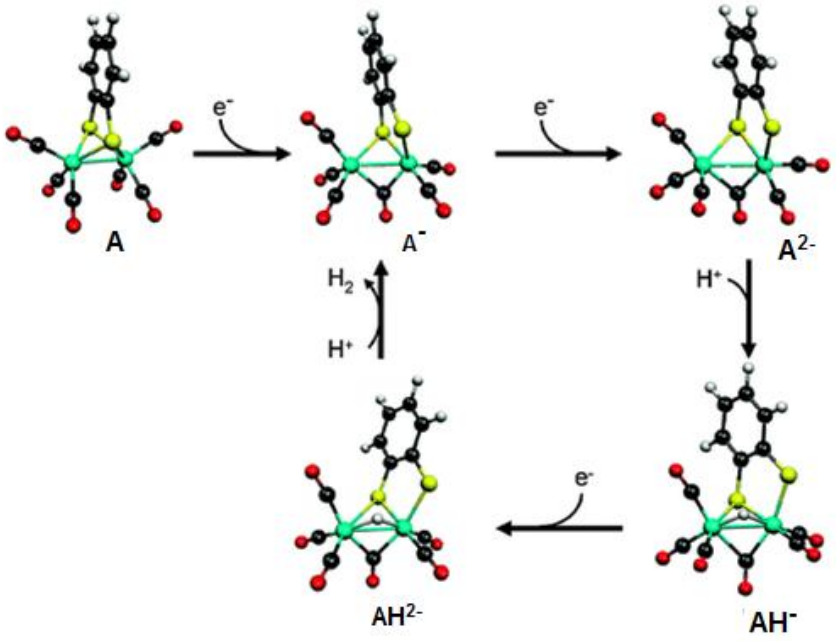


**Scheme 1.6.** Procatalyst initiation and ECEC mechanism for catalytic reduction of protons to $H_2$.

is able to modulate the potentials between oxidation states drastically in favor of electrochemical proton reduction [62]. Likewise, the coordination of the $bdt^{2-}$ ligand to the $\{Fe_2S_2\}$ core has a special ability to facilitate the electrocatalytic hydrogen production by lowering the potential difference between successive metal oxidation states in the catalytic cycle [59,60,62]. This has been explained by an interaction of the iron orbitals with a combination of the filled sulfur $p_\pi$ orbitals and the arene $p_\pi$ orbitals, which act to shield the change in electron density at the iron center as the oxidation state is changed, thus minimizing the changes in electron energies upon reduction. It is worth mentioning that the ene-1,2-dithiolate type ligand has been known to serve as an effective electron transfer pathway. Most of the dithiolate bridged $\{Fe^{I}Fe^{I}\}$ model complexes, that are inspired by the [FeFe]$H_2$ase active site, have been shown to be a promising class of molecular electrocatalysts for proton reduction from acids of varying strengths in non-aqueous media [47–50,59,60,62,63–68].

Sascha Ott and his co-workers described the use of complex $[Fe_2(\mu\text{-}Cl_2bdt)(CO)_6]$ ($Cl_2bdt$=3,6-dichlorobenzene-1,2-dithiolate) in a photocatalytic hydrogen production scheme that results in remarkably high turnover rates and numbers. In this scheme, $[Ru(bpy)_3]^{2+}$ (bpy=bipyridine) serves as a photosensitizer and ascorbic acid serves as a proton and sacrificial electron donor for homogeneous photochemical proton reduction [69]. And also they reported an inexpensive and robust photo electrochemical reduction system for the homogenous catalytic reduction of protons to hydrogen, which consists of an illuminated and biased *p*-type silicon (Si) photocathode, an [FeFe] electrocatalyst $[Fe_2(\mu\text{-bdt})(CO)_6]$ (bdt=benzene-1,2-dithiolate), a proton source ($HClO_4$) and a glassy carbon electrode [70].

## 1.5.2. Coordination Polymers based on metal *o*-dithiolate complexes

Recently, porous coordination polymers (metal-organic frameworks) have been synthesized based on bis(dithiolene) complexes $[Cu(pdt)_2]^-$ (Fig. 1.2) and $[Ni(pdt)_2]^-$ (Fig. 1.3) as building blocks [71,72]. These polymers ($Cu[Cu(pdt)_2]$ and $Cu[Ni(pdt)_2]$) show relatively high conductivity at room temperature with high porosity. In addition, conductivity of $Cu[Ni(pdt)_2]$ has been enhanced through partial oxidation of its framework as shown in Fig. 1.3. The increase in conductivity is due to oxidative doping and the resulting framework is a p-type semicounductor [72]. Metal-organic framewoks of these dithiolene based compounds exhibit reletively high elctrical conductvity. Because of such solid-state properties, these compounds can create a potentially versatile platform for genarating hybrid, ordered nanoscale elctronics. Given the wide range of metal dithiolene chemistry known, these properties suggest that the related metal organic framewoks may find applications as new electronic and photoactive microporous materials.

*1.5.2.1. Alkali metal based coordination Polymers of metal o-dithiolate complexes*

Rovira and co-workers have reported the alkali metal based coordination polymers of dithiolene complexes by using N-containing dithiolate ligands as building blocks. These coordination polymers have various applications in materials chemistry; very recently a simple route for the synthesis of alkali metal based coordination polymers of dithiolene complexes has been designed by our group. We have described that the synthesis of sodium metal based coordination polymers of diverse dimensionality (from 1D to 2D through 3D) based on a metal(III) dithiolene complex anion $[M^{III}(btdt)_2]^{1-}$ [M = Cu, Au]

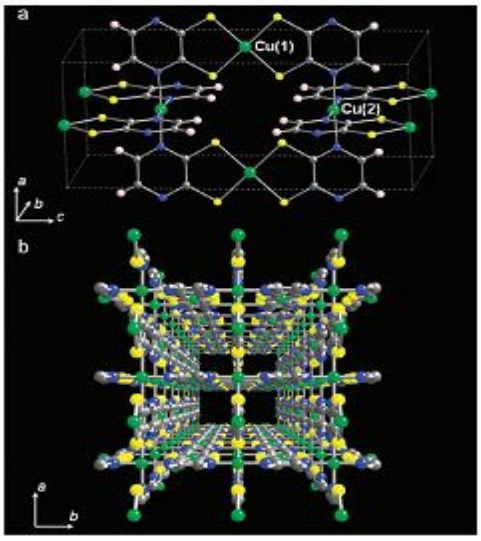


**Fig. 1.2.** (a) Crystal structure in Cu[Cu(pdt)2]. (b) Perspective view of the crystal structure of Cu[Cu(pdt)$_2$]. Color code: green, Cu; yellow, S; gray, C; blue, N; pink, H.

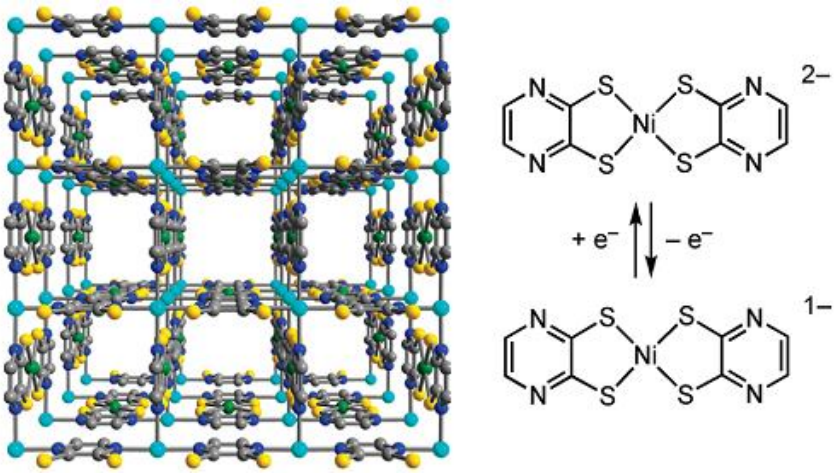


**Fig. 1.3.** Left: Portion of the structure of the metal-organic framework Cu[Ni(pdt)$_2$], with light blue, green, yellow, blue, and gray spheres representing Cu, Ni, S, N, and C atoms, respectively; H atoms are omitted for clarity. Right: Redox behavior associated with the $[Ni(pdt)_2]^{2-}$ units within the framework.

(btdt = 2,1,3-benzothiadiazole-5,6-dithiol) by simply changing the solvents of recrystallization as shown in Fig. 1.4(a) [73]. Interestingly, in this system, the dimensionality of a sodium coordination based polymers, coupled with a metal(III) (bis)dithiolene complex, can be regulated by the type of hybridization of the central carbon atom of the solvent coordinating to the sodium ion. We have investigated the solvent coordination to sodium ion more vigilantly. During recrystallization, the 1D coordination polymers were obtained from MeOH, and THF solvents in which the

hybridization of central carbon atom attached to the sodium-coordinated solvent atom (O) is $sp^3$ (Fig. 1.4(b)); likewise, the $sp^2$ hybridized central carbon atom (of acetone and DMF solvents) attached to the coordinating atom (O) leads to the formation of 2D coordination polymers. The 3D coordination polymers have been crystallized from $CH_3CN$, that includes N as coordinating solvent atom, which is attached to sp hybridized central carbon atom. These three observations clearly reveal that the diverse hybridizations of the central carbon atoms of the solvents (MeOH, THF, $CH_3COCH_3$, DMF and $CH_3CN$ in the present study), attached to the coordinating atoms, have a wonderful relationship with the dimensional-topologies of the sodium coordination polymers of these dithiolene system as shown in Fig. 1.4.

The more bulkier $sp^3$ hybridized orbitals (tetrahedral) of the central carbon atom of methanol and THF solvents occupy more space around the alkali metal ion (sodium cation) and prevent further coordination of more dithiolene complex units (through N or S donor atoms), thereby it allows the extension only in 1-dimension rather than 2-dimensions or 3-dimensions. The less bulkier sp hybridized orbitals (linear shape) of the central carbon atom of $CH_3CN$ occupy less space around sodium cation, thus allow more dithiolene complex units to coordinate sodium ion leading to 3-dimensional coordination polymers. The recrystallization from acetone and DMF type of coordinating solvents, the planar shape of $sp^2$ hybridized orbitals of the central carbon atom attached to coordinating donor atom of acetone and DMF solvents, direct towards the formation of 2-dimensional networks. Thus, the shape and space occupied by the hybridized orbitals of central carbon atom attached to the coordinating solvent atoms are the major factors in directing the dimensionality of coordination polymers of this system, which has been described in Table 1.1.

In this system (Fig. 1.4), Cu(III) analogues have given a opportunity to perform electrochemical studies and to carry out spectroscopy. The electrochemistry of the copper (III) complexes is very interesting in the sense that these complexes get reduced more easily. This indicates that the present system (Cu(III) dithiolate) might act as oxidation catalyst for organic transformations / oxidation reactions of industrial importance. To generalize the above concept (relation between the hybridization and dimensionality) by choosing an alkali metal ion (e.g., $K^+$ cations instead of $Na^+$ ions) coupled with a transition

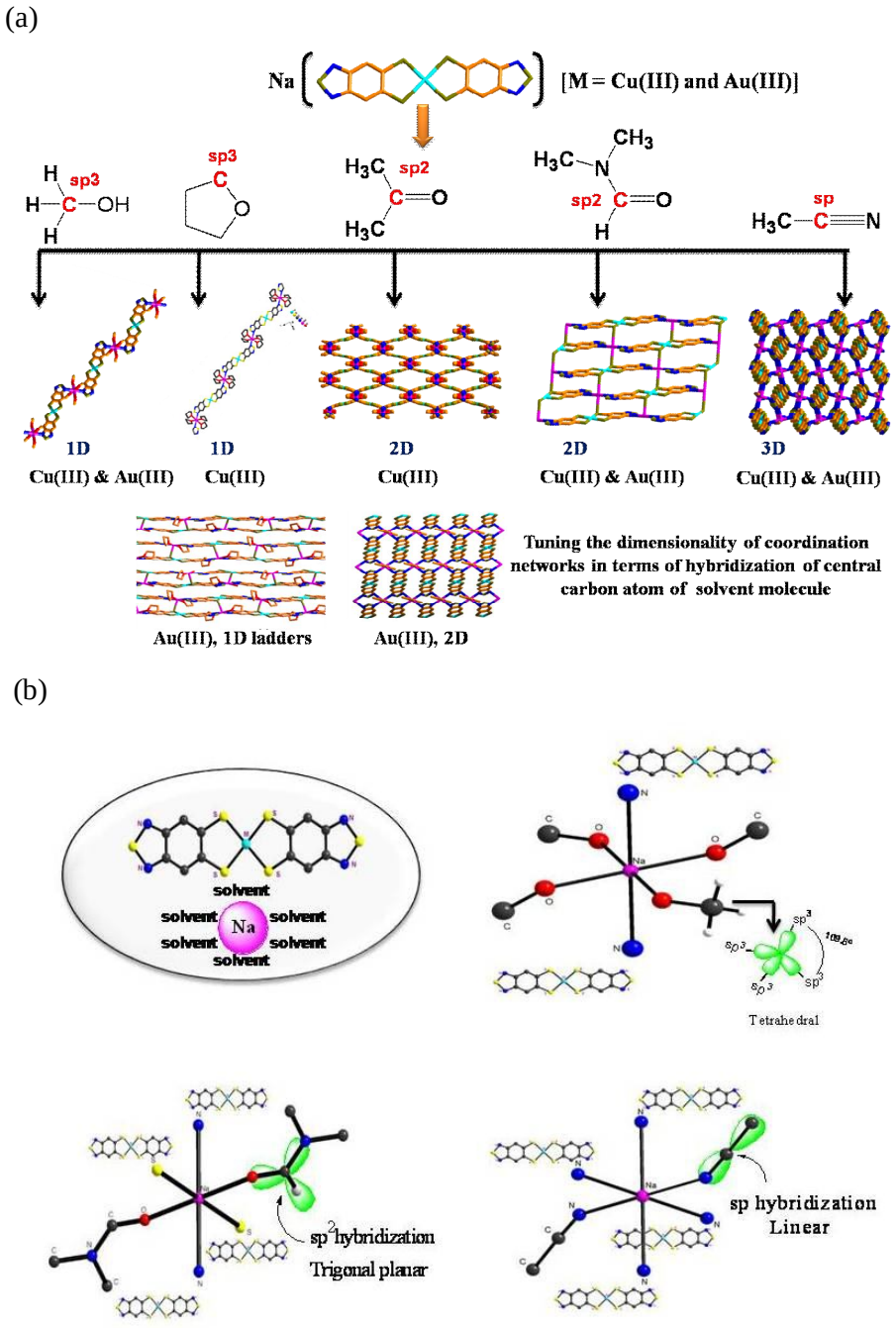


**Fig. 1.4.** (a) Extended networks (1D to 3D) observed in the crystals with different solvents, (b) $[Na(solvent)_n][M(btdt)_2]$ [M = Cu(III), Au(III)] complexes present in solution state (left above); crystallization from MeOH and THF ($sp^3$ hybridized orbitals of central carbon) directs the formation of 1D coordination polymer (right above); crystallizing in DMF and acetone ($sp^2$ hybridized orbitals of central carbon) influences the formation of 2D coordination polymer (left below); crystallization from $CH_3CN$ (sp hybridized orbitals of central carbon) directs the formation of 3D coordination polymer (right below).

metal(bis) dithiolene complex, additionally two new potassium metal coordination polymers were synthesized of diverse dimensionality based on a metal(III) dithiolene complex anion $[Cu^{III}(btdt)_2]^{1-}$ by changing the solvents of recrystallization [74].

**Table 1.1.** Role of coordinating solvent in directing the dimensionality of sodium based coordination polymer

| Recrystalizing solvent | Hybridization and geometry of central carbon | Dimensionality of coordination networks |
|---|---|---|
| MeOH | $sp^3$, Tetrahedral | 1D |
| THF | $sp^3$, Tetrahedral | 1D |
| Acetone | $sp^2$, Trigonal planar | 2D |
| DMF | $sp^2$, Trigonal planar | 2D |
| Acetonitrile | sp, Linear | 3D |

### 1.5.3. Polydentate *o*-dithiol ligands and their metal complexes in coordination chemistry

Till now we have discussed about bidentate mono *o*-dithiols. It is also to be noted that polydentate *o*-dithiols, such as, benzene-*o*-dithiolato donor groups are versatile building blocks in supramolecular coordination chemistry. The coordination chemistry of bis- and tris(benzene-*o*-dithiolato) ligands have been reported. Hahn and his coworkers have developed a method to synthesis

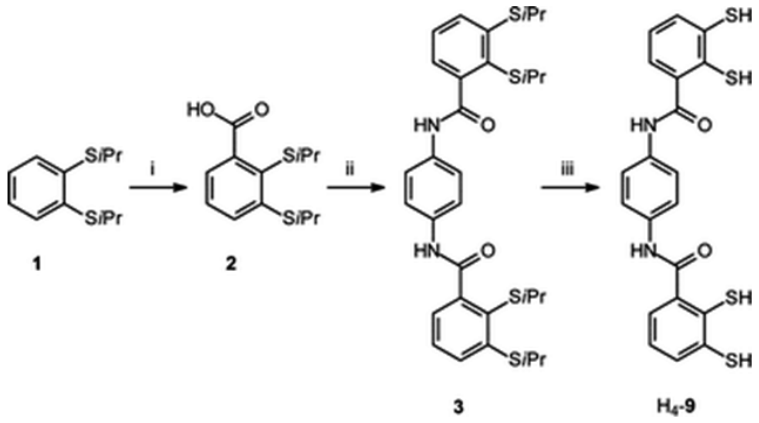


**Scheme 1.7.** Synthesis of ligand **$H_4$-9**. *Reagents and conditions*: (i) (1) *n*BuLi/TMEDA, (2) $CO_2$, (3) HCl-$H_2O$; (ii) (1) $SOCl_2$, (2) *p*-phenylenediamine, $NEt_3$; (iii) (1) Na/naphthalene, (2) HCl–$H_2O$.

such ligands starting from 1,2-di(isopropylmercapto)benzene **1** (Scheme 1.7), which can be obtained from 1,2-dichlorobenzene and sodium isopropylthiolate [75,76]. Compound **1** was *ortho*-lithiated and reacted with $CO_2$ which after acidic work-up gave the carboxylic acid **2,** which on further treated with $SOCl_2$ followed by reaction with 0.5 equiv. of a diamine (e.g. 1,4-diamino benzene) yielded the tetra-S-alkylated ligands. The isopropyl protection groups of compound **3** were removed with sodium/naphthalene in THF or with sodium in liquid ammonia. Hydrolysis with HCl-$H_2O$ gave the moderately air-sensitive bis(benzene-o-dithiol) ligands.

*1.5.3.1. Coordination chemistry of bis- and tris(benzene-o-dithiol) ligands*

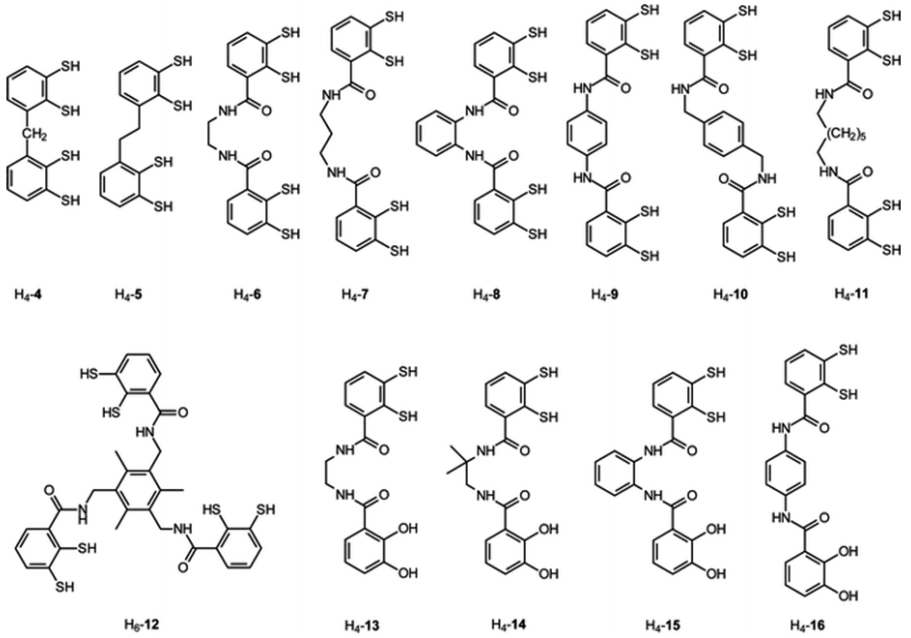


**Fig. 1.5.** Polydentate bis(benzene-*o*-dithiol) and benzene-*o*-dithiol/catechol ligands.

*1.5.3.1.1. Mononuclear chelate complexes*

Polydentate ligands are capable to form several different coordination compounds, depending on the topology of the ligand and the preferred coordination geometry of the metal ion. The bis(benzene-o-dithiol) ligand $H_4$-**11** (Fig. 1.5) with long and flexible backbone, for example, give mononuclear chelate complexes with $Co^{III}$ ions [77]. Complex $(NEt_4)$[Co(**11**)] can be obtained in simple metathesis reactions from $Na_4$-**11** with $CoCl_2.6H_2O$, followed by its aerial oxidation. Complex $(NEt_4)$[Co(**11**)] is stable in solution, which indicates that the cobalt atom is coordinated in a square-planar fashion.

This coordination geometry was confirmed for complex $(NEt_4)$[Co(**11**)] in the solid state (Fig. 1.6, left). In the molecular structure of $[(\eta^5\text{-}C_5H_5)Ti(\mathbf{10})]^-$ (as shown in Fig. 1.6 (middle)), Ti center is coordinated in a distorted tetragonal-pyramidal fashion. The four thiolate donors take the basal positions, whereas the Cp ligand assumes the apical position. Mononuclear chelate complexes have been obtained from the tris(benzene-*o*-dithiol) ligand $H_6$-**12** [78]: the reaction of $[Ti(OR)_4]$ with $Li_2CO_3$ results in the mononuclear complex $Li_2$[Ti(**12**)], which after cation exchange with $Ph_4AsCl$ yields $(Ph_4As)_2$[Ti(**12**)]. The structure determination with single crystals of $(Ph_4As)_2$[Ti(**12**)] (Fig. 1.6 (Right)) reveals a distorted octahedral coordination geometry around the metal center and the molecular parameters for $[Ti(\mathbf{12})]^{2-}$ indicate the unusual presence of intramolecular N–H···S hydrogen bonds.

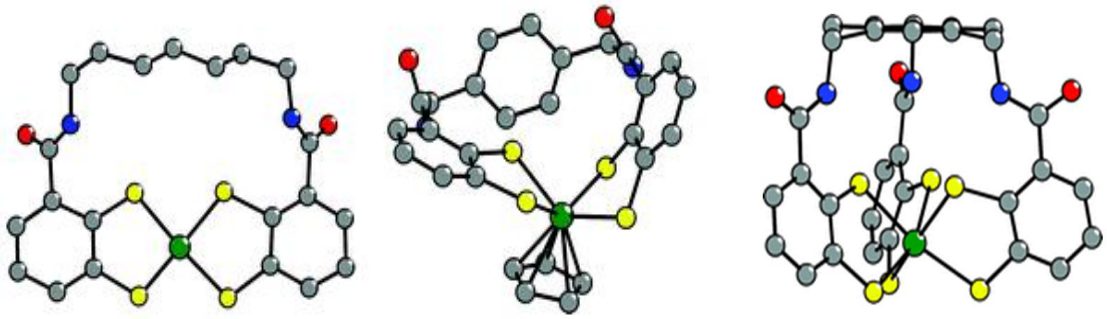

**Fig. 1.6.** Molecular structures of the anions $[Co(\mathbf{11})]^-$ (left), $[(\eta^5\text{-}C_5H_5)Ti(\mathbf{10})]^-$ (middle) and $[Ti(\mathbf{12})]^{2-}$ (right).

*1.5.3.1.2. Dinuclear double-stranded complexes*

Bis(benzene-*o*-dithiol) ligands with short or inflexible bridging units are no longer capable of forming mononuclear chelate complexes. It is well known that benzene-*o*-dithiolates give square-planar complexes with most metal ions from the first transition period [79]. This observation is also made with bis(benzene-*o*-dithiolato) ligands and thus leads to a large number of dinuclear double-stranded complexes. Ligands $H_4$-**5** and $H_4$-**6** (Fig. 1.5) form dinuclear double-stranded complexes with $Ni^{II}$ and, after aerial oxidation, $Ni^{III}$ ions [80]. The molecular structures of complex anions $[Ni^{II}_2(\mathbf{5})_2]^{4-}$ (Fig. 1.7c) and $[Ni^{II}_2(\mathbf{6})_2]^{4-}$ (Fig. 1.7a) confirm the expected square-planar coordination geometry at the nickel(II) centers. Both $Ni^{II}$ complex anions are air sensitive and are readily oxidized to the corresponding $Ni^{III}$ complexes $[Ni^{III}_2(\mathbf{5})_2]^{2-}$ and $[Ni^{III}_2(\mathbf{6})_2]^{2-}$. The X-ray diffraction study

for $(NEt_4)_2[Ni^{III}_2(\mathbf{6})_2]$ (Fig. 1.7b) revealed that the anions $[Ni^{II}_2(\mathbf{6})_2]^{4-}$ and $[Ni^{III}_2(\mathbf{6})_2]^{2-}$ possess similar structures with the exception that all amide NH protons are directed towards the sulfur donor groups in complex $[Ni^{II}_2(\mathbf{6})_2]^{4-}$ which indicates there is existence of (weak) N–H···S hydrogen bonds, while the amide protons in complex $[Ni^{III}_2(\mathbf{6})_2]^{2-}$ apparently are not involved in hydrogen bonds.

To synthesize the model compounds for iron only nitrogenase, Sellmann *et al.* investigated the reaction of ligand $H_4$-**7** (Fig. 1.5) with iron(III) ions. A dinuclear double-stranded complex $(AsPh_4)_2[Fe_2(\mathbf{7})_2]$ was obtained which differs significantly from that of the dinuclear nickel complexes [81]. The anion $[Fe_2(\mathbf{7})_2]^{2-}$ contains two $FeS_4$ units that are linked by two Fe–S–Fe bridges leading to two distorted square pyramidal, five coordinate iron centers as shown in Fig. 1.7d.

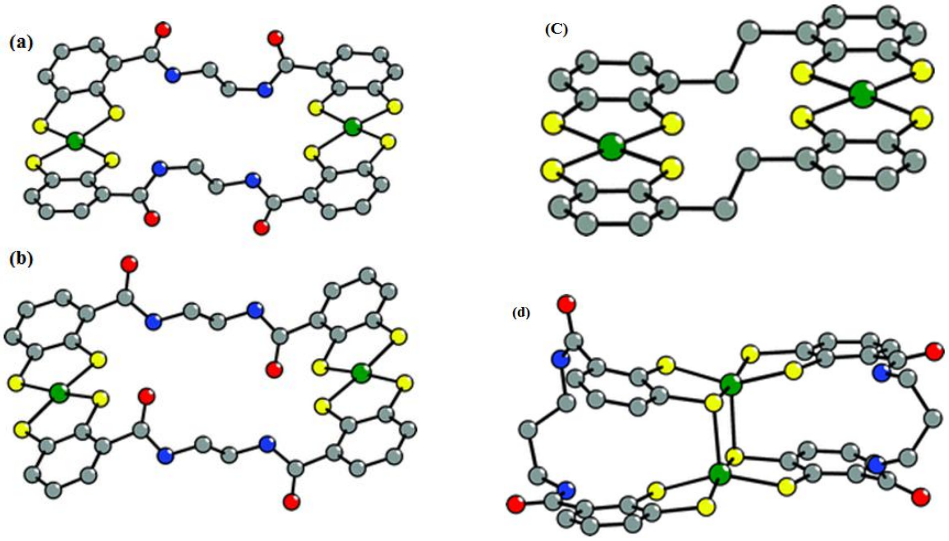


**Fig. 1.7.** Molecular structures of the anions (a) $[Ni^{II}_2(\mathbf{6})_2]^{4-}$, (b) $[Ni^{III}_2(\mathbf{6})_2]^{2-}$, (c) $[Ni_2(\mathbf{5})_2]^{4-}$ and (d) $[Fe_2(\mathbf{7})_2]^{2-}$.

Whe the ligand $H_4$-**8** (Fig. 1.5) was treated with $[Ti(OC_2H_5)_4]$ and $Li_2CO_3$ in methanol, this reaction did not lead to the formation of a triple-stranded helicate $[Ti_2(\mathbf{8})_3]^{4-}$, Instead, the dinuclear double-stranded complex $[Ti_2(\mathbf{8})_2(\mu\text{-}OCH_3)_2]^{2-}$ was obtained [82]. The single crystal X-ray diffraction analysis of $(Ph_4As)_2[Ti_2(\mathbf{8})_2(\mu\text{-}OCH_3)_2]$ revealed that the two metal centers are connected by two ligand strands $\mathbf{8}^{4-}$ in addition to two methoxo ligands which are part of a central four-membered $Ti_2(\mu\text{-}OCH_3)_2$ ring as shown in Fig. 1.8.

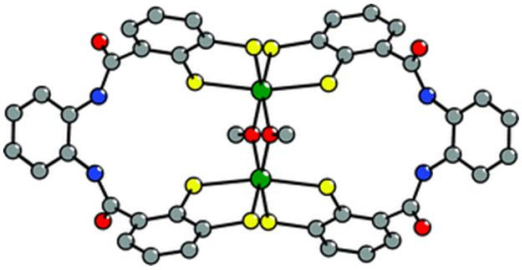

**Fig. 1.8.** Molecular structure of the anion $[Ti_2(\mathbf{8})_2(\mu\text{-}OCH_3)_2]^{2-}$.

The coordination geometry at the metal centers can be described as strongly distorted octahedral metal centers. The anion $[Ti_2(\mathbf{8})_2(\mu\text{-}OCH_3)_2]^{2-}$ resides on a crystallographic inversion center. Therefore the two titanium atoms must assume a different configuration (Λ and Δ) which leads to a *meso*-complex. However, in this dinuclear double-stranded complex, strong intramolecular N–H···O hydrogen bonds exist [82].

*1.5.3.1.3. Dinuclear triple-stranded helicates*

The first triple-stranded helicates with bis(benzene-*o*-dithiolato) ligands have been obtained only recently with ligands $H_4$-**6** and $H_4$-**9** (Fig. 1.5). The reaction of $[Ti(OC_2H_5)_4]$ with these ligands in the presence of $Li_2CO_3$ yields the dark red compounds $Li_4[Ti_2(\mathbf{6})_3]$ and $Li_4[Ti_2(\mathbf{9})_3]$ [82,83].

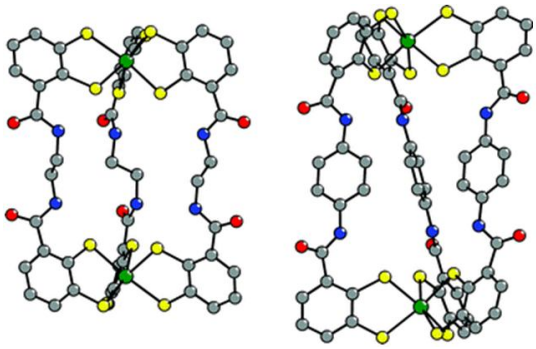

**Fig. 1.9.** Molecular structures of the anions $[Ti_2(\mathbf{6})_3]^{4-}$ (left) and $[Ti_2(\mathbf{9})_3]^{4-}$ (right).

The alkali metal salts have been found difficult to crystallize and therefore the salt metathesis reaction with (PNP)Cl has been carried out to give the complexes $Li(PNP)_3[Ti_2(\mathbf{6})_3]$ (Fig 1.9 left) and $(PNP)_4[Ti_2(\mathbf{9})_3]$ (Fig 1.9 right) in pure crystalline form. It should be noted that the exchange of the remaining lithium cation in $Li(PNP)[Ti_2(\mathbf{6})_3]$ could not be achieved, even when a large excess of (PNP)Cl was used in the relevant metathesis reaction [82,83]. The lithium cation in crystals of compound

$Li(PNP)_3[Ti_2(\mathbf{6})_3]\cdot 3DMF\cdot H_2O$ is coordinated by two carbonyl groups of two different anions $[Ti_2(\mathbf{6})_3]^{4-}$ and by a water and a DMF molecule in the asymmetric unit. This leads to indefinite polymeric chains $Li–[Ti_2(\mathbf{6})_3]^{4-}–Li–[Ti_2(\mathbf{6})_3]^{4-}$ in the crystal lattice (Fig 1.10). In contrast to this, the $[Ti_2(\mathbf{9})_3]^{4-}$-anions in compound $(PNP)_4[Ti_2(\mathbf{9})_3]\cdot 3DMF$ are well separated because there is no interactions between cations and anions [82,84].

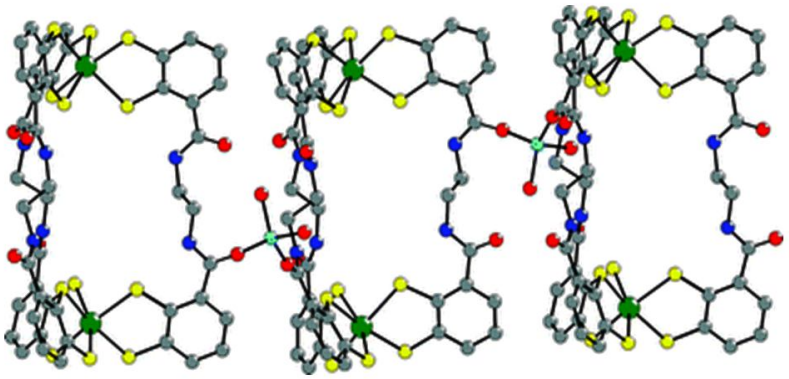

**Fig. 1.10.** Partial view of the polymeric chains in the crystal lattice of $Li(PNP)[Ti_2(\mathbf{6})_3]\cdot 3DMF\cdot H_2O$. No $PNP^+$ cations and only the oxygen atoms of the solvent molecules coordinating to the bridging lithium cation are shown.

### 1.5.3.2. Benzene-*o*-dithiol/catechol ligands

#### *1.5.3.2. 1. Dinuclear double-stranded complexes*

Tetradentate ligands with different donor groups, such as, benzene-*o*-dithiol/catechol derivatives (directional ligands) [85–88] are of special interest, since they offer the opportunity to prepare hetero dinuclear complexes as well as complexes with a different orientation of the ligand strands. The versatile coordination chemistry of bis(benzene-*o*-dithiol) ligands prompted us to substitute one of the benzene-*o*-dithiol groups for a catechol group, leading to ligands $H_4$-**13**–$H_4$-**16** (Fig. 1.5).

In order to investigate the coordination chemistry of mixed benzene-*o*-dithiol/catechol ligands, they reacted ligand $H_4$-**13** with $[TiO(acac)_2]$ and $Na_2CO_3$. Since the bis(benzene-*o*-dithiol) ligand $H_4$-**6** (Fig. 1.9) and its catechol homologue [89,90] with the same topology as $H_4$-**13** form dinuclear triple-stranded helicates $[Ti_2L_3]^{4-}$, they were expected to form a triple-stranded helicate $Na_4[Ti_2(\mathbf{13})_3]$. Surprisingly, all attempts to prepare the triple-stranded complex anion $[Ti_2(\mathbf{13})_3]^{4-}$ failed and the double-stranded complex $Na_2[Ti_2(\mathbf{13})_2(\mu\text{-}OCH_3)_2]$ was exclusively obtained [91]. The X-ray analysis of compound

$(AsPh_4)_2[Ti_2(\mathbf{13})(\mu\text{-}OCH_3)_2]$ (Fig. 1.11) indicates that the complex anions with an antiparallel orientation of the ligand stands are present in the crystal structure.

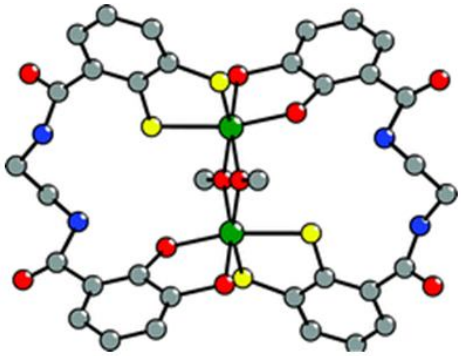

**Fig. 1.11.** Molecular structure of a centrosymmetric anion $[Ti_2(\mathbf{13})_2(\mu\text{-}OCH_3)_2]^{2-}$ present in crystals of $(AsPh_4)_2[Ti_2(\mathbf{13})_2(\mu\text{-}OCH_3)_2]$.

The double-stranded complex anion $[Ti_2(\mathbf{15})_2(\mu\text{-}OCH_3)_2]^{2-}$ was obtained from $[TiO(acac)_2]$ and the *o*-phenylenediamine bridged benzene-*o*-dithiol/catechol ligand $H_4$-**15** in methanol at room temperature [91]. Contrary to the observation for the anion $[Ti_2(\mathbf{13})_2(\mu\text{-}OCH_3)_2]^{2-}$, $^1H$ NMR spectroscopy indicated the formation of only one pair of enantiomers in solution. Only the amide protons linked to the catechoylamido groups form strong hydrogen bonds with the catecholato oxygen atoms which leads to a downfield shift of the resonance for these protons in the complex anion relative to the resonance for the free ligand $H_4$-**15**.

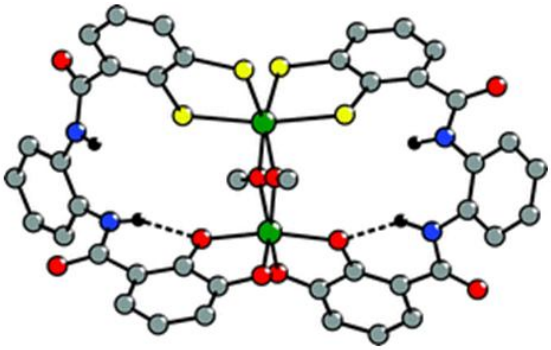

**Fig. 1.12.** Molecular structure of the anion $[Ti_2(\mathbf{15})_2(\mu\text{-}OCH_3)_2]^{2-}$.

Since the orientation of the ligand strands cannot be determined by NMR spectroscopy, a crystal structure analysis was carried out with single crystals of $(PNP)_2[Ti_2(\mathbf{15})_2(\mu\text{-}OCH_3)_2]$. It revealed a parallel orientation of the ligand strands (Fig. 1.12). The reasons for the parallel orientation of the ligand strands are at the moment subject to speculation. It is

reasonable to assume, that the formation of strong N–H···O hydrogen bonds that has been observed in the solid state has an influence on the orientation of the ligand strands.

*1.5.3.2. 2. Dinuclear triple-stranded complexes*

When the ligands $H_4$-**14** and $H_4$-**16** were reacted with $[TiO(acac)_2]$ and $Na_2CO_3$ in methanol, it exclusively resulted in the formation of the triple-stranded helicates $Na_4[Ti_2(\mathbf{14})_3]$ [91,92] and $Na_4[Ti_2(\mathbf{16})_3]$ [91]. Attempts to exchange all four sodium cations by $PNP^+$ cations failed in both cases even after addition of 10 equivalents of (PNP)Cl to methanolic solutions of $Na_4[Ti_2(\mathbf{14})_3]$ and $Na_4[Ti_2(\mathbf{16})_3]$. Only three sodium cations could be exchanged, resulting in the formation of complexes $Na(PNP)_3[Ti_2(\mathbf{14})_3]$ [91,92] and $Na(PNP)_3[Ti_2(\mathbf{16})_3]$ [91]. $^1$H NMR spectra of $Na(PNP)_3[Ti_2(\mathbf{14})_3]$ showed only one set of signals for the ligand strands (2 × t, 4 × d for the aromatic protons) which demonstrated the exclusive formation of the geometrical isomer with a parallel orientation of the ligand strands. A strong downfield shift of the catechoylamide NH proton in $[Ti_2(\mathbf{14})_3]^{4-}$ relative to the free ligand $H_4$-**14** indicates the formation of strong N–H···O hydrogen bonds, whereas no N–H···S hydrogen bonds were detected in the $[Ti_2(\mathbf{14})_3]^{4-}$ anion.

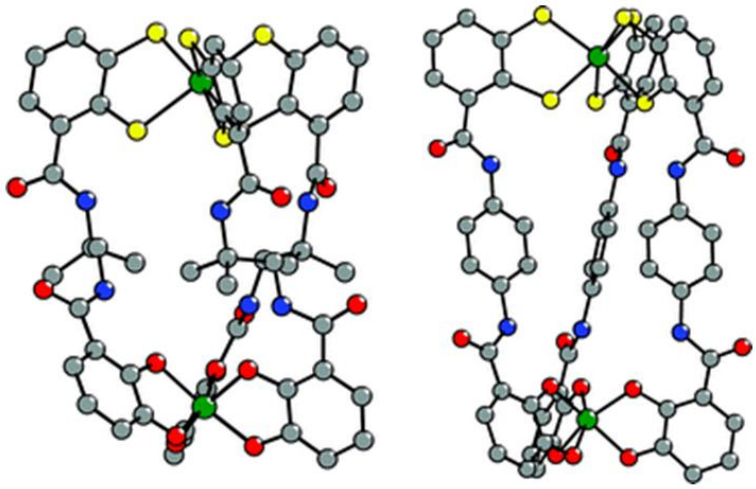

**Fig. 1.13.** Molecular structures of the anions $[Ti_2(\mathbf{14})_3]^{4-}$ (left) and $[Ti_2(\mathbf{16})_3]^{4-}$ (right).

Upon crystallization, spontaneous resolution into crystals containing exclusively the ΛΛ or the ΔΔ isomer (space group *P*1) occurred. The unit cell of $Na(PNP)_3[Ti_2(\mathbf{14})_3]$ contains one tetraanion $[Ti_2(\mathbf{14})_3]^{4-}$, three $PNP^+$ cations, one sodium cation and one molecule of water, methanol and diethyl ether. The sodium cation acts as a bridge between two

$[Ti_2(\mathbf{14})_3]^{4-}$ tetraanions by coordination of amide carbonyl functions of two different tetraanions and this leads to indefinite polymeric chains Na–$[Ti_2(\mathbf{14})_3]^{4-}$–Na–$[Ti_2(\mathbf{14})_3]^{4-}$ in the crystal lattice similar to those found for Li(PNP)$[Ti_2(\mathbf{6})_3]$ [82,83] (Fig. 1.10).

## 1.6. Functional Properties of Metal *o*-dithiolene complexes

### *1.6.1. Electrochemical Properties and Chemical Reactivity*

The electrochemical properties of metal-dithiolene complexes are very interesting because of their unique redox properties and noninnocent behavior. The extensive π-electron delocalization in metal bis-dithiolene complexes makes it possible for the existence of variable charge levels and also it is difficult to assign oxidation states of the metal and ligands. Interestingly, square planar bis(dithiolene) complexes undergo one-, two- and even three-reversible one electron redox processes and these can be explained by the following equation.

$$[M(\text{dithiolene})_2]^{+} \underset{-e^-}{\overset{+e^-}{\rightleftharpoons}} [M(\text{dithiolene})_2]^{0} \underset{-e^-}{\overset{+e^-}{\rightleftharpoons}} [M(\text{dithiolene})_2]^{-} \underset{-e^-}{\overset{+e^-}{\rightleftharpoons}} [M(\text{dithiolene})_2]^{2-}$$

Based on chemical, electrochemical, structural, and spectroscopic studies [3,8], the electron density in the metal orbitals does not change significantly as the charge level on the bis(dithiolene) complex is changed. Thus, the accessibility of a range of charge levels of dithiolene complex is possibly more related to the accessibility of a number of formal oxidation states of the dithiolene ligands. A large number of bis(dithiolene) complexes has been reported for the metals, such as, Ni, Pd, Pt, Cu, Au. The ease of oxidation of $[M(S_2C_2R_2)]^{z-}$ for a particular metal decreases in the order R = H > alkyl > aryl > $CF_3$ > CN. This series parallels to the electron donating-withdrawing ability of the substituent group R. For the transition metals Fe < Co < Ni < Cu, oxidative stability increases in this order for the dianion (Z = 2). This indicates that the participation of metal orbitals in the frontier orbitals of the dianionic species. Similarly, for $[M(bdt)_2]^{z-}$ (bdt = benzene-1,2-dithiolate), the redox potentials are dependent on the substituents on the aromatic ring. The potential of 0/-1 couple increases as the substituent group becomes more electron-withdrawing. Square-planar bis(dithiolene) complexes are subjected to theoretical investigations [7,93-95]. As from the density functional theory (DFT), the HOMO (highest occupied molecular orbital) for $[Ni(S_2C_2H_2)]$ is primarily ligand based orbital consisting of four $3p_z$ orbitals of sulfur, perpendicular to molecular XY plane, and four $2p_z$ orbitals

of carbons with opposite phases. The lowest unoccupied molecular orbital (LUMO) is a mixture of ligand–metal orbitals, but still mostly the ligand character [95]. In general, electrochemical data supports the molecular orbital descriptions, derived from quantum mechanical calculations. Because of rich redox chemistry of bis(dithiolene) chemistry and the redox active nature of the dithiolene ligands, these show much reactivity related to the redox properties. Recently, Wang and Stiefel have reported [96] the separation of simple olefins mediated by the metal bis(dithiolene) complex anions. They proposed that, it is reversible olefin binding, controlled electrochemically and the whole reversible process is generally described as follows: when the olefin bound adduct (metal complex) is reduced, the reductant dissociates and forms an olefin and the metal-dithiolene anion. When this anion is oxidized, the oxidant binds the olefin again and so on.

*Reactivity with Olefins*

Nowadays, in chemical and petrochemical industry, olefins are the major volume feed stock. In most of the metal-mediated reactions, the alkene coordinates to the metal in at least one step of the reaction sequence, description of such systems easily poisoned by impurities in crude alkenes, which often bind more strongly to the metal than the alkene. These metal-based systems are most probably poisoned by $C_2H_2$, CO, and $H_2S$. In this context, Wang and Stiefel [96] argued that the metal complexes bind alkenes through chelated ligands, instead of, at the metal center. Thus the concerned system should be more resistant to deactivation by contaminants. They reported that neutral nickel bis(dithiolene) complexes form adducts with linear alkenes, such as ethylene or 1-hexene, where the alkene binds through the ligand S-atoms, even in the presence of $H_2S$ or CO (Scheme 1.8).

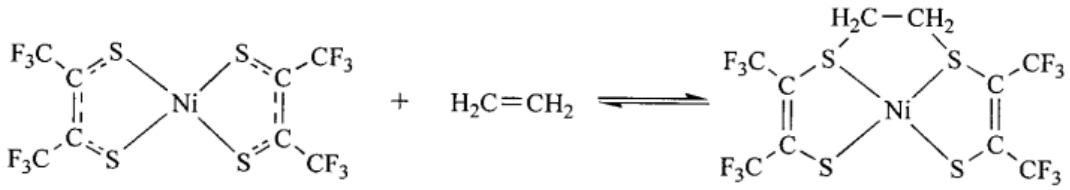

**Scheme 1.8.** Equilibrium reaction of metal(dithiolene) and with its olefin adduct.

This unusual tolerance toward poisoning led the authors to propose an olefin purification scheme in which the dithiolene-bound alkene is released by electrochemical reduction and it is regenerated by oxidation. Interestingly, the olefin binding and releasing

are controlled electrochemically in this case. Reversible olefin complexation to dithiolene complexes thus offers a novel approach in separating and purifying olefins [96,97].

As shown Scheme 1.9, the mono-anionic complex $[NiL_2]^-$ (L, ligand) is oxidized electrochemically, forming the neutral species $[NiL_2]$. A multicomponent stream (MCS) containing an olefin(s) is introduced where upon the olefin reacts with $[NiL_2]$, forming the adduct $[(olefin)NiL_2]$, while other (gaseous) components (such as alkanes, CO, $C_2H_2$, and so on.) pass unreacted. The olefin adduct is electrochemically reduced. The reduced olefin adduct $[(olefin)NiL_2]^-$ releases olefin (which is recovered) as $[NiL_2]^-$ is regenerated, completing the cycle. A similar scheme involves electrochemical reduction of the neutral species $[NiL_2]$ that is in equilibrium with the olefin adduct $[(olefin)NiL_2]$, which drives the release of the olefin from the adduct as the complexation equilibrium (Scheme 1.8) shifts to replenish the neutral species.

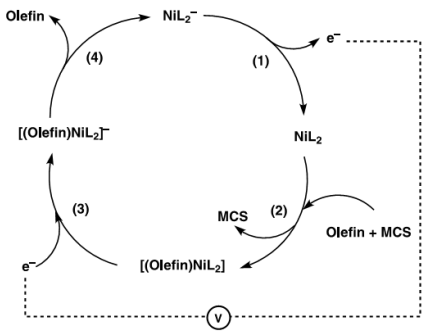


**Scheme 1.9.** Schematic representation for electrochemically driven olefin separation using nickel dithiolene complexes.

## 1.6.2. Solid-State Properties

Metal 1,2-dithiolene complexes exhibit the unusual solid-state properties, such as magnetic [98-100], conducting [101] and nonlinear optics [102] (NLO) properties. The electronically delocalized core comprising of the central metal, four sulphur atoms and the C=C units, accounts for a rich electrochemical behavior that often yields one or more reversible redox processes. The redox properties of these complexes are strongly dependent on the ligand and its large contribution to the frontier orbitals. The possible oxidation states of these complexes range from dianionic to cationic states and partial oxidation situations often occur, especially, in the solid state. Also different spin states such as S = 0, 1/2, 1 or 3/2, can be easily obtained, upon variation of both the transition

metal M and oxidation state make these complexes suitable units for magnetic materials. Moreover, the dithiolene complexes exhibit multiple oxidation states due to this stable ion-radical species that are available at various rodox potentials. Depending on the partial oxidation of these by electrochemical oxidation, it results in various nonintegral oxidation state (NIOS). Furthermore, these complexes also show a diversity of geometry, ranging from the more general case of purely square planar coordination, favorable to solid state extended $\pi$–$\pi$ interactions, to dimeric, trimeric [103] or even polymeric [104] arrangements. All these features have made dithiolene complexes suitable building blocks for the preparation of electrical and magnetic materials.

*Electrical Properties (Conducting and Super Conducting Properties)*

Over past few decades, large number of 1,2-dithiolene based conductor and superconductor materials have been developed. Although the first dithiolene ligands were synthesized in the early 1960's [105-107], electrical properties of the dithiolene complexes were reported only in 1969 [108]. These complexes exhibit low conductivity values in the range of $10^{-3}$–$10^{-5}$ S $cm^{-1}$ at room temperature. Then much effort has been devoted to design new analogues in order to improve the transition metal based conducting properties. In this context, the first observation of metallic behavior in crystalline metal-dithiolene was reported for $Li_{0.75}[Pt(mnt)_2]\cdot 2H_2O$ by Underhill *et al*. in 1981 [109,110]. In this complexes, the Pt···Pt distance is 3.639 Å, which indicates that there is no $5dz^2$ orbitals overlapping. This compound produces the uniform columnar structure. Therefore, the conduction band in molecular conductor originates from ligand $\pi$–orbitals or mixed metal($d$)–ligand($\pi$) orbitals, in which sulfur atoms play an important role as shown in Fig. 1.14.

From this, new aspect of molecular conductors, based on metal dithiolene complexes, has been developed. In order to improve the conductivity of molecular conductors, it needs the extension of delocalization and intermolecular interactions.

It was soon observed that a slight, even minute, modification of the cation may result in important, or even drastic, changes in the conducting behavior. To demonstrate, whether the cations play role for conductivity or not, in 1986 the $[Bu_4N]^+$ cation was replaced by TTF and the compound $(TTF)[Ni(dmit)_2]_2$ was reported to undergo the superconducting transition at 1.62 K under 7 kbar [111]. This was the first report on transition metal dithiolene complex based superconductor. Metal dithiolene complexes

show very interesting conducting behavior, which is mainly due to the involvement of sulfur-rich dithiolene ligands, owing to the intermolecular S···S interactions of the ligands. Few of the superconducting $[M(dmit)_2]^-$ salts are described in Table 1.2 [112-118].

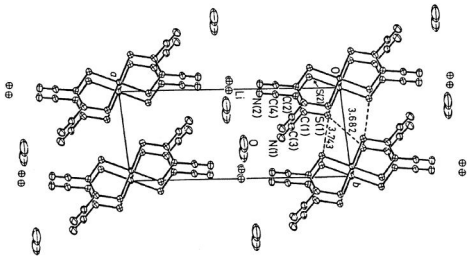

**Fig. 1.14.** Crystal structure of $(H_3O)_{0.33}Li_{0.8}[Pt(mnt)_2]\cdot 1.67H_2O$.

**Table 1.2**. Molecular superconductors based metal dithiolene complexes**.**

| **compound** | ***Tc*/K** | ***P*/kbar** |
|---|---|---|
| $(TTF)[Ni(dmit)_2]_2$ | 1.62 | 7 |
| α–(EDT-TTF)$[Ni(dmit)_2]$ | 1.3 | - |
| $(Me4N)[Ni(dmit)_2]_2$ | 5 | 7 |
| α'–$(TTF)[Pd(dmit)_2]_2$ | 5.93 | 24 |
| α–$(TTF)[Pd(dmit)_2]_2$ | 1.7 | 22 |
| β–$(Me_4N)[Pd(dmit)_2]_2$ | 6.2 | 6.5 |
| $(Et_2Me_2N)[Pd(dmit)_2]_2$ | 4.2 | 4 |
| β'–$(Et_2Me_2P)[Pd(dmit)_2]_2$ | 4 | 6.9 |
| β'–$(Me_4Sb)[Pd(dmit)_2]_2$ | 3 | 10 |
| β'–$(Me_4As)[Pd(dmit)_2]_2$ | 4 | 7(ap) |

## 1.6.3. Optical Materials

*1.6.3.1. Near–Infrared (NIR) absorbing dyes*

The near–infrared region is from about 800 nm to 2500 nm. Dyes for applications in the NIR region require small differences in the energy between HOMO and LUMO. The donor–acceptor concept was established by König [119] and Ismailsky [120] and further developed by Dilthey and Wizinger [121-123] and incorporated into the perturbation molecular orbital theory (PMO) model by Dewar [124]. According to this concept, long–wavelength absorption is expected if π–systems are substituted with donor (D) and acceptor (A) groups. Very strong donor and acceptor groups can be applied in a double arrangement according to building principle (**D — π — A — π — D**) and can cause long–wavelength absorption [125].

Metal bis(dithiolene) complexes have been used as good candidates for Near-IR dyes, because (1) metal bis(dithiolene) complexes show intense electronic absorption in the NIR region, especially Ni-dithiolene complexes. (2) Metal dithiolene complexes have their ability to exist in several clearly defined oxidation states which are fully connected through reversible redox steps. (3) Another characteristic property of dithiolene is their high thermal and photochemical stability. The absorption spectra of neutral [Ni(dithiolene)$_2$] have been discussed and the longest wavelength of these complexes has been assigned to $b_{1u}$–$b_{2g}$ ($\pi$–$\pi^*$) transition. The highest occupied MO ($b_{1u}$) is virtually a pure ligand orbital and the lowest empty MO ($b_{2g}$) has some Ni (metal) character as well as ligand character [126-129]. This absorption band can be smoothly tuned over desired wavelength region by simple and subtle changes on to the dithiolene ligands. Most of the dithiolene complexes used for the NIR dyes are derived from Ni because of the higher delocalization within these complexes compared to the Pd and Pt analogues. A detailed review by Mulller-Westerhoff *et al*. [130] is available on this NIR absorption topic and a number of Ni-based dithiolene complexes with absorption at wavelength > 700 nm have been described [131-137]. Some of the dithiolene ligands, involved in dithiolene complexes, exhibit such strong absorption as shown in Schemes 1.10 and 1.11. Many researchers aimed at increasing the intensity absorption maximum at low energy. Based on this research, it led to conclusion that the dithiolene complex should contain

(1) Coplanarity of ligand $\pi$-system and dithiolene;

(2) Presence of an extended $\pi$-system;

(3) Presence of electron donating substituents;

(4) Fixing of the substituents into rigid coplanarity with the ligand;

(5) Attachment of sterically bulky substituents to increase solubility;

(6) Variation of the central metal to obtain different shifts and to tune the relaxation time.

Although the dithiolene metal complexes show an absorption band in the NIR region, they are not useful as colorants in the recording layer of the optical DRAW disk [138-140], due to their low reflectivity of the GaAlAs diode lasers. But the dithiolene Ni complex has been applied to the optical DRAW disk as an inhibitor of laser induced fading [141]. The metal dithiolene complexes have also attracted much interest as Q–switching NIR dyes applications.

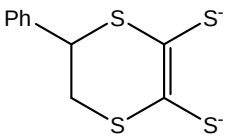


{phdt}$^{2-}$ 1028nm

(43,000) $C_6H_6$

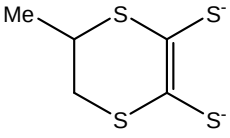


{medt}$^{2-}$ 1029nm

(36,000) $C_6H_6$

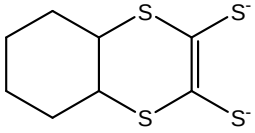


{bddt}$^{2-}$ 1035 nm

(63,000) $C_6H_6$

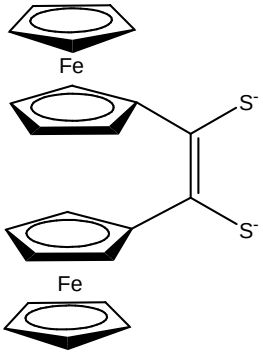


1310 nm

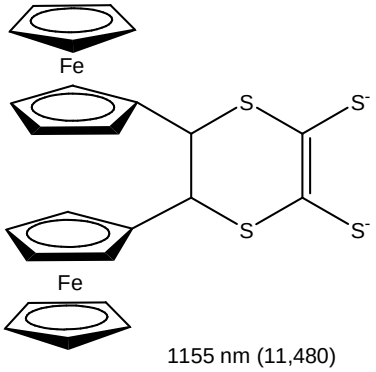


1155 nm (11,480)

**Scheme 1.10**

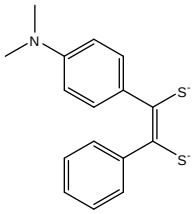


1060 nm (28,000)

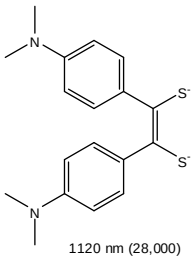


1120 nm (28,000)

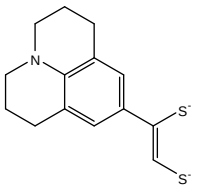


1180 nm (35,000)

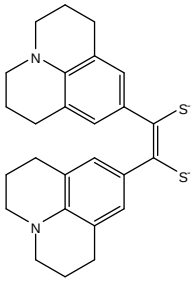


1270 nm (45,000)

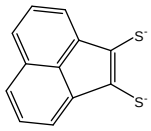


1140 nm (30,000)

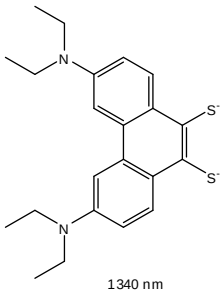


1340 nm

**Scheme 1.11**

### 1.6.3.2. Nonlinear Optical Materials

*Second-Order NLO*

The basic requirements for NLO active molecules, that possess large β values, contain an electron donor group (D) connected with an electron acceptor group (A) by a π–conjugated polarizable bridge [142,143]. The nonlinear optical properties of such dipolar, polarizable (D–π–A) molecules are characterized by low energy, D→A intermolecular charge transfer (ICT) excitations. However, much number of papers has appeared on organic molecule-based compound exhibiting NLO properties, especially for SHG, but only few are reported for inorganic molecule-based materials. In this context, metal dithiolene complexes have attracted interest for NLO properties owing to their highly delocalized electron configuration and the possibility of the transfer of electron density between metal and ligand which induces an intense near-IR absorption transition [144]. Unfortunately, symmetrical homoleptic bis(dithiolene) complexes do not exhibit any second harmonic generation (SHG), because the SHG materials require the lack of a center of symmetry. Symmetrical homoleptic dithiolene complexes, involved in SHG, are synthesized as counterions with push-pull active molecules such as hemicyanine dye (HCD) [145] as shown in Scheme 1.12. Replacement of iodide ion in (HCD)I by dmit-based complex dianion results in the compounds of general formula {(HCD)[M(dmit)$_2$] (M = Cd, Ni, Zn} [146,147]. Interestingly, LB films of these Zn-dmit compounds have been shown to improve SHG compared to the (HCD)I. This may be due to the fact that Zn complexes act as spacer avoiding aggregation and/or dispersion of the active chromofore (HCD) and allowing an ordered segregation of HCD in the films.

Interestingly, unsymmetrical homoleptic bis(dithiolene) and heteroleptic dithiolene complexes are better candidates for SHG, due to their nonzero dipole momentums. Some of the unsymmetrical bis(dithiolene) complexes (14–17) and heteroleptic dithiolene complexes (18–21), which exhibit second order NLO properties are shown in Schemes 1.13 and 1.14, respectively. In those, most promising and extensively studied compounds are heteroleptic Ni(diimine)(dithiolate) complexes as shown Scheme 1.15 [148-150].

In order to increase hyperpolarizability of the complexes, the best candidate system should be Pt, with electron donating substituents on the dithiolate ligands (to increase the donor strength), whereas electron withdrawing substituents should be placed on diimine as far as

Pt atom is concerned. These compounds exhibit $\beta_0$ values within the range from 0 to –16 × $10^{-30}$ esu, depending upon the substituents.

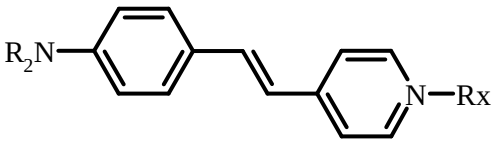


R = Me, Et, Bu, etc.

**Scheme 1.12**

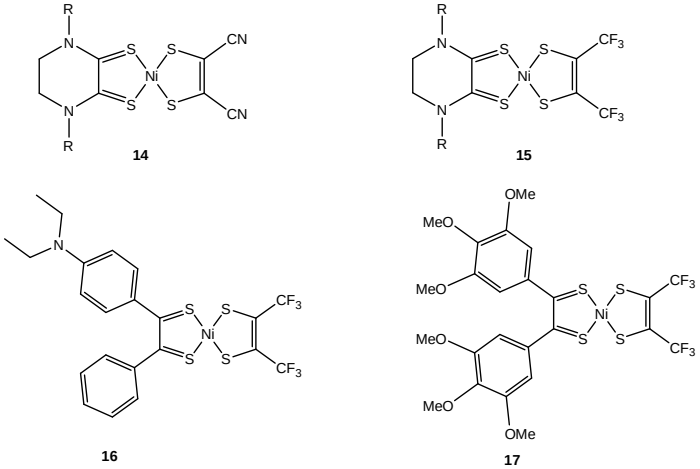


**Scheme 1.13**

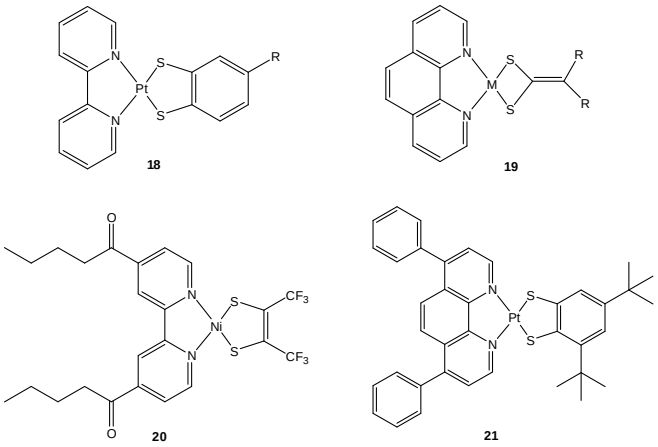


**Scheme 1.14**

*Third Order NLO*

The application of third order NLO effects have been known in various fields, such as, optical-phase configuration (to restore distorted images), all-optical-switching and computing [151]. Recently, more and more symmetrical bis(dithiolene) complexes with third-order optical nonlinearity or optical limiting effects have been explored because third order NLO effects do not require any symmetry restriction [152]. Some of the metal bis(dithiolene) complexes, exhibiting third order NLO, are shown in Scheme 1.15. Third order NLO properties of dmit-based and mnt-based metal complexes with sandwiched organometallic cations $[CpFe(\eta\text{-}C_6H_6)]^+$ have also been reported [153].

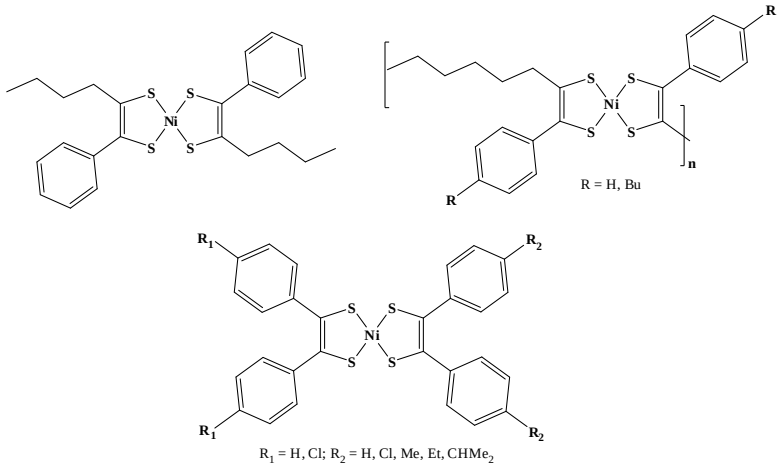


**Scheme 1.15**

Heteroleptic dithiolene complexes also have been studied for their third-order NLO properties that involve the dmit and mnt ligands as shown in Scheme 1.16 [154], in which, only the dmit based compounds exhibit a large third-order optical nonlinearity, due to their large planar conjugated system compared to the mnt analogues.

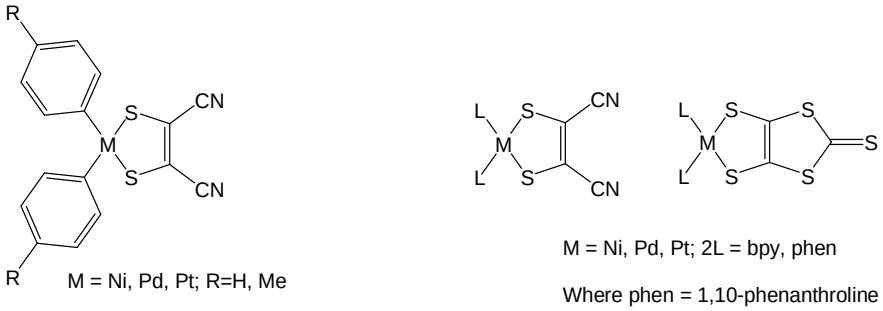


**Scheme 1.16**

## 1.7. Motivation of the present work

A great deal of coordination chemistry has emerged because we are curious to find out what happens when metals are coordinated by ligands. New chemistry generated by ligands is a strong incentive for designing and synthesizing new ligands such as mono-, bis- and tris(*o*-dithiol) ligands. The goal to model the active sites of metal enzymes with respect to their electronic properties, structure and reactivity represents another motive for ligand synthesis.

From the above description we have seen that, since last five decades, metal-dithiolene complexes have proved to be an interesting subclass of inorganic coordination compounds that have generated continued interest in structure, bonding and reactivity. The findings show that the dithiolene complexes have useful reactivity and sensing properties and they display remarkable solid state properties, such as, super conductivity, magnetic, and optical properties. Because of their rich properties, the literature on metal-dithiolene complexes is so vast.

The electronic spectral studies and redox properties would be greater interest in this area of *N*-heterocyclic based dithiolene chemistry. The photo-physical (luminescence) properties of platinum complexes of qdt-type ligand have been studied extensively by Eisenberg's group [155,156]. Additionally, qdt-type ligands are useful in the area of analytical chemistry to analyze the metal quantification in ppm levels due to their absorption in visible region with large molar extension coefficient values. These facts motivated us to design and synthesize new type of qdt-based ligands and to synthesize its metal bis(dithiolene) complexes, so that we can compare the chemistry of this new qdt-system with that of existing qdt compounds. Furthermore, H. B. Gray *et al.* studied that the effect of different substituents on the electronic structure of the $\{MS_4\}$ group in a systematic manner [12].

The coordination polymers of dithiolene based complexes are still rare in the literature. Metal coordination polymers are particularly interesting in materials chemistry. To accomplish these materials, the use of crystal engineering tools becomes crucial to achieve the adequate packing of the molecules that may lead to the desired properties. Very recently, two electro conductive coordination polymers $Cu[Cu(pdt)_2]$ and $Cu[Ni(pdt)_2]$ have been reported, and these show relatively high electrical conductivity at room temperature with high porosity based on pyrazine bis(dithiolate) building blocks

[73,74]. In addition, the conductivity of $Cu[Ni(pdt)_2]$ has been enhanced through partial oxidation of its framework. The increase in counducvity is due to oxidative doping and the resulting framework is a p-type semicounductor [74]. Metal-organic framewoks of these dithiolene based compounds exhibit reletively high elctrical conductvity with permenent porosity. This inspired us to choose metal bis(dithiolene) complexes as building blocks for the construction of metal-coordination polymers. Moreover, Rovira and co-workers have reported the alkali coordination polymers of dithiolene complexes by using *N*-containing dithiolate ligands as building blocks. Nature has has used dithiolene ligands in many matalloenzymes and this motivated us to use this 1,2 ene dithiol system in modeling the active sites of iron only hydrogeneases.

## 1.8. References


[1] K. D. Karlin, E. I. Stiefel, Prog. Inorg. Chem. John Wiley, New York, (2004), Volume 52.

[2] J. Locke, J. A. McCleverty, E. J. Wharton, C. J. Winscom, Chem. Commun. (1966) 677.

[3] J. A. McCleverty, Prog. Inorg. Chem. 10 (1968) 49.

[4] U. T. Müller–Westerhoff, B. Vance, in Comprehensive Coordination Chemistry, Vol. 2, G. Wilkinson, R. D. Gillard, J. A. McCleverty, Eds. Pergamon Press, Oxford, (1987) 595.

[5] L. J. Farrugia, J. Appl. Crystallogr. 32 (1997) 565.

[6] M. Cowie, M. J. Bennett, Inorg. Chem. 15 (1976) 1595.

[7] S. Alvarez, R. Vicente, R. Hoffmann, J. Am. Chem. Soc. 107 (1985) 6253.

[8] R. P. Burns, Mcauliffe, Adv. Inorg. Chem. Radiochem. 22 (1979) 303.

[9] A. L. Balch, I. G. Dance, R. H. Holm, J. Am. Chem. Soc. 90 (1968) 1139.

[10] G. N. Schrauzer, V. P. Mayweg, J. Am Chem. Soc. 84 (1962) 3221.

[11] A. E. Smith, G. N. Schrauzer, V. P. Mayweg, W. Heinrich, J. Am Chem. Soc. 87 (1965) 5798.

[12] M. J. Baker-Hawkes, E. Billig, H. B. Gray, J. Am. Chem. Soc. 88 (1966) 4870.

[13] S. I. Shupack, E. Billig, R. J. H. Clark, R. Williams, H. B. Gray, J. Am. Chem. Soc. 86 (1964) 4594.

[14] A. Davison, N. Edelstein, R. H. Holm, A. H. Maki, J. Am Chem. Soc. 85 (1963) 2029.

[15] R. Eisenberg, J. A. Ibers, R. J. H. Clark, H. B. Gray, J. Am Chem. Soc. 86 (1964) 113.

[16] R. Eisenberg, J. A. Ibers, Inorg. Chem. 4 (1965) 605.

[17] C. L. Beswick, J. M. Schulman, E. I. Stiefel, Prog. Inorg. Chem. 52 (2003) 55.

[18] S. Sproules, K. Wieghardt, Prog. Inorg. Chem. 52 (2003) 55.

[19] M. Roger, T. Arliguie, P. Thuery, M. Fourmigué; M. Ephri-tikhine, Inorg. Chem. 44 (2005) 594.

[20] E. M. Weis, C. L. Barnes; P. B. Duval, Inorg. Chem. 45 (2006) 10126.

[21] W. Paw, S. D. Cummings, M. A. Mansour, W. B. Connick, D. K. Geiger, R. Eisenberg, Coord. Chem. Rev. 171 (1998) 125.

[22] M. Hissler, J. E. McGarrah, W. B. Connick, D. K. Geiger, S. D. Cummings, R. Eisenberg, Coord. Chem. Rev. 208 (2000) 115.

[23] J. M. Bevilacqua, J. A. Zuleta, R. Eisenberg, Inorg. Chem. 33 (1994) 258.

[24] S.-K. Lee, K.-S. Shin, D.-Y.Noh, O. Jeannin, F. Barrière, J.-F. Bergamini, M. Fourmigué, Chem.–Asian J. 5 (2010) 169.

[25] S. J. N. Burgmayer, Prog. Inorg. Chem. 52 (2003) 491.

[26] J. McMaster, J. M. Tunney, C. D. Garner, Prog. Inorg. Chem. 52 (2003) 539.

[27] R. H. Holm, Coord. Chem. Rev. 100 (1990) 183.

[28] K. Kubo, A. Nakao, Y. Ishii, T. Yamamoto, M. Tamura, R. Kato, K. Yakushi; Matsubayashi, G. Inorg. Chem. 47 (2008) 5495.

[29] J. M. Bevilacqua, J. A. Zuleta; Eisenberg, Inorg. Chem., 32 **(**1993**)** 3689.

[30] R. Hille, Chem. Rev. 96 (1996) 2757.

[31] M. K. Johnson, D. C. Rees, M. W. W. Adams, Chem. Rev. 96 (1996) 2817.

[32] C. Kisker, H. Schindelin, D. C. Rees, Annu. Rev. Biochem. 66 (1997) 233.

[33] N. Ueyama, H. Oku, M. Kondo, T. Okamura, N. Yoshinaya, A. Nakamura, Inorg. Chem. 35 (1996) 643.

[34] J. C. Boyington, V. N. Gladyshev, S. V. Khangulov, T. C. Stadtman,; P. D. Sun, Science, 275 (1997) 1305.

[35] S. P. Kramer, J. L. Johnson, A. A. Ribeiro, D. S. Millington, K. V. Rajagopalan, J. Biol. Chem. 262 (1987) 16357.

[36] R. S. Pilato, E. I. Stiefel, in Bioinorganic catalysis, J. Reedijk, E. Bouwman, Eds.; Marcel Dekker, New York, 1999.

[37] K. V. Rajagopalan, Adv. Enzymol. Relat. Areas Mol. Biol. 64 (1991) 215–290.

[38] J. L. Johnson,;y Rajagopalan, K. V. Proc. Natl. Acad. Sci. U. S. A. 79 (1982) 6856.

[39] M. W. W. Adam, Biochim. Biophys. Acta 1020 (1990) 115–145.

[40] J. W. Peters, Curr. Opin. Struct. Biol. 9 (1999) 670–676.

[41] M. Frey, ChemBioChem 3 (2002) 152–160.

[42] E. C. Hatchikian, N. Forget, V. M. Fernandez, R. Williams, R. Cammack, Eur. J. Biochem. 209 (1992) 357–365.

[43] Y.Nicolet, C.Piras, P. Legrand, C. E. hatchikian, J. C. Fontecilla-Camps, Structure 7 (1998) 13.

[44] J. W. Peters, W. N. Lanzilotta, B. J. Lemon, L. C. Seefeldt, Science 282 (1998) 1853.

[45] P. Hoffmann, Tomorrow's Energy: Hydrogen, Fuel Cells, and the Prospect for a Cleaner Planet, MIT Press, Cambridge, Massachusetts and London, England, 2002.

[46] N. Lewis, D. Nocera, Proc. Natl. Acad. Sci. USA 103 (2006) 15729–15735.

[47] C. Tard, C. J. Pickett, Chem. Rev. 109 (2009) 2245–2274.

[48] F. Gloaguen, T. B. Rauchfuss, Chem. Soc. Rev. 38 (2009) 100–108.

[49] R. Lomoth, S. Ott, Dalton Trans. (2009) 9952–9959.

[50] G. A. N. Felton, C. A. Mebi, B. J. Petro, A. K. Vannucci, D. H. Evans, R. S. Glass, D. L. Lichtenberger, J. Organomet. Chem. 694 (2009) 2681–2699.

[51] S. J. Borg, S. K. Ibrahim, C. J. Pickett, S. P. Best, C. R. Chimie 11 (2008) 852–860.

[52] A. I. Stewart, I. P. Clark, M. Towrie, S. K. Ibrahim, A. W. Parker, C. J. Pickett, N. T. Hunt, J. Phys. Chem. B 112 (2008) 10023–10032.

[53] J. A. Wright, C. J. Pickett, Chem. Commun. (2009) 5719–5721.

[54] A. Jablonskyte, J. A. Wright, C. J. Pickett, Dalton Trans. 39 (2010) 3026–3034.

[55] M. Razavet, S. C. Davies, D. L. Hughes, and C. J. Pickett, Chem. Commun. (2001) 847–848.

[56] C. Tard, X. Liu, S. K. Ibrahim, M. Bruschi, L. De Gioia, S. C. Davies, X. Yang, L.-S.W, G. Sawers, and C. J. Pickett, Nature 433 (2005) 610–613.

[57] A. K. Justice, G. Zampella, L. De Gioia, T. B. Rauchfuss, J. I. van der Vlugt, and S. R. Wilson, Inorg. Chem. 46 (2007) 1655–1664.

[58] J. I. van der Vlugt, T. B. Rauchfuss, C. M. Whaley, and S. R. Wilson, J. Am. Chem. Soc. 127 (2005) 16012–16013.

[59] J. F. Capon, F. Gloaguen, P. Schollhammer, J. Talarmin, J. Electroanal. Chem. 566 (2004) 241–247.

[60] G. A. N. Felton, A. K. Vannucci, J. Chen, L. T. Lockett, N. Okumura, B. J. Petro, U. I. Zakai, D. H. Evans, R. S. Glass, D. L. Lichtenberger, J. Am. Chem. Soc. 129 (2007) 12521–12530.

[61] G. A. N. Felton, A. K. Vannucci, N. Okumura, L. T. Lockett, D. H. Evans, R. S. Glass, D. L. Lichtenberger, Organometallics 27 (2008) 4671–4679.

[62] J. F. Capon, F. Gloaguen, P. Schollhammer, J. Talarmin, J. Electroanal. Chem. 595 (2006) 47–52.

[63] F. Gloaguen, J. D. Lawrence, T. B. Rauchfuss, J. Am. Chem. Soc. 123 (2001) 9476 – 9477.

[64] S. Ott, M. Kritikos, B. Akermark, L. Sun, R. Lomoth, Angew. Chem. Int. Ed. 43 (2004) 1006 – 1009.

[65] S. J. Borg, T. Behrsing, S. P. Best, M. Razavet, X. Liu, C. J. Pickett, J. Am. Chem. Soc. 126 (2004) 16988 –16999.

[66] L. Schwartz, P. S. Singh, L. Eriksson, R. Lomoth, S. Ott, C. R. Chimie 11 (2008) 875–889.

[67] D. Chong, I. P. Georgakaki, R. Mejia-Rodriguez, J. Sanabria-Chinchilla, M. P. Soriaga, and M. Y. Darensbourg, J. Chem. Soc., Dalton. Trans. (2003) 4158–4163.

[68] S. Jiang, J. Liu, Y. Shi, Z. Wang, B. Åkermark, and L. Sun, Dalton Trans. (2007) 896–902.

[69] D. Streich, Y. Stuti, M. Orlandi, L. Schwartz, R. Lomoth, L. Hammarstrcm and S. Ott, Chem.–Eur. J. 16 (2010) 60–63.

[70] B. Kumar, M. Beyler, C. P. Kubiak and S. Ott, Chem.–Eur. J. 18 (2012) 1295–1298.

[71] Y. Kobayashi, B. Jacobs, M. D. Allendorf, J. R. Long, Chem. Mater. 22 (2010) 4120.

[72] S. Takaishi, M. Hosoda, T. Kajiwara, H. Miyasaka, M. Yamashita, Y. Nakanishi, Y. Kitagawa, K.Yamaguchi, A. Kobayashi, H. Kitagawa, Inorg. Chem. 48 (2009) 9048.

[73] R. Bolligarla and S. K. Das*, CrystEngComm 12 (2010) 3409–3412.

[74] R. Bolligarla, B. Tripuramallu, V. Sreenivasulu and S. K. Das*, Indian J. Chem. A 50 (2011) 1410-1417.

[75] L. Testaferri, M. Tiecco, M. Tingoli, D. Chianelli and M. Montanucci, Synthesis, (1983) 751.

[76] F. Maiolo, L. Testaferri, M. Tiecco and M. Tingoli, J. Org. Chem. 46 (1981) 3070.

[77] W. W. Seidel and F. E. Hahn, J. Chem. Soc., Dalton Trans. (1999) 2237.

[78] F. E. Hahn and W. W. Seidel, Angew. Chem., Int. Ed. 34 (1995) 2700.

[79] H. Alves, D. Simão, I. C. Santos, V. Gama, R. T. Henriques, H. Novais and M. Almeida, Eur. J. Inorg. Chem. (2004) 1318.

[80] H. V. Huynh, C. Schulze Isfort, W. W. Seidel, T. Lügger, R. Fröhlich, O. Kataeva and F. E. Hahn, Chem. –Eur. J. 8 (2002) 1327.

[81] D. Sellmann, K. P. Peters, R. M. Molina and F. W. Heinemann, Eur. J. Inorg. Chem. (2003) 903.

[82] T. Kreickmann, C. Diedrich, T. Pape, H. V. Huynh, S. Grimme and F. E. Hahn, J. Am. Chem. Soc. 128 (2006) 11808.

[83] F. E. Hahn, T. Kreickmann and T. Pape, Dalton Trans. (2006) 769.

[84] D. L. Kepert, Inorganic Stereochemistry: Inorganic Chemistry Concept 6, Springer Verlag, Berlin, (1982).

[85] Directional ligands with different donor groups: (a) C. Piguet, G. Hopfgartner, A. F. Williams and J.-C. Bünzli, J. Chem. Soc., Chem. Commun. (1995) 491.

[86] M. Albrecht and R. Fröhlich, J. Am. Chem. Soc. 119 (1997) 1656.

[87] Directional ligands with an unsymmetric bridge between the donor groups: (a) M. Albrecht, M. Napp, M. Schneider, P. Weis and R. Fröhlich, Chem. –Eur. J. 7 (2001) 3966.

[88] M. J. Hannon, S. Bunce, A. J. Clarke and N. W. Alcock, Angew. Chem., Int. Ed. 38 (1999) 1277.

[89] M. Albrecht, Chem. Soc. Rev. 27 (1998) 281.

[90] M. Albrecht, I. Janser and R. Fröhlich, Chem. Commun. (2005) 157.

[91] C. Schulze Isfort, T. Kreickmann, T. Pape, R. Fröhlich and F. E. Hahn, Chem. –Eur. J. 13 (2007) 2344.

[92] F. E. Hahn, C. Schulze Isfort and T. Pape, Angew. Chem., Int. Ed. 43 (2004) 4807.

[93] N. C. Schiødt, P. Sommer-Larsen, T. Bjørnholm, M. F. Nielsen, J. Larsen, K. Bechgaard, Inorg. Chem. 34 (1995) 3688.

[94] J. E. Huyyett, S. B. Choudhury, D. M. Eichhorn, P. A. Bryngelson, M. J. Maroney, B. M. Hoffman, Inorg. Chem. 37 (1998) 1361.

[95] M. C. Aragoni, M. Arca, F. Demartin, F. A. Devillanova, A. Garau, F. Isaia, F. Lelj, V. Lippolis, G. Verani, J. Am. Chem. Soc. 121 (1999) 7098.

[96] K. Wang, E. I. Stiefel, Science 291 (2001) 106.

[97] D. J. Harrison, N. Nguyen, A. J. Lough, U. Fekl, J. Am. Chem. Soc. 128 (2006) 11026.

[98] A. T. Coomber, D. Beljonne, R. H. Friend, J. L. Brédas, A. Charlton, N. Robertson, A. E. Underhill, M. Kurmoo, P. Day, Nature 380 (1996) 144.

[99] X. M. Ren, S. Nishihara, T. Akutagawa, S. Noro, T. Nakamura, Inorg. Chem. 45 (2006) 2229.

[100] N. Robertson, L. Cronin, Coord. Chem. Rev. 227 (2002) 93.

[101] R. Kato, Chem. Rev. 104 (2004) 5319.

[102] C. –T. Chen, S. –Y. Liao, K. –J. Lin, L. –L. Lai, Adv. Mater. 3 (1998) 334.

[103] V. Gama, R.T. Henriques, M. Almeida, L. Veiros, M. J. Calhorda, A. Meetsma, J. L. de Boer, Inorg. Chem. 32 (1993) 3705.

[104] V. Gama, R.T. Henriques, G. Bonfait, M. Almeida, A. Meetsma, S. Van Smaalen, J. L. de Boer, J. Am. Chem. Soc. 114 (1992) 1986.

[105] G. Bähr, G. Schleitzer, Chem. Ber. 90 (1957) 438.

[106] C. G. Krespan, B. C. Mckusick, T. L. Carirns, J. Am. Chem. Soc. 82 (1960) 1515.

[107] W. Schroth, Peschel, J. Chimia. 18 (1964) 171.

[108] G. N. Rosa Schrauzer, J. Phys. Chem. 73 (1969) 3132.

[109] A. E. Underhill, M. M. Ahmad, J. Chem. Soc., Chem. Commun. (1981) 67.

[110] A. Kobayashi, Y. Sasaki, H. Kobayashi, A. E. Underhill, M. M. Ahmad, J. Chem. Soc., Chem. Commun. (1982) 390.

[111] L. Brossard, M. Ribault, M. Bousseau, L. Valade, P. C. Cassoux, R. Acad. Sci., Ser. II 302 (1986) 205.

[112] A. Kobayashi, H. Kim, Y. Sasaki, R. Kato, H. Kobayashi, S. Moriyama, Y. Nishio, K. Kajita, W. Sasaki, Chem. Lett. (1987) 1819.

[113] H. Tajima, M. Inokuchi, A. Kobayashi, T. Ohta, R. Kato, H. Kobayashi, H. Kuroda, Chem. Lett. (1993) 1235.

[114] L. Brossard, H. Hurdequint, M. Ribault, L. Valade, L.-P. Legros, P. Cassoux, Synth. Met. 27 (1988) B157.

[115] L. Brossard, M. Ribault, L. Valade, P. Cassoux, J. Phys. (Paris) 50 (1989) 1521.

[116] A. Kobayashi, H. Kobayashi, A. Miyamoto, R. Kato, R. A. Clark, A. E. Underhill, Chem. Lett. (1991) 2163.

[117] H. Kobayashi, K. Bun, T. Naito, R. Kato, A. Kobayashi, Chem.Lett. (1992) 1909.

[118] R. Kato, Y. Kashimura, S. Aonuma, N. Hanasaki, H. Tajima, Solid State Commun. 105 (1998) 561.

[119] W. König, J. Prakt. Chem. 112 (1925) 1.

[120] W. Ismailsky, Dissertation, Univessität Dresden, (1913).

[121] W. Dilthey, R. Wizinger, J. Prakt. Chem. 118 (1928) 321.

[122] R. Wizinger, Chimia 15 (1961) 89.

[123] J. Griffiths, Colors and Constitution of Organic Molecules, Academic press, London, (1976) ISBN, 0–12–303550–3, LCCC 76–016971.

[124] M. J. S. Dewar, R. C. Dougherty, *The PMO Theory of Organic Compounds*, Akademie Verlag, Berlin, (1977) (Abh. Akad. Wiss. DDR Nr.8).

[125] H. Auler, G. Z. Banzer, Krebsforch. 53 (1942) 65.

[126] G. N. Schrauzer, V. P. Mayweb, J. Am. Chem. Soc. 87 (1965) 1483.

[127] G. N. Schrauzer, Acc. Chem. Res. 2 (1969) 72.

[128] Z. S. Herman, R. F. Kirchner, G. H. Loew, U. T. Mueller-Westerhoff, A. Nazzal, M. C. Zerner, Inorg. Chem. 21 (1982) 46.

[129] F. Lelj, A. Rosa, G. P. Ricciardi, M. Caserin, P. L. Christinziano, G. Morelli, Chem. Phys. Lett. 160 (1989) 39.

[130] U. T. Mueller-Westerhoff, B. Vance, D. I. Yoon, Tetrahedron 47 (1991) 909.

[131] U. T. Mueller-Westerhoff, B. Vance, D. I. Yoon, Coordination. Chem. Rev. 22 (1987) 595.

[132] U. T. Mueller-Westerhoff, D. I. Yoon, K. Plourde, Mol. Cryst. Liq. Cryst. 183 (1990) 291.

[133] S. B. Wikes, I. R. Butler, A. E. Underhill, M. B. Hursthouse, D. E. Hibbs, K. M. Abdul Malik, J. Chem. Soc., Dalton Trans. (1995) 897.

[134] F. Wang, Y. J. Qiu, J. R. Reynolds, Macromolecules 24 (1991) 4567.

[135] I. Tabushi, K. Yamamura, H. Nonoguchi, Chem. Lett. (1999) 1373.

[136] H. J. Lee, D. Y. Noh, Polyhedron 19 (2000) 425.

[137] F. Bigoli, P. Deplano, F. A. Devillanova, V. Lippolis, P. J. Lukes, M. L. Mercuri, M. A. Pellinghelli, E. F. Trogu, J. Chem. Soc., Chem. Commun. (1995) 371.

[138] H. Nakazumi, J. Soc. Dyers Color. 104 (1988) 121.

[139] H. Shiozaki, H. Nakazumi, T. Kitao, J. Soc. Dyers Color. 104 (1988) 173.

[140] N. J. Kuramoto, J. Soc. Dyers Color. 106 (1990) 181.

[141] K. Namba, Jpn. Kokai Tokkyo Koho JP 60 73891, 1985, Eur. Pat. Appl. EP 147083.

[142] J.-M. Lehn, Supramolecular Chemistry: Concepts and Perspectives, VCH: Weinheim, (1995).

[143] J. W. Steed, J. L. Atwood, Supramolecular Chemistry, John Wiley: Chichester, 2000.

[144] N. S. Nalwa, Appl. Organomet. Chem. 5 (1991) 349.

[145] Y. S. J. Veldhuizen, J. G. Hassnoot, J. Reedijk, Synth. Met. 86 (1997) 1827.

[146] J. Zhai, C. H. Huang, T. X. Wei, L. B. Gan, H. Cao, Polyhedron 18 (1999) 1513.

[147] D. Zhou, G. J. Ashwell, C. Huang, Chem. Lett. (1997) 7.

[148] C.-T. Chen, S. Y. Liao, K. J. Lin, T. Y. J. Lin, L. L. Lia, C. H. Chen, Nonlinear Optics, 22 (1999) 35.

[149] C.-T. Chen, S. Y. Liao, K. J. Lin, C. H. Chen, J. T. Y. Lin, Inorg. Chem. 38 (1999) 2734.

[150] K. Base, M. T. Tiernry, A. Fort, J. Muller, M. W. Grinstaff, Inorg. Chem. 38 (1999) 287.

[151] Special and Issue Chem. Rev. 94 (1994) 1.

[152] J.-F. Bai, J.-L. Zuo, W.-L. Tan, W.; Ji, Z. Shen, H.-K. Fun,; K.; Chinnakali, I. A. Razak, X.-Z. You,; C.-M. Che, J. Mater. Chem. 9 (1999) 2419.

[153] C. L. Yang, J. G. Qin, J. H. Si, Y. G. Wang, P. X. Ye, Y. L. Li, Synth. Met. 102 (1999) 1578.

[154] J. Si, Q. Yang, Q. X. Wang, P. Ye, S. Wang, J. Qin, D. Liu, Opt. Commun. 132 (1996) 311.

[155] S. D. Cummings, R. Eisenberg, Inorg. Chem. 34 (1995) 2007–2014.

[156] S. D. Cummings, R. Eisenberg, Inorg. Chem. 34 (1995) 3396–3403.

# Synthesis, structural characterization and electrochemical studies of $[Fe_2(\mu\text{-}L)(CO)_6]$ and $[Fe_2(\mu\text{-}L)(CO)_5(PPh_3)]$ (L = pyrazine-2,3-dithiolate, quinoxaline-2,3-dithiolate and pyrido[2,3-*b*]pyrazine-2,3-dithiolate): Towards modeling the active site of [FeFe]–Hydrogenase

2 Chapter

**Abstract:-** The reaction of heterocyclic 1,2-ene-dithiol ligands, namely, pyrazine-2,3-dithiol ($H_2$pydt), quinoxaline-2,3-dithiol ($H_2$qdt) and pyrido[2,3-*b*]pyrazine-2,3-dithiol ($H_2$ppdt) with $Fe_2(CO)_9$ yields the '[FeFe]–hydrogenase' model complexes $[Fe_2\{\mu\text{-pydt}\}(CO)_6]$ **(1)**, $[Fe_2\{\mu\text{-qdt}\}(CO)_6]$ **(2)** and $[Fe_2\{\mu\text{-ppdt}\}(CO)_6]$ **(3),** respectively. A further reaction of complexes **1**, **2** and **3** with $PPh_3$ in the presence of equimolar amount of decarbonylating agent $Me_3NO$ in $CH_3CN$ at room temperature resulted in the formation of unsymmetrical mono-$PPh_3$-substituted model complexes $[Fe_2\{\mu\text{-pydt}\}(CO)_5PPh_3]$ **(4)**, $[Fe_2\{\mu\text{-qdt}\}(CO)_5PPh_3]$ **(5)** and $[Fe_2\{\mu\text{-ppdt}\}(CO)_5PPh_3]$ **(6),** respectively. The complexes **1**–**6** were well characterized by routine elemental analysis, IR, $^1$H NMR, $^{13}$C NMR spectroscopy and unambiguously characterized by X–ray crystallographic analysis. IR spectroscopy and electrochemical analysis show that an increase of the electron– withdrawing character of the bridging ligands (where electron–withdrawing character is in the order of $pydt^{2-} > ppdt^{2-} \geq qdt^{2-}$) leads to a decreased electron density at the iron centers, which yield a milder reduction potential and higher CO stretching frequencies. All the compounds **1–6** are further characterized by electrochemical studies.

## 2.1. Introduction

Recent research has significantly advanced our understanding the nature's most efficient catalysts for hydrogen production, the [FeFe]-hydrogenases (Fig. 2.1) [1–3]. [FeFe]–hydrogenase ([FeFe]$H_2$ase), that catalyses the reductive generation of hydrogen (shown in eq. 1), has attracted intensive attention because the molecular hydrogen ($H_2$) is a clean and a highly efficient fuel [4–13].

$$2H^+ + 2e^- \xrightleftharpoons{\text{Hydrogenase enzymes}} H_2 \qquad (1)$$

The high resolution X-ray crystallographic structures have established that [FeFe]$H_2$ase, isolated from *Desulfovibrio desulfuricans* and *Clostridium pasteurianum,* features a butterfly 2Fe2S subunit as their active site (also called H–cluster) as shown in Fig. 2.1 [14–19]. In the active site, the iron centers are coordinated by carbon monoxide, cyanide ligands and by a dithiolate bridging ligand between the two iron centers; one of the iron centers ($Fe_p$) is coordinated by a cysteinyl–linked $Fe_4S_4$ cluster (Fig. 2.1). The well-defined/established structure of active site (H–cluster) and its remarkable hydrogen–producing ability provoked chemists to design and synthesize a range of model compounds. Several review articles, on the topic of [FeFe]–hydrogenase model complexes and their catalytic activity, have been published [20–24].

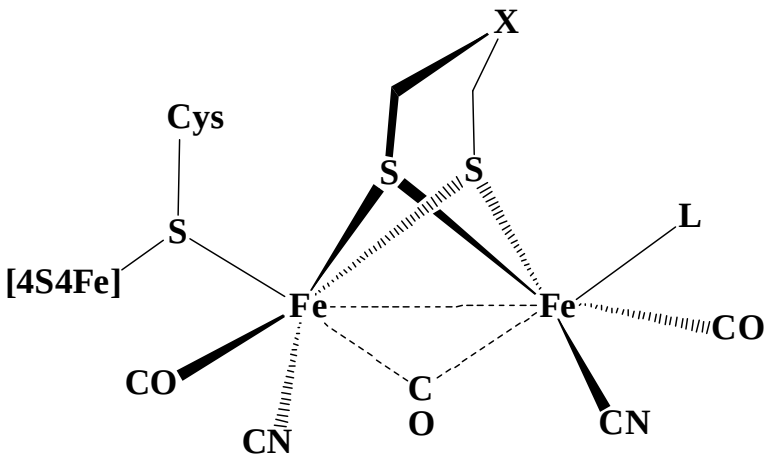


L = $H_2O$, H or Vacant X= C, N, O or S.

**Fig. 2.1**. The active site of [FeFe]–hydrogenase.

Numerous model diiron complexes, that are analogous to the active site of the iron only enzyme, have been shown as **A**–**F** representations in Scheme 2.1. Rauchfuss and co-workers reported the electrocatalytic reduction of strong acids like $H_2SO_4$, HCl etc. using a derivative of **A** (one CO of one iron is replaced by $PMe_3$ and one CO of other iron is replaced by $CN^-$) [25–28]. It was shown by Darensbourg and co–workers that **A** can electrocatalyze the di-hydrogen production from acetic acid (a weak acid) [29–32]. Borg *et al.* described detailed electrochemistry and spectroelectrochemical investigation on compound **A** in the context of number of electrons involved in the initial reduction of **A** [33–35]. Song and co-workers demonstrated ADT type model complex **B [**36, 37] and also have described that the model compound **C** catalyzes the reduction of $Et_3NHCl$ [38]. Ott, Sun, Akermark and their groups described the syntheses and characterizations of nitro-

and amino-functionalized diiron azadithiolate complexes (**B** in Scheme 1) and they have shown the electrocatalytic formation of hydrogen from acetic acid and $HClO_4$ proposing a CECE (chemical electrochemical chemical electrochemical) mechanism [39–41]. Electrocatalytic dihydrogen production has been demonstrated using systems **D** and **E** (Scheme 2.1) as the electrocatalysts [42].

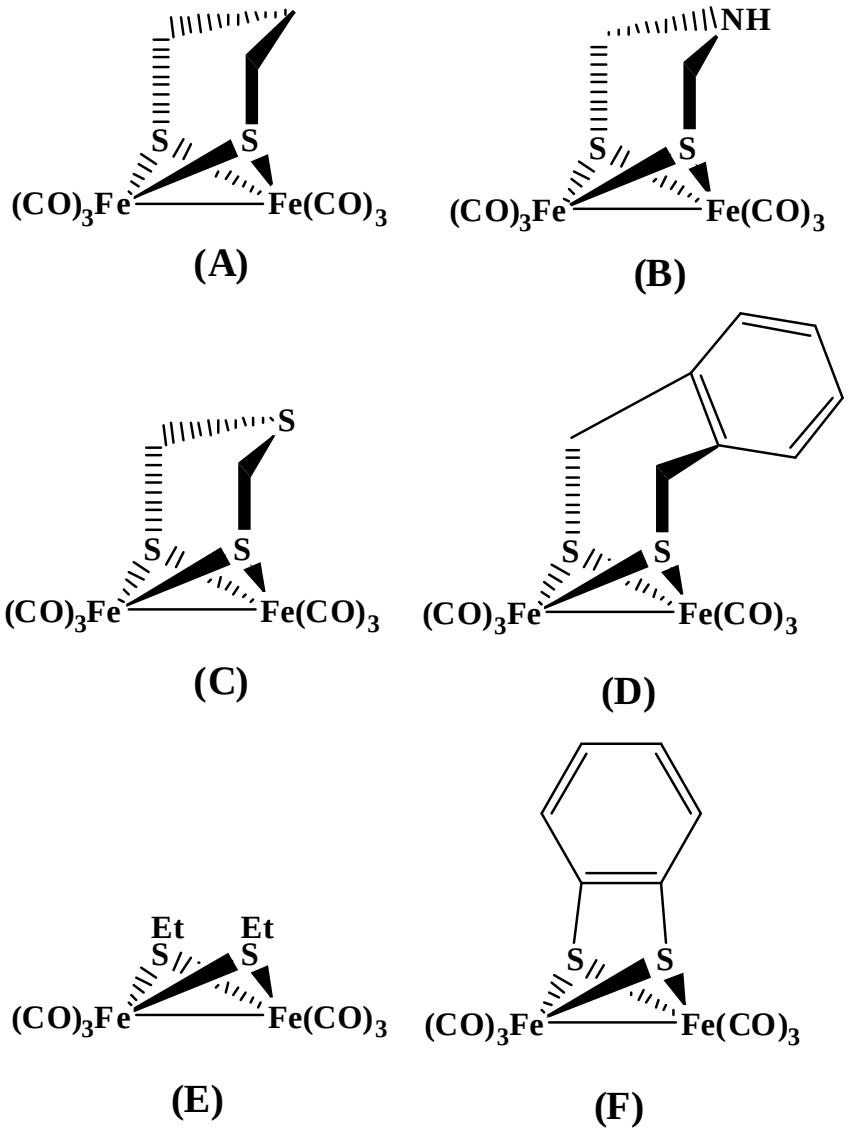


**Scheme 2.1.** [FeFe]–hydrogenase active site model complexes.

Capon and co-workers first reported the compound **F** as [FeFe]-hydrogenase active site model [43] and it has been further used by Lichtenberger, Evans, Glass and their co-workers to demonstrate electro catalytic hydrogen generation from weak acids [44,45].

They have described a novel mechanism deduced from both electrochemical and theoretical studies on compound **F**. For the system **F**, the ene-1,2-dithiolate ($bdt^{2-}$) ligand coordination is able to modulate the potentials between oxidation states drastically in favor of electrochemical proton reduction [46]. Likewise, the coordination of the $bdt^{2-}$ ligand to the $\{Fe_2S_2\}$ core has a special ability to facilitate the electrocatalytic hydrogen production by lowering the potential difference between successive metal oxidation states in the catalytic cycle [43,44,46]. This has been explained by an interaction of the iron orbitals with a combination of the filled sulfur $p_\pi$ orbitals and the arene $p_\pi$ orbitals, which act to shield the change in electron density at the iron center as the oxidation state is changed, thus minimizing the changes in electron energies upon reduction. It is worth mentioning that the ene-1,2-dithiolate type ligand has been known to serve as an effective electron transfer pathway. Moreover, '*Nature*' uses this type of ligand in the active sites of Mo/W metalloenzymes that catalyze range oxidation/reduction reactions with a variety of substrates (for example, sulfite, xanthine, trimethylamine etc.) [47–52]. It is obvious from the above discussion that the coordination of "ene-1,2-dithiolate" type of ligand (Scheme 2.2) with $\{Fe_2S_2\}$ core should afford potential model systems for the active sites of [FeFe]$H_2$ases as far as structural analogies are concerned. We wish to report herein the synthesis, detailed characterization and electrochemical reduction properties of a series of heterocyclic ene-1,2-dithiolate ligands (see in Scheme 2.3) based diiron complexes $[Fe_2\{\mu\text{-pydt}\}(CO)_6]$ ($pydt^{2-}$ = pyrazine-2,3-dithiolate) (**1**), $[Fe_2\{\mu\text{-qdt}\}(CO)_6]$ ($qdt^{2-}$ = quinoxaline-2,3-dithiolate) (**2**), $[Fe_2\{\mu\text{-ppdt}\}(CO)_6]$ ($ppdt^{2-}$ = pyrido[2,3-*b*]pyrazine-2,3-dithiolate) (**3**) and their triphenylphosphine derivatives $[(CO)_3Fe\{\mu\text{-pydt}\}Fe(CO)_2(PPh_3)]$ (**4**), $[(CO)_3Fe\{\mu\text{-qdt}\}Fe(CO)_2(PPh_3)]$ (**5**) and $[(CO)_3Fe\{\mu\text{-ppdt}\}Fe(CO)_2(PPh_3)]$ (**6**). Out of these, Sascha Ott and co-workers have already reported qdt-complex **2** in terms of synthesis and electrochemistry [53]. Here we have described the crystal structure of this compound for comparative studies.

The novelty of the present work lies in the fact that the present system offers relatively low reduction potentials, which is important in terms of proton reduction. In particular, compound **1** exhibits reduction potential at –1.08 V *vs* $Fe^{+/0}$, the lowest reduction potential as far as "ene-1,2-dithiolate" associated model systems are concerned.

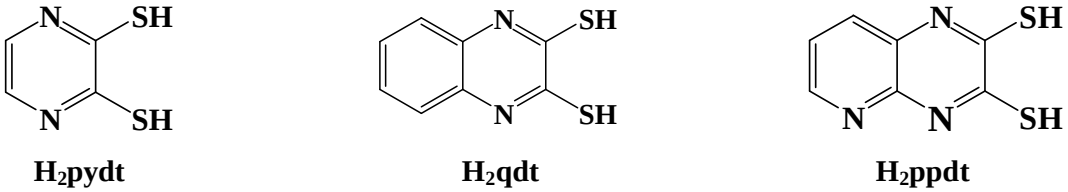


**Scheme 2.2.** *N*–heterocyclic 1,2-dithiolene ligands.

## 2.2. Results and Discussion

*2.2.1. Synthesis and spectroscopic characterization of model complexes **1–6***

Based on aforementioned considerations, we have synthesized and structurally characterized three relevant $\{Fe^{I}Fe^{I}\}$ carbonyl complexes bridging with 1,2-ethylene dithiolate ligands. As shown in Scheme 2.3, the treatment of heterocyclic 1,2-ethylene dithiolene ligands $H_2$pydt, $H_2$qdt and $H_2$ppdt with $Fe_2(CO)_9$ in THF at −10 °C to 20 °C, afford the complexes **1**, **2** and **3** respectively. Further treatment of complexes **1**, **2** and **3** in presence of equimolar amount of decarbonylating agent $Me_3NO$ with $Ph_3P$ in $CH_3CN$ at room temperature produced the unsymmetrical sole mono $Ph_3P$-substituted model complexes **4**, **5** and **6** respectively, in moderate yields [54, 55].

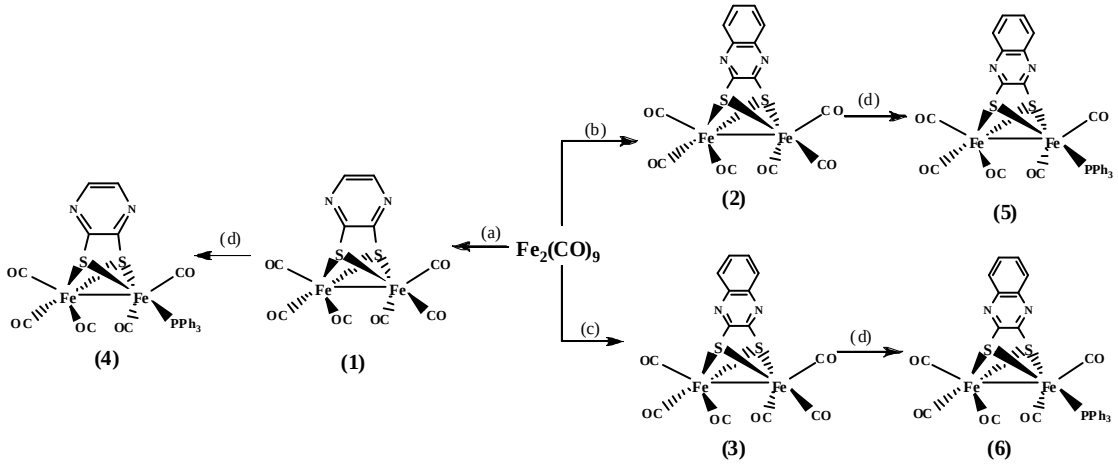


**Scheme 2.3.** (a) $H_2$pydt, THF, −10 °C to 20 °C, 1.5 h (b) $H_2$qdt, THF, reflux, 0.5 h (c) $H_2$ppdt, THF, −10 °C to 20 °C, 2 h (d) (i) $CH_3CN$, $Me_3NO$, 15 min. (ii) $PPh_3$, 0.5 h.

The complexes **1**–**6** were purified by column chromatography and characterized by IR, $^{1}$H NMR, $^{13}$C NMR spectroscopy and satisfactory elemental analysis. The APCI positive mode LC–MS spectra show the parent ion peak $[M + H]^{+}$ values at *m/z*: 422.85,

472.85 and 474.35 for compounds **1**, **2** and **3,** respectively. The IR spectra of complexes **1**, **2** and **3** in KBr exhibit strong absorption band frequencies in the region of 1950–2100 $cm^{-1}$, corresponding to the terminally coordinated carbonyl (CO) groups. The differences between aromatically bridged complexes (for example, with bdt ligand, representation **F**, Scheme 2.1) and aliphatically bridged complexes (such as pdt, propane 1,3-dithiol, representation **A**, Scheme 2.2) are remarkable [56,57]. The comparison between the IR spectra of these two complexes / systems (**F** and **A**, in Scheme 2.1) has been rationalized by a sizable delocalization of the electron density into the aromatic dithiolate ligands (in system **F** in Scheme 2.1), that makes the lower electron density at the iron centers resulting in less back bonding into the π*–orbital of the CO ligands which leads to a shift of the CO stretching frequencies towards the higher energy than those in aliphatic dithiolate ligand analogues (for example, system **A**, Scheme 2.1). Table 2.1 compares this situation. In the present system the bridging sulfur donating ligands are not only aromatic, but they are also heterocyclic containing ring nitrogen atom. This further lowers the electron density at the iron centers and for this reason, the CO frequencies in the IR spectra of the present system are shifted to even more higher energy (5 $cm^{-1}$ more compared to those reported for complex $[Fe_2\{\mu\text{-bdt}\}(CO)_6]$, ($bdt^{2-}$ = benzene 1,2-dithiolate) [58] and 10 $cm^{-1}$ compared to those in $[Fe_2\{\mu\text{-pdt}\}(CO)_6]$ [59]). The relevant comparison is shown in Table 2.1.

The more electron-withdrawing character of bridging ligand will decrease the electron density at the diiron core and thus make the iron centers more electrophilic. As a consequence, ligand substitutions with strong σ–donating ligands, such as $PPh_3$ will be facilitated. Because of the incorporation of the electron–donating $PPh_3$ ligand into butterfly $Fe_2S_2$ moiety, the IR spectra of complexes **4**, **5** and **6** shifted by approximately $\nu_{CO}$ = 30–50 $cm^{-1}$ towards the low-energy region compared to their respective hexacarbonyl analogues, suggesting that $PPh_3$ increases the electron density to the Fe(I)Fe(I) centers [59, 60]. Table 2.1 shows a comparison of the terminal CO bands in the IR spectra of complexes **1**–**6** and the related diiron benzene dithiolate complex $[Fe_2\{\mu\text{-bdt}\}(CO)_6]$, $[Fe_2\{\mu\text{-pdt}\}(CO)_6]$ and their analogues.

**Table 2.1.** A comparison of CO bands of analogous diiron heterocyclic 1,2–dithiolene complexes with diiron benzene dithiolene complex.

| Complex | CO bands/$cm^{-1}$ | Reference |
|---|---|---|
| $[Fe_2\{\mu\text{-pydt}\}(CO)_6]$ | 2084(s),2040(s), 2014(m), 1993(m) | present work |
| $[Fe_2\{\mu\text{-qdt}\}(CO)_6]$ | 2082(s), 2041(s), 2004(s), 1981(s) | present work |
| $[Fe_2\{\mu\text{-ppdt}\}(CO)_6]$ | 2083(s), 2047(m), 2029(s), 2004(m), 1981(s) | present work |
| $[Fe_2\{\mu\text{-pydt}\}(CO)_5]$ $pph_3$ | 2054(s), 2013(s), 1977(s), 1940(m) | present work |
| $[Fe_2\{\mu\text{-qdt}\}(CO)_5]$ $pph_3$ | 2050(s), 1988(s), 1940(s) | present work |
| $[Fe_2\{\mu\text{-ppdt}\}(CO)_5]$ $pph_3$ | 2050(vs), 1986(m), 1944(w) | present work |
| $[Fe_2\{\mu\text{-bdt}\}(CO)_6]$ | 2079(m), 2044(s), 2006(vs),1967(vw),1958(vw) | reference [58] |
| $[Fe_2\{\mu\text{-pdt}\}(CO)_6]$ | 2074 (m), 2036(s), 1995(s) | reference [59] |
| $[Fe_2\{\mu\text{-pdt}\}(CO)_5]$ $pph_3$ | 2044(s), 1984(s), 1931(m) | reference [59] |

$^1$H NMR spectrum of compound **1** displayed a singlet at $\delta$ 7.55 ppm for their pyrazine ring protons and three peaks for aromatic dithiolene ring appears in the range of $\delta$ 7.5–9.0 ppm, for compound **3**. For compounds **1** and **3,** $^{13}C\{^1H\}$ NMR spectra exhibited signals approximately in the range of $\delta$ 120–170 ppm for their aromatic carbons; these compounds give only one signal at around $\delta$ 206 ppm for their terminal carbonyls. Compounds **4**–**6** display two peaks for terminal carbonyl carbon atoms in $^{13}C\{^1H\}$ NMR spectra. $^{31}$P NMR spectra for complexes **4**–**6** show a peak in the region of $\delta$ 59.0–60.0 ppm.

*2.2.2. Description of crystal structures of complexes **1–6***

The molecular structures of complexes **1–3** and **4–6** were further confirmed by X-ray crystallography and thermal ellipsoidal plots are shown in Figs. 2.2 and 2.3, respectively. The crystallographic parameters, data collection and structure refinement of the compounds **1–3** and **4–6** are summarized in Tables 2.2 and 2.3, respectively. Selected bond lengths and angles for compounds **1–3** and **4–6** are listed in Tables 2.4 and 2.5, respectively. Wine-red colored crystals of complexes $[Fe_2\{\mu\text{-pydt}\}(CO)_6]$ (**1**) and $[Fe_2\{\mu\text{-ppdt}\}(CO)_6]$ (**3**), suitable for X–ray structure analysis, could be grown from the slow evaporation of the $MeOH/CH_2Cl_2$ solution at room temperature. On the other hand, the wine-red colored crystals of complex $[Fe_2\{\mu\text{-qdt}\}(CO)_6]$ (**2**), were grown by cooling $CH_2Cl_2$ solution at −10 °C.

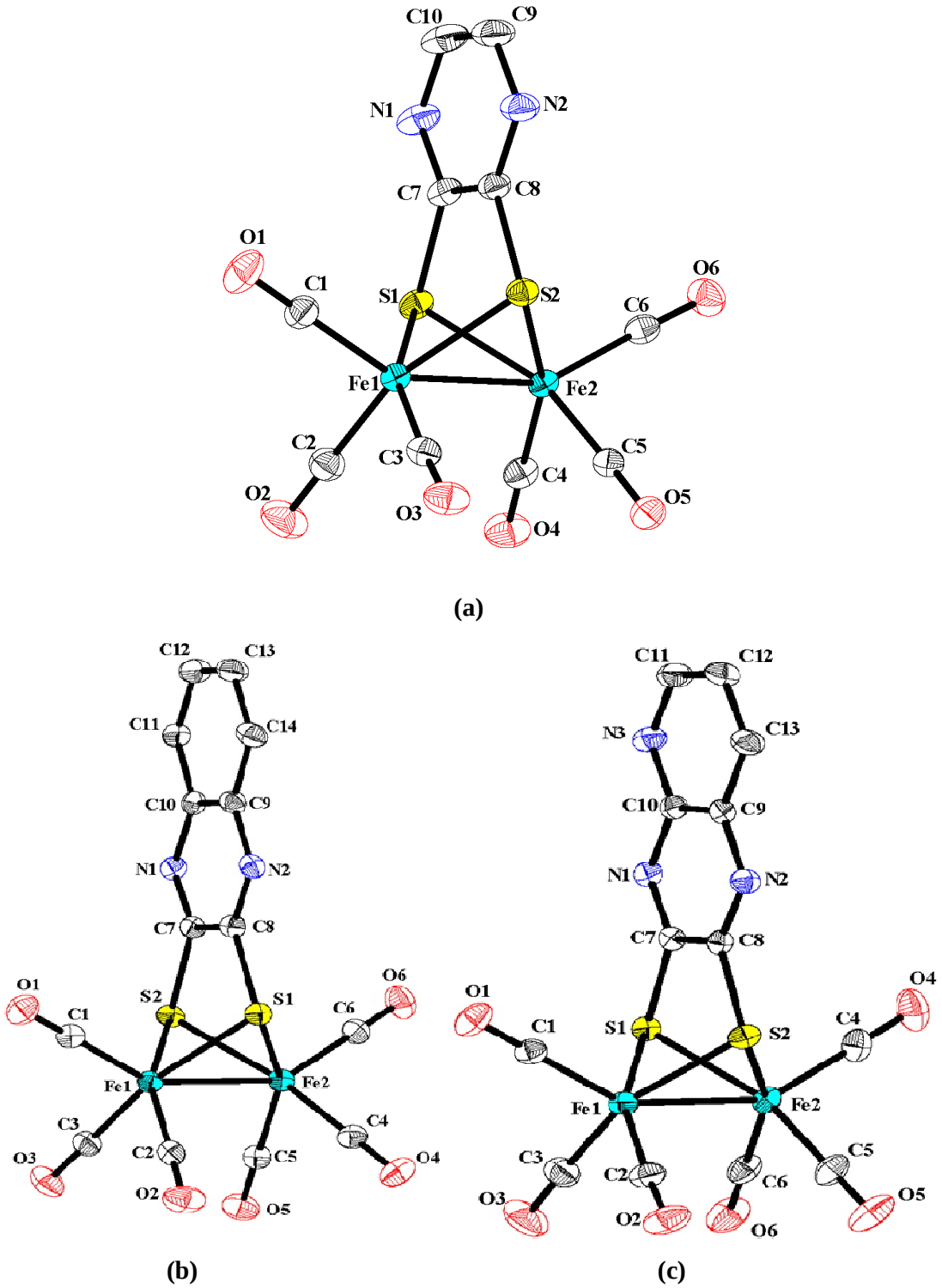


**Fig. 2.2.** Molecular structures of (a) compound **1**, (b) compound **2** and (c) compound **3** with thermal ellipsoids at 20% probability (Hydrogen atoms are omitted for clarity).

**Table 2.2.** Crystal data and structural refinement for complexes **1**–**3**.

| | **1** | **2** | **3** |
|---|---|---|---|
| Empirical formula | $C_{10}H_2Fe_2N_2O_6S_2$ | $C_{14}H_4Fe_2N_2O_6S_2$ | $C_{13}H_3Fe_2N_3O_6S_2$ |
| Formula weight | 421.96 | 472.01 | 473.0 |
| Temperature (K) | 298(2) | 298(2) | 298(2) |
| Crystal size (mm) | 0.50 x 0.42 x 0.38 | 0.40 x 0.22 x 0.12 | 0.24 x 0.18 x 0.04 |
| Crystal system | Monoclinic | Monoclinic | Monoclinic |
| Space group | $P2_1/c$ | $Pc$ | $P2_1/n$ |
| Z | 4 | 4 | 4 |
| Wavelength (Å) | 0.71073 | 0.71073 | 0.71073 |
| *a* [Å] | 9.8010 (15) | 18.292(4) | 9.1118(18) |
| *b* [Å] | 8.9085(13) | 7.5417 (15) | 20.152(4) |
| *c* [Å] | 16.998(3) | 12.483(3) | 9.5954(19) |
| β [°] | 96.305(2) | 101.17(3) | 102.42 (3) |
| Volume [$Å^3$] | 1475.1(4) | 1689.5(6) | 1720.7(6) |
| Calculated density ($Mg/m^{-3}$) | 1.900 | 1.856 | 1.826 |
| Reflections collected/ unique | 13596/2608 | 15283/5923 | 16076/3030 |
| R(int) | 0.0209 | 0.0288 | 0.0249 |
| F(000) | 832 | 936 | 936 |
| Max. and min. transmission | 0.4784 and0.3957 | 0.7954 and0.5020 | 0.9256 and0.6500 |
| Θ range for data collection (°) | 2.09 to 25.00 | 1.13 to 24.99 | 2.02 to 25.00 |
| Refinement method | Full-matrix Least -squares on $F^2$ | Full-matrix Least -squares on $F^2$ | Full-matrix Least -squares on $F^2$ |
| Data / restraints /parameters | 2608 / 0 / 199 | 5923 / 2 / 469 | 3030 / 0 / 235 |
| Goodness-of-fit on $F^2$ | 1.076 | 1.032 | 1.060 |
| $R_1/wR_2$ [I>2sigma(I)] | 0.0240 / 0.0645 | 0.0351 / 0.0912 | 0.0290 / 0.0724 |
| $R_1/wR_2$ (all data) | 0.0260 /0.0657 | 0.0373 / 0.0967 | 0.0350 / 0.0753 |
| Largest diff. peak and hole [$e.Å^{-3}$] | 0.287 and-0.243 | 0.780 and-0.325 | 0.447 and -0.210 |

**Table 2.3.** Crystal data and structural refinement for complexes **4**–**6**.

| | **4** | **5** | **6** |
|---|---|---|---|
| Empirical formula | $C_{27}H_{17}Fe_2N_2O_5PS_2$ | $C_{31}H_{19}Fe_2N_2O_5PS_2$ | $C_{30}H_{18}Fe_2N_3O_5PS_2$ |
| Formula weight | 656.22 | 706.27 | 707.26 |
| Temperature (K) | 298(2) | 298(2) | 298(2) |
| Crystal size (mm) | 0.20 x 0.14 x 0.10 | 0.40 x 0.24 x 0.18 | 0.32 x 0.28 x 0.22 |
| Crystal system | Monoclinic | Monoclinic | Monoclinic |
| Space group | $P2_1/c$ | $P2_1/c$ | $P2_1/c$ |
| Z | 8 | 4 | 4 |
| Wavelength (Å) | 0.71073 | 0.71073 | 0.71073 |
| *a* [Å] | 16.953(2) | 12.436(4) | 12.458(7) |
| *b* [Å] | 18.620(3) | 11.300(4) | 11.325(7) |
| *c* [Å] | 24.317(2) | 22.084(7) | 22.033(13) |
| β [°] | 132.899(5) | 100.824(5) | 100.640 (9) |
| Volume [$Å^3$] | 5623.1(12) | 3048.3(16) | 3055(3) |
| Calculated density ($Mg/m^{-3}$) | 1.550 | 1.539 | 1.538 |
| Reflections collected/ unique | 57706 / 11024 | 28550/5368 | 26043/5168 |
| R(int) | 0.0404 | 0.0394 | 0.0470 |
| F(000) | 2656 | 1432 | 1432 |
| Max. and min. transmission | 0.8829 and 0.7843 | 0.8151 and 0.6488 | 0.7809 and 0.7034 |
| Θ range for data collection (°) | 1.58 to 26.04 | 1.67 to 25.03 | 1.66 to 24.76 |
| Refinement method | Full-matrix least-squares on $F^2$ | Full-matrix least-squares on $F^2$ | Full-matrix least-squares on $F^2$ |
| Data / restraints /parameters | 11024 / 0 / 703 | 5368 / 0 / 388 | 5168 / 0 / 388 |
| Goodness-of-fit on $F^2$ | 1.124 | 1.103 | 1.009 |
| $R_1/wR_2$ [I>2sigma(I)] | 0.0534/ 0.1157 | 0.0435 / 0.0995 | 0.0335 / 0.0789 |
| $R_1/wR_2$ (all data) | 0.0651/ 0.1220 | 0.0525 /0.1044 | 0.0456 / 0.0834 |
| Largest diff. peak and hole [$e.Å^{-3}$] | 0.542 and -0.395 | 0.518 and -0.226 | 0.497 and -0.358 |

**Table 2.4.** Selected bond lengths [Å] and angles [°] for complexes **1**–**3**.

| | **1** | **2** | **3** |
|---|---|---|---|
| **Fe(1) −S(1)** | 2.2675(6) | 2.2696(13) | 2.2760(9) |
| **Fe(2) −Fe(1)** | 2.4677(5) | 2.4697(10) | 2.4795(7) |
| **O(1) −C(1)** | 1.120(3) | 1.116(6) | 1.115(3) |
| **C(7) −N(1)** | 1.318(3) | 1.295(6) | 1.296(3) |
| **S(1) −Fe(1) −Fe(2)** | 57.247(17) | 57.00(4) | 57.00(4) |
| **S(2) −Fe(1) −Fe(2)** | 57.214(17) | 57.15(4) | 57.15(4) |
| **Fe(1) −S(1) −Fe(2)** | 65.806(17) | 65.95(4) | 65.90(3) |

**Table 2.5**. Selected bond lengths [Å] and angles [°] for complexes **4**–**6**.

| | **4** | **5** | **6** |
|---|---|---|---|
| **Fe(1) −S(1)** | 2.2768(11) | 2.2737(11) | 2.2876(11) |
| **Fe(2) −Fe(1)** | 2.4822(7) | 2.4953(8) | 2.4973(11) |
| **O(1) −C(1)** | 1.132(5) | 1.126(4) | 1.136(3) |
| **C(4) −O(4)** | 1.134(4) | 1.137(4) | 1.143(3) |
| **Fe(2) −P(1)** | 2.2460(9) | 2.2572(10) | 2.2593(13) |
| **P(1) −Fe(2) −S(1)** | 105.04(4) | 106.34(4) | 106.35(4) |
| **S(1) −Fe(1) −Fe(2)** | 57.24(3) | 56.93(2) | 57.02(2) |
| **S(2) −Fe(1) −Fe(2)** | 57.37(3) | 57.54(3) | 57.42(4) |
| **Fe(1) −S(1) −Fe(2)** | 65.90(3) | 65.93(3) | 66.32(4) |

The crystal structure analyses show that the crystals of compounds **1**, **2** and **3** crystallize in monoclinic space groups $P2_1/c$, $Pc$ and $P2_1/n$, respectively. $Z' = 1$ for complexes **1** and **3** whereas $Z' = 2$ for complex **2**; bonding dimensions within the complexes are unexceptional as shown in Fig. 2.2. Single crystal X–ray diffraction analyses reveal that their molecular structures of complexes **1**, **2** and **3** are similar to the active site of [FeFe]–hydrogenase and the geometry around the iron centers has been found to be distorted square pyramidal, which is common in [FeFe]$H_2$ase model complexes. In the crystal

structures, two Fe atoms and two S atoms form a butterfly conformation as shown in thermal ellipsoid plots (Fig. 2.2). The two $Fe(CO)_3$ units are nearly eclipsed with Fe−Fe distance of 2.467(5) Å in **1**, 2.469(10) Å in **2** and 2.479(7) Å in **3**; these distances are relatively shorter than that found in *Desulfovibrio desulfuricans* [15] and *Clostridium pasteurianum* [14] (*ca*. 2.6 Å).

The displacement of CO group with triphenylphosphine, that coordinates to an apical site of Fe(2) of the complexes **1**, **2** and **3**, lengthens Fe−Fe bond distances in resulting unsymmetrical complexes **4**, **5** and **6** respectively due to the stronger σ–donor properties of $PPh_3$ ligand compared to carbonyl group, as shown in Table 2.4. Single crystals of compounds **4** and **5**, suitable for X–ray structure analysis, were grown by cooling the concentrated $CH_2Cl_2$ solution at −10 °C, whereas compound **6** was recrystallized by slow evaporation of the $CH_2Cl_2$/MeOH solution at room temperature. Accordingly, the C(1)–O(1) distances of 1.132(5) in **4**, 1.126(4) in **5** and 1.136(3) Å in **6** are shorter than the C(4)–O(4) distances of 1.134(4) in **4**, 1.137(4) in **5** and 1.143(3) Å in **6,** respectively (see Table 2.5)**.** The higher electron density of the Fe(2) centre leads to the stronger electron back-donation to π*-orbital of the C(4)–O(4) ligand as compared to the back-donation from the Fe(1) atom to π*-orbital of the C(1)–O(1) ligand. The crystal structure analyses show that the crystals of complex **4**, **5** and **6** crystallize in monoclinic space group $P2_1/c$, and the relevant thermal ellipsoidal plots are shown in Fig. 2.3. The $Z'$ is 2 for complex **4,** whereas $Z'$ is 1 for complexes **5** and **6.** Within each complex bonding dimensions are unexceptional.

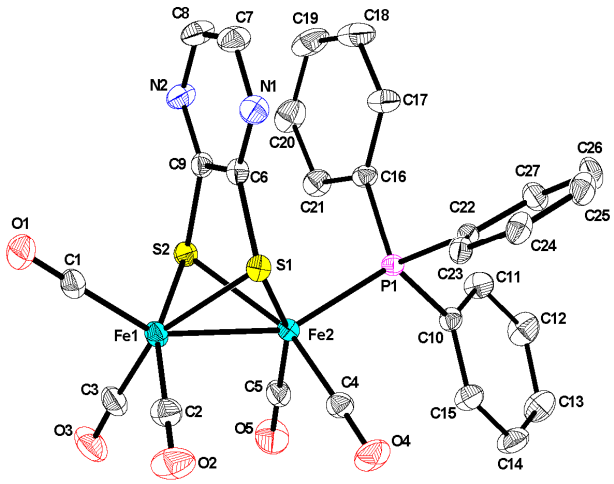


**(a)**

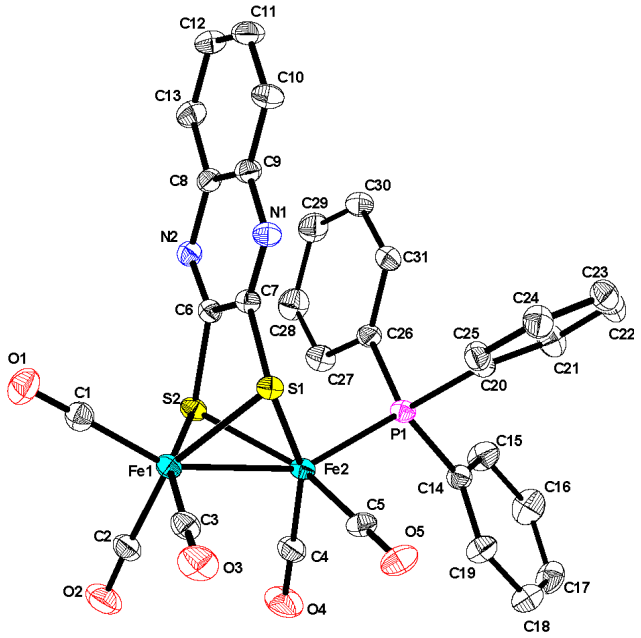


**(b)**

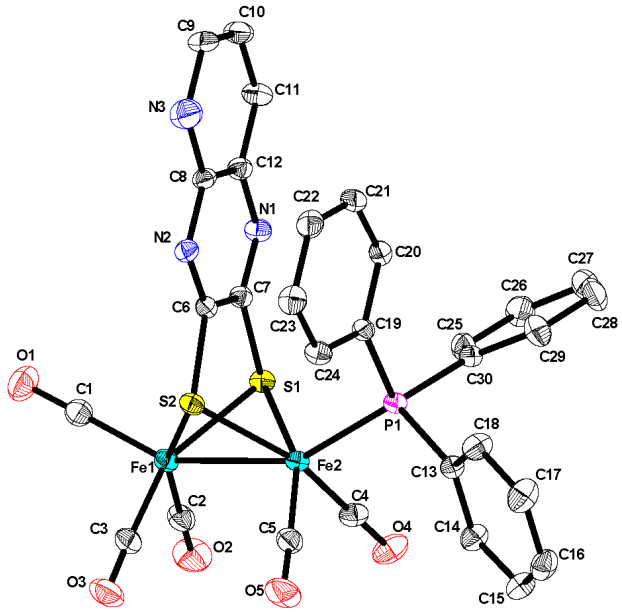


**(c)**

**Fig. 2.3.** Molecular structures of (a) compound **4**, (b) compound **5** and (c) compound **6** with thermal ellipsoids at 20% probability (Hydrogen atoms are omitted for clarity).

### *2.2.3. Electrochemistry of model complexes **1– 6***

The electrochemical behavior of **1–6** was investigated by cyclic voltammetry in $CH_3CN$ (with 0.1 M *n*-$Bu_4NClO_4$ as electrolyte, $v$ = 0.1 V/s) under argon atmosphere and the

electrochemical data were given in Table 5. The electrochemical reduction of compound **2** (qdt complex) has already been established as two-electron reduction process [53]. We have observed identical electro-chemical behavior for **2** as reported earlier. Based on established electrochemistry of compound **2** [53] and the fact that all arene-dithiolato-$Fe_2$-carbonyl complexes exhibit the fist reductive response of two electron process [20], we have assigned the reductive responses, exhibited by compounds **1** and **3**, as two-electron reduction. It is been observed that the present system is more easily reduced (Fig. 2.4 and Table 2.5) than the carbocyclic-arene complex (representation **F** in Scheme 2.1) in keeping with greater electronegativity of nitrogen (present system) compared to carbon (Compound **F**, Scheme 2.1). The cyclic voltammograms of complexes **1, 2** and **3** feature electrochemical responses at $E_{1/2}$ = –1.08 V, –1.22 V [53], –1.14 V (*vs.* $Fc^{+}/Fc^{0}$), respectively. The electrochemical behavior of the complex **F** (in Scheme 2.1) is already well-established and it shows that the first reduction potential of complex **F** is a two-electron process that occurs at $E_{1/2}$ = –1.27 V [44,53,46]. Thus, in comparison, the reduction potential of compound **1** (present work) is shifted towards more positive values by 190 mV, reflecting the strong electron-withdrawing character of the *N*–heterocyclic 1,2-ene dithiolates (Scheme 2.2) than benzene dithiolate ($bdt^{2-}$). As a consequence, the reductions of complexes **1**, **2** and **3** are thermodynamically more facile than that of complex **F** (Scheme 2.1) by 190, 50 and 130 mV, respectively (Table 2.6). When we compare the acidic property among heterocyclic dithiolene ligands $H_2$pydt, $H_2$qdt and $H_2$ppdt (Scheme 2.2), we found that the p$K_a$ value of pyrazine ($H_2$pydt) (0.67) [61] is less than that of quinoxaline ($H_2$qdt) (1.03) [62]. Therefore, pyrazine has more electron-withdrawing character than quinoxaline. Thus the reduction potential values of complexes **1** and **2** ($E_{1/2}$ = –1.08 V and $E_{1/2}$ = –1.22 V respectively) are consistent with their p$K_a$ values. In other words, the reduction potential value of compound **1** (with more electron–withdrawing ligation) is shifted to more positive side by 140 mV compared to the reduction potential value of compound **2** (with relatively less electron withdrawing ligand).

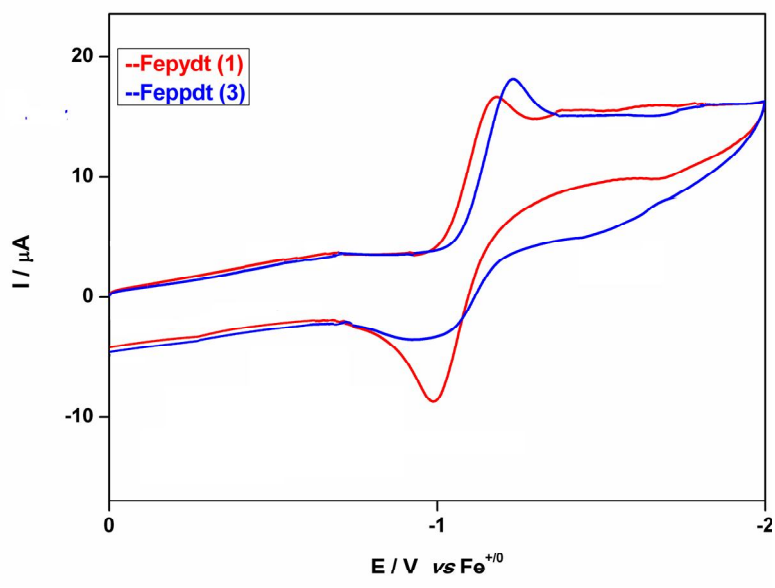


**Fig. 2.4.** Cyclic voltammograms of complexes **1** (red) and **3** (blue) (1.0 mM) in 0.1 M *n*-$Bu_4NClO_4$/MeCN at a scan rate of 100 $mVs^{-1}$. Potentials are *vs.* $Fc^{+/0}$.

The cyclic voltammogram of complex **3** displays the reduction potential value at $E_{1/2}$ = –1.14 V showing the potential shift to more negative value by 60 mV compared to that of complex **1**. Thus, based on electrochemical analyses, pyrido[2,3-*b*]pyrazine dithiolate ($ppdt^{2-}$) has more electron-withdrawing character than quinoxaline dithiolate ($qdt^{2-}$) and less electron-withdrawing character than pyrazine dithiolate ($pydt^{2-}$); accordingly the electron-withdrawing character order is $pydt^{2-} > ppdt^{2-} \geq qdt^{2-} > bdt^{2-}$.

**Table 2.6.** Cyclic voltammetric data (*vs.* $Fc^{+/0}$) for complexes **1**, **3**–**6** in MeCN[a]

| | **1** | **3** | **4** | **5** | **6** |
|---|---|---|---|---|---|
| $E_{pc}$ (V) | –1.17 | –1.23 | –1.38 | –1.41 | –1.42 |
| | — | — | –1.65 | –1.70 | –1.70 |
| $E_{pa}$ (V) | –1.01 | –1.05 | — | — | — |
| $E_{1/2}^{red}$ (V) | –1.08 | –1.14 | — | — | — |

[a] *n*-$Bu_4NClO_4$ (0.1 M) in $CH_3CN$; scan rate 100 mV $s^{-1}$; working electrode: glassy carbon electrode of diameter 3 mm; reference electrode: non-aqueous $Ag/Ag^+$ electrode (0.01 M $AgNO_3$ in $CH_3CN$); counter electrode: platinum wire.

The incorporation of strong electron donating $PPh_3$ ligand to $Fe_2S_2$ model complexes makes the reduction of the Fe–Fe site more difficult but the oxidation easier. Thus

compared to the hexacarbonyl analogues, the electron-donating $PPh_3$ ligand shift the reduction potentials of **1**, **2** and **3** by about 300–600 mV towards more negative potentials. The $PPh_3$–substituted $Fe_2S_2$ model complexes **4**–**6** show two irreversible reduction waves. The cyclic voltammograms for complexes **4**–**6** are shown in Fig. 2.5. Comparing the current heights of compounds **1** and **3** (Fig. 2.4) with those of **4**–**6** (Fig. 2.5), the two irreversible reductive responses for compounds **4**–**6** can be described as two one- electron reduction processes.

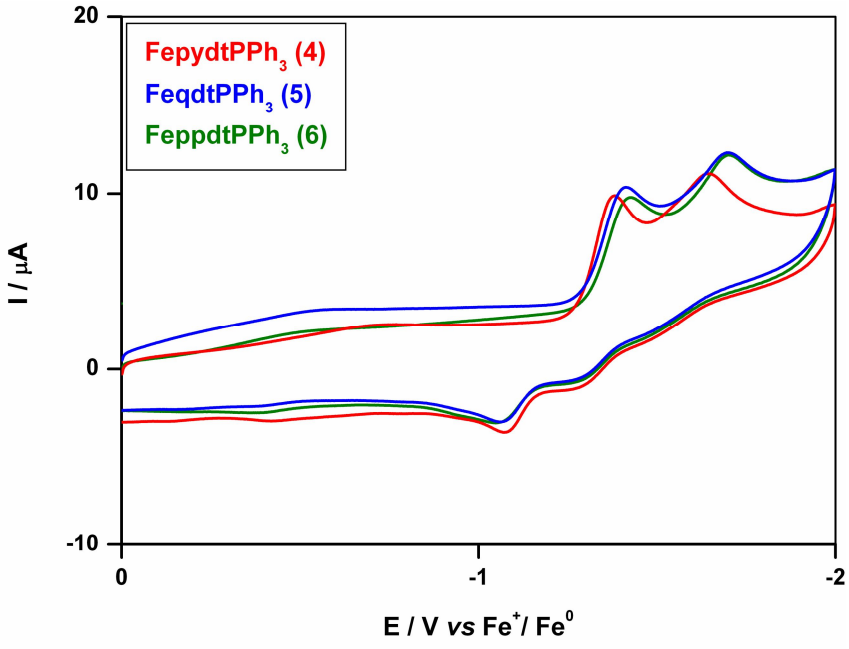


**Fig. 2.5.** Cyclic voltammograms of complexes **4** (red)**, 5** (blue) and **6** (green) (1.0 mM) in 0.1 M *n*-$Bu_4NClO_4$/MeCN at a scan rate of 100 $mVs^{-1}$. Potential are *vs*. $Fc^{+/0}$.

### *2.2.4. Electrocatalytic proton reduction by complex **1***

The electrochemical behavior of catalytic proton reduction by compound **1** was studied by recording cyclic voltammograms in the presence of strong acid, such as, *p*-toluenesulfonic acid (*p*-HOTs, $pK_a$ = 8.7) in $CH_3CN$ (Fig. 2.6) with the concentration range of 0–12 mM. Upon the addition of *p*-HOTs, the reduction potential shifts to more anodic side by 250 mV ($E_{pc}$ = –0.90 V) and a new peak appeared at –1.42 V (Fig. 2.6). On further addition of *p*-HOTs, complex **1** shows a significant electrocatalytic response, that the current intensity of the peak at –1.42 V gradually increases further with increasing acid concentration. This is the characteristic of proton reduction. Similar electrocatalytic situation was observed for the ADT (bridging ligand)-associated $\{Fe_2S_2\}$ compound, for which protonation of ligand

N was suggested [40]. The present system also has ring nitrogen atoms that can be easily protonated. Based on this, we propose a CECE (chemical–electrochemical–chemical–electrochemical) mechanism.

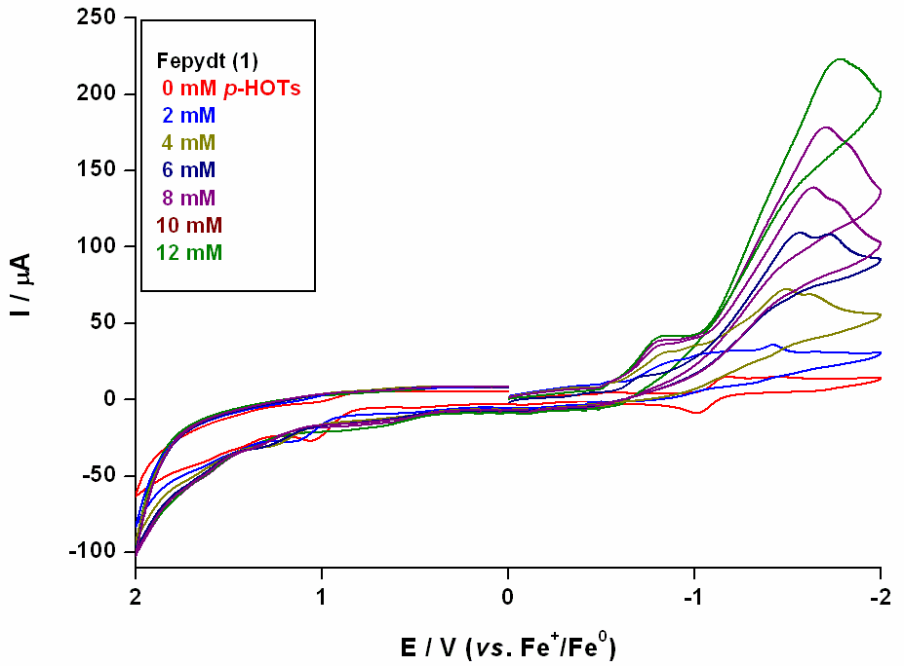


**Fig. 2.6.** Cyclic voltammogram of complex **1** with 1.0 mM complex and 0–8 mM *p*-HOTs in $CH_3CN$ solution (0.1 M *n*-$Bu_4NClO_4$) at a scan rate of 100 mV $s^{-1}$.

It is interesting that complex **1** exhibit relatively low reductio potential and undergoes electrocatalytic proton reduction of a stron acid , *p*–toluenesulfonic acid (*p*–HOTs). The value of $E^o_{HA}$ of the acid to be reduced can be used to evaluate the efficiency of a given catalyst. The $E^o_{p\text{-}HOTs}$ for *p*-HOTs is –0.65 V *vs.* $Fc^+/Fc^0$ in acetonitrile [63]. This indicates that the least negative potential of the catalyst, that will allow reduction of *p*-HOTs to dihydrogen, should be more negative than –0.65 V *vs.* $Fc^+/Fc^0$. It is thermodynamically impossible to achieve catalyst at a less negative potential. In the present study, we have shown electrocatalytic proton reduction catalyzed by the complex $[Fe_2\{\mu\text{-pydt}\}(CO)_6]$ (**1**). The cyclic voltammogram of complex **1** features electrochemical response at $E_{1/2}$ = –1.08 V *vs.* $Fc^+/Fc^0$ in the absence of acid *p*-HOTs and the catalyzed reduction of p-HOTs occurs at about –1.42 V *vs.* $Fc^+/Fc^0$ V. Thus catalysis occurs with 0.77 V overpotential. On the same ground, it can be concluded that the compound **1,** thermodynamically, will not allow

the catalytic reduction of weak acid (e.g. HOAc) to dihydrogen because the $E^0_{AcOH}$ for AcOH is –1.46 V *vs.* $Fc^+/Fc^0$ in acetonitrile [63].

## 2.3. Experimental section

*2.3.1. General procedures*

Pyrazine-2,3-dithiol ($H_2$pydt) [64], quinoxaline-2,3-dithiol ($H_2$qdt) [53] and Pyrido[2,3-b]pyrazine-2,3-dithiol ($H_2$ppdt) [65] were prepared according to literature procedures. Dichloromethane was distilled from $CaH_2$, THF from sodium/benzophenone ketyl, and MeOH, EtOH from Mg powder under a $N_2$ atmosphere. $Fe_2(CO)_9$ and $Me_3NO$ were purchased from Aldrich and directly used without further purification. All the reactions were carried out using standard Schlenk and vacuum-line technique under an atmosphere of nitrogen. Micro analytical (C, H, N) data were obtained with a FLASH EA 1112 Series CHNS Analyzer. The IR spectra (with KBr pellet) were recorded in the range of 400–4000 $cm^{-1}$ on a JASCO FT/IR-5300 spectrometer and Thermo Nicolet FT/IR–5700. Electronic spectra were obtained on a Cary 100 Bio UV–Visible spectrophotometer. $^1$H NMR and $^{13}$C NMR spectra were recorded on Bruker DRX–400 spectrometer using $Si(CH_3)_4$ (TMS) as an internal standard. Solution mass spectra (LCMS) were obtained on a LCMS–2010A Shimadzu spectrometer. Melting points were measured in open capillary tubes and are uncorrected.

*2.3.2. A general synthetic procedure for complexes **1** and **3***

A mixture of $Fe_2(CO)_9$ (2.0 g, 5.49 mmol) and equimolar amount of thiol ($H_2$pydt 0.8 g for compound **1** and $H_2$ppdt 1.07 g for compound **3**) was stirred in THF (25 mL) at –10 °C to 20 °C for 2–3 hrs to give a blood-red colored solution that contained some black solid as suspension. The mixture was filtered, and the solvent was removed under the reduced pressure. The residue was subjected to column chromatography by using hexane/$CH_2Cl_2$ (4:1 v/v) as an eluent. From the major red band, a red solid of respective compounds **1** and **3** was obtained.

**[$Fe_2${μ-pydt}$(CO)_6$] (1):** Yield: 0.4 g (18% based on thiol ($H_2$pydt)). It was recrystallized by slow evaporation of the MeOH/$CH_2Cl_2$ solution. m.p. 110–112 ºC, LC-MS: *m/z* = 423 $[M + H]^+$. IR (KBr pellet, $cm^{-1}$): 2926m, 1693m, 1550m, $\nu_{(S\text{-}C=)}$845m $\nu_{(C\equiv O)}$ 2084s, 2040s, 2014m, 1993m. $^1$H NMR (400 MHz, $CDCl_3$): $\delta$ 7.55 (s, 2H) ppm. $^{13}$C NMR (100 MHz, $CDCl_3$): $\delta$ 206.3, 169.1, 137.3 ppm. Anal. Calc. for $C_{10}H_2N_2O_6S_2Fe_2$: C, 28.46; H, 0.48; N, 6.64. Found: C, 28.35; H, 0.43; N, 6.78%.

**[$Fe_2${μ-ppdt}$(CO)_6$] (3):** Yield: 0.5 g (20% based on thiol ($H_2$ppdt)). It was recrystallized in MeOH/$CH_2Cl_2$ solution. m.p. 170–172 ºC, LC–MS: *m/z* = 474.3 $[M + H]^+$. IR (KBr pellet, $cm^{-1}$): 2687m, 761s $\nu_{(C\equiv O)}$ 2083s, 2047m, 2029s, 2004m, 1981s. $^1$H NMR (400 MHz, $CDCl_3$): $\delta$ 8.90 (s, 1H), 8.07 (d, *J* = 3.2 Hz, 1H), 7.56 (t, *J* = 3.0 Hz, 1H) ppm. $^{13}$C NMR (100 MHz, $CDCl_3$): $\delta$ 205.9, 169.0, 167.5, 154.0, 146.3, 137.0, 132.5, 126.1 ppm. Anal. Calc. for $C_{13}H_3N_3O_6S_2Fe_2$: C, 33.01; H, 0.64; N, 8.88. Found: C, 33.21; H, 0.66; N, 8.79%.

*2.3.3. A general synthetic procedure for complexes* ***4–6*****.**

One portion of $Me_3NO$ (0.064 g, 0.864 mmol) was added to a solution of 0.86 mmol of [$Fe_2${μ-L}$(CO)_6$] (L = pydt, qdt, ppdt for compounds **1**, **2** and **3** respectively) in MeCN (30 mL) under $N_2$. The mixture was stirred for 15 min. followed by the addition of the triphenylphosphine ligand $PPh_3$ (0.226 g, 0.864 mmol). After 30 min the volatiles were removed *in vacuo*. The resulting respective solids (**4**, **5** and **6**) were purified by column chromatography on silica gel with hexane/$CH_2Cl_2$ (3:2 v/v) as gradient eluent.

**[$Fe_2${μ-pydt}$(CO)_5PPh_3$] (4):** Yield: 0.37 g (65%). Single crystals suitable for X–ray analysis were obtained by slow evaporation of the $CH_2Cl_2$ solution at −10 ºC. IR (KBr pellet, $cm^{-1}$): 2962m, $\nu_{(C\equiv O)}$ 2054s, 2013s, 1977m, 1940m, 1479m, 1433m, 1336m, 1261m, 1217m, 1130v, 1091m, 1024m, 800m, 746s. $^1$H NMR (400 MHz, $CDCl_3$): $\delta$ 7.52 (br, 7H), 7.40 (br, 10H) ppm. $^{13}$C NMR (100 MHz, $CDCl_3$): $\delta$ 212.8, 208.13, 135.9, 134.9, 134.5, 133.1, 133.0, 130.3, 128.9, 128.8 ppm. $^{31}$P NMR (161.6 MHz, $CDCl_3$): $\delta$ 59.9 ppm. Anal. Calc. for $C_{27}H_{17}Fe_2N_2O_5PS_2$: C, 49.41; H, 2.61; N, 4.27. Found: C, 49.28; H, 2.65; N, 4.35%.

**[$Fe_2${μ-qdt}$(CO)_5PPh_3$] (5):** Yield: 0.4 g (65%). Single crystals suitable for X–ray analysis were obtained by slow evaporation of the $CH_2Cl_2$ solution at −10 ºC. IR (KBr pellet, $cm^{-1}$): 2964m, $\nu_{(C\equiv O)}$ 2050s, 1988s, 1940s, 1479m, 1433m, 1261m, 1093m, 800m, 690s. $^1$H NMR (400 MHz, $CD_3CN$): $\delta$ 7.51–6.87 (m, 19H) ppm. $^{13}$C NMR (100 MHz, $CDCl_3$): $\delta$ 213.0, 208.0, 164.8, 137.0, 134.5, 133.1, 130.2, 129.8, 128.7, 127.9 ppm. $^{31}$P NMR (161.6 MHz, $CDCl_3$): $\delta$ 59.0 ppm. Anal. Calc. for $C_{31}H_{19}Fe_2N_2O_5PS_2$: C, 52.72; H, 2.71; N, 3.96. Found: C, 52.61; H, 2.66; N, 3.85%.

**[$Fe_2${μ-ppdt}$(CO)_5PPh_3$] (6):** Yield: 0.330 g (54%). Single crystals suitable for X–ray analysis were obtained by slow evaporation of the MeOH/$CH_2Cl_2$ solution. IR (KBr pellet, $cm^{-1}$): 3057w, 2922m, 1433m, 1259m, 1172m, 1103m, 1022w, 800m, 765s, 746s, 692s,

621m, 561m, 518m, $\nu_{(C\equiv O)}$ 2050s, 1986s, 1944s. $^{1}$H NMR (400 MHz, $CDCl_3$): $\delta$ 7.71–7.75 (m, 3H), 7.41–7.52 (m, 15H) ppm. $^{13}$C NMR (100 MHz, $CDCl_3$): $\delta$ 213.0, 208.0, 164.8, 137.0, 134.5, 134.0, 133.0, 132.3, 131.5, 130.2, 129.7, 128.6, 127.8 ppm. $^{31}$P NMR (161.6 MHz, $CDCl_3$): $\delta$ 59.0 ppm. Anal. Calc. for $C_{30}H_{18}Fe_2N_3O_5PS_2$: C, 50.95; H, 2.56; N, 5.94. Found: C, 51.12; H, 2.53; N, 5.86%.

*2.3.4. Single crystal structure determination of complexes **1–6***

All the data were measured at room temperature for compounds **1–6** on a Bruker SMART APEX CCD, area detector system [λ (Mo Kα) = 0.7103 Å], graphite monochromator, 2400 frames were recorded with an ω scan width of 0.3°, each for 8 s, crystal-detector distance 60 mm, collimator 0.5 mm. Data reduction by SAINTPLUS [66], absorption correction using an empirical method SADABS [67] structure solution using SHELXS–97 [68] and refined using SHELXL–97 [68]. All the non hydrogen atoms were refined anisotropically. Hydrogen atoms on the aromatic rings were introduced on calculated positions and included in the refinement riding on their respective parent atoms.

*2.3.5. Electrochemical studies of complexes **1–6***

Acetonitrile (Finar, HPLC grade) used for performance of electrochemistry was dried with molecular sieve (4 Å) and then freshly distilled from $CaH_2$ under $N_2$. A solution of 0.1 M [*n*-$Bu_4N$][$ClO_4$] (TBAP) (Across, electrochemical grade) in $CH_3CN$ was used as supporting electrolyte. Electrochemical measurements were recorded by using a BAS electrochemical analyzer. The electrolyte solution was degassed by bubbling with dry Argon for 10 min. before measurement. Cyclic voltammograms were obtained in a three–electrode cell under argon. The working electrode was a glassy carbon disc (diameter 3 mm) successively polished with 0.3-μm alumina paste and sonicated in iron–free water for 10 min ethanol and finally rinsed with acetone, then air dried before usage. The home-built reference electrode was a silver wire in contact with a solution of 0.1 M *n*-$Bu_4NClO_4$ and 0.01 M $AgNO_3$ in acetonitrile. The reference electrode was separated from the contents of the cell by means of a porous Vycor frit. When not in use, the reference electrode assembly was kept immersed in 0.1 M *n*-$Bu_4NClO_4$ / acetonitrile to prevent drying of the frit. The auxiliary electrode was a platinum wire. The potentials reported here are referenced to the potential of the ferrocene couple.

## 2.4. Conclusion

In summary, we have successfully synthesized three heterocyclic ene-1,2-dithiolate bridged diiron complexes $[Fe_2\{\mu\text{-pydt}\}(CO)_6]$ (**1**), $[Fe_2\{\mu\text{-qdt}\}(CO)_6]$ (**2**), $[Fe_2\{\mu\text{-ppdt}\}(CO)_6]$ (**3**) and their triphenylphosphine derivatives $[(CO)_3Fe\{\mu\text{-pydt}\}Fe(CO)_2(PPh_3)]$ (**4**), $[(CO)_3Fe\{\mu\text{-qdt}\}Fe(CO)_2(PPh_3)]$ (**5**) and $[(CO)_3Fe\{\mu\text{-ppdt}\}Fe(CO)_2(PPh_3)]$ (**6**). Electronic properties of the diiron site can be modified by choosing the suitable aromatic dithiol ligand. We have characterized compounds **1**–**6** not only by single crystal X-ray structure determinations, but also by spectroscopic analyses. Electrochemical investigation shows that the electron-withdrawing character of the ligand decreases in the order pyrazine-2,3-dithiolate ($pydt^{2-}$) > pyrido[2,3-*b*]pyrazine-2,3-dithiolate ($ppdt^{2-}$) ≥ quinoxaline-2,3-dithiolate ($qdt^{2-}$) > benzene-1,2-dithiolate ($bdt^{2-}$).

## 2.5. References


[1] J. C. Fontecilla-Camps, A. Volbeda, C. Cavazza., Y. Nicolet, Chem. Rev. 107 (2007) 4273–4303.

[2] P. E. M. Siegbahn, J. W. Tye, M. B. Hall, Chem. Rev. 107 (2007) 4414–4435.

[3] P. M. Vignais, B. Billoud, Chem. Rev. 107 (2007) 4206–4272.

[4] M. W. W. Adams, Biochim. Biophys. Acta 1020 (1990) 115–145.

[5] R. Cammack, Nature 397 (1999) 214–215.

[6] Y. Nicolet, B. J. Lemon, J. C. Fontecilla-Camps, J. W. Peters, Trends Biochem. Sci. 25 (2000) 138–143.

[7] M. Y. Darensbourg, E. J. Lyon, X. Zhao, I. P. Georgakaki, Proc. Natl. Acad. Sci. U.S.A. 100 (2003) 3683–3688.

[8] D. J. Evans, C. J. Pickett, Chem. Soc. Rev. 32 (2003) 268–275.

[9] J. Alper, Science 299 (2003) 1686–1687.

[10] L. C. Song, Acc. Chem. Res. 38 (2005) 21–28.

[11] M. W. W. Adams, E. I. Stiefel, Science 282 (1998) 1842–1843.

[12] M. Frey, ChemBioChem. 3 (2002) 153–160.

[13] K. A. Vincent, A. Parkin, F. A. Armstrong, Chem. Rev. 107 (2007) 4366–4413.

[14] J. W. Peters, W. N. Lanzilotta, B. J. Lemon, L. C. Seefeldt, Science 282 (1998) 1853–1858.

[15] Y. Nicolet, C. Piras, P. Legrand, E. C. Hatchikian, J. C. Fontecilla-Camps, Structure 7 (1999) 13–23.

[16] B. Bennett, B. J. Lemon, J. W. Peters, Biochemistry 39 (2000) 7455–7460.

[17] B. J. Lemon, J. W. Peters, Biochemistry 38 (1999) 12969–12973.

[18] B. J. Lemon, J. W. Peters, J. Am. Chem. Soc. 122 (2000) 3793–3974.

[19] Y. Nicolet, A. L. de Lacey, X. Vernede, V. M. Fernandez, E. C. Hatchikian, J. C. Fontecilla-Camps, J. Am. Chem. Soc. 123 (2001) 1596–1601.

[20] G. A. N. Felton, C. A. Mebi, B. J. Petro, A. K. Vannucci, D. H. Evans, R. S. Glass and D. L. Lichtenberger, J. Organomet. Chem. 694 (2009) 2681–2699.

[21] D. M. Heinekey, J. Organomet. Chem. 694 (2009) 2671–2680.

[22] C. Tard and C. J. Pickett, Chem. Rev. 109 (2009) 2245–2274.

[23] J.-F. Capon, F. Gloaguen, F. Y. Petillon, P. Schollhammer, J. Talarmin, C. R. Chimie 11 (2008) 842–851.

[24] J.-F. Capon, F. Gloaguen, F.Y. Petillon, P. Schollhammer, J. Talarmin, Coord. Chem. Rev. 253 (2009) 1476–1494.

[25] F. Gloaguen, J. D. Lawrence, T. B. Rauchfuss, J. Am. Chem. Soc. 123 (2001) 9476–9477.

[26] F. Gloaguen, J. D. Lawrence, T. B. Rauchfuss, M.-M. Rohmer, Inorg. Chem. 41 (2002) 6573–6582.

[27] K. A. Justice, R. C. Linck, T. B. Rauchfuss, S. R. Wilson, J. Am. Chem. Soc. 126 (2004) 13214–13215.

[28] A. C. Boyke, T. B. Rauchfuss, S. R. Wilson, M.-M. Rohmer, M. Benard, J. Am. Chem. Soc. 126 (2004) 15151–15160.

[29] R. Mejia-Rodriguez, D. Chong, J. H. Reibenspies, M. P. Soriaga, M. Y. Darensbourg, J. Am. Chem. Soc. 126 (2004) 12004–12014.

[30] X. Zhao, I. P. Georgakaki, L. M. Miller, R. Mejia-Rodriguez, C.-Y. Chiang, M. Y. Darensbourg, Inorg. Chem. 41 (2002) 3917–3928.

[31] X. Zhao, C.-Y. Chiang, M. L. Miller, M. V. Rampersad, M. Y. Darensbourg, J. Am. Chem. Soc. 125 (2003) 518–524.

[32] T. Liu, M. Y. Darensbourg, J. Am. Chem. Soc. 129 (2007) 7008–7009.

[33] S. J. Borg, T. Behrsing, S. P. Best, M. Razavet, X. Liu, C. J. Pickett, J. Am. Chem. Soc. 126 (2004) 16988–16999.

[34] M. H. Cheah, S. J. Borg, S. P. Best, Inorg. Chem. 46 (2007) 1741–1750.

[35] S. J. Borg, J. W. Tye, M. B. Hall, S. P. Best, Inorg. Chem. 46 (2007) 384–394.

[36] L.-C. Song, M.-Y. Tang, S.-Z. Mei, J.-H. Huang, Q.-M. Hu, Organometallics

26 (2007) 1575–1577.

[37] L.-C. Song, L.-X. Wang, M.-Y. Tang, C.-G. Li, H.-B. Song, Q.-M. Hu, Organometallics 28 (2009) 3834–3841.

[38] L.-C. Song, Z. Y. Yang, Y. J. Hua, H. T. Wang, Y. Liu, Q. M. Hu, Organometallics 26 (2007) 2106–2110.

[39] S. Ott, M. Kritikos, B. Akermark, L. Sun, Angew. Chem. Int. Ed. 42 (2003) 3285–3288.

[40] T. Liu, M. Wang, Z. Shi, H. Cui, W. Dong, J. Chen, B. Akermark, L. Sun, Chem.–Eur. J. 10 (2004) 4474–4479.

[41] S. Ott, M. Kritikos, B. Akermark, L. Sun, R. Lomoth, Angew. Chem. Int. Ed. 43 (2004) 1006–1009.

[42] D. Chong, I. P. Georgakaki, R. Mejia-Rodriguez, J. Sanabria-Chinchilla, M. P. Soriaga, M. Y. Darensbourg, Dalton Trans. (2003) 4158–4163.

[43] J. F. Capon, F. Gloaguen, P. Schollhammer, J. Talarmin, J. Electroanal. Chem. 566 (2004) 241–247.

[44] G. A. N. Felton, A. K. Vannucci, J. Chen, L. T. Lockett, N. Okumura, B. J. Petro, U. I. Zakai, D. H. Evans, R. S. Glass, D. L. Lichtenberger, J. Am. Chem. Soc. 129 (2007) 12521–12530.

[45] G. A. N. Felton, A. K. Vannucci, N. Okumura, L. T. Lockett, D. H. Evans, R. S. Glass, D. L. Lichtenberger, Organometallics 27 (2008) 4671–4679.

[46] J. F. Capon, F. Gloaguen, P. Schollhammer, J. Talarmin, J. Electroanal. Chem. 595 (2006) 47–52.

[47] H. K. Joshi, F. E. Inscore, J. T. Schirlin, I. K. Dhawan, M. D. Carducci, T. G. Bill, J. H. Enemark, Inorg. Chim. Acta 337 (2002) 275–286.

[48] H. K. Joshi, J. J. A. Cooney, F. E. Inscore, N. E. Gruhn, D. L. Lichtenberger, J. H. Enemark, Proc. Natl. Acad. Sci. U.S.A. 100 (2003) 3719–3724.

[49] H. K. Joshi, J. H. Enemark, J. Am. Chem. Soc. 126 (2004) 11784–11785.

[50] J. J. A. Cooney, M. A. Cranswick, N. E. Gruhn, H. K. Joshi, J. H. Enemark, Inorg. Chem. 43 (2004) 8110–8118.

[51] A. Majumdar, J. Mitra,; K. Pal, S. Sarkar, Inorg. Chem. 47 (2008) 5360–5364.

[52] A. Majumdar, K. Pal, S. Sarkar, J. Am. Chem. Soc. 128 (2006) 4196–4197.

[53] L. Schwartz, P. S. Singh, L. Eriksson, R. Lomoth, S. Ott, C. R. Chimie 11 (2008) 875–889.

[54] N. Wang, M. Wang, T. Liu, P. Li, T. Zhang, M. Y. Darensbourg, L. Sun, Inorg. Chem. 47 (2008) 6948–6955.

[55] P. Li, M. Wang, L. Chen, J. Liu, Z. Zhao, L. Sun, Dalton Trans. (2009) 1919–1926.

[56] D. Streich, M. Karnahl, Y. astute, C-W. Cady, L. Hammarström, R. Lomoth and S. Ott, Eur. J. Inorg. Chem. (2011) 1106–1111.

[57] L. Schwartz, L. Eriksson, R. Lomoth, F. Teixidor, C. Vinas and S. Ott, Dalton Trans. (2008) 2379–2381.

[58] J. A. Cabeza, A. Martinez-Garcia, V. Riera, Organometallics 17 (1998) 1471–1477.

[59] P. Li, M. Wang, C. He, G. Li, X. Liu, C. Chen, B. Akermark, L. Sun, Eur. J. Inorg. Chem. (2005) 2506–2513.

[60] P. Li, M. Wang, C. He, X. Liu, K. Jin, L. Sun, Eur. J. Inorg. Chem. (2007) 3718–3727.

[61] O. Kasende and Th. Zeegers-Huyskens, J. Phys. Chem. 88 (1984) 2132–2137.

[62] J. H. Markgraf and R. J. Katt, J. Org. Chem. 37 (1972) 717–718.

[63] G. A. N. Felton, R. S. Glass, D. L. Lichtenberger, D. H. Evans, Inorg. Chem. 45 (2006) 9181-9184.

[64] X. Ribas, J. C. Dias, J. Morgado, K. Wurst, E. Molins, E. Ruiz, M. Almeida, J. Veciana, C. Rovira, Chem.–Eur. J. 10 (2004) 1691–1704.

[65] R. Bolligarla, G. Durgaprasad, S. K. Das, Inorg. Chem. Commun. 12 (2009) 355–358.

[66] Software for the CCD Detector System; Bruker Analytical X-Ray Systems, Inc.: Madison, WI, 1998.

[67] Sheldrick, G. M., SADABS, Program for Absorption Correction with the Siemens SMART Area-Detector System; University of Göttingen: Göttingen, Germany, 1996.

[68] G. M. Sheldrick, Acta. Cryst. A64 (2008) 112–122.

# 1,2-Ene dithiolate bridged diiron carbonyl-phosphine and -phosphite complexes in relevance to the active site of [FeFe]-hydrogenases: Synthesis, characterization and electrocatalysis

3 Chapter

**Abstract:-** A series of binuclear $Fe^{I}Fe^{I}$ complexes have been prepared by the treatment of *N*–heterocyclic 1,2-dithiols, such as, quinoxaline-6,7-dithiol ($H_2$6,7-qdt), 2,3-diphenyl-6,7-quinoxaline dithiol ($H_2$diph-6,7-qdt) and 2,1,3-benzothiadiazole-5,6-dithiol ($H_2$btdt) with $Fe_2(CO)_9$ resulting in the formation of $[Fe_2\{\mu\text{-}6,7\text{-qdt}\}(CO)_6]$ (**1**), $[Fe_2\{\mu\text{-diph-}6,7\text{-qdt}\}(CO)_6]$ (**2**) and $[Fe_2\{\mu\text{-btdt}\}(CO)_6]$ (**9**) respectively. These complexes have now been examined to explore structural, electronic and electrochemical effects on substituting one or two CO group(s) with other good donor ligands, e.g., phosphine and phosphite ligands. Mono-phosphine substituted compounds $[Fe_2\{\mu\text{-}6,7\text{-qdt}\}(CO)_5PPh_3]$ **(3)**, $[Fe_2\{\mu\text{-diph-}6,7\text{-qdt}\}(CO)_5PPh_3]$ **(4)** and $[Fe_2\{\mu\text{-btdt}\}(CO)_5PPh_3]$ **(10)** are synthesized by the reactions of **1**, **2** and **3**, respectively with $PPh_3$ in the presence of $Me_3NO$. Interestingly, treatment of **1**, **2** and **3** with controlled amount of $P(OEt)_3$ affords the mono-substituted phosphite derivatives $[Fe_2\{\mu\text{-}6,7\text{-qdt}\}(CO)_5P(OEt)_3]$ **(5),** $[Fe_2\{\mu\text{-diph-}6,7\text{-qdt}\}(CO)_5P(OEt)_3]$ **(6),** $[Fe_2\{\mu\text{-btdt}\}(CO)_5\ P(OEt)_3]$ **(11)** respectively. The same reaction with an excess amount of $P(OEt)_3$ affords the di-substituted phosphite derivatives $[Fe_2\{\mu\text{-}6,7\text{-qdt}\}(CO)_4\{P(OEt)_3\}_2]$ **(7),** $[Fe_2\{\mu\text{-diph-}6,7\text{-qdt}\}(CO)_4\{P(OEt)_3\}_2]$ **(8)** and $[Fe_2\{\mu\text{-btdt}\}(CO)_4\{P(OEt)_3\}_2]$ **(12)** correspondingly. These new complexes **1–12** have been characterized by IR, $^{1}H$, $^{13}C$, and $^{31}P\{^{1}H\}$ NMR and mass spectroscopy including elemental analysis. The solid state structures for all compounds have been determined by single-crystal X-ray structure analyses. The electrochemistry of **1–12** was performed by cyclic voltammetry to evaluate the effects of phosphine and phosphite ligands on the reduction potentials of the iron atoms of the model complexes. The electrocatalytic activities of model complexes **2**, **9** and **10–12** toward proton reduction of a strong acid *p*–HOTs have been described.

## 3.1. Introduction

The hydrogenase enzymes are vital enzymes, in which [FeFe]hydrogenases have received special attention, largely due to their unusual structures and particularly their highly catalytic ability for production of hydrogen, an alternative ‘clean’ and renewable fuel [1–3]. [FeFe]-hydrogenase enzyme, isolated from *Desulfovibrio desulfuricans* and

*Clostridium pasteurianum* [4–5], consists of an unusual [2Fe2S] subunit bridged to an ordinary [4Fe4S] cubane via a single cysteinyl sulfur atom, typically with a vacant coordination site on one iron atom ($Fe_p$) and the iron atoms are coordinated by biologically unusual ligands (CO, $CN^-$), which were first detected by FTIR spectroscopy as shown in Fig. 3.1(i) [6,7]. Eventually, such a structure has inspired the organometallic chemists to do an extensive work on developing simple and robust structural analogues to mimic the [FeFe]-hydrogenase active site. Several review articles have been published in recent times that are associated with hydrogenase model complexes and their catalytic activities [8–12]. The catalytic property for the hydrogen generation, mediated by [FeFe]$H_2$ase model complexes, can be tuned by the substitution of the CO ligands of di-iron carbonyl complexes. Thus, displacement of one or two CO ligands from [FeFe]$H_2$ase model complexes by various good ligands such as $CN^-$, phosphine, phosphite, and carbene has been reported [13–21]. These carbonyl substituted complexes also serve as synthetic models of the active site of [FeFe]$H_2$ases. Most of the dithiolate bridged $\{Fe^IFe^I\}$ model complexes, that are inspired by the [FeFe]$H_2$ase active site, have been shown to be a promising class of molecular electrocatalysts for proton reduction from acids of varying strengths in non-aqueous media [22–34]. To date, a large number of biomimetic models for the active site of [FeFe] hydrogenase has been prepared and structurally characterized [35–40]. Among such models, we are particularly interested in 1,2-ethylene-dithiol bridged 2Fe2S core, such as, benzene dithiolate ($bdt^{2-}$) bridged di-iron core (representation **A**, shown below in Fig. 3.1(ii)) type models [41–44].

Capon and co-workers first reported the compound **A** as [FeFe]-hydrogenase active site model system [27] and further Lichtenberger, Evans, Glass and their co-workers have successfully demonstrated electrocatalytic hydrogen generation from weak acid (HOAc) by using the same system **A**. They proposed a novel mechanism, deduced from both electrochemical and theoretical studies on complex **A [**29,45**]**. Sascha Ott and his coworkers worked on arene dithiolate bridged diiron complexes extensively [30, 46–49].

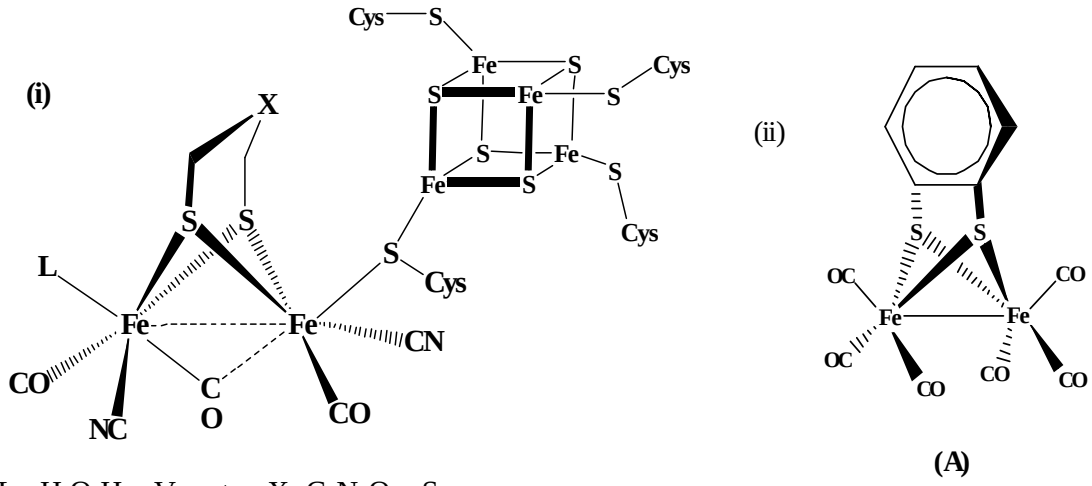


**Fig. 3.1.** (i) Schematic view of the active site of [FeFe]Hydrogenase. (ii) **A** represents benzene dithiol bridged diiron complex as a model of [FeFe]Hydrogenase active site.

For the system A, the benzene dithiolate ($bdt^{2-}$) ligand has a special ability; it assists to modulate the redox reactions of the catalyst by lowering the potential difference between the successive reduction states. This has been explained by an interaction of the metal d-orbitals with a combination of the filled sulfur $p_\pi$ orbitals and the arene $p_\pi$ orbitals, which acts to shield the change in electron density at the iron center as the oxidation state is changed, thus minimizing the changes in electron energies upon reduction. The importance of 1,2-ethylene-dithiolate in such model complexes can also be realized by the fact that "Nature" has used this ligand in the active site of Mo/W-oxotransferase redox enzymes because of its unique electronic property [50,51].

Thus, the rational design and syntheses of 1,2-ethylene-dithiolate-coordinated 2Fe2S complexes are challenging tasks for synthetic chemists in modeling the active sites of [FeFe]$H_2$ases. In view of this, recently we have reported pyrazine dithiolate bridged diiron complexes as [FeFe]hydrogenase active site model complexes [52]. In the present contribution, we preferred and synthesized the following *N*–heterocyclic ene-1,2-dithiol (benzene ring attached *o*-dithiols) ligands, such as, quinoxaline-6,7-dithiol ($H_2$6,7-qdt), 2,3-diphenyl-6,7-quinoxaline dithiol ($H_2$diph-6,7-qdt) and 2,1,3-benzothiadiazole-5,6-dithiol ($H_2$btdt) as shown in Scheme 3.1.

We have synthesized model complexes [$Fe_2\{\mu$-6,7-qdt$\}(CO)_6$] (**1**), [$Fe_2\{\mu$-diph-6,7-qdt$\}(CO)_6$] (**2**) and [$Fe_2\{\mu$-btdt$\}(CO)_6$] (**9**) using these N-heterocyclic 1,2-dithiol ligands.

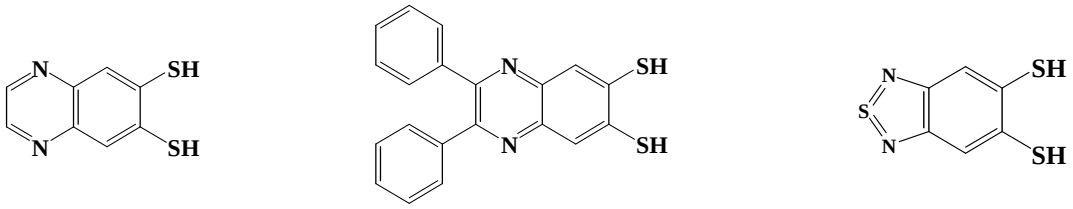

$H_2$6,7-qdt $H_2$diph-6,7-qdt $H_2$btdt

**Scheme 3.1.** *N*–heterocyclic 1,2-dithiol ligands.

The phosphorus-containing ligands are more commonly used to alter the electron density of the metal carbonyl complexes that emulate the donor properties of the biological $CN^-$ ligand, without the complications of reactivity at the cyanide nitrogen. So good donor ligands, such as $PPh_3$ and $P(OEt)_3$, have been introduced to iron-coordinated CO ligands from the all carbonyl di-iron complexes **1**, **2** and **9** by CO displacement to result in the isolations of $[Fe_2\{\mu\text{-}6,7\text{-qdt}\}(CO)_5PPh_3]$ **(3)**, $[Fe_2\{\mu\text{-diph-}6,7\text{-qdt}\}(CO)_5PPh_3]$ **(4)**, $[Fe_2\{\mu\text{-btdt}\}(CO)_5\ PPh_3]$ **(10)**, $[Fe_2\{\mu\text{-}6,7\text{-qdt}\}(CO)_5P(OEt)_3]$ **(5),** $[Fe_2\{\mu\text{-diph-}6,7\text{-qdt}\}(CO)_5P(OEt)_3]$ **(6),** $[Fe_2\{\mu\text{-btdt}\}(CO)_5\ P(OEt)_3]$ **(11)**, and $[Fe_2\{\mu\text{-}6,7\text{-qdt}\}(CO)_4\{P(OEt)_3\}_2]$ **(7)**, $[Fe_2\{\mu\text{-diph-}6,7\text{-qdt}\}(CO)_4\{P(OEt)_3\}_2]$ **(8)**, $[Fe_2\{\mu\text{-btdt}\}(CO)_4\{P(OEt)_3\}_2]$ **(12).** Here we describe the syntheses, spectroscopic characterization, X-ray crystallography and electrochemical studies of complexes **1**–**12**. Based on the electro-catalytic hydrogen generation experiments by cyclic voltammetric studies, plausible catalytic mechanisms for the production of molecular hydrogen have been proposed.

## 3.2. Results and discussion

*3.2.1. Synthesis and characterization of N–heterocyclic 1,2-dithiol ligands.*

**$H_2$6,7-qdt.** It was prepared by literature procedure [53].

**$H_2$diph-6,7-qdt.** The starting precursor for this sysnthesis is 4,5-bis(thiocyanato)-benzene-1,2-diamine, which was prepared from benzene-1,2-diamine and $KSCN/Br_2$ by following reported literature procedure [54]. 2,3-Diphenyl-6,7-bis-thiocyanato-quinoxaline (**B**) (see Scheme 3.2) was prepared according to modified literature procedure [55,56], which was obtained by a condensation reaction between the 4,5-bis(thiocyanato)-benzene-1,2-diamine and benzil by using iodine as a catalyst in acetonitrile solution at room temperature for 1 h affording a quantitative yield. Finally $H_2$diph-6,7-qdt was synthesized by treating compound **B** with $Na_2S$ followed by acidification, which gives a good yield

(90%) as shown in Scheme 3.2. Compound **B** and ligand $H_2$diph-6,7-qdt were characterized by regular IR, NMR, LC-MS spectral and elemental analysis.

**$H_2$btdt.** It was synthesized by a reported literature procedure [54].

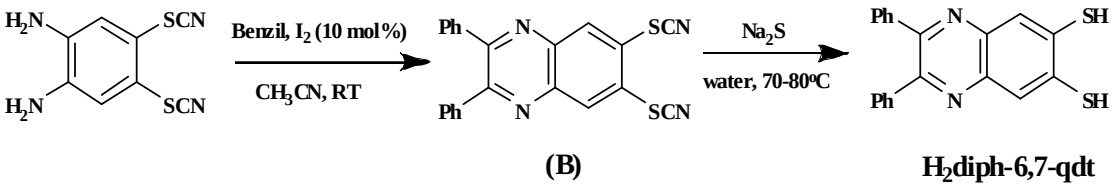


**(B)** **$H_2$diph-6,7-qdt**

**Scheme 3.2.** Synthetic route of $H_2$diph-6,7-qdt.

*3.2.2. Synthesis and characterization of model complexes [$Fe_2${$\mu$-6,7-qdt}$(CO)_6$] **(1)**, [$Fe_2${$\mu$-diph-6,7-qdt}$(CO)_6$] **(2)** and [$Fe_2${$\mu$-btdt}$(CO)_6$] **(9)***

We have synthesized [FeFe]-hydrogenase model compounds [$Fe_2${$\mu$-6,7-qdt}$(CO)_6$] **(1)**, [$Fe_2${$\mu$-diph-6,7-qdt}$(CO)_6$] **(2)** and [$Fe_2${$\mu$-btdt}$(CO)_6$] **(9)** by treating 6,7-quinoxaline-dithiol ($H_2$6,7-qdt), diphenyl-6,7-quinoxaline dithiol ($H_2$diph-6,7-qdt) and 2,1,3-benzothiadiazole-5,6-dithiol ($H_2$btdt) respectively with $Fe_2(CO)_9$ in THF at 50 °C as shown in Scheme 3.3 and 3.4. Complexes **1, 2** and **9** are air stable red solids and purified directly by column chromatography, which have been fully characterized by IR, $^1$H, and $^{13}$C NMR spectroscopy and elemental analysis. The IR spectra of complexes **1, 2** and **9** show four to five strong absorption bands in the region of 2080-1950 $cm^{-1}$, that are assigned to the terminal carbonyl groups as shown in Fig. 3.2. The $^1$H NMR spectrum (in $CDCl_3$ solution at 298 K) of complex **1** displays two singlets at $\delta$ 8.66 and 7.86 ppm. Compound **2** shows one singlet at $\delta$ 7.94 and one multiplet for two phenyl groups at $\delta$ 7.43–7.29 ppm whereas for compound **9**, only one singlet at $\delta$ 7.85 ppm is observed in their respective NMR spectra. The $^{13}$C NMR spectra of complexes **1**, **2** and **9** exhibit only one peak at $\delta$ 207 ppm for their terminal carbonyl group.

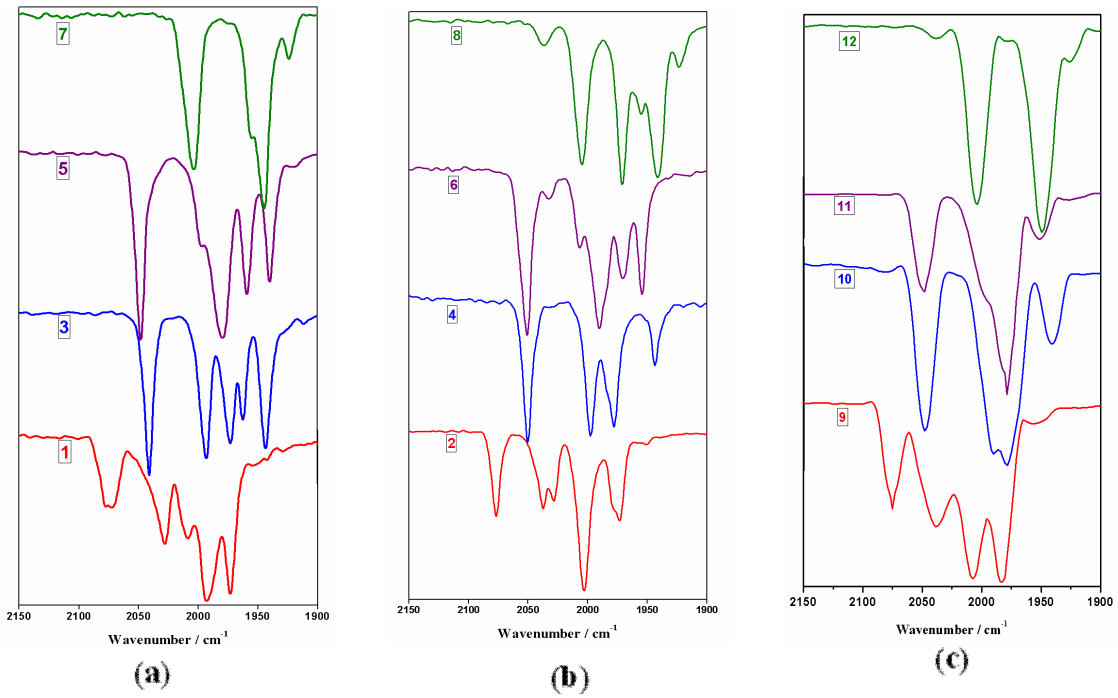


**Fig. 3.2.** IR spectra of (a) complexes **1**, **3**, **5** and **7** (b) **2**, **4**, **6** and **8** (c) **9**, **10**, **11** and **12**.

The molecular structures of **1**, **2** and **9** are unambiguously confirmed by X-ray diffraction technique and thermal ellipsoidal plots are shown in Fig. 3.3. Table 3.1 lists their selected bond lengths and bond angles. The wine-red colored crystals of complexes **1**, **2** and **9** are grown by cooling respective $CH_2Cl_2$ solutions at −10 °C. The crystal structure analyses show that the complexes **1**, **2** and **9** crystallize in monoclinic space groups $P2_1/c$, $C2/c$ and $P2_1/c$ respectively. $Z' = 1$ for complexes **1**, **2** and **9** and bonding dimensions within the complexes are unexceptional as shown in Fig. 3.3. The central 2Fe2S structures of all three diiron 1,2-ene dithiolate bridged complexes (**1**, **2** and **9**) are in the butterfly conformation and each iron atom is coordinated with a pseudo square–pyramidal geometry as in previously reported relevant models [13,19,57–61]. In addition, the Fe···Fe separation in the crystal structures of complexes **1**, **2** and **9** are 2.4900, 2.5023 and 2.4907 Å respectively, that are somewhat longer than that of complex **A** (2.480(2) Å) (Fig. 3.1) [42] and relatively shorter than those found in *Desulfovibrio desulfuricans*[5] and *Clostridium pasteurianum*[4] (*ca*. 2.6 Å). Interestingly, complex **9** shows non-covalent interactions, such as, weak S···N and S···S supramolecular contacts.

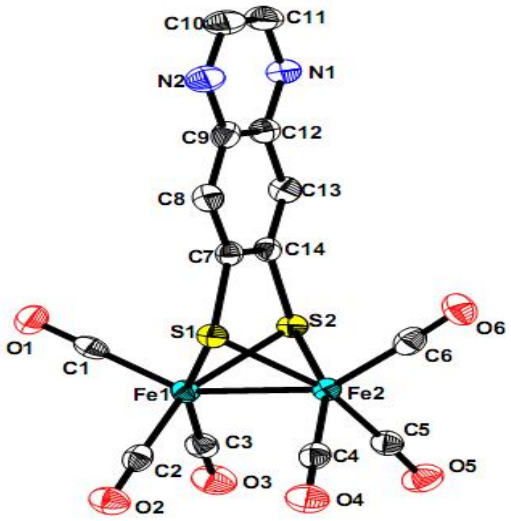


**(a)**

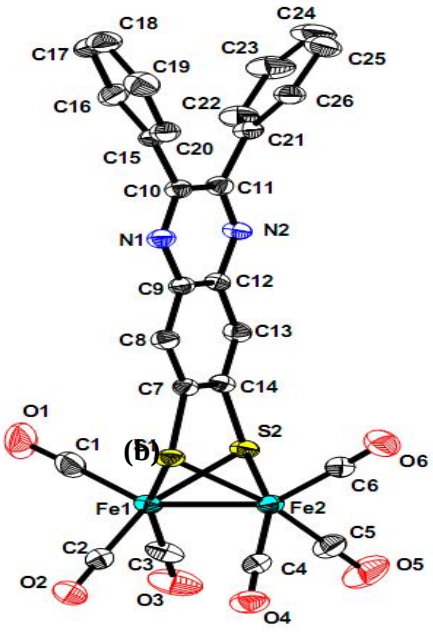


**(b)**

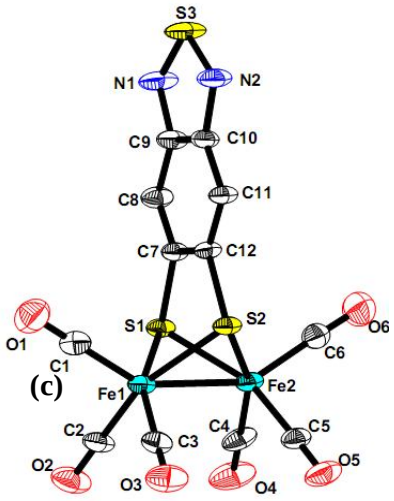


**(c)**

**Fig. 3.3.** Molecular structures of compounds (a) **1**, (b) **2** and (c) **9** with thermal ellipsoids at 50% probability. Hydrogen atoms are omitted for clarity.

The S···N contact distance is 3.0701(1), which is less than the sum of their van-der Waals radii (1.55 Å for nitrogen and 1.80 Å for sulphur) [62]. The non-covalent S···S interactions are described by a distance of 3.641(1) Å. These combined weak S···N and S···S non-

covalent interactions result in the formation of one dimensional chainlike arrangement as shown in Fig. 3.4.

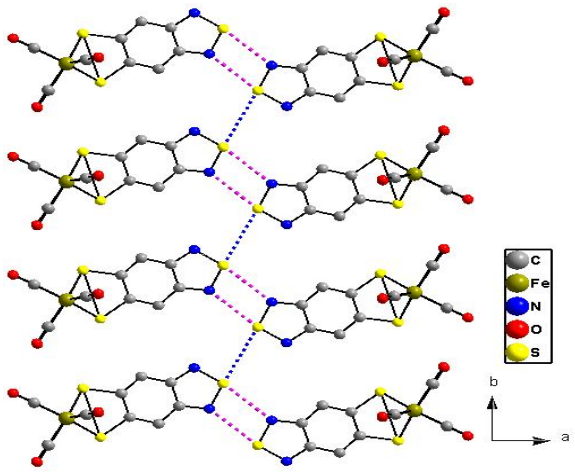


**Fig. 3.4.** The molecular packing diagram of compound **9**, characterized by S–N···S and N– S···S weak interactions, when viewed down to the crystallographic *c* axis.

*3.2.3. Synthesis and characterization of phosphine substituted model complexes [$Fe_2${μ-6,7-qdt}$(CO)_5PPh_3$] (**3**), [$Fe_2${μ-diph-6,7-qdt}$(CO)_5PPh_3$] (**4**) and [$Fe_2${μ-btdt}$(CO)_5$ $PPh_3$] (**10**).*

Complexes **1**, **2** and **9** react with $PPh_3$ in $CH_3CN$ in the presence of decarbonylating agent $Me_3NO$ at room temperature to produce a series of solo unsymmetrical mono-phosphine substituted complexes **3**, **4** and **10** respectively as shown in Schemes 3.3 and 3.4. The IR spectra of **3**, **4** and **10** display four to five absorption bands in the range of 2050–1940 $cm^{-1}$, which can be assigned to the terminal carbonyl groups. These $\nu$(C≡O) values of **3**, **4** and **10** are markedly shifted towards lower frequencies relative to those of their respective parent complexes **1**, **2** and **9** as shown in Fig. 3.2. The $^{13}C$ NMR spectra of complexes **3**, **4** and **10** exhibit two peaks around $\delta$ 213.5 and 207 ppm for their terminal carbonyl groups. $^{31}P$ NMR spectra of **3**, **4** and **10** show one peak in the range of $\delta$ 60–61 ppm.

The crystals of complexes **3**, **4** and **10** were grown by cooling $CH_2Cl_2$ solution at −10 °C. The crystal structure analyses show that the crystals of complexes **3** and **10** crystallize in monoclinic space groups $P2_1/c$, whereas **4** crystallizes in triclinic space group *P*-1. $Z'$ = 1 for complexes **3**, **4** and **10**. The bonding dimensions within the complexes are unexceptional. The thermal ellipsoidal plots of the molecular structures of **3**, **4** and **10** are shown in Fig. 3.5. Selected bond lengths and bond angles are listed in

Table 3.2. The central 2Fe2S structures of these complexes are all in the butterfly conformation as shown in previously reported model compounds [13,18,58,59,63,64]. The displacement of CO group with $PPh_3$, that coordinates to an apical site of Fe(2) of the complexes **1**, **2** and **9**, lengthens Fe···Fe separations in resulting unsymmetrical complexes

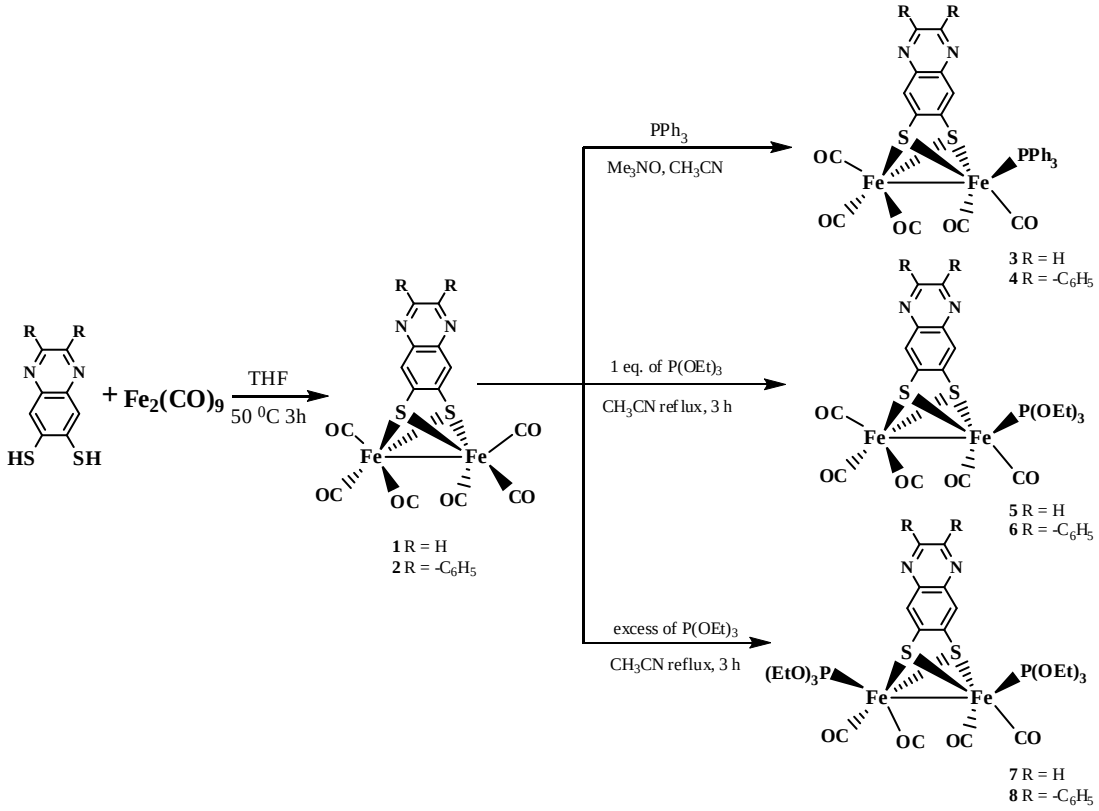


**Scheme 3.3.** Schematic representation of synthesis of complexes **1–8**

**3**, **4** and **10** respectively due to the stronger σ–donor properties of $PPh_3$ ligand compared to carbonyl group, as shown in Table 3.2. In complexes **3**, **4** and **10**, the Fe(2)–C(4) (1.776 Å in **3**, 1.766 Å in **4** and 1.769 Å in **10**) distances are notably shorter than Fe(1)–C(1) (1.805 Å in **3**, 1.818 Å in **4** and 1.809 Å in **10**) distances. Accordingly, the C(4)–O(4) (1.144 Å in **3**, 1.150 Å in **4** and 1.139 Å in **10**) distances are longer than the C(1)–O(1) (1.136 Å in **3**, 1.129 Å in **4** and 1.132 Å in **10**) distances in $Fe(CO)_3$ unit. The reasonable explanation is that the higher electron density of Fe(2) atom leads to the stronger electron back-donation from Fe(2) to the C(4) / C(5) as compared to the back-donation from Fe(1) center to the Fe(1)-coordinated CO ligands.

*3.2.4. Synthesis and characterization of mono- and di-phosphite substituted model complexes [$Fe_2$\{μ-6,7-qdt\}$(CO)_5P(OEt)_3$] (**5**), [$Fe_2$\{μ-diph-6,7-qdt\}$(CO)_5P(OEt)_3$] (**6**),[$Fe_2$\{μ-btdt\}$(CO)_5$ $P(OEt)_3$] (**11**) and [$Fe_2$\{μ-6,7-qdt\}$(CO)_4${$P(OEt)_3$}$_2$] (**7**), [$Fe_2$\{μ-diph-6,7-qdt\}$(CO)_4${$P(OEt)_3$}$_2$] (**8**), [$Fe_2$\{μ-btdt\}$(CO)_4$ {$P(OEt)_3$}$_2$] (**12**).*

The relatively weaker nucleophile, $P(OEt)_3$ results in slower CO displacement on reaction with **1**, **2** and **9**, and thereby this needs more stringent conditions. Thus treatment of complexes **1**, **2** and **9** with equimolar and excess amount of triethylphosphite in $CH_3CN$ at

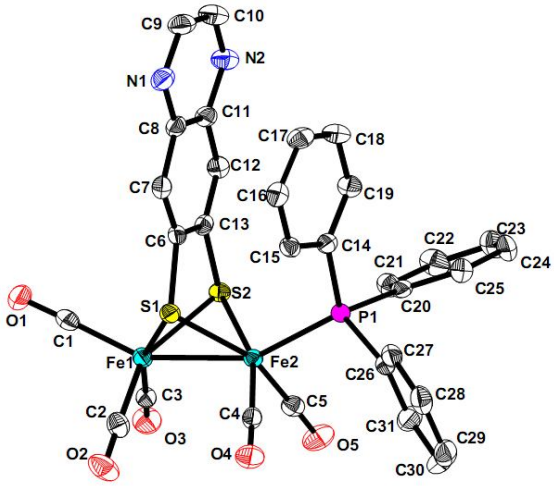


**(a)**

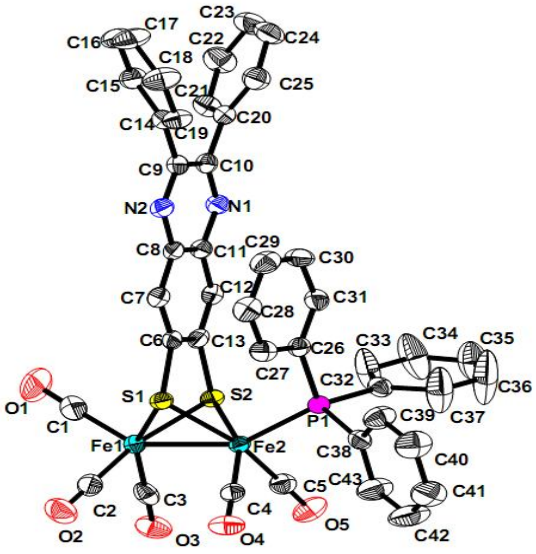


**(b)**

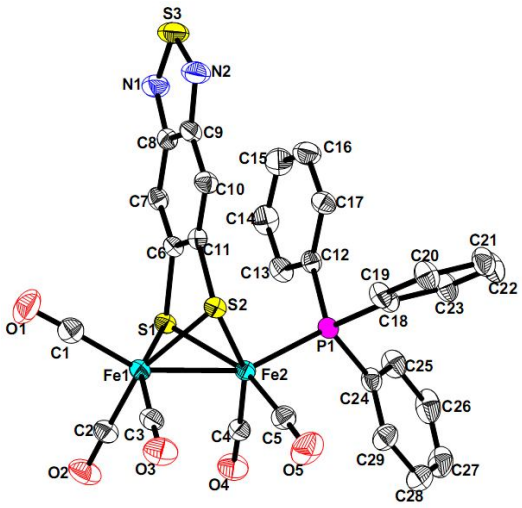


**(c)**

**Fig. 3.5.** Molecular structures of compounds (a) **3**, (b) **4** and (c) **10** with thermal ellipsoids at 50% probability. Hydrogen atoms are omitted forclarity.

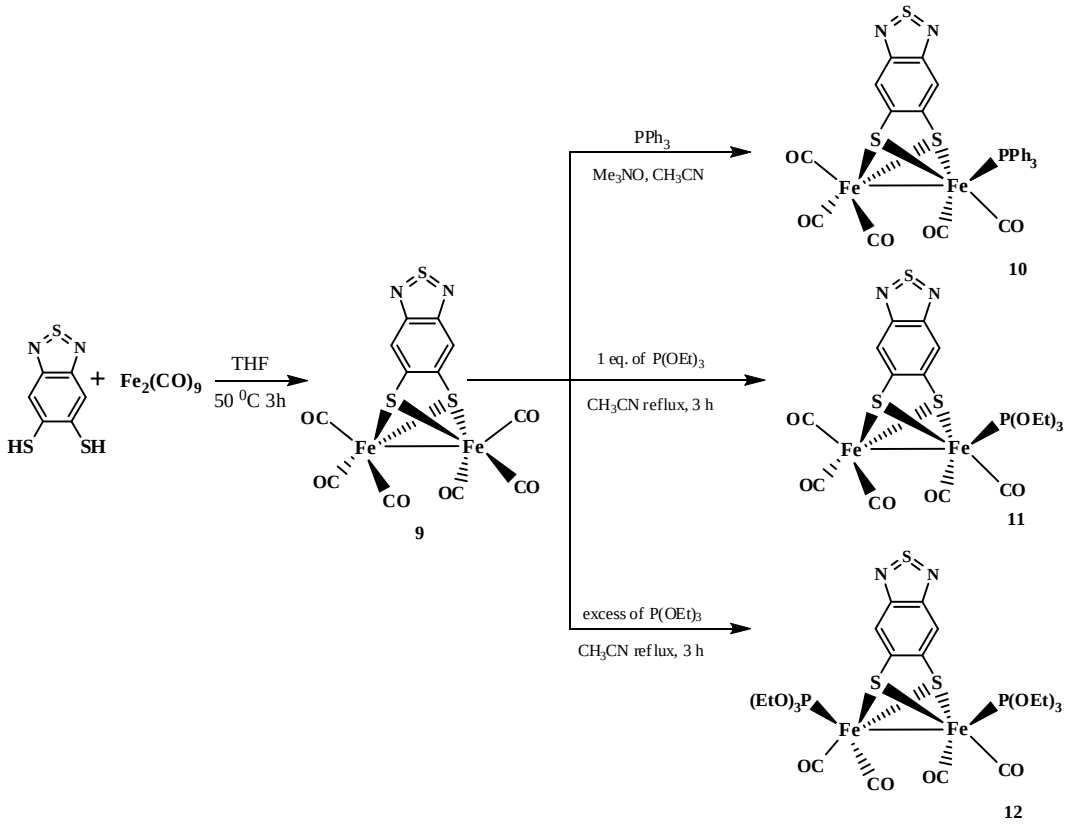


**Scheme 3.4.** Schematic representation of synthesis of complexes **9–12.**

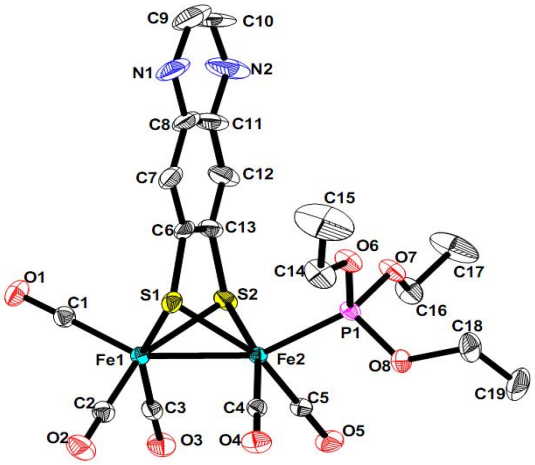

**(a)**

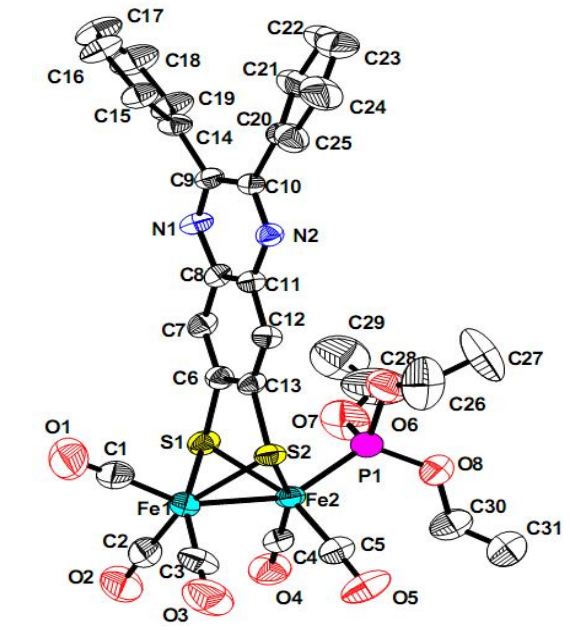


**(b)**

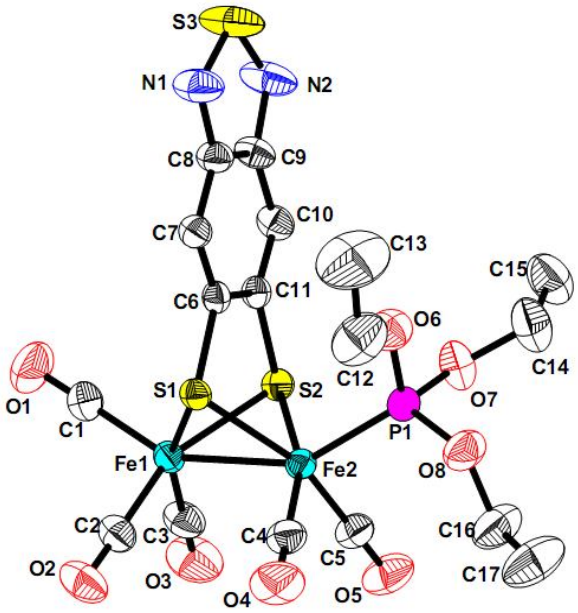


**(c)**

**Fig. 3.6.** Molecular structures of compounds (a) **5**, (b) **6** and (c) **11** with thermal ellipsoids at 50% probability. Hydrogen atoms are omitted for clarity.

reflux condition for 3 h affords mono-substituted derivatives **5**, **6** and **11**, and di-substituted $P(OEt)_3$ compounds, **7**, **8** and **12** respectively, as shown in Schemes 3.3 and 3.4. The $\nu(C{\equiv}O)$ bands are considered as useful indicator for detecting the variation in the

electron density at the 2Fe2S core influenced by electron donating phosphine and phosphite ligand substitution. Complexes **5**, **6** and **11** show around 30 $cm^{-1}$ red-shifted value for four $\nu_{CO}$ bands in the region of 2048–1940 $cm^{-1}$ compared to the corresponding all carbonyl parent complexes **1**, **2** and **9** respectively. On the other hand, in complexes **7**, **8** and **12**, the di-substitution of $P(OEt)_3$, adds more electron density on the Fe centers, thereby exhibiting more red-shift (of approximately 70 $cm^{-1}$) of three $\nu_{CO}$ bands around 2004–1926 $cm^{-1}$ compared to complexes **1**, **2** and **9** respectively, as shown in Fig. 3.2. The $^1H$ NMR spectra of all the mono- and di-phosphite substituted complexes exhibit one quartet at $\delta$ 4.06–4.08 ppm ($-OCH_2$) and one triplet at $\delta$ 1.24–1.29 ppm ($-CH_3$). The $^{13}C$ NMR spectra of all mono substituted complexes **5**, **6** and **11** show two peaks at $\delta$ 213 and 208 ppm, whereas di-substituted complexes **7**, **8** and **12** display only one peak at $\delta$ 213.8 ppm. In addition, the $^{31}P$ NMR spectra of mono-substituted complexes (**5**, **6** and **11**) show one peak in the range of $\delta$ 166.5–167.5 ppm and that of di-substituted compounds (**7**, **8** and **12**) show a peak in the range of $\delta$ 170.1–172.5 ppm for their phosphorus atoms coordinated to Fe atoms of the diiron subunit.

Single crystals of **5**–**7** and **11**, **12** suitable for single crystal X-ray structure analysis, were grown by slow evaporation of respective $CH_2Cl_2$ solutions at room temperature. Single-crystal X-ray diffraction studies were carried out on complexes **5, 6, 11** and **7**, **12** to determine the coordination conformations of the phosphite ligands in the diiron complexes. The crystal structure analyses show that the crystals of complexes **5** and **6** crystallize in monoclinic space groups $P2_1/c$ and complex **11** crystallizes in triclinic space group *P*-1. Compounds **7** and **12** crystallize in monoclinic space groups $P2_1$. While ORTEP diagrams for **5**, **6** and **11** are shown in Fig. 3.6, those of **7** and **12** are presented in Fig. 3.7; their selected bond lengths and angles are presented in Tables 3.3 and 3.4.

As expected, the overall molecular geometries of **5**, **6**, **11** and **7**, **12** are analogous to those of their parent arene dithiolate diiron complexes **1**, **2** and **9**. In the molecular structures of mono-substituted complexes **5**, **6** and **11**, $P(OEt)_3$ is coordinated to an apical site of Fe(2) atom, whereas **7** and **12** affords only one isomer ap/ap, as shown in Fig. 3.7. The crystal structure of complex **8** could not be determined because of the poor quality of the relevant crystals.

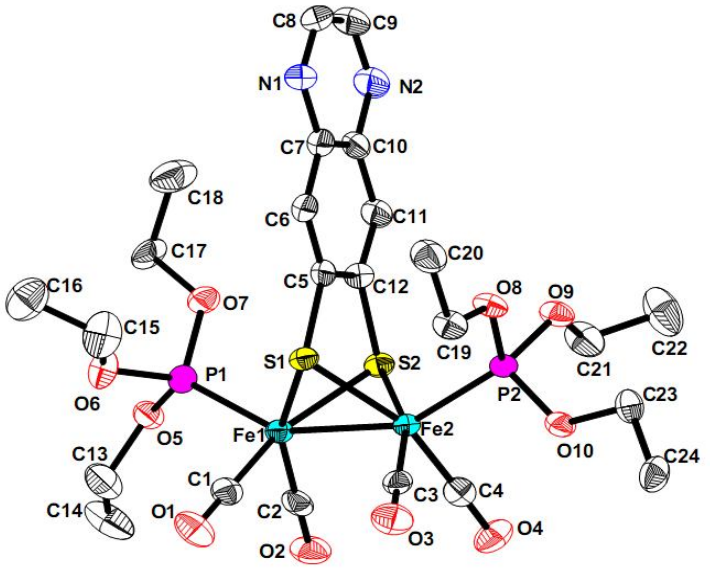


**(a)**

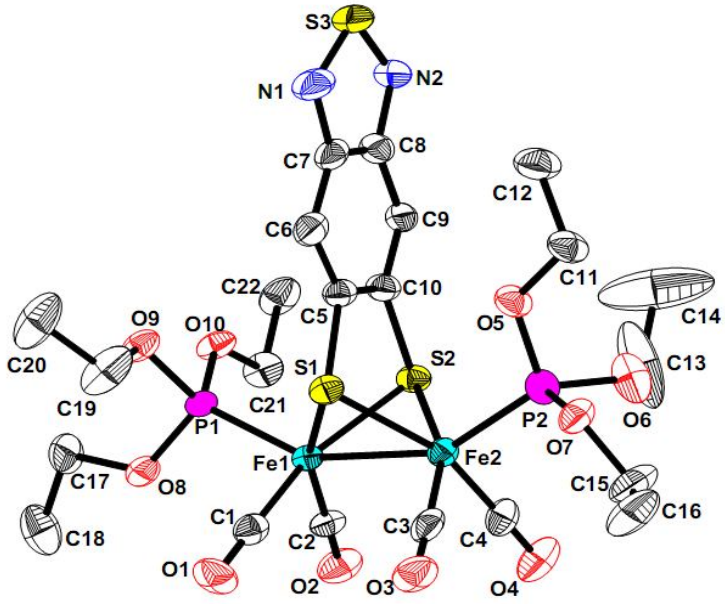


**(b)**

**Fig. 3.7.** Molecular structures of compounds (a) **7** and (b) **12** with thermal ellipsoids at 50% probability (Hydrogen atoms are omitted for clarity).

**Table 3.1.** Selected bond lengths [Å] and angles [°] for complexes **1, 2** and **9.**

| | **1** | **2** | **9** |
|---|---|---|---|
| **Fe(1)-S(1)** | 2.2658(7) | 2.2632(16) | 2.267(2) |
| **Fe(2)-Fe(1)** | 2.4740(5) | 2.4772(11) | 2.490(18) |
| **O(1)-C(1)** | 1.136(3) | 1.128(8) | 1.147(9) |
| **C(9)-N(1)** | 1.366(3) | 1.359(6) | 1.357(8) |
| **Fe(1)-C(1)** | 1.807(3) | 1.801(7) | 1.785(9) |
| **S(1)-Fe(1)-Fe(2)** | 56.96(2) | 56.96(4) | 56.52(6) |
| **S(2)-Fe(1)-Fe(2)** | 56.819(19) | 56.56(4) | 56.60(6) |
| **Fe(1)-S(1)-Fe(2)** | 66.15(2) | 66.28(4) | 66.73(6) |

**Table 3.2.** Selected bond lengths [Å] and angles [°] for complexes **3, 4** and **10.**

| | **3** | **4** | **10** |
|---|---|---|---|
| **Fe(1)-S(1)** | 2.2790(6) | 2.2575(8) | 2.2694(13) |
| **Fe(2)-Fe(1)** | 2.4900(4) | 2.5023(5) | 2.4842(10) |
| **O(1)-C(1)** | 1.136(2) | 1.129(4) | 1.132(6) |
| **C(4)-O(4)** | 1.144(2) | 1.150(3) | 1.139(5) |
| **Fe(2)-P(1)** | 2.2372(6) | 2.2503(8) | 2.2374(12) |
| **P(1)-Fe(2)-S(1)** | 105.85(2) | 100.75(3) | 104.81(5) |
| **S(1)-Fe(1)-Fe(2)** | 56.870(16) | 56.85(2) | 56.89(3) |
| **S(2)-Fe(1)-Fe(2)** | 56.940(15) | 56.53(2) | 57.02(3) |
| **Fe(1)-S(1)-Fe(2)** | 66.237(17) | 67.00(2) | 66.32(4) |

**Table 3.3.** Selected bond lengths [Å] and angles [°] for complexes **5, 6** and **11.**

| | **5** | **6** | **11** |
|---|---|---|---|
| **P(1)-O(7)** | 1.616(3) | 1.600(5) | 1.610(2) |
| **Fe(2)-Fe(1)** | 2.5201(13) | 2.4800(13) | 2.4918(8) |
| **O(1)-C(1)** | 1.148(6) | 1.147(8) | 1.132(4) |
| **C(4)-O(4)** | 1.161(6) | 1.139(5) | 1.136(3) |
| **Fe(2)-P(1)** | 2.2013(16) | 2.1747(19) | 2.1776(10) |
| **P(1)-Fe(2)-S(1)** | 105.18(5) | 99.55(7) | 103.40(3) |
| **S(1)-Fe(1)-Fe(2)** | 56.92(4) | 56.67(5) | 56.56(3) |
| **S(2)-Fe(1)-Fe(2)** | 56.82(4) | 57.04(5) | 56.44(3) |
| **Fe(1)-S(1)-Fe(2)** | 66.01(5) | 66.11(5) | 66.48(3) |

**Table 3.4.** Selected bond lengths [Å] and angles [°] for complexes **7** and **12.**

| | **7** | **12** |
|---|---|---|
| **Fe(1)-S(1)** | 2.2661(12) | 2.2677(10) |
| **Fe(2)-Fe(1)** | 2.4798(8) | 2.4788(7) |
| **O(1)-C(1)** | 1.143(5) | 1.146(4) |
| **C(4)-O(4)** | 1.147(5) | 1.145(4) |
| **Fe(1)-P(1)** | 2.1805(12) | 2.1662(10) |
| **P(1)-Fe(1)-S(2)** | 100.68(4) | 102.02(4) |
| **S(1)-Fe(1)-Fe(2)** | 56.83(3) | 57.04(3) |
| **S(2)-Fe(1)-Fe(2)** | 57.02(3) | 57.03(3) |
| **Fe(1)-S(1)-Fe(2)** | 66.34(3) | 66.16(3) |

*3.2.5. Electrochemistry of model complexes **1– 12***

The electrochemical properties of complexes **1–12** were investigated by cyclic voltammetry (CV) studies in MeCN (with 0.1 M *n*–$Bu_4NClO_4$ as supporting electrolyte, *v* = 0.1 V/s) solution under an atmosphere of Ar. Table 3.5 lists the electrochemical data and Figs. 3.8(a–d) shows the cyclic voltammograms of the complexes **1–12**. They were initiated from the open circuit and scanned in the cathodic direction as indicated in Figs. 3.8a–d. It is shown that complexes **1**, **2** and **9** display one quasi–reversible two electron reduction process at $E_{1/2}$ = –1.23, –1.24 and –1.25 V (*vs.* $Fc^0/Fc^+$) respectively, as shown in Fig. 3.8a. The electrochemical behavior of the complex **A** (Fig. 3.1) was already well–established and it shows that the first reduction potential undergoes a two–electron process

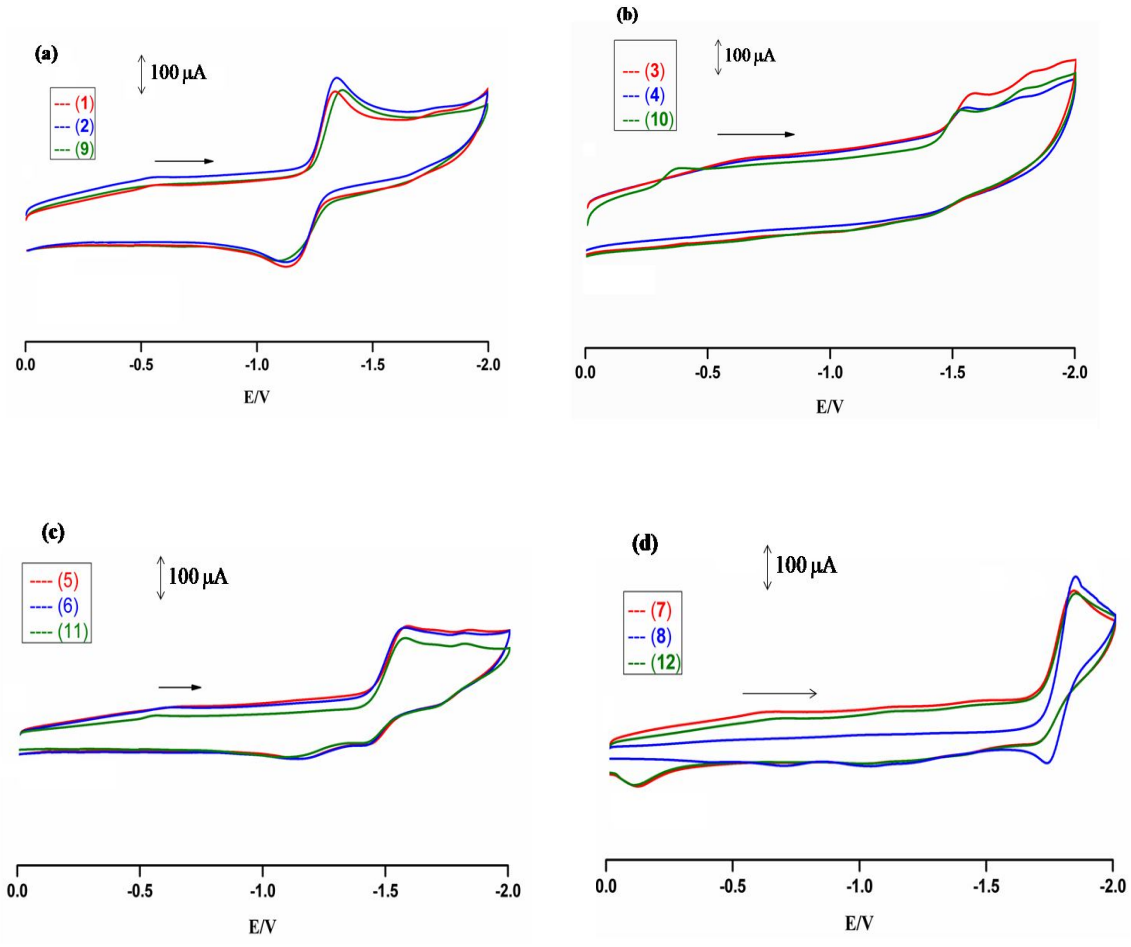


**Fig. 3.8.** Cyclic voltammograms of complexes (a)**1** (red), **2** (blue) and **9** (olive); (b) **3** (red), **4** (blue) and **10** (olive); (c) **5** (red), **6** (blue) and **11** (olive); (d) **7** (red), **8** (blue) and **12** (olive) (1.0 mM) in 0.1 M *n*-$Bu_4NClO_4$/MeCN at a scan rate of 100 $mVs^{-1}$. Potential are *vs.* $Fc^{0/+}$.

that occurs at $E_{1/2}$ = –1.27 V [28,29,30]. This reflects that the present ligand system (*N*–heterocyclic 1,2-ene dithiolates (Scheme 3.1) is of more electron-withdrawing character than benzene dithiolate ($bdt^{2-}$) in complex **A**, thereby, shifting the reduction potentials of complexes **1**, **2** and **9** to relatively more anodic side by 40, 30 and 20 mV, respectively (see Table 3.5) than complex **A** with benzene dithiolate ($bdt^{2-}$) ligand. As a consequence, complexes **1**, **2** and **9** are thermodynamically more facile than that of complex **A** as far as reduction is concerned. The reduction potential of the related model compound, quinoxaline 2,3-dithiol ($H_2$qdt) bridged diiron complex [$Fe_2\{\mu$-qdt$\}(CO)_6$], is comparable ($E_{1/2}$ = –1.22 V) [30, 52] to those of complexes **1**, **2** and **9**. In all these cases, the electron withdrawing nature of the ligands decreases the electron density around the iron centers, making the reduction process easier [30].

The cyclic voltammograms (CVs) of mono-substituted diiron phosphine complexes (**3**, **4** and **10**) and mono- and di-substituted diiron phosphite complexes (**5**, **6**, **11** and **7**, **8**, **12**) were studied to evaluate the effects of different phosphine and phosphite ligands on the redox properties of the parent all-carbonyl diiron complexes **1**, **2** and **9**. In case of mono-phosphine substituted diiron complexes **3**, **4** and **10**, the cyclic voltammograms show two irreversible reduction waves at $E^1_{pc}$ = –1.55 V and $E^2_{pc}$ = –1.85 V for **3**, $E^1_{pc}$ = –1.56 V and $E^2_{pc}$ = –1.80 V for **4**, and $E^1_{pc}$ = –1.56 V and $E^2_{pc}$ = –1.83 V (*vs.* $Fc/Fc^+$) for **10**. The relevant CV plots are shown in Fig. 3.8b. Comparing the current heights of the CVs of compounds **3**, **4** and **10** (Fig. 3.8b) with those of **1**, **2** and **9** (Fig. 3.8a), the two irreversible reductive responses for compounds **3**, **4** and **10** can be described as two one–electron reduction processes. The incorporation of electron-donating phosphine ligand into the $Fe_2S_2$ core in these model complexes makes the reduction of the Fe–Fe site more difficult but the oxidation easier. As a result, first reduction potential ($E^1_{pc}$) of complexes **3**, **4** and **10** shifts to more negative value by 220–180 mV compared to their corresponding hexa- carbonyl parent complexes **1**, **2** and **9** respectively as shown in Fig. 3.8b.

The cyclic voltammograms of mono phosphite substituted di-iron complexes **5**, **6**, **11** feature electrochemical responses of two electron reduction at $E^1_{pc}$ = –1.58 V for **3**, –1.57 V for **4** and –1.60 V for **8**, which show little cathodic shift compared to complexes **3**, **4** and **10** as shown in Fig. 3.8c. In case of di-phosphite substituted complexes **7**, **8** and **12**, introduction of second $P(OEt)_3$ ligand to mono substituted diiron complex increases the

electron density at the iron centers and renders the reduction of the iron core more difficult. Thus complexes **7**, **8** and **12** exhibit electrochemical reductive responses (of two electron reduction) at $E^{1}_{pc}$ = –1.9 V for **7**, –1.82 V for **8** and $E_{1/2}$ = –1.86 V for **12** as shown in Fig. 3.8d. Thus, with the conversion from all carbonyl diiron complexes of mono- and di- substituted $P(OEt)_3$ derivatives, the reduction potentials shift in a more cathodic direction by *ca.* 560, 500 and 510 mV, respectively, as compared to that of the parent complexes **1**, **2** and **9**. This is indicative of a considerable influence of different phosphine and phosphite ligands on the redox properties of all carbonyl parent [FeFe]–model complexes **1**, **2** and **9**.

**Table 3.5.** Voltammetric data (*vs.* $Fc^{0/+}$) for complexes **1–12** in MeCN[a]

| | **1** | **2** | **3** | **4** | **5** | **6** | **7** | **8** | **9** | **10** | **11** | **12** |
|---|---|---|---|---|---|---|---|---|---|---|---|---|
| $E^{1}_{pc}$ **(V)** | –1.34 | –1.34 | –1.55 | –1.56 | –1.58 | –1.57 | –1.9 | –1.84 | –1.35 | –1.56 | –1.6 | –1.86 |
| $E^{2}_{pc}$ **(V)** | – | – | –1.85 | –1.80 | – | – | – | – | – | –1.82 | – | – |
| $E^{1}_{pa}$ **(V)** | –1.12 | –1.13 | – | – | – | – | – | –1.80 | –1.15 | – | – | – |
| $E_{1/2}^{red}$ **(V)** | –1.23 | –1.24 | – | – | – | – | – | –1.82 | –1.25 | – | – | – |

[a]0.1 M *n*-$Bu_4NClO_4$ in $CH_3CN$; scan rate 100 mV $s^{-1}$; working electrode: glassy carbon electrode of diameter 3 mm; reference electrode: non-aqueous $Ag/Ag^+$ electrode (0.01 M $AgNO_3$ in $CH_3CN$); counter electrode: platinum wire.

### *3.2.6. Electrocatalytic hydrogen formation from p-toluenesulfonic acid (p-HOTs)*

The behavior of electrocatalytic proton reductions by compounds **2** and **9–12** was performed by cyclic voltammograms in the presence of a strong acid *p*-toluenesulfonic acid (*p*-HOTs). The $E^{o}_{p\text{-HOTs}}$ for *p*-HOTs is –0.65 V *vs.* $Fc^0/Fc^+$ in acetonitrile [65]. This indicates that the least negative potential of the catalyst, that will allow reduction of *p*-HOTs to dihydrogen, should be more negative than –0.65 V *vs.* $Fc^0/Fc^+$. As described in preceding section, the *E* values obtained from the electrochemical reductive responses of compounds **2** and **9–12** qualify the requirement of reducing *p*-HOTs to dihydrogen.

For compound $[Fe_2\{\mu\text{-diph-6,7-qdt}\}(CO)_6]$ (**2**), upon the addition of 2 mmol of *p*-HOTs, a new peak appeared at $E_{pc}$ = –0.53 V and the current intensity of the reduction at $E_{pc}$ = –1.35 V increased with a cathodic shift by 40 mV. The height of this reduction peak at $E_{pc}$ = –1.35 V continuously grew as the acid concentrations increase from 2–12 mM with final cathodic shift by 260 mV (Fig. 3.9). On the other hand, the current intensity of the anodic shifted peak $E_{pc}$ = –0.53 V (appeared on addition of 2 mmol of *p*-HOTs) did not grow up further with sequential increments of the acid concentrations (4–12 mM).

This observation indicates the protonation of one of the ring nitrogens present in the ligand system of compound **2**. This is supported by electronic absorption spectral changes, occurred on addition of 10–60 $\mu$L *p*-HOTs to the acetonitrile solution of complex **2** is also observed on energies of the IR bands as shown in the FTIR spectrum (Fig. 3.11) of compound **2** solution ($CH_3CN$) treated with *p*-HOTs. As shown in Fig. 3.11, the IR spectrum exhibited significant changes in the carbonyl region. When protonation occurs, there is a considerable shift of the CO bands to higher frequencies (energy) region. The IR peaks at 2076, 2037, 2028, 2003, 1973 $cm^{-1}$ (compound **2**) shift to 2081, 2049, 2012 $cm^{-1}$ on protonation. The N−H bond, formed on protonation, displays a strong and broad

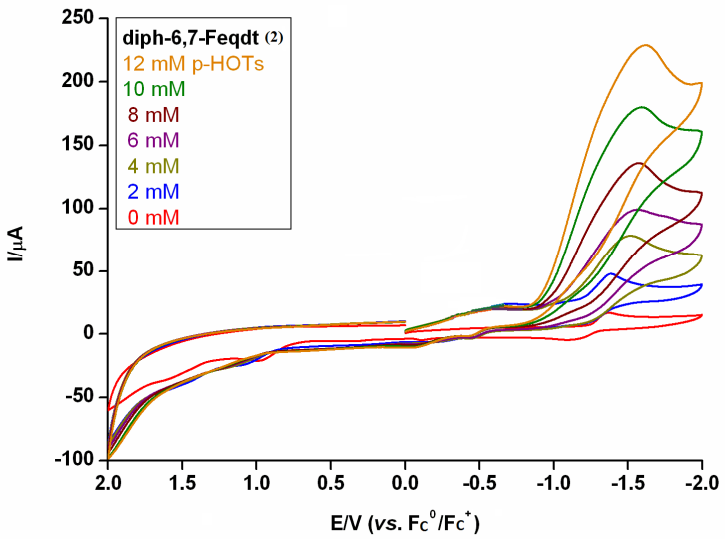


**Fig. 3.9.** Cyclic voltammogram of complex **2** with 1.0 mM complex and 0–12 mM *p*-HOTs in $CH_3CN$ solution (0.1 M *n*-$Bu_4NClO_4$) at a scan rate of 100 mV $s^{-1}$.

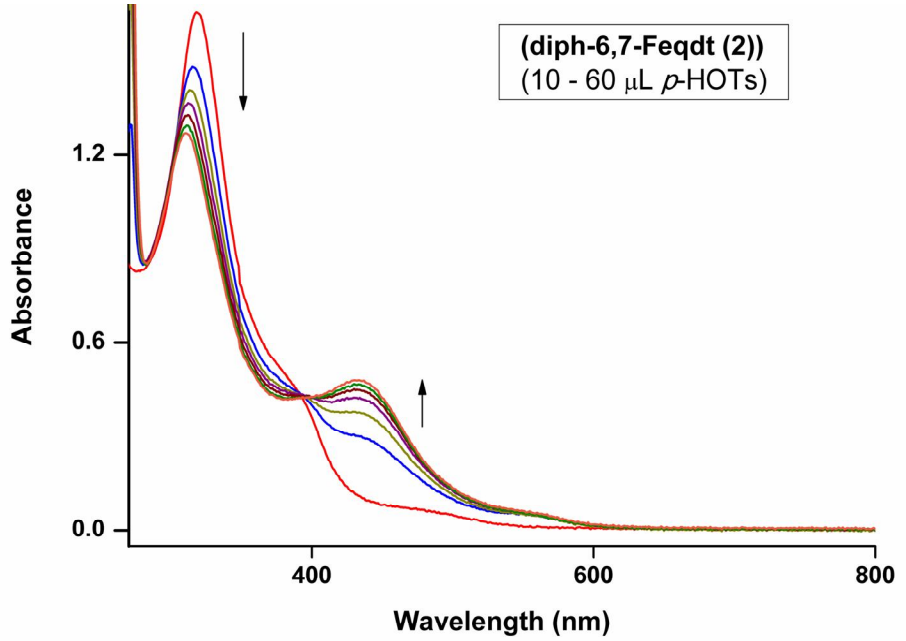


**Fig. 3.10.** Changes in the absorption spectra of compound **2,** (5.0X $10^{-5}$ M) upon the addition of 10 –60 $\mu$L aliquots of dilute *p*–HOTs (0.1mM) in $CH_3CN$.

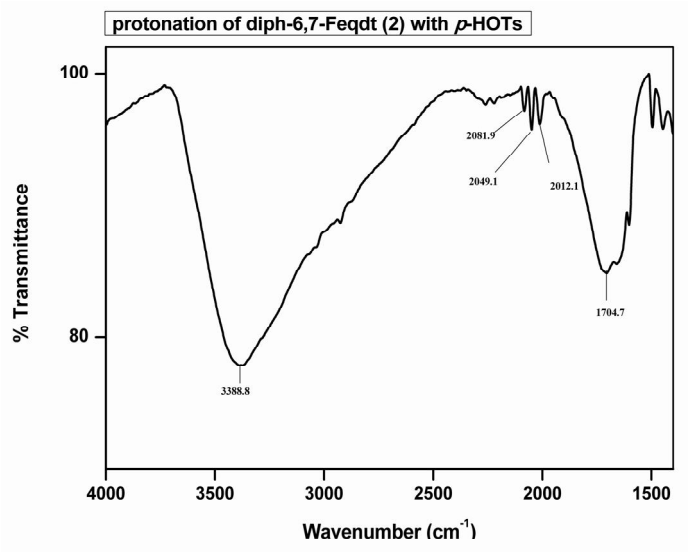


**Fig. 3.11.** FTIR spectrum of acetonitrile solution of compound **2** treated with *p*–HOTs. 5 mg of *p*-HOTs was added to a $CH_3CN$ solution (2 mL) of complex **2** (10 mg).

absorption band at 3388 $cm^{-1}$ region because of N−H stretching vibrations (Fig. 3.11). The continuous growth of the reduction peak at $E_{pc}$ = –1.35 V with final cathodic shift of 260 mV (on addition of 2–12 mM *p*-HOTs) is characteristic of an electrochemical catalytic reduction of *p*-HOTs to hydrogen. The catalyzed reduction of *p*-HOTs occurs at about –1.61 V *vs*. $Fc/Fc^+$ with overpotential of 0.96 V. The cyclic voltammograms (Fig.

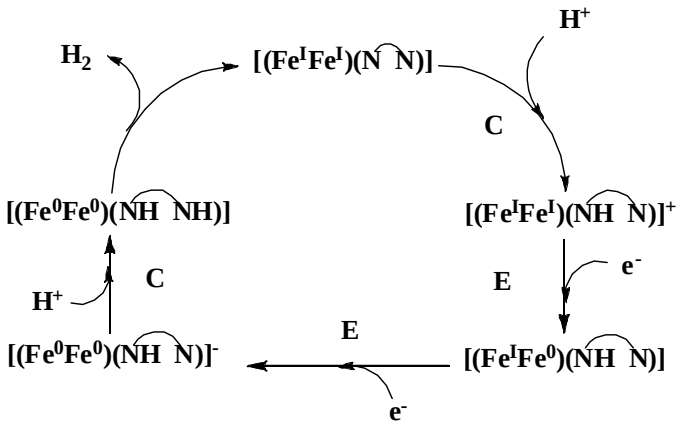


**Fig. 3.12.** A schematic representation of plausible CEEC mechanism for electrocatalytic proton reduction in the presence of *p*–HOTs for compound **2**.

3.9) and the spectroscopic evidences (Fig. 3.10 and 3.11) suggest a CEEC (chemical-electrochemical-electrochemical-chemical) mechanism (Fig. 3.12) for the electrocatalytic proton reduction by diph-6,7-qdt-bridged all-carbonyl $\{Fe^1Fe^1\}$ compound **2**. A possible CECE (chemical-electrochemical-chemical-electrochemical) mechanism can be ruled out by the fact that the catalyzed reduction of *p*-HOTs occurs (present study) with cathodic shift instead of anodic shift; earlier report of the ADT-diiron complex $[\{(\mu\text{-}SCH_2)_2N(4\text{-}NO_2C_6H_4)Fe_2(CO)_6]$ catalyzed acid reduction has been described by a CECE mechanism, for which the catalyzed acid reduction occurs with an anodic shift [66].The hexa carbonyl compound $[Fe_2\{\mu\text{-btdt}\}(CO)_6]$ (**9**) exhibits the electro-catalytic proton reduction with *p*-HOTs as shown in Fig. 3.13. In this case, protonation of oxidized $\{Fe^IFe^I\}$ species does not occur as shown by electronic absorption spectral scans, recorded on addition of 10–60 $\mu$L *p*-HOTs to the acetonitrile solution of complex **9** that do not show any spectral changes (Fig. 3.14). The current height of the reduction potential at $E_{pc}$ = –1.35 V continuously increased with increased acid concentration (2–12 mM *p*-HOTs) with final cathodic shift of 290 mV indicating a catalytic proton reduction. The concerned cyclic voltammograms (Fig. 3.13) and unchanged electronic spectra (Fig. 3.14) on acid addition suggest an EC (electrochemical-chemical) mechanism as shown in Fig. 3.15.

Compounds **[**$Fe_2\{\mu\text{-btdt}\}(CO)_5PPh_3$] (**10**), $[Fe_2\{\mu\text{-btdt}\}(CO)_5P(OEt)_3]$ (**11**) and $[Fe_2\{\mu\text{-btdt}\}(CO)_4\{P(OEt)_3\}_2]$ (**12**) show comparable situation in terms of electro-catalytic proton reduction of *p*-HOTs. Upon the addition of *p*-HOTs, the reduction potential shifts to more anodic side by 300 mV ($E_{pc}$ = –1.24 V for compound **10**), 300 mV ($E_{pc}$ = –1.24 V for compound **11**), 500 mV ($E_{pc}$ = –1.40 V for compound **12**). On further

addition of *p*-HOTs, complexes show a significant electrocatalytic response (current heights of the reductions grew up continuously further towards more cathodic side), with sequential increasing acid concentration (2–12 mM *p*-HOTs) as shown in Figs. 3.16–3.18 respectively. This is the characteristic of proton reduction for hydrogen generation. This anodic shift indicates that the proton is directly attached to the iron center instead of dithiolate N atom; this is because of the more basicity at the iron centers due to the presence of electron donating groups, such as $PPh_3$ and $P(OEt)_3$. But in case of parent all-carbonyl $Fe^{I}Fe^{I}$ model complex **[**$Fe_2\{\mu$-btdt$\}(CO)_6$], the addition of *p*-HOTs shows the shift of the reduction potential towards cathodic side and it shows continuous increase of current height with increasing acid concentration suggesting electrocatalytic proton reduction [67]. The complete distinct electrochemical behavior of the phosphine and phosphite substituted diiron complexes **10**–**12** from their parent btdt bridged all-carbonyl diiron complex **9** is due to the increase the basicity by the incorporation of the electron-donor ligands to iron centers in complexes **10**–**12**. We have not attempted to propose mechanisms for the electrocatalytic reductions described here.

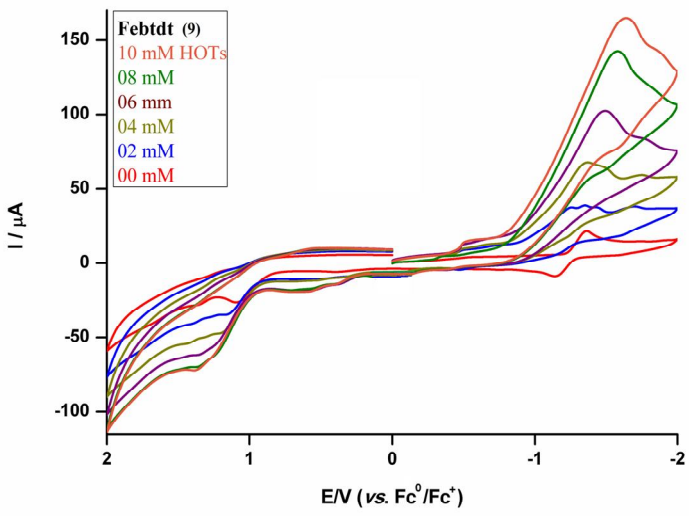


**Fig. 3.13.** Cyclic voltammogram of complex **9** with 1.0 mM complex and 0–10 mM *p*-HOTs in $CH_3CN$ solution (0.1 M *n*-$Bu_4NClO_4$) at a scan rate of 100 mV $s^{-1}$.

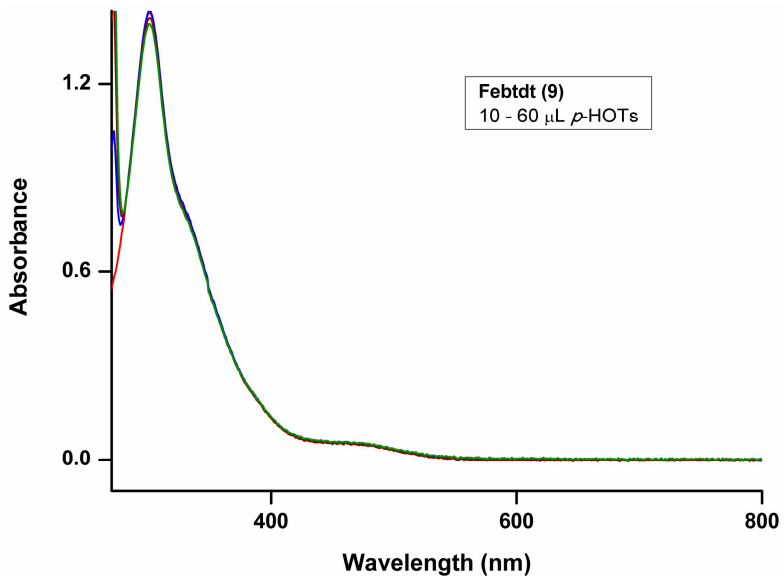


**Fig.3.14.** Changes in the absorption spectra of compound **9,** (5.0X $10^{-5}$ M) upon the addition of 10 –60 $\mu$L aliquots of dilute *p*–HOTs (0.1mM) in $CH_3CN$.

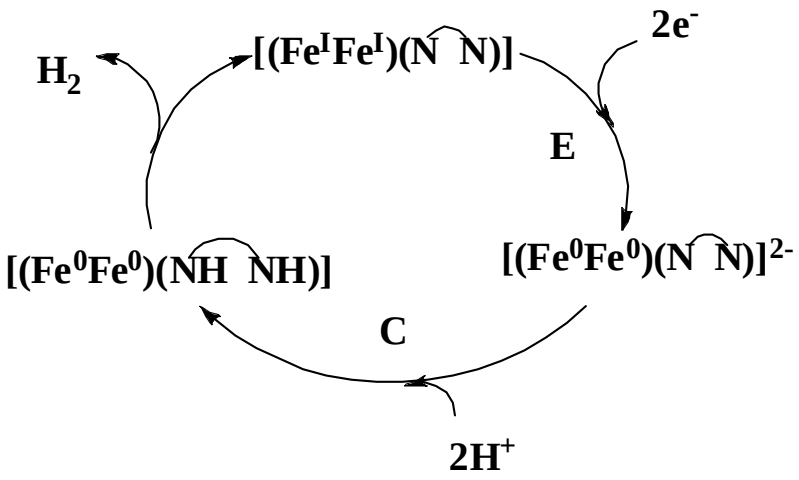


**Fig. 3.15.** A schematic representation of plausible EC mechanism for electrocatalytic proton reduction in the presence of *p*–HOTs for compound **9.**

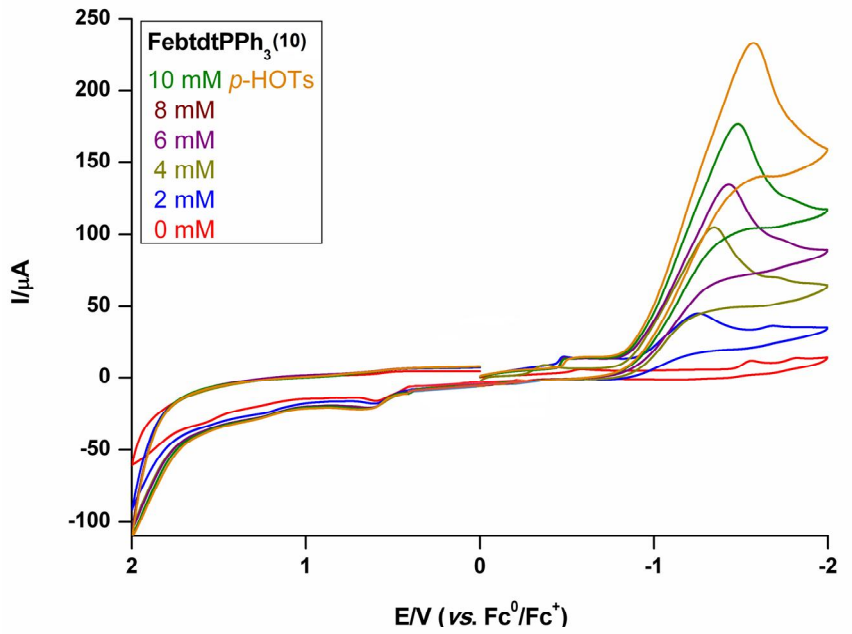


**Fig. 3.16.** Cyclic voltammograms of complex **10** with 1.0 mM complex and 0–12 mM *p*-HOTs in $CH_3CN$ solution (0.1 M *n*-$Bu_4NClO_4$) at a scan rate of 100 mV $s^{-1}$.

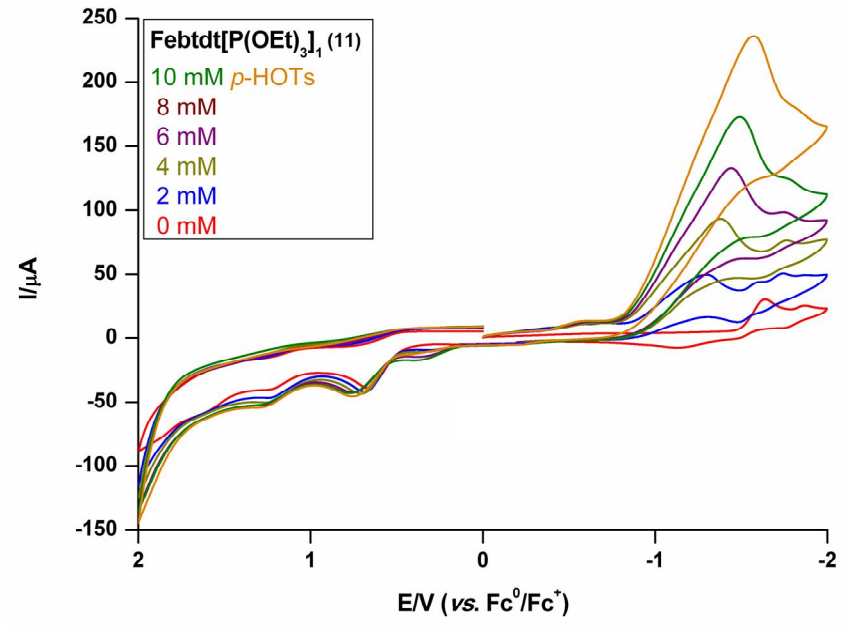


**Fig. 3.17.** Cyclic voltammograms of complex **11** with 1.0 mM complex and 0–12 mM *p*-HOTs in $CH_3CN$ solution (0.1 M *n*-$Bu_4NClO_4$) at a scan rate of 100 mV $s^{-1}$.

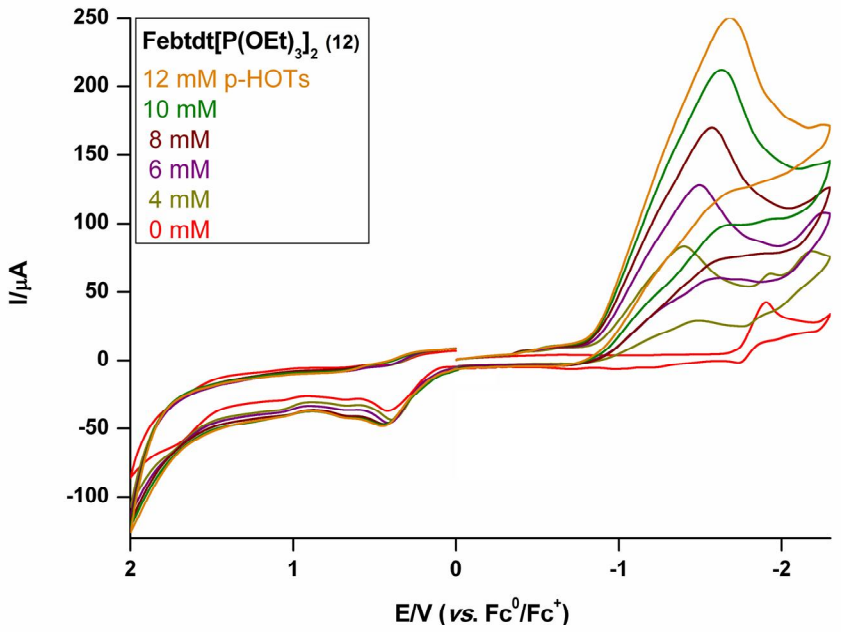


**Fig. 3.18.** Cyclic voltammograms of complex **12** with 1.0 mM complex and 0–12 mM *p*-HOTs in $CH_3CN$ solution (0.1 M *n*-$Bu_4NClO_4$) at a scan rate of 100 mV $s^{-1}$.

## 3.3. EXPERIMENTAL SECTION

### *3.3.1. General procedures*

All the reactions were carried out using standard schlenk and vacuum-line technique under an atmosphere of nitrogen. Dichloromethane was distilled from $CaH_2$, THF from sodium/benzophenone ketyl, and MeOH, EtOH from Mg powder under a $N_2$ atmosphere. 1,2-diamino benzene (from Loba), $Fe_2(CO)_9$ and $Me_3NO$ were purchased from Aldrich and directly used without further purification. Micro analytical (C, H, N) data were obtained with a FLASH EA 1112 series CHNS Analyzer. The IR spectra (with KBr pellet) were recorded in the range of 400–4000 $cm^{-1}$ on a JASCO FT/IR-5300 spectrometer. Electronic spectra were obtained on a Cary 100 Bio UV–Visible spectrophotometer. $^1H$, $^{13}C$ and $^{31}P\{^1H\}$ NMR spectra were recorded on Bruker DRX–400 spectrometer using $Si(CH_3)_4$ (TMS) as an internal standard. Mass spectra were obtained on a BRUKER MAXIS type ESI TOF HRMS spectrometer. Solution mass spectra (LCMS) were obtained on a LCMS–2010A Shimadzu spectrometer.

*3.3.2. Single crystal structure determination of complexes **1–12***

Single crystals suitable for facile structural determination for the compounds **1**–**5**, **7**, **9**, **10**, and **12** were measured on a three circle Bruker SMART APEX CCD, area detector system under [λ (Mo Kα) = 0.7103 Å], graphite monochromator X-ray beam, 2400 frames were recorded with an ω scan width of 0.3°, each for 8 s, crystal-detector distance 60 mm, collimator 0.5 mm. Data reduction performed by SAINTPLUS [68]. Empirical absorption corrections using equivalent reflections performed program SADABS [68]. Crystal data for compounds **6**, **8** and **11** were collected on Oxford, Gemini Diffractometer equipped with EOS CCD detector. Monochromatic Mo Kα radiations (0.71073 Å) were used for the measurements. Absorption corrections using multi Ψ-scans were applied. The structures were solved by direct methods and least-square refinement on $F^2$ for all the compounds 1–12 by using SHELXS-97 [69]. All the non hydrogen atoms were refined anisotropically. Hydrogen atoms on the aromatic rings were introduced on calculated positions and included in the refinement riding on their respective parent atoms. The crystallographic parameters, data collection and structure refinement of the compounds **1–6** and **7, 9**–**12** are summarized in Tables 3.6, 3.7, 3.8 and 3.9, respectively.

*3.3.3. Electrochemical studies of complexes **1–12***

Acetonitrile (Finar, HPLC grade) used for performance of electrochemistry was dried with molecular sieve (4 Å) and then freshly distilled from $CaH_2$ under $N_2$. A solution of 0.1 M $[nBu_4N][ClO_4]$ (TBAP) (Across, electrochemical grade) in $CH_3CN$ was used as supporting electrolyte. Electrochemical measurements were recorded by using a BAS electrochemical analyzer. The electrolyte solution was degassed by bubbling with dry Argon for 10 min. before measurement. Cyclic voltammograms were obtained in a three–electrode cell under argon. The working electrode was a glassy carbon disc (diameter 3 mm) successively polished with 0.3–$\mu$m alumina paste and sonicated in iron–free water for 10 min., ethanol and finally rinsed with acetone, then air dried before usage. The home-built reference electrode was a silver wire in contact with a solution of 0.1 M *n*–$Bu_4NClO_4$ and 0.01 M $AgNO_3$ in acetonitrile. The reference electrode was separated from the contents of the cell by means of a porous Vycor frit. When not in use, the reference electrode assembly was kept immersed in 0.1 M *n*–$Bu_4NClO_4$ / acetonitrile to prevent drying of the frit. The auxiliary electrode was a platinum wire. The potentials, reported here, are quoted against the ferrocene/ferrocenium ($Fc/Fc^+$) couple.

*3.3.4. Preparation of 2,3-diphenyl-6,7-bis-thiocyanato-quinoxaline (B)*

A mixture containing 1,2-diaminobenzene-bis(thiocyanate) (300 mg, 1.35 mmol), benzil (316 mg, 1.50 mmol) and iodine (10 mol%) in $CH_3CN$ (10.0 mL) was stirred for 1 h. The resulting yellow precipitate was separated by filtration, washed with little $CH_3CN$, and dried in *vaccuo*. Yield: 0.45 g (84.0%); Yellow solid; LC–MS: *m/z* = 395 $[M–H]^+$. IR (KBr pellet, $cm^{-1}$): 3067(C–H Str, Ar), 2160 (C≡N str), 1653, 1597, 1537, 1435, 1390, 1338, 1253, 1194, 1057, 1022, 952, 893, 871, 769, 723, 698, 597, 543, 493. $^1$H NMR (400 MHz, $CDCl_3$) $\delta$: 8.66 (s, 2H), 7.55 (d, 4H), 7.36-7.46 (m, 6H) ppm. $^{13}$C NMR ($CDCl_3$): $\delta$ 156.32, 141.47, 137.75, 134.35, 129.95, 129.88, 128.53, 126.72, 107.91 ppm. Anal. Calc. for $C_{22}H_{12}N_4S_2$: C, 66.64; H, 3.05; N, 14.13%. Found: C, 66.48; H, 3.14; N, 14.25%.

*3.3.5. Preparation of 2,3-diphenyl-quinoxaline-6,7-dithiol ($H_2$diph-6,7-qdt)*

2,3-diphenyl-6,7-bis-thiocyanato-quinoxaline (0.3 g, 0.757 mmol) was added as a solid to a solution of $Na_2S$ (0.3 g, 3.85 mmol) in 100 mL of degassed water and the mixture was heated to 70–80 °C for 24 h to produce a clear, orange-red solution. The mixture was cooled to room temperature, and 20 mL of 10% HCl was added drop-wise to afford a heavy, brown precipitate. The precipitate was filtered off, washed with water, and air-dried. Thus dithiol ligand **$L_2$** is obtained. Yield: 0.180 g (68.6%). LC–MS: *m/z* = 347 $[M–H]^+$. IR (KBr pellet, $cm^{-1}$): 3057 (C–H Str, Ar), 2530 (S–H str), 1581, 1533, 1433, 1388, 1338, 1253, 1188, 1059, 1022, 960, 869, 765, 727, 694, 596, 543. $^{13}$C NMR (DMSO-$d^6$): $\delta$ 145.2, 140, 136.5, 134, 131.0, 129, 128.5, 127.0 ppm. Anal. Calc. for $C_{20}H_{14}N_2S_2$: C, 69.33; H, 4.07; N, 8.09%. Found: C, 69.86; H, 3.92; N, 7.82%.

**$[Fe_2\{\mu$-6,7-qdt$\}(CO)_6]$ (1).** A mixture of $Fe_2(CO)_9$ (0.9 g, 2.474 mmol) and $H_2$6,7-qdt (0.48 g, 2.474 mmol) was refluxed in THF (25 mL) for 3 h to give a blood red solution containing some black solid in suspension. The mixture was filtered, and the solvent was removed under the reduced pressure, the residue was subjected to column chromatography by using hexane/$CH_2Cl_2$ (4:1 v/v) as eluents. The major red band was obtained as a red solid. Yield: 0.3 g (25.6% based on thiol). It was recrystallized by cooling at –10 °C. LC–MS: *m/z* = 473.0 $[M + H]^+$. IR (KBr pellet, $cm^{-1}$): 2945(m), 1541(m), 760(vs) $\nu_{(C\equiv O)}$ 2072(s), 2028(s), 2008(s), 1993(s), 1973(s). $^1$H NMR (400 MHz, $CDCl_3$) $\delta$: 8.66 (s, 2H), 7.86 (s, 2H) ppm. $^{13}$C NMR ($CDCl_3$, $\delta$): 207.0, 148.3, 145.8, 142.0, 128.2 ppm. Anal.

Calc. for $C_{14}H_4Fe_2N_2O_6S_2$: C, 35.62; H, 0.85; N, 5.93%. Found: C, 35.55; H, 0.87; N, 6.05%.

**[$Fe_2$\{$\mu$-diph-6,7-qdt\}$(CO)_6$] (2).** A mixture of $Fe_2(CO)_9$ (0.902 g, 2.482 mmol) and $H_2$diph-6,7-qdt (0.860 g, 2.482 mmol) was refluxed in THF (25 mL) for 3 h and followed same procedure for the preparation of **1.** The residue was subjected to column chromatography by using hexane/$CH_2Cl_2$ (4:1 v/v) as eluents. It was recrystallized by cooling at –10 °C. Yield: 0.5 g, (33% based on thiol). IR (KBr pellet, $cm^{-1}$): 2950(m), 1550(m), 765(vs) $\nu_{(C\equiv O)}$ 2076(s), 2037(s), 2028(s), 2003(s), 1973(s). $^1$H NMR (400 MHz, $CDCl_3$) $\delta$: 7.94 (s, 2H), 7.43–7.29 (m, 10H) ppm. $^{13}$C NMR ($CDCl_3$, $\delta$): 207.0, 147.8, 140.07, 138.3, 129.6, 129.1, 128.3, 128.0 ppm. Anal. Calc. for $C_{26}H_{12}Fe_2N_2O_6S_2$: C, 50.03; H, 1.93; N, 4.48%. Found: C, 50.12; H, 2.05; N, 4.38%.

**[$Fe_2$\{$\mu$-btdt\}$(CO)_6$] (3).** A mixture of $Fe_2(CO)_9$ (0.91 g, 2.5mmol) and $H_2$btdt (0.5 g, 2.5 mmol) was refluxed in THF (25 mL) for 3 h and followed same procedure as discussed for the preparation of **1.** It was recrystallized by cooling at –10 °C. Yield: 0.3 g, (25.1% based on thiol). LC–MS: *m/z* = 479.3 $[M + H]^+$. IR (KBr pellet, $cm^{-1}$): 2964(m), 2928(m), 1649(m), 1506(m), 1425(m), 1261(m), 1095(m), 850(m), 760(vs), $\nu_{(C\equiv O)}$ 2075(s), 2038(s), 2007(s), 1983(s). $^1$H NMR (400 MHz, $CDCl_3$) $\delta$: 7.85 (s, 2H) ppm. $^{13}$C NMR ($CDCl_3$, $\delta$): 206.9, 153.7, 147.7, 120.2 ppm. Anal. Calc. for $C_{12}H_2Fe_2N_2O_6S_3$: C, 30.15; H, 0.42; N, 5.86%. Found: C, 30.21; H, 0.48; N, 5.76%.

*3.3.6. Protonation experiment*

5 mg of *p*-HOTs was added to a solution of complex **2** (10 mg) in $CH_3CN$ (2 mL). The solution was stirred for 5 min. The red solution turned into dark red. This dark red solution was then subjected to FTIR studies. As expected, the IR spectrum exhibited significant changes in the carbonyl region (*vide supra*).

*3.3.7. A general synthetic procedure for complexes **3**, **4** and **10***

One portion of decarbonylating agent $Me_3NO$ (0.016 g, 0.2118 mmol) was added to a solution of 0.2118 mmol of compound [$Fe_2$\{$\mu$-L\}$(CO)_6$] (L = 6,7-qdt, diph-6,7-qdt and btdt, for **3**, **4** and **10** respectively) in MeCN (10 mL) under $N_2$. The mixture was stirred for 15 min, whereby color turned to dark red and triphenylphosphine ligand $PPh_3$ (55.4 mg, 0.2118 mmol) was subsequently added. After 30 min, the volatiles were removed *in*

*vacuo*. The resulting respective solids (**3**, **4** and **10**) were purified by column chromatography on silica gel with hexane/$CH_2Cl_2$ (7:3 v/v) as gradient eluents. The analytically pure red powders are collected from the red band after removal of solvent. The analytical data for **3**, **4** and **10** are given below:

**[$Fe_2$\{$\mu$-6,7-qdt\}$(CO)_5PPh_3$] (3).** Yield: 0.075 g, (50.1%). Single crystals, suitable for X–ray analysis, were obtained by cooling of the $CH_2Cl_2$ solution at –10 $^0$C. IR (KBr pellet, $cm^{-1}$): 2964(m), 1479(m), 1433(m), 1261(m), 1093(m), 800(m), 690(s) $\nu_{(C\equiv O)}$ 2040(s), 1993(s), 1973(s), 1962(s), 1943(s). $^1$H NMR (400 MHz, $CDCl_3$) $\delta$: 7.29 –7.66 (m, 19H) ppm; $^{13}$C NMR ($CDCl_3$, $\delta$): 213.5, 208.7, 149.4, 144.7, 141.6, 135.2, 134.8, 133.1, 133.0, 132.0, 130.1, 128.4, 128.3, 127.4 ppm. $^{31}$P NMR ($CDCl_3$, $\delta$): 60.75 ppm. ESI-MS: *m/z* 706.9173 $[M+1]^+$. Anal. Calcd for $C_{31}H_{19}Fe_2N_2O_5PS_2$: C, 52.72; H, 2.71; N, 3.96%. Found: C, 52.63; H, 2.75; N, 3.85%.

**[$Fe_2$\{$\mu$-diph-6,7-qdt\}$(CO)_5PPh_3$] (4).** Yield: 0.106 g, (58.2%). Single crystals, suitable for X-ray analysis, were obtained by cooling of the $CH_2Cl_2$ solution at –10 $^0$C. IR (KBr pellet, $cm^{-1}$): 2964(m), 2950(m), 1550(m), 1479(m), 1433(m), 1261(m), 1093(m), 800(m), 765(vs), 690(s), $\nu_{(C\equiv O)}$ 2050(s), 1997(s), 1978(s), 1943(s). $^1$H NMR (400 MHz, $CDCl_3$) $\delta$: 7.32–7.62 (m, 27H) ppm; $^{13}$C NMR ($CDCl_3$, $\delta$): 213.56, 208.84, 153.2, 148.9, 139.6, 138.6, 135.3, 134.9, 133.2, 133.1, 132.1, 130.09, 129.60, 128.93, 128.45, 128.43, 128.32, 127.29 ppm. $^{31}$P NMR ($CDCl_3$, $\delta$): 61.08 ppm. ESI-MS: *m/z* 858.9797 $[M+1]^+$, 880.9595 $[M+Na]^+$. Anal. Calcd for $C_{43}H_{27}Fe_2N_2O_5PS_2$: C, 60.16; H, 3.17; N, 3.26%. Found: C, 60.28; H, 3.09; N, 3.38%.

**[$Fe_2$\{$\mu$-btdt\}$(CO)_5$ $PPh_3$] (10).** Yield: 0.075 g, (47.8%). Single crystals, suitable for X–ray analysis, were obtained by cooling of the $CH_2Cl_2$ solution at –10 °C. IR (KBr pellet, $cm^{-1}$): 3059(m), 1477(m), 1431(m), 1261(m), 1091(m), 844(m), 812(m), 744(vs), $\nu_{(C\equiv O)}$ 2047(s), 1990(m), 1979(s), 1940(s). $^1$H NMR (400 MHz, $CDCl_3$) $\delta$: 7.46–7.23 (m, 17H) ppm; $^{13}$C NMR ($CDCl_3$, $\delta$): 213.5, 208.7, 153.5, 148.8, 135.1, 134.7, 133.1, 133.0, 130.1, 128.4, 128.3, 119.4 ppm. $^{31}$P NMR ($CDCl_3$, $\delta$): 60.4 ppm. ESI-MS: *m/z* 712.9 $[M+1]^+$, 734.8 $[M+Na]^+$. Anal. Calcd for $C_{29}H_{17}Fe_2N_2O_5PS_3$: C, 48.90; H, 2.40; N, 3.93%. Found: C, 48.79; H, 2.44; N, 4.13%.

*3.3.8. A general synthetic procedure for complexes **5**, **6** and **11***

The equimolar (0.642 mmol) amount of $[Fe_2\{\mu\text{-}6,7\text{-qdt}\}(CO)_6]$ (0.303 g) for compound **5**, $[Fe_2\{\mu\text{-diph-}6,7\text{-qdt}\}(CO)_6]$ (0.4 g) for compound **6** and $[Fe_2\{\mu\text{-btdt}\}(CO)_6]$ (0.3 g) for compound **11** with $P(OEt)_3$ (0.11 mL, 0.642 mmol) was refluxed in $CH_3CN$ (14 mL) for 3 h to give a dark red solution; the solvent was removed under the reduced pressure and the residue was subjected to column chromatography by using hexane/EtOAc (3:2 v/v) as eluents. From the major red band we obtained red solids of respective compounds **5, 6** and **11**. Their analytical data are given below.

**$[Fe_2\{\mu\text{-}6,7\text{-qdt}\}(CO)_5P(OEt)_3]$ (5).** Yield: 0.13 g, (33.1%). It was recrystallized by slow evaporation of $CH_2Cl_2$ solution at room temperature. IR (KBr pellet, $cm^{-1}$): 2964(m), 1479(m), 1433(m), 1261(m), 1093(m), 800(m), 690(s) $\nu_{(C\equiv O)}$ 2048(s), 1979(s), 1959(s), 1940(s). $^1H$ NMR (400 MHz, $CDCl_3$) $\delta$: 8.58 (s, 2H), 7.76 (s, 2H), 4.07 (q, $J$ = 6.8 Hz, 6H), 1.24 (t, $J$ = 6.4 Hz, 9H) ppm; $^{13}C$ NMR ($CDCl_3$, $\delta$): 212.1, 208.9, 151.3, 145.0, 142.0, 127.0, 61.5, 16.0 ppm. $^{31}P$ NMR ($CDCl_3$, $\delta$): 166.7 ppm. ESI-MS: *m/z* 610.9019 $[M+1]^+$, 632.8833 $[M+Na]^+$. Anal. Calcd for $C_{19}H_{19}Fe_2N_2O_8PS_2$: C, 37.40; H, 3.13; N, 4.59%. Found: C, 37.54; H, 3.18; N, 4.64%.

**$[Fe_2\{\mu\text{-diph-}6,7\text{-qdt}\}(CO)_5P(OEt)_3]$ (6).** Yield: 0.16 g, (32.6%) It was recrystallized by slow evaporation of $CH_2Cl_2$ solution at room temperature. IR (KBr pellet, $cm^{-1}$): 2964(m), 2950(m), 1550(m), 1479(m), 1433(m), 1261(m), 1093(m), 800(m), 765(vs), 690(s), $\nu_{(C\equiv O)}$ 2050(s), 2029(s), 2002(s), 1990(s), 1970(s), 1954(s). $^1H$ NMR (400 MHz, $CDCl_3$) $\delta$: 7.85 (s, 2H), 7.41–7.28 (m, 10H), 4.10 (q, $J$ = 6.8 Hz, 6H), 1.29 (t, $J$ = 6.8 Hz, 9H) ppm; $^{13}C$ NMR ($CDCl_3$, $\delta$): 212.1, 209.0, 153.6, 150.7, 140.0, 138.6, 129.6, 128.8, 128.2, 126.8, 61.5, 16.0 ppm. $^{31}P$ NMR ($CDCl_3$, $\delta$): 167.5 ppm. ESI-MS: *m/z* 762.9645 $[M+1]^+$. Anal. Calcd for $C_{31}H_{27}Fe_2N_2O_8PS_2$: C, 48.84; H, 3.57; N, 3.67%. Found: C, 48.35; H, 3.52; N, 3.61%.

**$[Fe_2\{\mu\text{-btdt}\}(CO)_5$ $P(OEt)_3]$ (11).** Yield: 0.13 g, (32.8%). It was recrystallized by slow evaporation of $CH_2Cl_2$ solution at room temperature. IR (KBr pellet, $cm^{-1}$): 3518(m), 2982(m), 1425(m), 1385(m), 1153(m), 1020(m), 947(m), 814(m), 783(m), 620(s) $\nu_{(C\equiv O)}$ 2048(s), 1978(s), 1996(s), 1951(s). $^1H$ NMR (400 MHz, $CDCl_3$) $\delta$: 7.74 (s, 2H), 4.06 (q, $J$ = 4.0 Hz, 6H), 1.25 (t, $J$ = 4.0 Hz, 9H) ppm; $^{13}C$ NMR ($CDCl_3$, $\delta$): 212.01, 208.86, 153.9,

150.71, 118.81, 61.58, 16.0 ppm. $^{31}$P NMR ($CDCl_3$, $\delta$): 166.4 ppm. ESI-MS: *m/z* 616.8651 $[M+1]^+$, 638.8464 $[M+Na]^+$. Anal. Calcd for $C_{17}H_{17}Fe_2N_2O_8PS_3$: C, 33.13; H, 2.78; N, 4.58%. Found: C, 33.25; H, 2.71; N, 4.48%.

*3.3.9. A general synthetic procedure for complexes **7**, **8** and **12***

The excess amount of $P(OEt)_3$ (0.4237 mmol) was added to the $CH_3CN$ solution (15 mL) $[Fe_2\{\mu\text{-}6,7\text{-qdt}\}(CO)_6]$ (0.2 g for compound **7**), $[Fe_2\{\mu\text{-diph-}6,7\text{-qdt}\}(CO)_6]$ (0.264 g for compound **8**), and $[Fe_2\{\mu\text{-btdt}\}(CO)_6]$ (0.203 g for compound **12**); it was refluxed for 3 h to give a dark red solution and the solvent was removed under the reduced pressure. The residue was subjected to column chromatography by using hexane/EtOAc (2:3 v/v) as eluents. From the major red band we obtained red solid of respective compounds **7, 8** and **12**. Their analytical data are provided below.

**$[Fe_2\{\mu\text{-}6,7\text{-qdt}\}(CO)_4\{P(OEt)_3\}_2]$ (7).** Yield: 0.16 g (50.4%). It was recrystallized by slow evaporation of $CH_2Cl_2$ solution at room temperature. IR (KBr pellet, $cm^{-1}$): 2964(m), 1479(m), 1433(m), 1261(m), 1093(m), 800(m), 690(s) $\nu_{(C\equiv O)}$ 2003(s), 1944(s), 1924(s). $^1$H NMR (400 MHz, $CDCl_3$) $\delta$: 8.51 (s, 2H), 7.66 (s, 2H), 4.09 (q, $J$ = 6.4 Hz, 12H), 1.27 (t, $J$ = 6.4 Hz, 18H) ppm; $^{13}$C NMR ($CDCl_3$, $\delta$): 213.8, 153.5, 144.0, 142.0, 126.1, 60.8, 16.0 ppm. $^{31}$P NMR ($CDCl_3$, $\delta$): 170.2 ppm. ESI-MS: *m/z* 748.9829 $[M+1]^+$. Anal. Calcd for $C_{24}H_{34}Fe_2N_2O_{10}P_2S_2$: C, 38.52; H, 4.57; N, 3.74%. Found: C, 38.45; H, 4.61; N, 3.65%.

**$[Fe_2\{\mu\text{-diph-}6,7\text{-qdt}\}(CO)_4\{P(OEt)_3\}_2]$ (8).** Yield: 0.23 g (60.1%). It was recrystallized by slow evaporation of $CH_2Cl_2$ solution at room temperature. IR (KBr pellet, $cm^{-1}$): 2984(m), 2965(m), 1550(m), 1464(m), 1426(m), 1261(m), 1093(m), 800(m), 765(vs), 689(s), $\nu_{(C\equiv O)}$ 2035(m), 2004(s), 1971(s) 1941(s), 1915(s). $^1$H NMR (400 MHz, $CDCl_3$) $\delta$: 7.77 (s, 2H), 7.39–7.28 (m, 10H), 4.09 (q, $J$ = 6.4 Hz, 12H), 1.27 (t, $J$ = 6.8 Hz, 18H) ppm; $^{13}$C NMR ($CDCl_3$, $\delta$): 214.12, 153.0, 140.1, 138.8, 129.6, 128.6, 128.2, 126.0, 60.8, 16.1 ppm. $^{31}$P NMR ($CDCl_3$, $\delta$): 171.2 ppm. ESI-MS: *m/z* 901.0455 $[M+1]^+$. Anal. Calcd for $C_{36}H_{42}Fe_2N_2O_{10}P_2S_2$: C, 48.02; H, 4.70; N, 3.11%. Found: C, 48.15; H, 4.65; N, 3.21%.

**$[Fe_2\{\mu\text{-btdt}\}(CO)_4\{P(OEt)_3\}_2]$ (12).** Yield: 0.18 g (56.3%). It was recrystallized by slow evaporation of $CH_2Cl_2$ solution at room temperature. IR (KBr pellet, $cm^{-1}$): 3435(w), 2982(m), 1442(m), 1388(m), 1261(m), 1244(m), 1157(m), 1018(m), 945(m), 858(m),

781(m), 634(s) $\nu_{(C\equiv O)}$ 2033(s), 2004(s), 1949(s), 1926(w). $^1$H NMR (400 MHz, $CDCl_3$) $\delta$: 7.64 (s, 2H), 4.05 (q, $J$ = 4.0 Hz, 12H), 1.21 (t, $J$ = 4.0 Hz, 18H) ppm; $^{13}$C NMR ($CDCl_3$, $\delta$): 213.83, 154.09, 153.12, 117.94, 60.8, 16.0 ppm. $^{31}$P NMR ($CDCl_3$, $\delta$): 170.2 ppm. ESI-MS: *m/z* 754.9430 $[M+1]^+$, 776.9192 $[M+Na]^+$. Anal. Calcd for $C_{22}H_{32}Fe_2N_2O_{10}P_2S_3$: C, 35.03; H, 4.27; N, 3.71%. Found: C, 35.12; H, 4.21; N, 3.65%.

## 3.4. Conclusion

We have described the synthesis, characterization and electrochemistry of three *N*-heterocyclic cis-1,2 dithiolato bridged di-iron complexes as potential models for the active sites of the [FeFe] hydrogenase. *N*-heterocyclic cis-1,2 dithiols belong to an important ligand system as far as the active sites of many metalloenzymes are concerned. Molybdopterin, a well characterized co-factor associated the active sites molybdenum hydroxylases, contains *N*-heterocyclic cis-1,2 dithiol as a ligand coordinated to the metal center and this class of enzymes catalyses many essential oxidation –reduction reactions. It was proposed that cis-1,2 dithiolato (non-innocent) ligand plays an important role in these red-ox / electron transfer reactions. The metallo-enzyme of the present context, iron only hydrogenase is also known as an important redox enzyme catalyzing an acid to dihydrogen. Therefore, complexes that contains *N*-heterocyclic cis-1,2 dithiolato bridged di-iron centers would serve as potential models for iron only hydrogenases. Even through, the number of reports of modeling the active sites of iron only hydrogenases is not anymore limited, the number of di-iron model systems that contains bridged *N*-heterocyclic cis-1,2 dithiolato ligand is very limited.

All three model complexes **1**–**12**, reported in the present study, are *N*-heterocyclic cis-1,2 dithiolato bridged di-iron complexes. Interestingly, out of 12, three all carbonyl complexes **1**, **2** and **9** display one quasi–reversible two electron reduction at relatively very low potentials ($E_{1/2}$ = –1.23, –1.24 and –1.25 V *vs*. $Fc/Fc^+$ for **1**, **2** and **9** respectively) compared to other related model compounds. We have demonstrated the electrocatalytic proton reduction of a strong acid *p*-toluenesulfonic acid mediated by compounds **2** and **9**. For the electro-catalytic proton reduction by the all carbonyl compound $[Fe_2\{\mu\text{-diph-6,7-qdt}\}(CO)_6]$ (**2**), we have proposed CEEC mechanism. The hexa carbonyl compound $[Fe_2\{\mu\text{-btdt}\}(CO)_6]$ (**9**) does not undergo protonation with *p*-toluenesulfonic acid in its $\{Fe^IFe^I\}$ oxidation state, probably due to the involvement / delocalization of lone pair of

electrons of ring nitrogen with ring sulfur pi-electrons. Accordingly an EC electrocatalytic reduction mechanism is proposed for compound **9**.

For continuation of our work, we have attempted to alter the electron density at the iron centers and thereby to demonstrate the change in catalytic activity. IR spectroscopic, crystallographic and electrochemical investigations show that bridging dithiolate ligands (bdt, pdt and adt) play an important role on diiron complexes. If we compare the aromatic dithiolate (bdt)-bridged diiron complex (complex A in Fig. 1) with aliphatic dithiolate (such as, pdt, propane 1,3-dithiolate)- bridged diiron complex, the delocalization of the electron density into the aromatic dithiolate ligands (for example, in system **A** in Fig. 1) lowers the electron density at the iron centers (in the case of aromatic system A in Fig. 1 and present work) resulting in lowering the basicity of the diiron core. Because of lowering the basicity, it decreases the extent of protonation and thereby reduces the catalytic activity.

In the present study, in order to increase the basicity of 2Fe2S core through the substitution of CO ligands with $PPh_3$ or $P(OEt)_3$, we synthesized compounds **3**–**8** and **10–12**. The shifts in the infrared carbonyl stretching frequencies and in the reduction potentials of complexes **3**–**8** and **10–12** indicates the increase in electron density at the 2Fe2S core. We have demonstrated that the newly synthesized complexes **10–12** successfully electro-catalyze the reduction of *p*-HOTs to $H_2$.

**Table 3.6.** Crystal data and structural refinement for complexes **1**, **2** and **9**

| | **1** | **2** | **9** |
|---|---|---|---|
| Empirical formula | $C_{14}H_4Fe_2N_2O_6S_2$ | $C_{27}H_{14}Fe_2N_2O_6S_2Cl_2$ | $C_{12}H_2Fe_2N_2O_6S_3$ |
| Formula weight | 472.01 | 709.12 | 478.04 |
| Temperature (K) | 298(2) | 100(2) | 298(2) |
| Crystal size (mm) | 0.24 x 0.18 x 0.04 | 0.50 x 0.42 x 0.38 | 0.33 x 0.25 x 0.19 |
| Crystal system | Monoclinic | Monoclinic | Monoclinic |
| Space group | $P2_1/c$ | $C2/c$ | $P2_1/c$ |
| Z | 4 | 8 | 4 |
| Wavelength (Å) | 0.71073 | 0.71073 | 0.71073 |
| *a* [Å] | 18.0645(13) | 36.976(6) | 22.247(8) |
| *b* [Å] | 6.8573(5) | 7.5657 (11) | 6.877(3) |
| *c* [Å] | 13.2585(10) | 25.353(4) | 14.146(5) |
| α (°) | 90.0 | 90.0 | 90.0 |
| β [°] | 96.8580(10) | 124.119(5) | 94.152(7) |
| γ (°) | 90.0 | 90.0 | 90.0 |
| Volume [$Å^3$] | 1630.6(2) | 5871.8(15) | 2151.7(14) |
| Calculated density ($Mg/m^{-3}$) | 1.923 | 1.604 | 1.472 |
| Reflections collected/ unique | 6956/3139 | 23565/5175 | 19265/3741 |
| R(int) | 0.0228 | 0.0511 | 0.1160 |
| F(000) | 936 | 2848 | 944 |
| Max. and min. transmission | 0.9217 and0.6363 | 0.6268 and0.5504 | 0.7434 and 0.6105 |
| Θ range for data collection (°) | 1.14 to 25.98 | 1.33 to 25.06 | 1.84 to 24.98 |
| Refinement method | Full-matrix Least -squares on $F^2$ | Full-matrix Least -squares on $F^2$ | Full-matrix Least -squares on $F^2$ |
| Data / restraints /parameters | 3139 / 0 / 235 | 5175/0/370 | 3741/0/226 |
| Goodness-of-fit on $F^2$ | 1.053 | 1.069 | 1.037 |
| $R_1/wR_2$ [I>2sigma(I)] | 0.0313 / 0.0764 | 0.0647 / 0.01567 | 0.0746/0.1559 |
| $R_1/wR_2$ (all data) | 0.0353 /0.0785 | 0.0789 / 0.1655 | 0.1372/0.1782 |
| Largest diff. peak and hole [$e.Å^{-3}$] | 0.531 and-0.319 | 1.193 and-0.952 | 0.652 and -0.513 |

**Table 3.7.** Crystal Data and Structural Refinement for Complexes **3–5**

| | **3** | **4** | **5** |
|---|---|---|---|
| Empirical formula | $C_{31}H_{19}Fe_2N_2O_5PS_2$ | $C_{44}H_{29}Fe_2N_2O_5PS_2Cl_2$ | $C_{19}H_{19}Fe_2N_2O_8PS_2$ |
| Formula weight | 706.27 | 943.38 | 610.15 |
| Temperature (K) | 173(2) | 100(2) | 298(2) |
| Crystal size (mm) | 0.42 x 0.24 x 0.14 | 0.32 x 0.28 x 0.22 | 0.34 x 0.25 x 0.18 |
| Crystal system | Monoclinic | Triclinic | Monoclinic |
| Space group | $P2_1/c$ | *P-1* | $P2_1/c$ |
| Z | 4 | 2 | 4 |
| Wavelength (Å) | 0.71073 | 0.71073 | 0.71073 |
| *a* [Å] | 17.1199(16) | 11.9477(9) | 14.300(6) |
| *b* [Å] | 10.8452(10) | 12.1462(9) | 15.065(7) |
| *c* [Å] | 16.5940(15) | 17.3212(12) | 12.837(6) |
| α (°) | 90.0 | 106.2240(10) | 90.0 |
| β [°] | 110.2860 (10) | 95.2610(10) | 92.689(7) |
| γ (°) | 90.0 | 116.3910(10) | 90.0 |
| Volume [$Å^3$] | 2889.9(5) | 2092.8(3) | 2762(2) |
| Calculated density ($Mg/m^{-3}$) | 1.623 | 1.497 | 1.467 |
| Reflections collected/ unique | 27118/5151 | 20369/7482 | 27607/6060 |
| R(int) | 0.0294 | 0.0350 | 0.0784 |
| F(000) | 1432 | 960 | 1240 |
| Max. and min. transmission | 0.8445 and 0.6220 | 0.8089 and 0.7388 | 0.7996 and 0.6661 |
| Θ range for data collection (°) | 1.27 to 25.15 | 1.95 to 25.24 | 1.43 to 27.46 |
| Refinement method | Full-matrix Least -squares on $F^2$ | Full-matrix least-squares on $F^2$ | Full-matrix least-squares on $F^2$ |
| Data / restraints /parameters | 5151/0/388 | 7482/0/523 | 6060 / 0 / 310 |
| Goodness-of-fit on $F^2$ | 1.070 | 1.047 | 1.037 |
| $R_1/wR_2$ [I>2sigma(I)] | 0.0276/0.0694 | 0.0418/0.1009 | 0.0636/0.1498 |
| $R_1/wR_2$ (all data) | 0.0291/0.0706 | 0.0463/0.1038 | 0.0851/0.1611 |
| Largest diff. peak and hole [$e.Å^{-3}$] | 0.414 and -0.244 | 1.286 and -1.191 | 0.655 and -0.439 |

**Table 3.8.** Crystal Data and Structural Refinement for Complexes **6, 7** and **10**

| | **6** | **7** | **10** |
|---|---|---|---|
| Empirical formula | $C_{31}H_{27}Fe_2N_2O_8PS_2$ | $C_{24}H_{34}Fe_2N_2O_{10}P_2S_2$ | $C_{30}H_{19}Fe_2N_2O_5PS_3$ |
| Formula weight | 762.34 | 748.29 | 797.22 |
| Temperature (K) | 298(2) | 100(2) | 298(2) |
| Crystal size (mm) | 0.40 x 0.22 x 0.12 | 0.42 x 0.38 x 0.22 | 0.38 x 0.28 x 0.20 |
| Crystal system | Monoclinic | Monoclinic | Monoclinic |
| Space group | $P2_1/c$ | $P2_1$ | $P2_1/c$ |
| Z | 4 | 4 | 4 |
| Wavelength (Å) | 0.71073 | 0.71073 | 0.71073 |
| *a* [Å] | 19.5969(8) | 11.2607(14) | 12.397(4) |
| *b* [Å] | 12.7253(14) | 14.4324(17) | 11.680(4) |
| *c* [Å] | 14.2226(9) | 20.570(3) | 23.340(8) |
| α (°) | 90.0 | 90.0 | 90.0 |
| β [°] | 105.710 (5) | 105.106(2) | 104.148(6) |
| γ (°) | 90.0 | 90.0 | 90.0 |
| Volume [$Å^3$] | 3414.3(5) | 3227.5(7) | 3277.1(19) |
| Calculated density ($Mg/m^{-3}$) | 1.483 | 1.540 | 1.616 |
| Reflections collected/ unique | 12457/5818 | 33035/12689 | 30922/5889 |
| R(int) | 0.0609 | 0.0374 | 0.0808 |
| F(000) | 1560 | 1544 | 1608 |
| Max. and min. transmission | 0.8824 and 0.6744 | 0.7812 and 0.6369 | 0.7767 and 0.6318 |
| Θ range for data collection (°) | 2.61 to 24.71 | 1.03 to 26.09 | 1.69 to 25.22 |
| Refinement method | Full-matrix least-squares on $F^2$ | Full-matrix Least -squares on $F^2$ | Full-matrix least-squares on $F^2$ |
| Data / restraints /parameters | 5818/0/418 | 12689/1/769 | 5889/0/406 |
| Goodness-of-fit on $F^2$ | 0.893 | 1.027 | 1.037 |
| $R_1/wR_2$ [I>2sigma(I)] | 0.0539/0.0706 | 0.0407/0.0895 | 0.0508/0.1232 |
| $R_1/wR_2$ (all data) | 0.1239/0.0937 | 0.0446/0.0913 | 0.0727/0.1345 |
| Largest diff. peak and hole [$e.Å^{-3}$] | 0.516 and -0.410 | 0.746 and-0.300 | 0.728 and -0.642 |

**Table 3.9.** Crystal Data and Structural Refinement for Complexes **11** and **12**

| | **11** | **12** |
|---|---|---|
| Empirical formula | $C_{17}H_{17}Fe_2N_2O_8PS_3$ | $C_{22}H_{32}Fe_2N_2O_{10}P_2S_3$ |
| Formula weight | 616.18 | 754.32 |
| Temperature (K) | 298(2) | 100(2) |
| Crystal size (mm) | 0.60 x 0.40 x 0.30 | 0.20 x 0.14 x 0.10 |
| Crystal system | Triclinic | Monoclinic |
| Space group | *P-1* | $P2_1$ |
| Z | 2 | 4 |
| Wavelength (Å) | 0.71073 | 0.71073 |
| *a* [Å] | 9.2183(18) | 11.1968(12) |
| *b* [Å] | 11.372(2) | 14.5453(16) |
| *c* [Å] | 12.043(2) | 20.071(2) |
| α (°) | 94.22(3) | 90.00 |
| β [°] | 91.69(3) | 105.026 (2) |
| γ (°) | 93.39(3) | 90.00 |
| Volume [$Å^3$] | 1256.1(4) | 3157.0(6) |
| Calculated density ($Mg/m^{-3}$) | 1.629 | 1.587 |
| Reflections collected/ unique | 18355/9572 | 30084/11096 |
| R(int) | 0.0277 | 0.0241 |
| F(000) | 624 | 1552 |
| Max. and min. transmission | 1.0000 and 0.93414 | 0.8834 and 0.7851 |
| Θ range for data collection (°) | 3.28 to 33.14 | 1.75 to 25.00 |
| Refinement method | Full-matrix least-squares on $F^2$ | Full-matrix least-squares on $F^2$ |
| Data / restraints /parameters | 9572/0/301 | 11096/1/751 |
| Goodness-of-fit on $F^2$ | 0.985 | 1.055 |
| $R_1/wR_2$ [I>2sigma(I)] | 0.0473 / 0.1141 | 0.0300/0.0727 |
| $R_1/wR_2$ (all data) | 0.0952/0.1301 | 0.0306/0.0730 |
| Largest diff. peak and hole [$e.Å^{-3}$] | 0.707 and -0.569 | 0.476 and -0.371 |

## 3.5. References

[1] R. Cammack, Nature 397 (1999) 214–215.

[2] D. J. Evans, C. J. Pickett, Chem. Soc. Rev. 32 (2003) 268–275.

[3] M. Frey, ChemBioChem 3 (2002) 153–160.

[4] J. W. Peters, W. N. Lanzilotta, B. J. Lemon, L. C. Seefeldt, Science 282 (1998) 1853–1858.

[5] Y. Nicolet, C. Piras, P. Legrand, C. E. Hatchikian, J. C. Fontecilla- Camps, Strcture 7 (1999) 13–23.

[6] R. P. Happe, W. Roseboom, A. J. Pierik, S. P. Albracht, K. A.Bagley, Nature 385 (1997) 126.

[7] A. J. Pierik, W. Roseboom, R. P. Happe, K. A. Bagley, S. P. J. Albracht, J. Biol. Chem. 274 (1999) 3331–3337.

[8] G. A. N. Felton, C. A. Mebi, B. J. Petro, A. K. Vannucci, D. H. Evans, R. S. Glass, D. L. Lichtenberger, J. Organomet. Chem. 694 (2009) 2681–2699.

[9] D. M. Heinekey, J. Organomet. Chem. 694 (2009) 2671–2680.

[10] C. Tard, and C. J. Pickett, Chem. Rev. 109 (2009) 2245–2274.

[11] J.-F. Capon, F. Gloaguen, F.Y. Petillon, P. Schollhammer, J. Talarmin, C. R. Chimie. 11 (2008) 842–851.

[12] J.-F. Capon, F. Gloaguen, F.Y. Petillon, P. Schollhammer, J. Talarmin, Coord. Chem. Rev. 253 (2009) 1476–1494.

[13] F. Gloaguen, J. D. Lawrence, M. Schmidt, S. R. Wilson, T. B. Rauchfuss, J. Am. Chem. Soc. 123 (2001) 12518–12527.

[14] E. J. Lyon, I. P. Georgakaki, J. H. Reibenspies, M. Y. Darensbourg, J. Am. Chem. Soc. 123 (2001) 3268–3278.

[15] J. D. Lawrence, H. Li, T. B. Rauchfuss, M. Benard, M. M. Rohmer, Angew. Chem. Int. Ed. 40 (2001) 1768–1771.

[16] J. Windhager, H. Görls, H. Petzold, G. Mloston, G. Linti, W. Weigand, Eur. J. Inorg. Chem. 28 (2007) 4462–4471.

[17] L.-C. Song, Z. Y. Yang, H. Z. Bian, Y. Liu, H. T. Wang, X. F. Liu, Q. M. Hu, Organometallics 24 (2005) 6126–6135.

[18] P. Li, M. Wang, C. He, G. Li, X. Liu, C. Chen, B. Akermark, L. Sun, Eur. J. Inorg. Chem. (2005) 2506–2513.

[19] J. F. Capon, S. E. Hassnaoui, P. Schollhammer, J. Talarmin, Organometallics 24 (2005) 2020–2022.

[20] J. W. Tye, J. Lee, H. Wang, R. Mejia-Rodriguez, J. H. Reibenspies, M. B. Hall, M. Y. Darensbourg, Inorg. Chem. 44 (2005) 5550–5552.

[21] L. Duan, M. Wang, P. Li, Y. Na, N. Wang, L. Sun, Dalton Trans. (2007) 1277–1283.

[22] F. Gloaguen, T. B. Rauchfuss, Chem. Soc. Rev. 38 (2009) 100–108.

[23] R. Lomoth, S. Ott, Dalton Trans. (2009) 9952–9959.

[24] F. Gloaguen, J. D. Lawrence, T. B. Rauchfuss, J. Am. Chem. Soc. 123 (2001) 9476 – 9477.

[25] S. Ott, M. Kritikos, B. Akermark, L. Sun, R. Lomoth, Angew. Chem. Int. Ed. 43 (2004) 1006 – 1009.

[26] S. J. Borg, T. Behrsing, S. P. Best, M. Razavet, X. Liu, C. J. Pickett, J. Am. Chem. Soc. 126 (2004) 16988 –16999.

[27] J. -F. Capon, F. Gloaguen, P. Schollhammer, J. Talarmin, J. Electroanal. Chem. 566 (2004) 241–247.

[28] J. -F. Capon, F. Gloaguen, P. Schollhammer, J. Talarmin, J. Electroanal. Chem. 595 (2006) 47–52.

[29] G. A. N. Felton, A. K. Vannucci, J. Chen, L. T. Lockett, N. Okumura, B. J. Petro, U. I. Zakai, D. H. Evans, R. S. Glass, D. L. Lichtenberger, J. Am. Chem. Soc. 129 (2007) 12521 – 12530.

[30] L. Schwartz, P. S. Singh, L. Eriksson, R. Lomoth, S. Ott, C. R. Chimie 11 (2008) 875–889.

[31] D. Chong, I. P. Georgakaki, R. Mejia-Rodriguez, J. Sanabria-Chinchilla, M. P. Soriaga, and M. Y. Darensbourg, J. Chem. Soc., Dalton. Trans. (2003) 4158–4163.

[32] S. Jiang, J. Liu, Y. Shi, Z. Wang, B. Åkermark, and L. Sun, Dalton Trans. (2007) 896–902.

[33] D. Morvan, J.-F. Capon, F. Gloaguen, A. Le Goff, M. Marchivie, F. Michaud, P. Schollhammer, J. Talarmin, J.-J. Yahouanc, R. Pichon, and N. Karvarec, Organometallics 26 (2007) 2042–2052.

[34] R. Mejia-Rodriguez, D. Chong, J. H. Reibenspies, M. P. Soriaga, and M. Y. Darensbourg, J. Am. Chem. Soc. 126 (2004) 12004–12014.

[35] F. Gloaguen, J. D. Lawrence, T. B. Rauchfuss, M. Benard, M.-M. Rohmer, Inorg. Chem. 41 (2002) 6573–6582.

[36] K. A. Justice, R. C. Linck, T. B. Rauchfuss, S. R. Wilson, J. Am. Chem. Soc. 126 (2004) 13214–13215.

[37] A. C. Boyke, T. B. Rauchfuss, S. R. Wilson, M. -M. Rohmer, M. Benard, J. Am. Chem. Soc. 126 (2004) 15151–15160.

[38] L.-C. Song, M.-Y. Tang, S.-Z. Mei, J.-H. Huang, Q.-M. Hu, Organometallics 26 (2007) 1575–1577.

[39] L.-C. Song, L.-X. Wang, M.-Y. Tang, C.-G. Li, H.-B. Song, Q.-M. Hu, Organometallics 28 (2009) 3834–3841.

[40] L.-C. Song, Z. Y. Yang, Y. J. Hua, H. T. Wang, Y. Liu, Q. M. Hu, Organometallics 26 (2007) 2106–2110.

[41] J. Chen, A. K. Vannucci, C. A. Mebi, N. Okumura, S. C. Borowski, M. Swenson, T. Lockett, D. H. Evans, R. S. Glass, and D. L. Lichtenberger, Organometallics 29 (2010) 5330–5340.

[42] J. A. Cabeza, A. Martinez-Garcia, V. Riera, Organometallics 17 (1998) 1471–1477.

[43] M. M. Hasan, M. B. Hursthouse, S. E. Kabir, K. M. Abdul Malik, Polyhedron 20 (2001) 97–101.

[44] A. K. Vannucci, S. Wang, G. S. Nichol, D. L. Lichtenberger, D. H. Evans, and R. S. Glass, Dalton Trans. 39 (2010) 3050–3056.

[45] G. A. N. Felton, A. K. Vannucci, N. Okumura, L. T. Lockett, D. H. Evans, R. S. Glass, D. L. Lichtenberger, Organometallics 27 (2008) 4671–4679.

[46] D. Streich, M. Karnahl, Y. Astuti, C. W. Cady, L. Hammarström, R. Lomoth, and S. Ott, Eur. J. Inorg. Chem. (2011) 1106–1111.

[47] S. Ezzaher, A. Gogoll, C. Bruhn, and S. Ott, Chem. Commun. 46 (2010) 5775–5777.

[48] D. Streich, Y. Astuti, M. Orlandi, L. Schwartz, R. Lomoth, L. Hamarström, and S. Ott, Chem. –Eur. J. 16 (2010) 60–63.

[49] L. Schwartz, L. Eriksson, R. Lomoth, F. Teixidor, C. Viñas, and S. Ott, Dalton Trans. (2008) 2379–2381.

[50] A. Majumdar, J. Mitra, K. Pal and S. Sarkar, Inorg. Chem. 47 (2008) 5360–5364.

[51] A. Majumdar, K. Pal and S. Sarkar, J. Am. Chem. Soc. 128 (2006) 4196–4197.

[52] G. Durgaprasad, R. Bolligarla, S. K. Das, J. Organomet. Chem. 696 (2011) 3097–3105.

[53] R. Bolligarla, G. Durgaprasad, S. K. Das, Inorg. Chem. Commun. 14 (2011) 809–813.

[54] J. L. Brusso, O. P. Clements, R. C. Haddon, M. E. Itkis, A. A. Leitch, R. T. Oakley, R. W. Reed, and J. F. Richardson, J. Am. Chem. Soc. 126 (2004) 8256–8265.

[55] S. V. More, M. N. V. Sastry, C.-C. Wang, and C.-F. Yao, Tetrahedron Letters 46 (2005) 6345–6348.

[56] R. Bolligarla, and S. K. Das, Tetrahedron Letters 52 (2011) 2496–2500.

[57] A. L. Cloirec, S. P. Best, S. Borg, S. C. Davies, D. J. Evans, D. L. Hughes, C. J. Pickett, Chem. Commun. (1999) 2285–2286.

[58] E. J. Lyon. I. p. Georgakaki, J. H. Reibenspies, M. Y. Darensbourg, Angew. Chem., Int. Ed. 38 (1999) 3178–3180.

[59] X. Zhao, I. P. Georgakaki, M. L. Miller, J. C. Yarbrough, M. Y. Darensbourg, J. Am. Chem. Soc. 123 (2001) 9710–9711.

[60] J. L. Nehring, D. M. Heinekey, Inorg. Chem. 42 (2003) 4288–4292.

[61] J. D. Lawrence, T. B. Rauchfuss, S. R. Wilson, Inorg. Chem. 41 (2002) 6193–6195.

[62] A. Bondi, Vander waals volumes and radii, J. Phy. Chem. 68 (1964) 441–451.

[63] M Schmidt, S. M. Contakes and T. B. Rauchfuss, J. Am. Chem. Soc. 121 (1999) 9736–9737.

[64] X. Zhao, I. P. Georgakaki, M. L. Miller, R. Mejia-Rodriguez, C. Y. Chiang and M. Y. Darensbourg, Inorg. Chem. 41 (2002) 3917–3928.

[65] G.-A. N. Felton, R. S. Glass, D. L. Lichtenberger, and D. H. Evans, Inorg. Chem. 45 (2006) 9181–9184**.**

[66] T. Liu, M. Wang, Z. Shi, H. Cui, W. Dong, J. Chen, B. Akermark, and L. Sun, Chem. –Eur. J. 10 (2004) 4474–4479.

[67] G. Durgaprasad, R. Bolligarla, S. K. Das, J. Organomet. Chem. 706–707 (2012) 37–45.

[68] Bruker. *SADABS*, *SMART*, *SAINT* and *SHELXTL*, 2000 (Bruker AXS Inc., Madison, Wisconsin, USA).

[69] G. M. Sheldrick, A short history of **SHELX** , Acta Crystallogr. Sect. A 64 (2008) 112–122.

# Influence of coordinated crystallizing solvents and bulkiness of ligands in tuning the structural diversity and dimensionality of alkali metal based coordination polymers of metal bis(dithiolene) complexes

4 Chapter

**Abstract:–** In order to investigate the influence of coordinating solvent and bulkiness of the dithiol ligand (diph-6,7-qdt$^{2-}$ = 2,3-diphenylquinoxaline-6,7-dithiolate) on structural diversity of sodium coordinated M(III) bis dithiolene complexes (M = Cu(III), Au(III)), we have synthesized six coordination complexes $[Na(CH_3OH)_3][Cu(diPh\text{-}6,7\text{-}qdt)_2]\cdot MeOH$ (**1**), $[Na(THF)_2(OH_2)_2(C_2H_5OC_2H_5)][Cu(diPh\text{-}6,7\text{-}qdt)_2]$ (**2**), $[Na(CH_3COCH_3)_2(OH_2)][Cu(diPh\text{-}6,7\text{-}qdt)_2]$ (**3**), $\{[Na(CH_3CN)][Cu(diPh\text{-}6,7\text{-}qdt)_2]\}_n$ (**4**), $[Na(THF)_2(OH_2)_2(C_2H_5OC_2H_5)][Au(diPh\text{-}6,7\text{-}qdt)_2]$ (**5**) and $[Na(CH_3COCH_3)_2(OH_2)][Au(diPh\text{-}6,7\text{-}qdt)_2]$ (**6**) by varying the coordinating solvents in respective recrystallization process. We have described comparative studies of the above mentioned complexes with sodium-based [M(btdt)] (M = Cu and Au) (btdt$^{2-}$ = 2,1,3-benzenethiadiazole-5,6-dithiolate) coordination polymers reported by us. All these compounds **1**–**6** have been structurally characterized unambiguously by single crystal X-ray crystallography and routine spectral characterization techniques. Interestingly, copper compounds **1**–**4** show one quasi-reversible reduction response at $E_{1/2}$ = –0.19 V *vs* Ag/AgCl in DMF solutions

## 4.1. Introduction

Metal–organic materials (MOMs) [1-10], also known as metal based coordination polymers, hybrid inorganic–organic materials, and metal–organic frameworks (MOFs), represent an emerging class of materials that have attracted the imagination of solid-state chemists because many MOMs combine unprecedented levels of porosity with a range of other functional properties that occur through the metal moiety and/or the organic ligand. The design and syntheses of coordination polymers or metal-organic frameworks (MOFs), that involve attentive selection of organic ligands with suitable functional groups and metal ions, have attracted considerable attention because such solid-functional materials have potential to be used as gas storage, nonlinear optical, conducting and magnetic materials [11–40]. Controlling self-assembly of coordination polymers in terms of their

dimensionality (1D, 2D and 3D) is a challenging task. This is because the properties of these coordination polymers can be tuned by the structural diversity and dimensionality of polymeric materials. Thus, by precise prediction of diversity and dimensionality of self-assembled-coordination networks, we can control the properties of solid-functional materials [41–48]. In the self-assembly process of a coordination polymer, generally, the structural diversity and dimensionality are greatly affected by the choice of the ligands [49–55], metal/ligand ratios [56–59], solvents [60–71] and counterions [72]. Among these factors, influence of solvents and bulkiness of the ligands are particularly important because, simply, the variations in solvents and ligands, result in a variety of self assembled structures [60–72]. Generally, a solvent can influence the structure assemblies of coordination architecture either by playing role as reaction medium or in the re-crystallization process. In the course of crystallization, the solvents can control the crystal structure of coordination networks by its lattice formation without their involvement in the final product or their incorporation as guests into the structures without coordination to the complexing moiety or their involvement in the coordination to metal ion by coordinate covalent bonds [60–71]. In the latter case (their coordination to a metal ion), solvents can directly influence the dimensionality of self-assembled network, due to difference in their shape, size and polarity. Effects of solvents on the dimensionality of self-assembled coordination networks are demonstrated in previous reports [60–71]. Even then, the role of a coordinating solvent on the structure assemblies of coordination networks is still not been well understood.

Square-planar metal-dithiolene complexes have been used as building blocks for the construction of polymeric compounds as conducting, magnetic and non linear optical materials [73–79]. However, the investigation of influence of solvents on the coordination networks, based on a square-planar metal bis(dithiolene) complex, is hardly explored. In the present chapter, we have demonstrated a systematic study of influence of bulkiness of the ligand molecule and the solvent effect on the formation of crystalline coordination networks of diverse dimensionalities (ion pair complex, descrete and 1D) by employing different coordinating solvents such as, THF, MeOH, $CH_3COCH_3$, and $CH_3CN$ through their coordination with the sodium cation. We have recently reported that the geometry of the central carbon of crystallizing coordinating solvents plays an important role in directing the dimensionality of coordination polymers. In that we have described that,

during recrystallization process, $sp^3$ hybridized central carbon containing solvents, such as, MeOH and THF solvents lead to 1D coordination polymers, $sp^2$ hybridized central carbon containing solvents, such as, DMF and acetone solvents lead to 2D coordination polymers and sp hybridized central carbon containing solvents, such as, acetonitrile solvent leads to 3D coordination polymers.

We have described four new coordination complexes **1–4** based on $[Cu^{III}(diph\text{-}6,7\text{-}qdt)_2]^{1-}$ and two new coordination complexes **5** and **6** based on $[Au^{III}(diph\text{-}6,7\text{-}qdt)_2]^{1-}$ (diph-6,7-$qdt^{2-}$ = 2,3-diphenylquinoxaline-6,7-dithiolate) systems by varying the coordinating solvents. All these compounds have been structurally characterized unambiguously by single crystal X-ray crystallography including with their spectral characterizations (IR and NMR), and elemental analysis. We have also described electrochemical properties of compounds **1**–**4** in solution state.

$[Na(CH_3OH)_3][Cu(diPh\text{-}6,7\text{-}qdt)_2]\cdot MeOH$ (**1**),

$[Na(THF)_2(OH_2)_2(C_2H_5OC_2H_5)][Cu(diPh\text{-}6,7\text{-}qdt)_2]$ (**2**),

$[Na(CH_3COCH_3)_2(OH_2)][Cu(diPh\text{-}6,7\text{-}qdt)_2]$ (**3**),

$\{[Na(CH_3CN)][Cu(diPh\text{-}6,7\text{-}qdt)_2]\}_n$ (**4**),

$[Na(THF)_2(OH_2)_2(C_2H_5OC_2H_5)][Au(diPh\text{-}6,7\text{-}qdt)_2]$ (**5**),

$[Na(CH_3COCH_3)_2(OH_2)][Au(diPh\text{-}6,7\text{-}qdt)_2]$ (**6**).

## 4.2. Results and discussion

*4.2.1. Synthesis and Spectroscopic Characterization*

The synthetic route for the compounds **1**–**4** are shown in Scheme 4.1. Copper complexes **1**–**4** were obtained from different solvent recrystallization of dark green colored solid which was obtained from the reaction of one mole equivalent of $CuCl_2$ with two mole equivalents of $H_2$diph-6,7-qdt in MeOH treated with excess amount of NaOH in presence of open atmosphere. Recrystallization from the acetonitrile/ether diffusion leads to the formation of 1D coordination polymers, whereas MeOH/ether, THF/ether and acetone/ether diffusion leads to formation of discrete molecule instead of forming coordination polymers. During the reaction process Cu(II) oxidizes to Cu(III) by air oxidation. In all these compounds **1**–**4**, $Na^+$ ion is the counter cation. In the same way, we have synthesized gold compounds **5** and **6**, by using $HAuCl_4\cdot 3H_2O$ instead of

$CuCl_2 \cdot 2H_2O$, in the reaction procedure, as shown in Scheme 4.2. For the compounds **5** and **6** also, $Na^+$ ion acts as counter cation, for that NaOH was used as base to de-protonate thiol group (Scheme 4.2).The green colored solid compound was obtained from the reaction and they were recrystallized separately from THF and acetone / ether diffusions that lead to the formation of discrete molecules. All the Compounds **1**–**6** have been characterized by single crystal X-ray crystallography and further characterized by IR, $^1H$ & $^{13}C$ NMR and including their elemental analysis (experimental section).

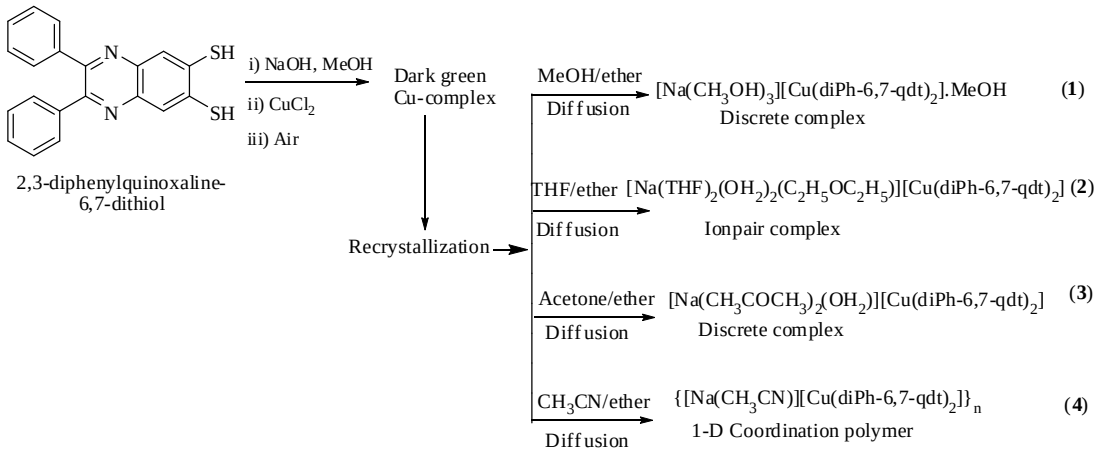


**Scheme 4.1.** Synthesis of Cu coordinated complexes **1**–**4**.

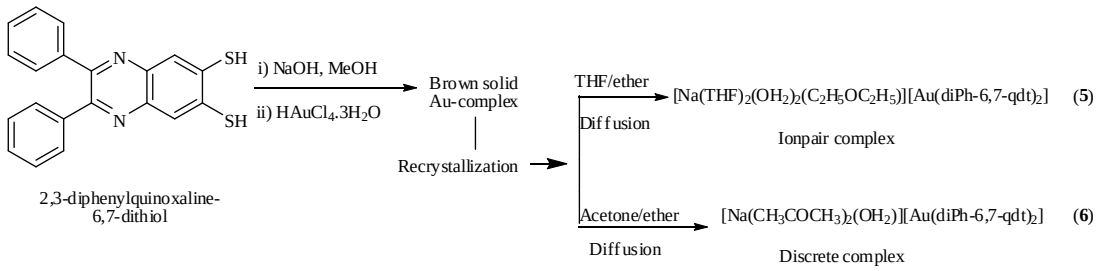


**Scheme 4.2.** Synthesis of gold coordinated complexes **5**–**6**.

*Spectroscopic studies*

*IR Spectroscopy*

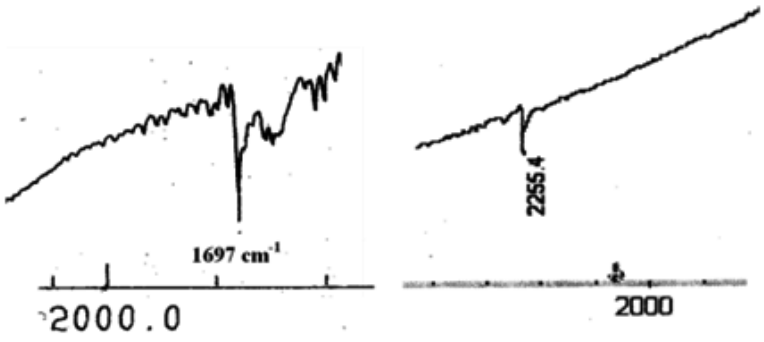


(a) (b)

**Fig. 4.1.** IR spectra of (a) compound **3** ($\upsilon_{C=O}$) and (b) compound **4** ($\upsilon_{C\equiv N}$) in the frequency regions of their respective coordinating solvents.

From the IR spectra (Fig. 4.1), we have observed two bands at 1697 and 2255 $cm^{-1}$. The presence of these peaks are due to the coordinated solvent molecules such as acetone ($\upsilon_{C=O}$) in complexes **3** and $CH_3CN$ ($\upsilon_{C\equiv N}$) in complex **4**, respectively. All complexes **1**–**6** shows a broad IR bands at 3466 and 3369 $cm^{-1}$, which are due to the O–H stretching frequency, that conforms the presence of water molecule in all compounds.

*$^1$H NMR Spectroscopy*

$^1$H NMR spectra of Cu-coordination complexes **1**–**4** show three narrow peaks at 7.69, 7.43 and 7.34 ppm in DMSO-$d_6$ corresponding to the four benzene and two quinoxaline ring protons from the diph-6.7-qdt ligands. As representative example, the $^1$H NMR spectrum of compound **3** in DMSO-$d_6$ solution is shown in Fig. 4.2. According to the nature and position of the signal, copper compounds in the present study are diamagnetic square planar Cu(III) $d^8$ coordination complexes, as expected [75]. As in the case of Au-coordination polymers **5** and **6**, also we have observed three narrow peaks at 7.69, 7.43 and 7.34 ppm in DMSO-$d_6$ related to the four benzene rings and two quinoxaline ring protons from the diph-6.7-qdt ligands.

*ESR Spectroscopy*

None of these copper compounds exhibit any ESR signals confirming again that these complexes are Cu(III) complexes.

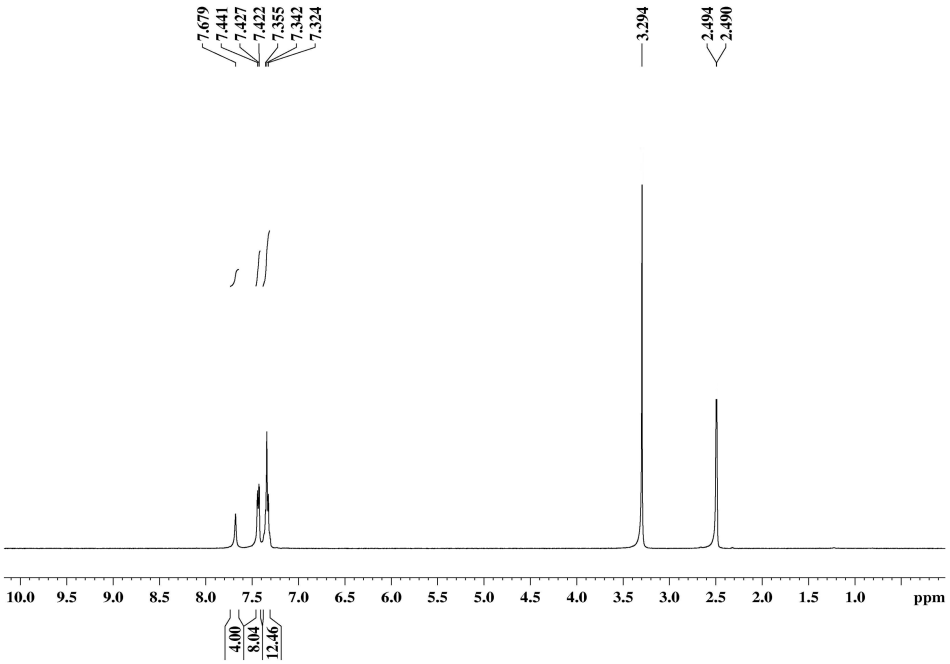


**Fig. 4.2**. $^{1}$H NMR spectrum of compound **3** in DMSO-$d_6$.

*4.2.2. Electrochemical Studies*

In cyclic voltammetric studies of Cu-compounds **1**–**4**, a common Cu(III)/Cu(II) redox couple appears as almost reversible reduction wave at $E_{1/2}$ = –0.187 V ($E_{red}$ = –0. 231 V, $E_{oxd}$ = –0.144 V) *vs* Ag/AgCl ($\Delta E$= 87 mV) in DMF solutions with scan rate 100 $mVs^{-1}$ as shown in Fig. 4.3 for compound **2**. Interestingly, this is some what low reduction potential for a Cu(III)-coordination complex. Interestingly, the reduction potential of compound **2** is more when we compare with $[Cu^{III}(btdt)_2]^{1-}$ ($btdt^{2-}$ = 2,1,3-benzenethiadiazole-5,6-dithiolate) that has $E_{1/2}$ = –0.13 V *vs* Ag/AgCl ($\Delta E$= 90 mV) reported by Das and co-workers [80] and even it is less than that of reported Cu(III) compound of pds ligand [$E_{1/2}$ = –0.54 V (quasi-reversible)], reported by Rovira and co-workers [75]. Thus it shows that the present system $[Cu^{III}(diph\text{-}6,7\text{-}qdt)_2]^{1-}$ is relatively difficult to reduce, when we compare with $[Cu^{III}(btdt)_2]^{1-}$ and it is relatively easy to reduce, when we compare with $[Cu^{III}(pds)_2]^{1-}$. From the above discussion,it can be said that Cu(III)-compounds **1**–**4** have been prepared by simple and rapid air oxidation. We could not isolate the Cu(II) compounds of $H_2$diph-6,7-qdt ligand because reaction of $CuCl_2$ with $Na_2$diph-6,7-qdt results in the formation of immediate precipitate as a Cu(III) dark green-coloured solid (Scheme 4.1.).

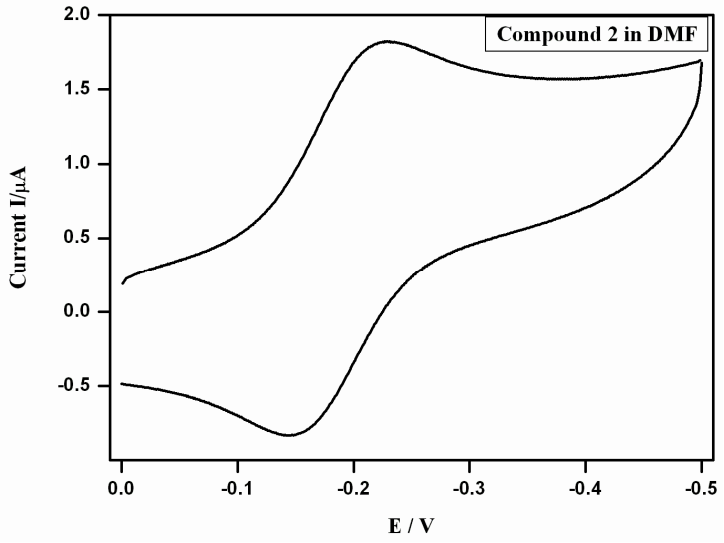


**Fig. 4.3.** Cyclic voltammetry of complex **2** in DMF with a scan rate 100 mV $s^{-1}$ ($n$Bu$_4$NClO$_4$ as supporting electrolyte).

### *4.2.3. Description of Crystal Structures*

*Recrystallization from MeOH Solvent: Compound **1***

Single crystals of compound [Na(CH$_3$OH)$_3$][Cu(diPh-6,7-qdt)$_2$]·MeOH (**1**) were grown from MeOH solvent and crystallize in triclinic space group *P-1*. The asymmetric unit in the crystal structure of

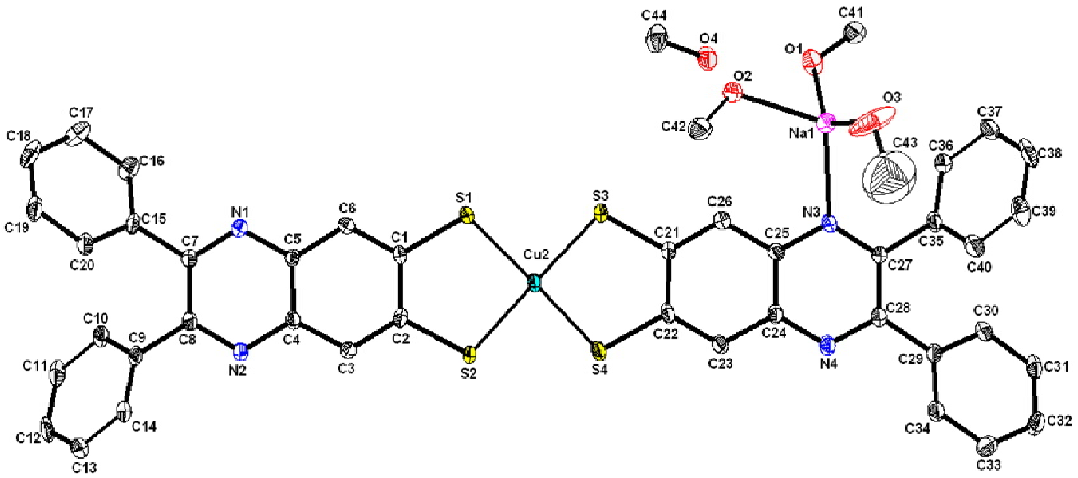


**Fig. 4.4.** Thermal ellipsoid plot of compound **1** (70% probability, hydrogen atoms omitted for clarity).

complex **1** [represented as labeled atoms] contain one {Cu(diPh-6,7-qdt)}$^{1-}$ complexic anion, one sodium counter cation which is coordinated by three MeOH solvent molecules and one lattice MeOH solvent molecule as shown in Fig. 4.4. The structure of complex **1**

shows square planar geometry around the Cu(III) ion, with the average Cu–S bond distance 2.178 ± 0.002 Å and there is a deviation between the two SCuS planes with the dihedral angle of 7.27°. In addition to dihedral angle, there is a deviation in planarity of dithiolene chelating rings with bending angles ($\eta$) of 2.54° and 5.44° between the {S1Cu1S2} and {S1C1C2S2} planes and {S3Cu1S4} and {S3C21C22S4} planes present in the {Cu1S1S2C1C2} and {Cu1S3S4C21C22} chelating rings represented as in Fig. 4.5(a). In the crystal structure of complex **1,** only one nitrogen atom of dithiolene complex is coordinated to $Na^+$ counter ion (Mode I, Scheme 4.3, vide infra). When we consider the geometry around $Na^+$ ion, it is found to be in almost tetrahedral environment, in which each $Na^+$ ion is coordinated by one nitrogen atom from dithiolene complexic anion and the remaining three coordination sites are occupied by three different MeOH solvent molecules. The Na–N1 bond distance is 2.520 Å in the crystal structure of complex **1** which are in good agreement with relevant literature reports [84–87]. The Na–$O_{(solvent)}$ coordination bond distances lie in the range of 2.336 to 2.352 Å.

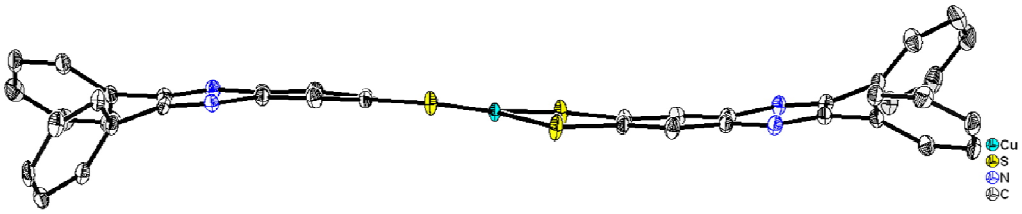


(a)

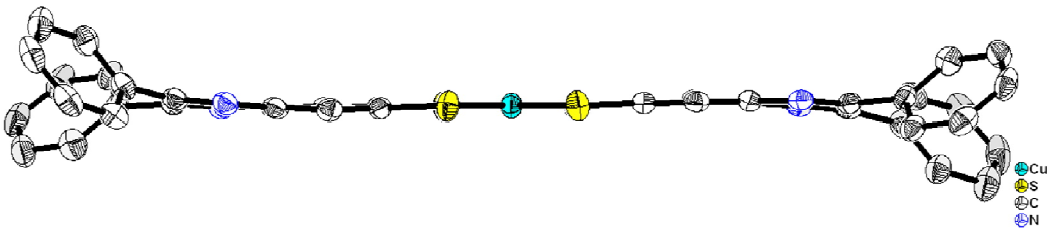


(b)

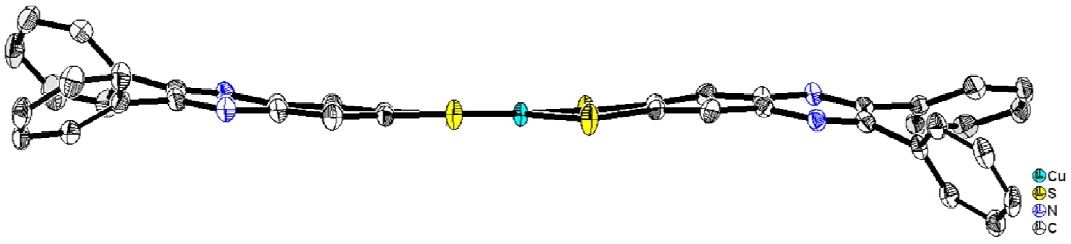


(c)

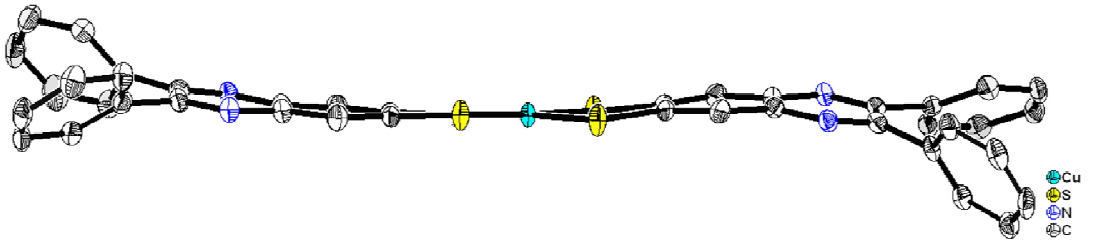


(d)

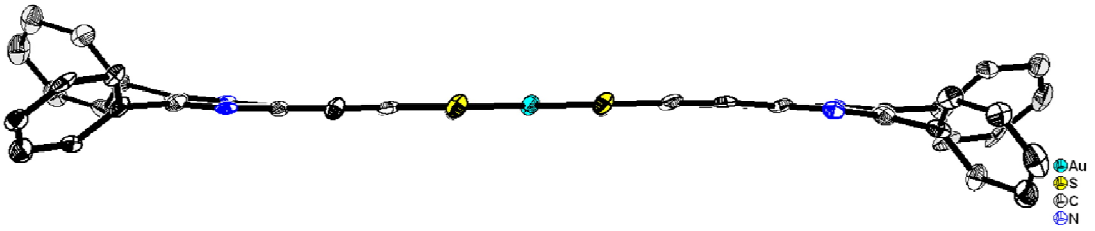


(e)

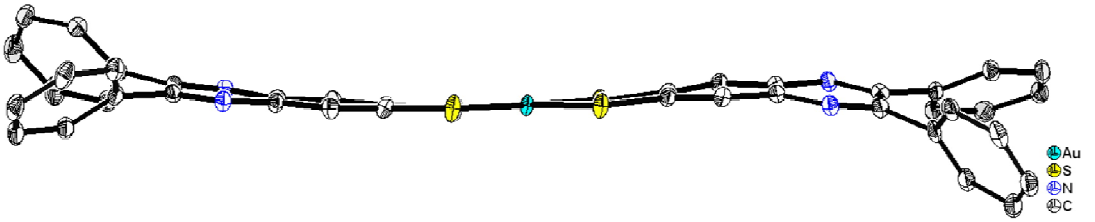


(f)

**Fig. 4.5.** (a) Anionic complex units through side view of: (a) compound **1**; (b) compound **2**; (c) compound **3**; (d) compound **4**; (e) compound **5** and (f) compound **6**.

*Recrystallization from THF solvent: Compounds **2** and **5***

Crystal structures of the complexes $[Na(THF)_2(OH_2)_2(C_2H_5OC_2H_5)][Cu(diPh\text{-}6,7\text{-}qdt)_2]$ (**2**) and $[Na(THF)_2(OH_2)_2(C_2H_5OC_2H_5)][Au(diPh\text{-}6,7\text{-}qdt)_2]$ (**5**) are isomorphous and these complexes crystallize in triclinic space group *P*-1. The asymmetric unit in the crystal structures of the both complexes **2** and **5** (represented as labeled atoms) contain an ion pair complex, having $\{Cu(diPh\text{-}6,7\text{-}qdt)\}^{1-}$ complexic anion, and $[Na(THF)_2(OH_2)_2(C_2H_5OC_2H_5)]^+$ complexic cation as shown in Fig. 4.6 and Fig. 4.7. This system shows a square planar geometry around the M(III) ion with the average Cu–S and Au–S bond distances 2.178 ± 0.002 Å and 2.305 ± 0.000 Å in complexes **2** and **5**, respectively. However, there are less deviations in the planar rings of dithiolene chelates (anionic fragment) with respect to {SMS} (M = Cu, Au) plane with dihedral angle 0.70° and 0.39° respectively as shown in Fig. 4.5(b) and 4.5(e).

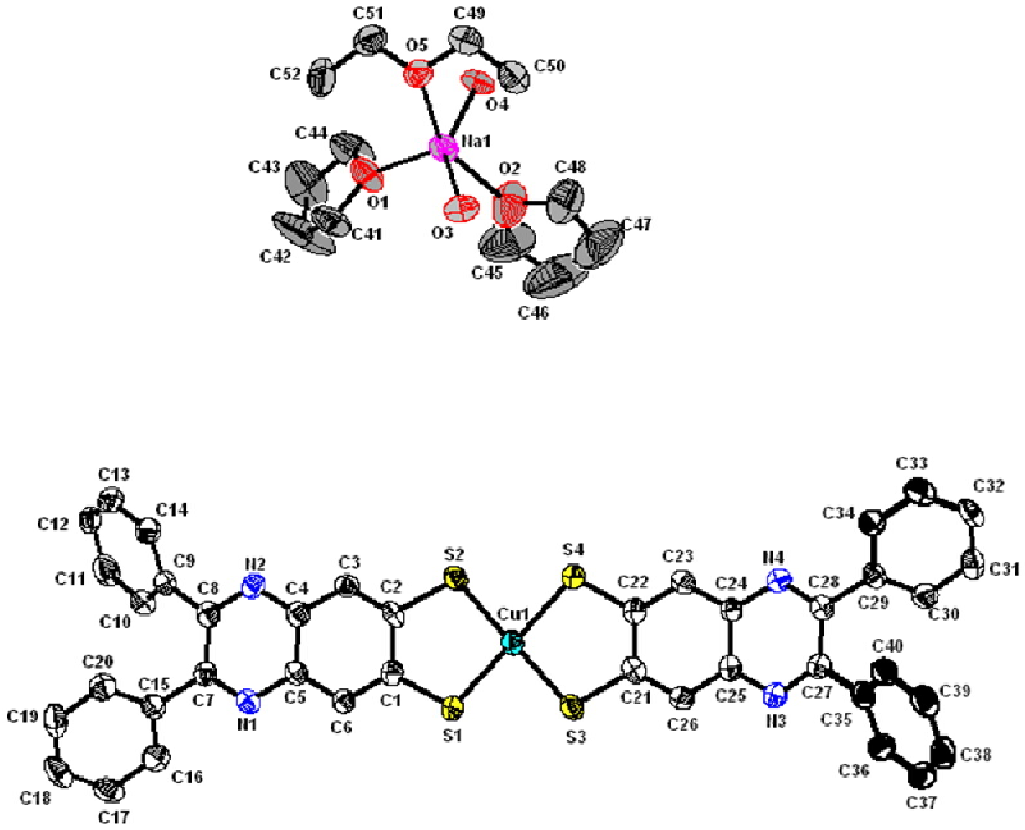


**Fig. 4.6**. Thermal ellipsoid plot of compound **2** (70% probability, hydrogen atoms omitted for clarity).

The bending deviation ($\eta$) between the SMS plane and SCCS plane is characterized by the dihedral angle i.e., the bending deviations ($\eta$) of planarity between {S1Cu1S2} and {S1C1C2S2} planes and {S3Cu1S4} and {S3C21C22S4} planes present in the {Cu1S1S2C1C2} and {Cu1S3S4C21C22} chelating rings with angles 0.81° and 1.94°, respectively in the complex **2**. The bending deviations ($\eta$) of planarity between {S1Au1S2} and {S1C1C2S2} planes and {S3Au1S4} and {S3C21C22S4} planes present in the {Au1S1S2C1C2} and {Au1S3S4C21C22} dithiolate-chelating rings with angles 0.41° and 0.47°, respectively in the complex **5**.

In the crystal structures of the complexes **2** and **5**, the complexic cationic unit is $[Na(THF)_2(OH_2)_2(C_2H_5OC_2H_5)]^+$. Interestingly, in these complexes $Na^+$ ion is not coordinating with any one of the nitrogen atoms of the dithiolene anionic complex, may be due to more steric hindrance created by two THF solvent molecules around Na cation. When we observe coordination environment around the $Na^+$ ion, it was found to be

slightly distorted square pyramidal geometry that includes coordination by two oxygen donor atoms of water molecules, one oxygen atom of diethyl ether and the remaining two coordination sites are occupied by two different THF molecules as shown in Fig. 4.6 and Fig. 4.7 (thermal ellipsoidal plots). The Na–$O_{(solvent)}$ coordination bond distances lie in the range of 2.229–2.497 Å.

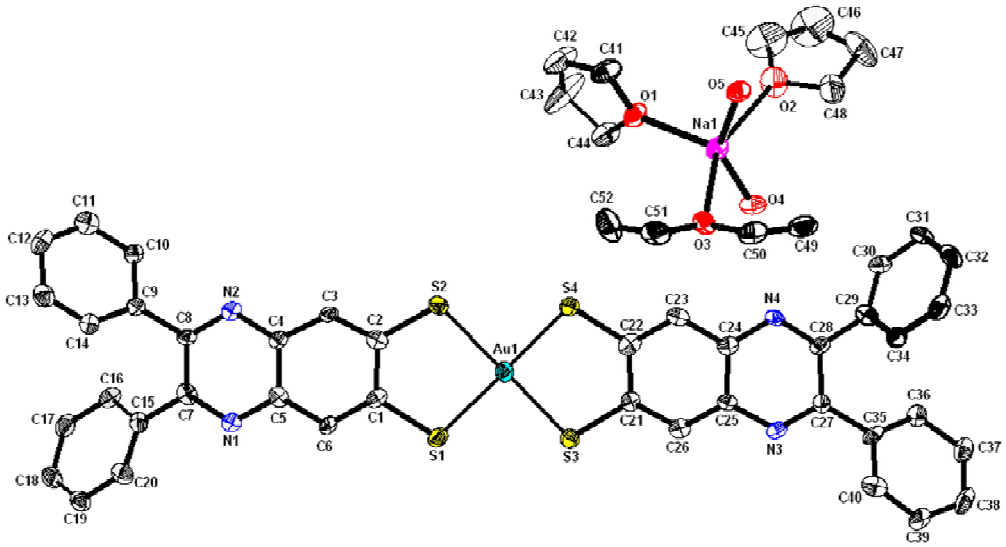


**Fig. 4.7**. Thermal ellipsoidal plot of compound **5** (40% probability, hydrogen atoms are omitted for clarity).

*Recrystallization from Acetone Solvent: Compounds 3 and **6***

Both complexes {[$Na(CH_3COCH_3)_2(OH_2)$][$Cu(diPh\text{-}6,7\text{-}qdt)_2$] (**3**) and complex [$Na(CH_3COCH_3)_2(OH_2)$][$Au(diPh\text{-}6,7\text{-}qdt)_2$] (**6**) crystallize in triclinic space group *P*-1. The asymmetric unit in the crystal structures of the both complexes **3** and **6** (represented as labeled atoms) contain one $\{Cu(diPh\text{-}6,7\text{-}qdt)\}^{1-}$ complexic anion, one sodium coordination complex which is coordinated by two acetone solvent molecules and one water molecule being located at symmetry center as shown in Figs. 4.8(a) and 4.8(b).

The structures of the both complexes show a square planar geometry around the M(III) (Cu(III) and Au(III)) ion with the average Cu–S and Au–S bond distances 2.180 ± 0.002 Å and 2.304 ± 0.000 Å in complexes **3** and **6**, respectively. However, there are deviations in the planar rings of dithiolene chelates (anionic fragment) with respect to {SMS} (M = Cu, Au) plane with dihedral angles 4.01° and 1.86° respectively as shown in Fig. 4.5(c) and 4.5(f).

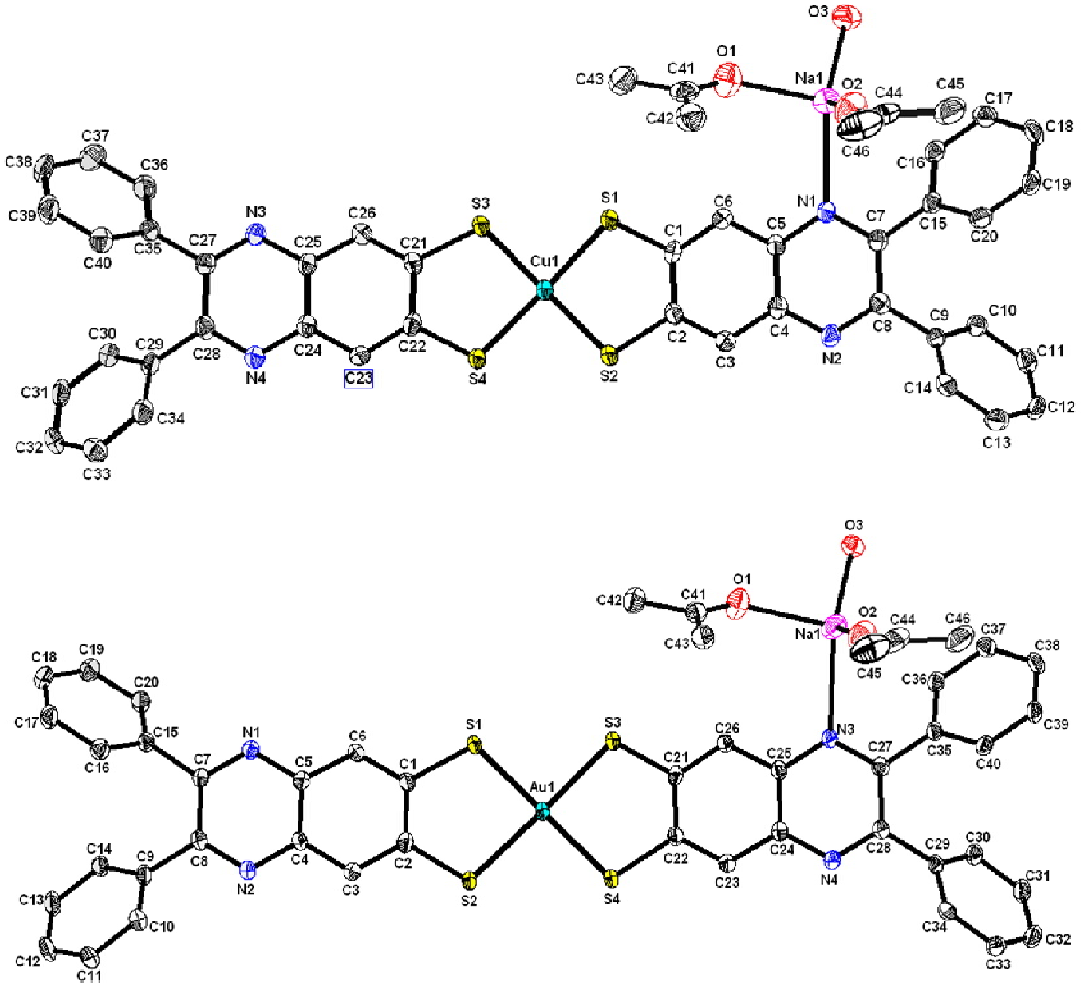


**Fig. 4.8**. Thermal ellipsoid plots of: (a) compound **3** (40% probability) (b) compound **6** (40% probability, hydrogen atoms omitted for clarity).

The bending deviations ($\eta$) of planarity between {S1Cu1S2} and {S1C1C2S2} planes and {S3Cu1S4} and {S3C21C22S4} planes present in the {Cu1S1S2C1C2} and {Cu1S3S4C21C22} chelating rings are the angles of 7.25° and 0.99°, respectively in the complex **3.** The bending deviations ($\eta$) of planarity between {S1Au1S2} and {S1C1C2S2} planes and {S3Au1S4} and {S3C21C22S4} planes present in the {Au1S1S2C1C2} and {Au1S3S4C21C22} dithiolate-chelating rings are 3.06° and 5.08°, respectively in the complex **6**.

In the crystal structure of complexes **3** and **6,** only one nitrogen atom of dithiolene complex is coordinated to $Na^+$ counter ion (Mode I, Scheme 4.3, vide infra). When we observe the coordination around $Na^+$ ion, it is found to be in almost tetrahedral environment, $Na^+$ ion is coordinated by one nitrogen atom from dithiolene complexic

anion, one water molecule and the remaining two coordination sites are occupied by two oxygen atoms of two different acetone (solvent) molecules as shown in Figs. 4.8(a) and 4.8(b), for complexes **3** and **6** respectively. The Na–N1 bond distances are 2.597 Å and 2.622 Å in complexes **3** and **6** respectively**,** which are in good agreement with relevant literature reports [84–87]. The Na–$O_{(solvent)}$ coordination bond distances lie in the range of 2.336 to 2.352 Å.

*Recrystallization from Acetonitrile Solvent: Compound **4***

Crystals of the complex $\{[Na(CH_3CN)][Cu(diPh\text{-}6,7\text{-}qdt)_2]\}_n$ (**4**) were grown from acetonitrile solvent and it crystallizes in monoclinic space group $P2_1/c$. The asymmetric unit in the crystal structure of complex **4** [represented as labeled atoms, in Fig. 4.9(a)] contains one $\{diph\text{-}6,7\text{-}qdt\}^{2-}$ ligand and two acetonitrile (solvent) molecules, one Cu in general position and one Cu and Na atom, that are located at symmetry center as shown in Fig. 4.9(a).

The structure of complex **4** shows perfect square planar geometry around the Cu(III) ion because it has no bending deviation (0.0°) in the planarity of the dithiolene chelating rings (CSSC plane) with respect to the {SMS} plane in complex **4** as shown in Fig. 4.5(d). The average Cu–S bond distance is 2.180 ± 0.003 Å in complex **4**. There is a deviation in planarity of dithiolene chelating ring with bending angle ($\eta$) of 5.01° between the {S1Cu1S2} and {S1C1C2S2} planes present in the {Cu1S1S2C1C2} chelating ring are shown in Fig. 4.5(d).

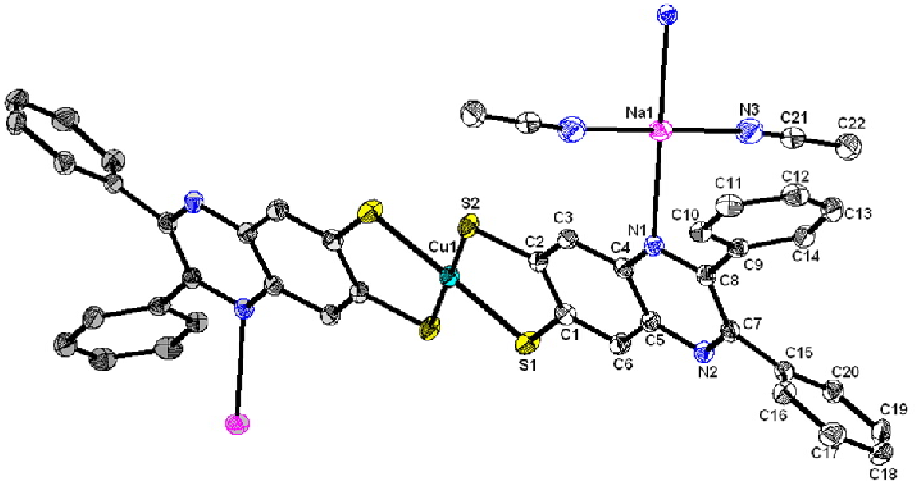

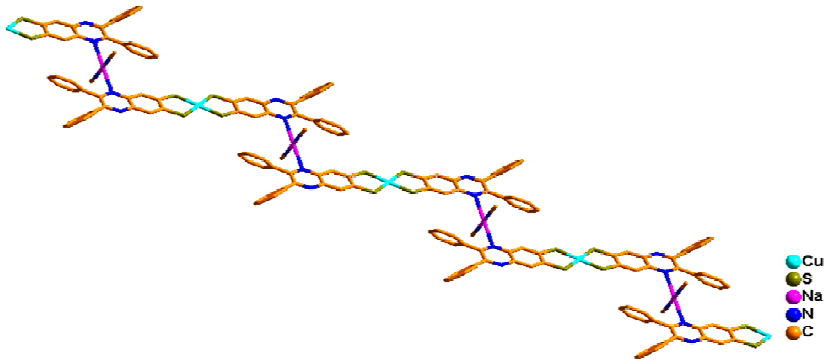


**Fig. 4.9.** Thermal ellipsoid plots of: (a) compound **4** (40% probability); (b) extended 1D network in the crystal structure of the compound **4 (**Hydrogen atoms omitted for clarity).

In the crystal structure of complex **4**, one of the nitrogen atoms of quinoxaline moiety of dithiolene complex is coordinated to $Na^+$ counter ion (Mode II, Scheme 4.3, vide infra). When we consider the geometry around $Na^+$ ion, it is found to be in almost tetrahedral environment: $Na^+$ ion is coordinated by two nitrogen atoms from two different $[M(diph\text{-}6,7\text{-}qdt)_2]^{1-}$ anions that are parallel to each other and the remaining two coordination sites are occupied by two different acetonitrile molecules. This way, complexes **4**, in their crystal structures, are extended to one-dimensional coordination polymers as shown Fig. 4.9(b). The Na–N1 bond distance is 2.503 Å in complex **4**, which is a good agreement with relevant literature reports [81–84]. The $Na–N3_{(solvent)}$ coordination bond distances lie in the range of 2.406 Å.

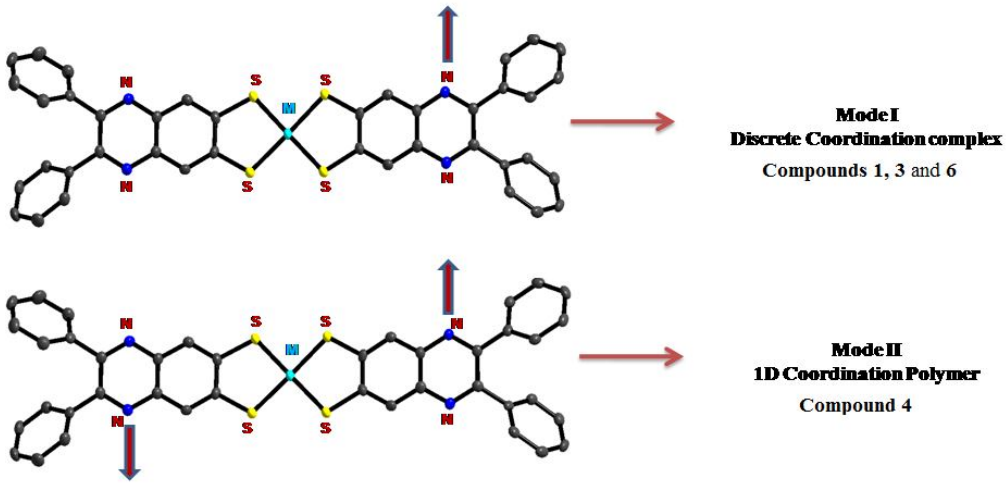


**Scheme 4.3.** Observed coordination modes of counter ion with $[M(diPh\text{-}6,7\text{-}qdt)_2]^{1-}$ (M = Cu and Au) in the coordination complexes **1–6**.

**Influential role of bulky coordinating molecules in obtaining the low dimensional compounds:**

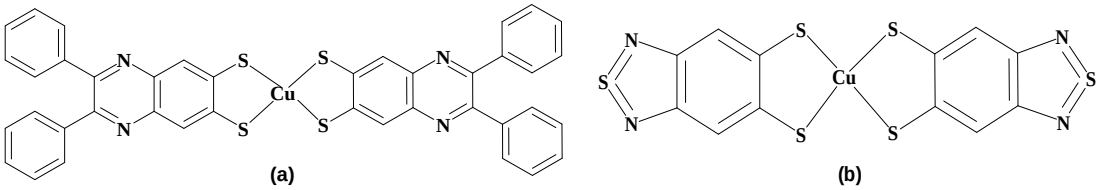


**Scheme 4.4.** (a) Complexic anion $[Cu(diph\text{-}6,7\text{-}qdt)_2]^-$ (b) Complexic anion $[Cu(btdt)_2]^-$ ($btdt^{2-}$ = 2,1,3-benzenethiadiazole-5,6-dithiolate)

The compounds **1–3, 5** and **6** presented in the study are discrete compounds and compound **4** is one dimensional compound. The size of the solvent molecules, the hybridization of the central carbon atom attached to the coordinating atom of the solvent molecule and the size, bulkiness of the dithiolene moiety are major factors in obtaining the molecular and low dimensional solids. In continuation to our previous work of tuning the dimensionality of coordination networks in terms of the geometry of central carbon of solvents through their coordination with sodium metal ion, we have now extended the concept to bulky dithiolene ligands. In this progression, we synthesized a bulky $H_2$diPh-6,7-qdt type dithiolene ligand as shown in the scheme 4.4, in which the four phenyl groups are attached to the quinoxaline ring that imparts the bulkiness in terms of size of the ligand in comparison to the btdt ligand.

The dimensionality of the Na-btdt compounds in our previous work [83] mainly depends on the number of btdt ligands connected to the sodium metal ion (first coordination sphere). As the number of the btdt ligands in the sodium coordination sphere increases the dimensionality increases which is reflected in the acetonitrile mediated Na-btdt 3D compound in which four btdt ligands are present in the coordination sphere. The accommodation of more number of btdt ligands in combination with the solvent molecules in the sodium coordination sphere is mainly dependent upon the crowdedness created by the dithiolene ligands and solvent molecules. When we compare with the $H_2$btdt ($btdt^{2-}$ = 2,1,3-benzenethiadiazole-5,6-dithiolate)ligand, the $H_2$diPh-6,7-qdt ligand is more bulkier and creates huge crowdedness in the metal coordination sphere; as a result in the compounds **1**–**6**, the coordination numbers of sodium ion is restricted to only four and five rather than six coordination (which is observed in the Na-btdt compounds) [83]. The

bulkiness of the ligand $H_2$diPh-6,7-qdt allows coordination around Na ion with less coordination number which is the primarily the reason accountable for the low dimensional and discrete compounds.

In case of compound **1** the coordination sphere contains one $H_2$diPh-6,7-qdt ligand connected to the sodium ion and the remaining three coordination sites are occupied by the three methanol molecules thereby prevents the spatial expansion as shown in Fig. 4.10. The bulkiness of the dithiolene ligand in the coordination sphere and the low coordination number of the central sodium ion favors to accommodate the solvent methanol molecules in to the residual coordination sites rather than another bulky dithiolene ligand. The solvent molecule methanol is regarded as bulky moiety in terms of the hybridization of the carbon atom ($sp^3$) attached to the coordinating atom and known to form low dimensional compounds revealed from our previously reported compound 1D $\{[Na(CH_3OH)_4][Cu(btdt)_2]\}_n$ [83]. Based on aforementioned discussion, the tetra co-ordinated Na in the compound **1** experiences a huge crowdedness due to both bulky coordinated solvent molecules and bulky dithiolene ligand.

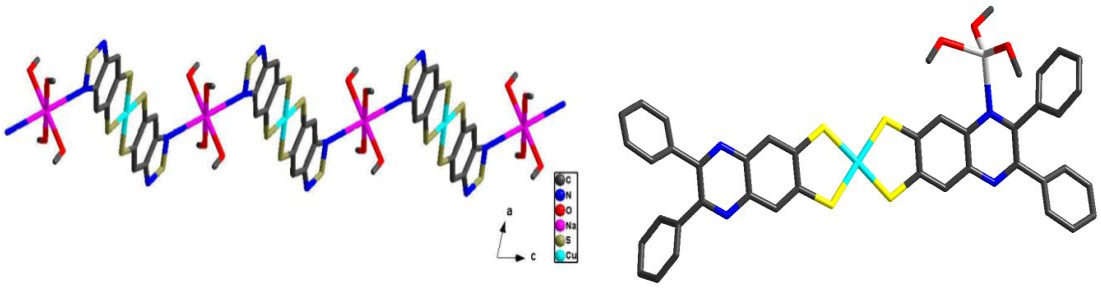

**Fig. 4.10.** 1D coordination polymer $\{[Na(CH_3OH)_4][Cu(btdt)_2]\}_n$ (left) and discrete $[Na(CH_3OH)_3][Cu(diPh\text{-}6,7\text{-}qdt)_2]\cdot MeOH$ (right).

But interestingly, when THF is used as recrystallizing solvent, an ion-pair discrete compound $[Na(THF)_2(OH_2)_2(C_2H_5OC_2H_5)][Cu(diPh\text{-}6,7\text{-}qdt)_2]$ (**2**) is formed. The coordination number of the sodium metal ion the in cationic part is five. The bulky THF molecules in the sodium coordination sphere do not allow even one dithiolene ligand to coordinate with the sodium ion which results in the formation of ion-pair compound. This

example clearly shows the affect of bulkiness of the coordinating solvents in tuning the dimensionality of the final architecture (Fig. 4.6).

To rationalize the concept in terms of the bulkiness of the coordinating ligands, we have chosen acetone (in which the carbon atom attached to coordinated oxygen atom is $sp^2$ hybridized) as recrystallizing solvent resulting in the formation of discrete compound $[Na(CH_3COCH_3)_2(OH_2)][Cu(diPh\text{-}6,7\text{-}qdt)_2]$ (**3**). In this case also, the bulky dithiolene ligand diPh-6,7-qdt and coordinated acetone molecules do not favor to accommodate the other dithiolene moiety in to the coordination sphere resulting in the formation of discrete compound rather than coordination polymer. Even though the hybrid orbitals on the carbon atom attached to the coordinated oxygen atom is less bulkier (i.e. $sp^2$), but it does not allow the other dithiolene moiety to enter into the coordination sphere to coordinate with the sodium ion due to the bulkiness of the diph-6,7-qdt molecule. Only two acetone molecules are coordinated to the sodium ion and the other coordination site is occupied by the water molecule; this is because the steric hindrance created by the methyl groups in the acetone molecule does not allow the other (i.e. third acetone) in to the coordination sphere. But when acetone molecule is used as recrystallizing solvent in case of btdt ligand, it results in the formation of 2D compound $\{[Na(CH_3COCH_3)_2][Cu(btdt)_2]\}_n$ as shown in Fig. 4.11 . The sodium coordination sphere in this compound consists of four dithiolene ligands and two acetone molecules which results in spatial expansion to form a 2D compound as shown in Fig. 4.11.

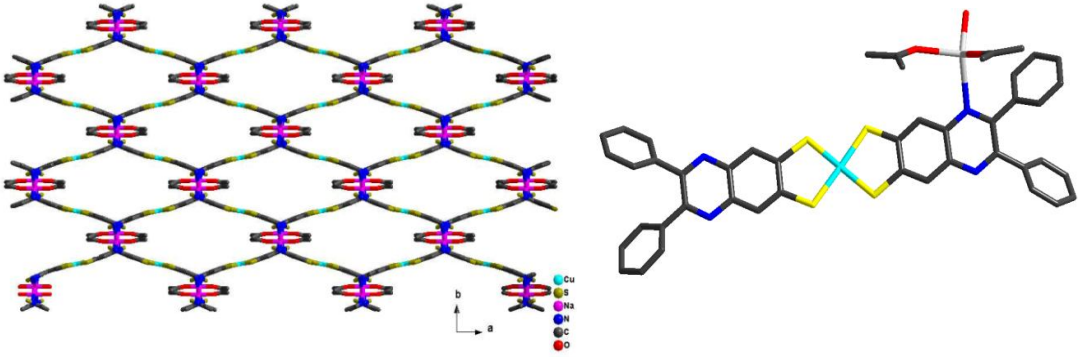


**Fig. 4.11.** 2D coordination polymer $\{[Na(CH_3COCH_3)_2][Cu(btdt)_2]\}_n$ (left) and discrete $[Na(CH_3COCH_3)_2(OH_2)][Cu(diPh\text{-}6,7\text{-}qdt)_2]$ (right).

Finally when we use acetonitrile as recrystallizing solvent, it results in the formation of 1D $\{[Na(CH_3CN)][Cu(diPh\text{-}6,7\text{-}qdt)_2]\}_n$ chain. In this compound, the sodium coordination sphere contains two dithiolene moieties and two coordinated solvent

molecules. Due to less bulky (sp) hybrid orbitals on the carbon atom attached to the coordinating atom of solvent molecule, in this compound the sodium coordination sphere favors to accommodate the other bulkier dithiolene moiety in to the coordination sphere which is not favored in the case of methanol ($sp^3$), acetone ($sp^2$). Also from our previously reported 3D compound $\{[Na(CH_3CN)_2][Cu(btdt)_2]\}_n$, acetonitrile is known to form a higher dimensional compounds (3D) as shown in Fig. 4.12 .

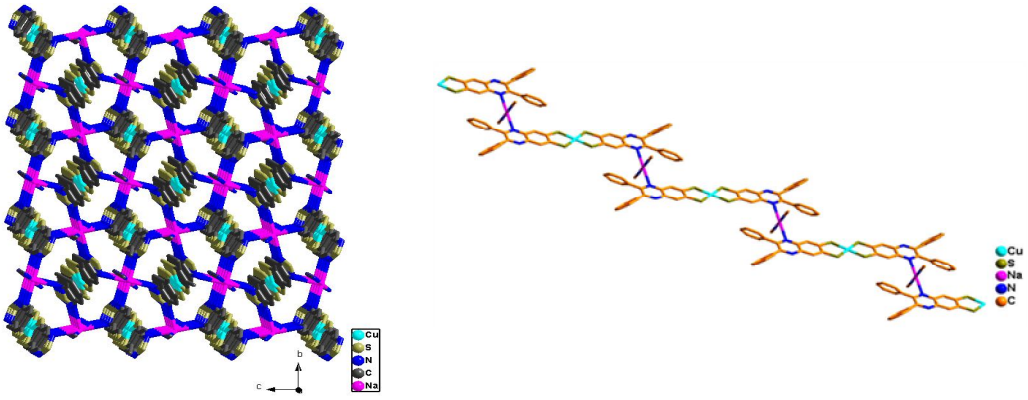


**Fig. 4.12.** 3D coordination polymer $\{[Na(CH_3CN)_2][Cu(btdt)_2]\}_n$ (left) and 1D coordination polymer $\{[Na(CH_3CN)][Cu(diPh\text{-}6,7\text{-}qdt)_2]\}_n$ (right).

The use of less bulky solvent molecule, acetonitrile (associated with sp hybridisation) allows sodium to accommodate two bulkey ligands (in compound **4**), which is not possible in compounds **1**-**3** and **5**-**6**. Table 4.1 shows the comparison of the dimensionality of compounds containing $btdt^{2-}$ and $diph\text{-}6,7\text{-}qdt^{2-}$ lingad anions.

**Table 4.1.** Table showing comparison of the dimensionality of the compounds containing $btdt^{2-}$ and $diPh\text{-}6,7\text{-}qdt^{2-}$ ligands.

| **Solvent (hybridization of the central carbon)** | **$H_2$btdt** | **$H_2$diPh-6,7-qdt** |
|---|---|---|
| Methanol ($sp^3$) | 1D | Discrete |
| THF ($sp^3$) | 1D | Discrete Ion-pair |
| Acetone ($sp^2$) | 2D | Discrete |
| Acetonitrile (sp) | 3D | 1D |

## 4.3. Experimental Details

### *4.3.1. General procedures*

FLASH EA series 1112 CHNS analyzer was used for elemental analyses. Infrared spectra were recorded as KBr pellets on a JASCO–5300 FT–IR spectrophotometer at 298K. Electronic absorption spectra of solutions were recorded on a Cary 100 Bio UV-vis spectrophotometer. Diffuse reflectance spectra of solid compounds were recorded on a UV-3600 Shimadzu UV-vis-NIR spectrophotometer. NMR spectra were recorded in Bruker 400 MHz spectrometer. The chemical shifts ($\delta$) are reported in ppm. A Cypress model CS-1090/CS-1087 electro analytical system was used for cyclic voltammetric experiments. The electrochemical experiments were performed in DMF containing $[Bu_4N][ClO_4]$ as a supporting electrolyte, using a conventional cell consisting of two platinum wires as working and counter electrodes, and a Ag/AgCl electrode as a reference. The potentials reported here are uncorrected for junction contributions.

### *4.3.2. Materials*

All the reagents for the syntheses were commercially available and used as received. 2,3-diphenylquinoxaline-6,7-dithiol ($H_2$diPh-6,7-qdt) ligand was synthesized according to literature procedure [85]. Syntheses of metal complexes were performed under $N_2$ using standard inert-atmosphere techniques. Solvents were dried by standard procedures.

***Synthesis of Copper Complexes 1-4***

The diPh-6,7-qdt dianion is generated, *in situ*, by treatment of $H_2$diPh-6,7-qdt (0.20 g, 0.577 mmol) with excess amount of NaOH (0.057 g, 1.44 mmol) in MeOH (10.0 mL). To the resulting clear red solution, solid $CuCl_2$ (0.038 g, 0.288 mmol) was added and the reaction mixture was stirred for 30 min in presence of open atmosphere. The resulting dark black micro crystalline solid was separated by filtration and air dried. Yield: 0.10 g**.** IR (KBr, $cm^{-1}$): 3400w, 1635m, 1527w, 1433s, 1344s, 1250m, 1192s, 1097vs, 1060s, 1022m, 964w, 862w, 827m, 771s, 729w, 698s. $^1$H NMR (400 MHz, $\delta$ ppm) (DMSO-$d_6$): 7.679 (s, 4H), 7.427 (dd, 8H), 7.342 (qt, 12H). Copper complexes **1**–**4** have been prepared from the different solvent recrystallization of this dark green colored solid.

The Characterization data for **1**–**4** are described below.

**$[Na(CH_3OH)_3][Cu(diPh\text{-}6,7\text{-}qdt)_2]\cdot MeOH$ (1).** Dark green colored crystals of compound **1** were obtained from the vapor diffusion of diethyl ether into a solution of the black solid compound dissolved in MeOH solvent. Anal. Calcd. for $C_{44}H_{40}CuN_4NaO_4S_4$: C, 58.48; H,

4.46; N, 6.20%. Found: C, 58.45; H, 4.44; N, 6.19%. IR (KBr, $cm^{-1}$): 3400w, 1635m, 1527w, 1433s, 1344s, 1250m, 1192s, 1097vs, 1060s, 1022m, 964w, 862w, 827m, 771s, 729w, 698s. $^1$H NMR (400 MHz, $\delta$ ppm) (DMSO-$d_6$): 7.679 (s, 4H), 7.427 (dd, 8H), 7.342 (qt, 12H).

**$[Na(THF)_2(OH_2)_2(C_2H_5OC_2H_5)][Cu(diPh\text{-}6,7\text{-}qdt)_2]$ (2).** Dark green colored crystals of compound **2** were obtained from the vapor diffusion of diethyl ether into a solution of the black solid compound dissolved in THF solvent. Anal. Calcd. for $C_{52}H_{54}CuN_4NaO_5S_4$: C, 60.65; H, 5.28; N, 5.44%. Found: C, 60.62; H, 5.24; N, 5.41%. IR (KBr, $cm^{-1}$): 3400w, 1635m, 1527w, 1433s, 1344s, 1250m, 1192s, 1097vs, 1060s, 1022m, 964w, 862w, 827m, 771s, 729w, 698s. $^1$H NMR (400 MHz, $\delta$ ppm) (DMSO-$d_6$): 7.679 (s, 4H), 7.427 (dd, 8H), 7.342 (qt, 12H).

**$[Na(CH_3COCH_3)_2(OH_2)][Cu(diPh\text{-}6,7\text{-}qdt)_2]$ (3).** Dark green colored crystals of compound **3** were obtained from the vapor diffusion of diethyl ether into a solution of the black solid compound dissolved in acetone solvent. Anal. Calcd. for $C_{46}H_{38}CuN_4NaO_3S_4$: C, 60.74; H, 4.21; N, 6.16%. Found: C, 60.70; H, 4.19; N, 6.13%. IR (KBr, $cm^{-1}$): 3400w, 1635m, 1527w, 1433s, 1344s, 1250m, 1192s, 1097vs, 1060s, 1022m, 964w, 862w, 827m, 771s, 729w, 698s. $^1$H NMR (400 MHz, $\delta$ ppm) (DMSO-$d_6$): 7.679 (s, 4H), 7.427 (dd, 8H), 7.342 (qt, 12H).

**$\{[Na(CH_3CN)][Cu(diPh\text{-}6,7\text{-}qdt)_2]\}_n$ (4**). Dark green colored crystals of compound **4** were obtained from the vapor diffusion of diethyl ether into a solution of the black solid compound dissolved in acetonitrile solvent. Anal. Calcd. for $C_{44}H_{30}CuN_6NaS_4$: C, 61.63; H, 3.52; N, 9.79%. Found: C, 61.59; H, 3.51; N, 9.77%. IR (KBr, $cm^{-1}$): 3400w, 1635m, 1527w, 1433s, 1344s, 1250m, 1192s, 1097vs, 1060s, 1022m, 964w, 862w, 827m, 771s, 729w, 698s. $^1$H NMR (400 MHz, $\delta$ ppm) (DMSO-$d_6$): 7.679 (s, 4H), 7.427 (dd, 8H), 7.342 (qt, 12H).

**Syntheses of Gold Complexes 5 and 6**

The diPh-6,7-qdt dianion is generated, *in situ*, by treatment with $H_2$diPh-6,7-qdt (0.05 g, 0.144 mmol) with excess amount of NaOH (0.014 g, 0.360 mmol) in MeOH (10 mL). To the resulting clear red solution, solid $HAuCl_4 \cdot 3H_2O$ (0.028 g, 0.072 mmol) was added and the reaction mixture was stirred for 30 min under nitrogen atmosphere. The resulting brown solid was separated by filtration and air dried. Yield: 0.080 g. IR (KBr, $cm^{-1}$): 3400w, 1635m, 1527w, 1433s, 1344s, 1250m, 1192s, 1097vs, 1060s, 1022m, 964w, 862w,

827m, 771s, 729w, 698s. $^1$H NMR (400 MHz, $\delta$ ppm) (DMSO-$d_6$): 7.679 (s, 4H), 7.427 (dd, 8H), 7.342 (qt, 12H). Gold complexes **5**–**6** have been prepared from the various solvent recrystallization of the above mentioned brown-colored solids as described below.

**[Na(THF)$_2$(OH$_2$)$_2$(C$_2$H$_5$OC$_2$H$_5$)][Au(diPh-6,7-qdt)$_2$] (5).** The red colored crystals of compound **5** was obtained from the vapor diffusion of ether into a solution of the brown solid compound dissolved in THF. Anal. calcd. for $C_{52}H_{54}AuN_4NaO_5S_4$: C, 53.69; H, 4.67; N, 4.81%. Found: C, 53.66; H, 4.66; N, 4.81%. IR (KBr, cm$^{-1}$): 3400w, 1635m, 1527w, 1433s, 1344s, 1250m, 1192s, 1097vs, 1060s, 1022m, 964w, 862w, 827m, 771s, 729w, 698s. $^1$H NMR (400 MHz, $\delta$ ppm) (DMSO-$d_6$): 7.679 (s, 4H), 7.427 (dd, 8H), 7.342 (qt, 12H).

**[Na(CH$_3$COCH$_3$)$_2$(OH$_2$)][Au(diPh-6,7-qdt)$_2$] (6).** Red colored crystals of compound **6** were obtained from the vapor diffusion of ether into a solution of the brown colored solid compound dissolved in acetone solvent. Anal. calcd. for $C_{46}H_{38}AuN_4NaO_3S_4$: C, 52.97; H, 3.67; N, 5.37%. Found: C, 52.94; H, 3.65; N, 5.36%. IR (KBr, cm$^{-1}$): 3400w, 1635m, 1527w, 1433s, 1344s, 1250m, 1192s, 1097vs, 1060s, 1022m, 964w, 862w, 827m, 771s, 729w, 698s. $^1$H NMR (400 MHz, $\delta$ ppm) (DMSO-$d_6$): 7.679 (s, 4H), 7.427 (dd, 8H), 7.342 (qt, 12H).

*4.3.4 Single crystal structure determination of complexes **1**–**6***

Single crystals, suitable for facile structural determination for the compounds (**1**–**6**), were measured on a three circle Bruker SMART APEX CCD area detector system under Mo–K$\alpha$ ($\lambda$ = 0.71073 Å) graphite monochromatic X–ray beam. The frames were recorded with an $\omega$ scan width of 0.3º, each for 8 s, crystal-detector distance 60 mm, collimator 0.5 mm. Data reduction performed by using SAINTPLUS [86]. Empirical absorption corrections were performed using equivalent reflections performed program SADABS [86]. The Structures were solved by direct methods and least-square refinement on $F^2$ for all the compounds **1**–**6** by using SHELXS-97 [87]. All non-hydrogen atoms were refined anisotropically. The hydrogen atoms were included in the structure factor calculation by using a riding model. Selected bond lengths and angles for the compounds **1**–**6** are listed in Tables 4.2 – 4.7. The crystallographic parameters, data collection and structure refinement of the compounds **1**–**6** are summarized in Tables 4.8 and 4.9.

**Table 4.2**. Crystal data and structural refinement for complexes **1**–**3**.

| **Identification code** | **1** | **2** | **3** |
|---|---|---|---|
| Empirical formula | $C_{44}H_{40}CuN_4NaO_4S_4$ | $C_{52}H_{54}CuN_4NaO_5S_4$ | $C_{46}H_{38}CuN_4NaO_3S_4$ |
| Formula weight | 903.57 | 1029.76 | 909.57 |
| Temperature | 100(2) K | 100(2) K | 100(2) K |
| Wavelength | 0.71073 Å | 0.71073 Å | 0.71073 Å |
| Crystal system | Triclinic | Orthorhombic | Triclinic |
| Space group | *P* -1 | *P*2(1)2(1)2(1) | *P* -1 |
| Unit cell dimensions | a = 13.2345(17) Å | a = 10.8504(10) Å | a = 9.908(2) Å, |
| | b = 13.5236(17) Å | b = 21.147(2) Å | b = 11.154(2) Å |
| | c = 13.8584(17) Å | c = 21.720(2) Å | c = 19.409(4) Å |
| | α = 63.310(2)° | α = 90° | α = 97.52(3)° |
| | β = 65.795(2)° | β = 90° | β = 99.35(3)° |
| | γ = 72.523(2)° | γ = 90° | γ = 93.70(3)° |
| Volume | 2000.6(4) $Å^3$ | 4983.8(8) $Å^3$ | 2090.2(7) $Å^3$ |
| Z | 2 | 4 | 2 |
| Density (calculated) | 1.500 $Mg/m^3$ | 1.372 $Mg/m^3$ | 1.445 $Mg/m^3$ |
| F(000) | 936 | 2152 | 940 |
| Crystal size($mm^3$) | 0.42 x 0.18 x 0.06 | 0.46 x 0.22 x 0.06 | 0.42 x 0.12 x 0.06 |
| Theta range for data collection | 1.70 to 25.99° | 1.34 to 26.00° | 1.07 to 25.97° |
| Reflections collected | 20298 | 51954 | 16140 |
| Independent reflections | 7766 [R(int) = 0.0405] | 9774 [R(int) = 0.0544] | 8050 [R(int) = 0.0278] |
| Completeness to theta = 25.97° | 98.6 % | 99.9 % | 98.4 % |
| Max. and min. transmission | 0.9527 and 0.7256 | 0.9611 and 0.7493 | 0.9547 and 0.7353 |
| Data / restraints / parameters | 7766 / 0 / 542 | 9774 / 0 / 622 | 8050 / 0 / 544 |
| Goodness-of-fit on $F^2$ | 1.035 | 1.069 | 1.046 |
| Final R indices [I>2sigma(I)] | R1 = 0.0437, wR2 = 0.1088 | R1 = 0.0517, wR2 = 0.1186 | R1 = 0.0383, wR2 = 0.0880 |
| R indices (all data) | R1 = 0.0580, wR2 = 0.1172 | R1 = 0.0582, wR2 = 0.1224 | R1 = 0.0528, wR2 = 0.0945 |
| Largest diff. peak and hole | 0.857 and -0.644 e.$Å^{-3}$ | 0.836 and -0.317 e.$Å^{-3}$ | 0.628 and -0.304 e.$Å^{-3}$ |

**Table 4.3.** Crystal data and structural refinement for complexes **4**–**6**.

| **Identification code** | **4** | **5** | **6** |
|---|---|---|---|
| Empirical formula | $C_{44}$ $H_{30}$ Cu $N_6$ Na $S_4$ | $C_{52}$ $H_{54}$ Au $N_4$ Na $O_5$ $S_4$ | $C_{46}$ $H_{38}$ Au $N_4$ Na $O_3$ $S_4$ |
| Formula weight | 857.51 | 1163.19 | 1043.00 |
| Temperature | 100(2) K | 100(2) K | 100(2) K |
| Wavelength | 0.71073 Å | 0.71073 Å | 0.71073 Å |
| Crystal system | Monoclinic | Orthorhombic | Triclinic |
| Space group | *P*21/c | *P*2(1)2(1)2(1) | *P*-1 |
| Unit cell dimensions | a = 8.0075(7) Å | a = 10.9197(13) Å | a = 9.9685(9) Å |
| | b = 17.5571(15) Å | b = 21.229(3) Å | b = 11.2317(10) Å |
| | c = 16.0207(11) Å | c = 21.680(3) Å | c = 19.4759(17) Å |
| | α = 90° | α = 90° | α = 97.7230(10)° |
| | β = 117.247(3)° | β = 90° | β = 99.9190(10)° |
| | γ = 90° | γ = 90° | γ = 94.1730(10)° |
| Volume | 2002.4(3) $Å^3$ | 5025.7(10) $Å^3$ | 2118.2(3) $Å^3$ |
| Z | 2 | 4 | 2 |
| Density (calculated) | 1.422 $Mg/m^3$ | 1.537 $Mg/m^3$ | 1.635 $Mg/m^3$ |
| Absorption coefficient | 0.806 $mm^{-1}$ | 3.153 $mm^{-1}$ | 3.727 $mm^{-1}$ |
| F(000) | 880 | 2352 | 1040 |
| Crystal size($mm^3$) | 0.56 x 0.32 x 0.06 | 0.36 x 0.18 x 0.06 | 0.36 x 0.16 x 0.04 |
| Theta range for data collection | 1.84 to 24.96° | 1.34 to 26.05° | 1.84 to 25.00° |
| Reflections collected | 18777 | 38841 | 19095 |
| Independent reflections | 3506 [R(int) = 0.0277] | 9898 [R(int) = 0.1098] | 7322 [R(int) = 0.0260] |
| Completeness to theta = 25.97° | 99.9 % | 99.8 % | 98.3 % |
| Max. and min. transmission | 0.9533 and 0.6611 | 0.8334 and 0.3965 | 0.8652 and 0.3472 |
| Data / restraints / parameters | 3506 / 0 / 257 | 9898 / 0 / 606 | 7322 / 0 / 536 |
| Goodness-of-fit on $F^2$ | 1.063 | 1.030 | 1.026 |
| Final R indices [I>2sigma(I)] | R1 = 0.0278, wR2 = 0.0785 | R1 = 0.0914, wR2 = 0.2135 | R1 = 0.0305, wR2 = 0.0742 |
| R indices (all data) | R1 = 0.0291, wR2 = 0.0799 | R1 = 0.1415, wR2 = 0.2446 | R1 = 0.0332, wR2 = 0.0757 |
| Largest diff. peak and hole | 0.340 and -0.228 e.$Å^{-3}$ | 5.389 and -1.879 e.$Å^{-3}$ | 2.904 and -0.873 e.$Å^{-3}$ |

**Table 4.4.** Selected bond lengths [Å] and angles [°] for complex **1**.

| | | | |
|---|---|---|---|
| Cu(2)-S(4) | 2.1668(8) | S(4)-Cu(2)-S(1) | 174.86(3) |
| Cu(2)-S(3) | 2.1776(8) | S(4)-Cu(2)-S(2) | 87.49(3) |
| S(1)-C(1) | 1.748(3) | S(1)-Cu(2)-S(2) | 92.12(3) |
| N(1)-C(7) | 1.318(3) | C(1)-S(1)-Cu(2) | 104.65(9) |
| N(3)-Na(1) | 2.496(2) | C(7)-N(1)-C(5) | 117.8(2) |
| C(36)-Na(1) | 3.003(3) | C(27)-N(3)-Na(1) | 121.60(17) |
| O(1)-C(41) | 1.420(4) | C(6)-C(1)-S(1) | 120.7(2) |
| O(1)-Na(1) | 2.242(3) | C(41)-O(1)-Na(1) | 131.11(19) |
| O(1)-H(1O) | 0.79(4) | O(3)-Na(1)-O(1) | 138.84(12) |
| O(2)-C(42) | 1.421(4) | O(3)-Na(1)-O(2) | 97.18(12) |
| O(2)-Na(1) | 2.313(2) | O(1)-Na(1)-O(2) | 87.69(9) |
| Na(1)-O(3) | 2.240(3) | O(3)-Na(1)-N(3) | 112.76(10) |
| O(4)-C(44) | 1.417(4) | O(1)-Na(1)-N(3) | 101.30(9) |
| O(4)-H(4O) | 0.73(4) | O(2)-Na(1)-N(3) | 115.77(8) |
| O(3)-C(43) | 1.447(9) | C(43)-O(3)-Na(1) | 120.1(4) |

**Table 4.5.** Selected bond lengths [Å] and angles [°] for complex **2**

| | | | |
|---|---|---|---|
| Cu(1)-S(2) | 2.1732(10) | O(3)-Na(1)-O(4) | 146.23(14) |
| S(2)-C(2) | 1.758(4) | O(3)-Na(1)-O(1) | 110.60(13) |
| N(1)-C(7) | 1.315(5) | O(4)-Na(1)-O(1) | 100.37(12) |
| N(2)-C(8) | 1.327(5) | O(3)-Na(1)-O(2) | 83.16(15) |
| Na(1)-O(3) | 2.216(3) | O(4)-Na(1)-O(2) | 80.50(15) |
| Na(1)-O(1) | 2.288(3) | O(1)-Na(1)-O(2) | 95.96(14) |
| Na(1)-O(2) | 2.456(4) | O(3)-Na(1)-O(5) | 92.54(12) |
| Na(1)-O(5) | 2.497(3) | O(4)-Na(1)-O(5) | 88.71(12) |
| O(1)-C(44) | 1.434(5) | O(1)-Na(1)-O(5) | 110.75(13) |
| O(5)-C(51) | 1.415(5) | O(2)-Na(1)-O(5) | 152.64(13) |
| S(2)-Cu(1)-S(4) | 86.95(4) | C(44)-O(1)-C(41) | 109.0(3) |
| S(2)-Cu(1)-S(3) | 179.40(4) | C(44)-O(1)-Na(1) | 123.5(3) |
| S(4)-Cu(1)-S(3) | 92.54(4) | C(51)-O(5)-C(49) | 111.5(3) |
| C(2)-S(2)-Cu(1) | 104.38(13) | C(51)-O(5)-Na(1) | 121.8(3) |
| C(27)-N(3)-C(25) | 118.7(3) | C(45)-O(2)-Na(1) | 135.5(4) |

**Table 4.6.** Selected bond lengths [Å] and angles [°] for complex **3**

| | | | |
|---|---|---|---|
| Cu(1)-S(3) | 2.1743(9) | S(3)-Cu(1)-S(2) | 176.61(3) |
| Cu(1)-S(1) | 2.1799(9) | S(4)-Cu(1)-S(2) | 88.88(3) |
| S(1)-C(1) | 1.750(2) | C(21)-S(3)-Cu(1) | 105.10(8) |
| N(2)-C(8) | 1.327(3) | C(7)-N(1)-Na(1) | 115.96(14) |
| N(1)-Na(1) | 2.597(2) | C(5)-N(1)-Na(1) | 123.93(15) |
| O(1)-C(41) | 1.222(3) | C(23)-C(22)-S(4) | 120.64(18) |
| O(1)-Na(1) | 2.283(2) | N(3)-C(27)-C(35) | 116.9(2) |
| C(41)-C(42) | 1.485(4) | C(41)-O(1)-Na(1) | 140.11(19) |
| O(2)-C(44) | 1.217(3) | O(1)-C(41)-C(42) | 122.2(3) |
| O(2)-Na(1) | 2.231(2) | C(44)-O(2)-Na(1) | 156.0(2) |
| O(3)-Na(1) | 2.307(2) | O(2)-Na(1)-O(1) | 101.48(8) |
| S(3)-Cu(1)-S(4) | 91.74(3) | O(2)-Na(1)-O(3) | 123.13(9) |
| S(3)-Cu(1)-S(1) | 87.38(3) | O(1)-Na(1)-O(3) | 93.30(8) |
| S(4)-Cu(1)-S(1) | 177.49(3) | O(2)-Na(1)-N(1) | 99.61(8) |
| C(1)-S(1)-Cu(1) | 104.14(8) | O(1)-Na(1)-N(1) | 102.44(8) |
| S(1)-Cu(1)-S(2) | 92.14(3) | O(3)-Na(1)-N(1) | 130.31(9) |

**Table 4.7.** Selected bond lengths [Å] and angles [°] for complex **4**.

| | | | |
|---|---|---|---|
| Cu(1)-S(1)#1 | 2.1664(4) | S(1)-Cu(1)-S(2) | 92.278(16) |
| Cu(1)-S(2)#1 | 2.1804(4) | C(1)-S(1)-Cu(1) | 104.51(6) |
| S(1)-C(1) | 1.7479(16) | N(3)#2-Na(1)-N(3) | 180.0 |
| Na(1)-N(3) | 2.4065(17) | N(3)-Na(1)-N(1)#2 | 98.78(5) |
| N(3)-C(21) | 1.139(2) | N(3)-Na(1)-N(1) | 81.22(5) |
| Na(1)-N(1) | 2.5030(13) | C(8)-N(1)-C(4) | 117.87(14) |
| Na(1)-C(10) | 3.0350(17) | C(8)-N(1)-Na(1) | 108.53(10) |
| N(1)-C(8) | 1.328(2) | C(4)-N(1)-Na(1) | 126.95(10) |
| S(1)#1-Cu(1)-S(1) | 180.00(2) | C(21)-N(3)-Na(1) | 173.17(15) |
| S(1)#1-Cu(1)-S(2) | 87.722(16) | C(6)-C(1)-S(1) | 119.98(13) |

**Table 4.8.** Selected bond lengths [Å] and angles [°] for complex **5**.

| | | | |
|---|---|---|---|
| Au(1)-S(2) | 2.305(4) | O(4)-Na(1)-O(5) | 143.6(6) |
| Au(1)-S(1) | 2.320(4) | O(4)-Na(1)-O(1) | 109.6(5) |
| S(2)-C(2) | 1.742(16) | O(5)-Na(1)-O(1) | 103.4(5) |
| C(8)-N(2) | 1.316(19) | O(4)-Na(1)-O(2) | 81.9(6) |
| O(4)-Na(1) | 2.215(13) | O(5)-Na(1)-O(2) | 79.9(6) |
| Na(1)-O(1) | 2.289(14) | O(1)-Na(1)-O(2) | 95.3(6) |
| Na(1)-O(2) | 2.464(17) | O(4)-Na(1)-O(3) | 92.4(5) |
| Na(1)-O(3) | 2.498(13) | O(5)-Na(1)-O(3) | 89.7(5) |
| O(3)-C(51) | 1.37(3) | O(1)-Na(1)-O(3) | 111.5(6) |
| O(1)-C(44) | 1.41(2) | O(2)-Na(1)-O(3) | 152.9(6) |
| S(2)-Au(1)-S(4) | 89.47(15) | C(51)-O(3)-C(50) | 114.9(17) |
| S(2)-Au(1)-S(3) | 179.69(17) | C(51)-O(3)-Na(1) | 123.7(13) |
| S(4)-Au(1)-S(3) | 90.45(15) | C(44)-O(1)-Na(1) | 126.8(12) |
| C(2)-S(2)-Au(1) | 104.5(6) | C(45)-O(2)-C(48) | 108(2) |
| C(21)-S(3)-Au(1) | 102.7(5) | C(45)-O(2)-Na(1) | 138(2) |

**Table 4.9.** Selected bond lengths [Å] and angles [°] for complex **6**.

| | | | |
|---|---|---|---|
| Au(1)-S(1) | 2.3031(10) | C(25)-N(3)-Na(1) | 124.0(3) |
| Au(1)-S(4) | 2.3124(10) | N(4)-C(28)-C(29) | 115.5(4) |
| S(1)-C(1) | 1.763(4) | C(27)-C(28)-C(29) | 122.8(4) |
| N(1)-C(7) | 1.317(5) | N(3)-C(27)-C(35) | 116.7(4) |
| N(3)-Na(1) | 2.622(4) | C(28)-C(27)-C(35) | 123.0(4) |
| O(2)-C(44) | 1.203(6) | C(44)-O(2)-Na(1) | 157.8(5) |
| O(2)-Na(1) | 2.238(5) | O(2)-C(44)-C(45) | 118.7(6) |
| C(44)-C(45) | 1.454(9) | O(2)-C(44)-C(46) | 121.3(6) |
| O(1)-Na(1) | 2.278(4) | C(45)-C(44)-C(46) | 120.0(6) |
| O(3)-Na(1) | 2.330(4) | O(2)-Na(1)-O(1) | 100.70(16) |
| S(1)-Au(1)-S(2) | 89.60(4) | O(2)-Na(1)-O(3) | 125.76(17) |
| S(1)-Au(1)-S(3) | 89.21(4) | O(1)-Na(1)-O(3) | 94.00(14) |
| S(2)-Au(1)-S(3) | 178.47(4) | O(2)-Na(1)-N(3) | 97.90(15) |
| C(1)-S(1)-Au(1) | 104.22(14) | O(1)-Na(1)-N(3) | 102.39(15) |
| C(27)-N(3)-Na(1) | 115.4(3) | O(3)-Na(1)-N(3) | 129.39(14) |

## 4.4. Conclusion

In summary, We have demonstrated here, the synthesis of sodium metal based coordination complexes/polymer of diverse architectures (from discrete to 1D) based on a Metal(III) dithiolene complex anion $[M^{III}(diph\text{-}6,7\text{-}qdt)_2]^{1-}$ [M = Cu(III), Au(III)] by varying the solvents of recrystallization. We have shown that dimensionality of a sodium coordination based polymer system, coupled with a Metal(III) (bis)dithiolene complex, can be regulated by various factors such as the size of the solvent molecules, the hybridization of the central carbon atom attached to the coordinating atom of the solvent molecule and the size. These factors are exemplified by comparing Metal(III) dithiolene complex anions $[M^{III}(diph\text{-}6,7\text{-}qdt)_2]^{1-}$ with $[M^{III}(btdt)_2]^{1-}$. When MeOH, THF and acetone were used as recrystallizing solvent, 1D and 2D coordination polymer has been formed with btdt ligand. Whereas in case of diph-6,7-qdt ligand, only discrete molecule has been formed due to bulkiness of the dithiol ligand. Finally when we used acetonitrile as recrystallizing solvent, it results in the formation of 3D network with btdt ligand, whereas 1D chain with diph-6,7-qdt ligand. In compounds **1**–**6** the coordination numbers of sodium ion is restricted to only four and five rather than six coordination (which is observed in the Na-btdt (co-ordination no. of Na is six) compounds)

The compounds presented in the study, clearly demonstrate the effect of bulkier dithiolene ligand in obtaining the discrete and lower dimensional structures (Table 4.9). But the effect of the hybrid orbitals of the carbon atom attached to the coordinating atom follows the same fashion as observed in the case of less bulkier dithiolene ligands. These compounds rationalize the concept (developed in our laboratory) of bulkiness of the coordinating moieties that limit the coordination extension.

In order to get good conducting and magnetic coordination polymeric materials based on dithiolene complexes, we are now attempting to synthesize a new class of coordination polymers system by choosing an alkali metal ion (e.g., $Na^+$, $K^+$ cations etc.,) coupled with a transition metal(bis) dithiolene complex such as, Ni(III)(bis) dithiolene complexes. Finally it is worth mentioning that we have established a new class of dithiolene-based materials, where hybridization of central carbon atom of the coordinating solvent plays an important role in determining the dimensionality of the resulting coordination polymer. This work is not only importance in terms of practical applications, but also it serves in understanding the basic principle of supramolecular chemistry.

## 4.5. References


[1] J. H. Rayner and H. M. Powell, J. Chem. Soc. (1952) 319–328.

[2] R. Baur and G. Schwarzenbach, Helv. Chim. Acta 43 (1960) 842–847.

[3] K. V. Krishnamurty and G. M. Harris, Chem. Rev. 61 (1961), 213–246.

[4] W. P. Griffin, Q. Rev., Chem. Soc. 16 (1962) 188–207.

[5] R. D. Billard and G. Wilkinson, J. Chem. Soc. (1963) 3193–3200.

[6] R. A. Walton, Q. Rev., Chem. Soc. 19 (1965) 126–143.

[7] T. Iwamoto, T. Nakano, M. Morita, T. Miyoshi, T. Miyamoto and Y. Sasaki, Inorg. Sasaki, Inorg. Chim. Acta 2 (1986) 313–316.

[8] K. V. Krishnamurty, G. M. Harris and V. S. Sastri, Chem. Rev. 70 (1970) 171–197.

[9] T. Iwamoto, M. Kiyoki, Y. Ohtsu and Y. Takeshige-Kato, Bull. Chem. Soc. Jpn. 51 (1978) 488–491.

[10] A. E. Underhill and D. M. Watkins, Chem. Soc. Rev. 9 (1980) 429–448.

[11] B. Moulton, M. Zaworotko, J. Chem. Rev. 101 (2001) 1629.

[12] Design and Construction of Coordination Polymers, John Wiely & Sons, NewYork, (2009).

[13] S. R. Batten, R. Robson, Angew. Chem., Int. Ed. 37 (1998) 1460.

[14] O. M. Yagi, M. O'Keeffe, N. W. Ockwig, H. K. Chae, M. Eddaouji, J. Kim, Nature 423 (2003) 705.

[15] K. Biradha, CrystEngComm 5 (2003) 374.

[16] C. Janiak, Dalton Trans. (2003) 2781.

[17] M. Fujita, K. Umemoto, M. Yoshizawa, N. Fujita, T. Kusukawa, K.Biradha, Chem. Commun. (2001) 509.

[18] A. J. Blake, N. R. Champness, P. Hubberstey, W.-S. Li, M. A. Withersby, M. Schröder, Coord. Chem. Rev. 183 (1999) 117.

[19] G. F. Swiegers, T. J. Malefetse, Chem. Rev. 100 (2000) 3483.

[20] C. B. Aakeröy, N. R. Champness, C. Janiak, CrystEngComm 12 (2010) 22.

[21] D. Miao, B. Xianhe, Prog. in Chem. 21 (2009) 2458.

[22] S. L. James, Chem. Soc. Rev. 32 (2003) 276.

[23] S. Rabaça, M. Almeida, Coord. Chem. Rev. 254 (2010) 1493.

[24] J. J. Perry IV, J. A. Perman, M. J. Zaworotko, Chem. Soc. Rev. 38 (2009) 1400.

[25] K. Adachi, S. Kawata, Md. K. Kabir, H. Kumagai, I K. noue, S. Kitagawa, Chem. Lett. 30 (2001) 50.

[26] R. Matsuda, R. Kitaura, S. Kitagawa, Y. Kubota, R. V. Belosludov, T. C. Kobayashi, H. Sakamoto, T. Chiba, M. Takata, Y. Kawazoe, Y. Mita, Nature 436 (2005) 238.

[27] J. L. C. Rowsell, O. M. Yaghi, Angew. Chem., Int. Ed. 44 (2005) 4670.

[28] O. R. Evans, W. Lin, Chem. Mater. 13 (2001) 2705.

[29] Y. Geng, X.-J. Wang, B. Chen, H. Xue, Y.-P. Zhao, S. Lee, C.-H. Tung, L.-Z. Wu, Chem. –Eur. J. 15 (2009) 5124.

[30] T. Okubo, N. Tanaka, K. H. Kim, H. Yone, M. Maekawa, T. Kuroda-Sowa, Inorg. Chem. 49 (2010) 3700.

[31] X.-Y. Wang, Z.-M. Wang, S. Gao, Chem. Commun. (2008) 281.

[32] M. Todokoro, S. Yasuzuka, M. Nakamura, T. Shinoda, T. Tatenuma, M. Mitsumi, Y. Ozawa, K. Toriumi, H. Yoshino, D. Shiomi, K. Sato, T. Takui, T. Mori, K. Murata, Angew. Chem., Int. Ed. 45 (2006) 5144.

[33] E. Coronado, J. R. Galán-Mascarós, C. J. Gómez-García, V. Laukhin, Nature 408 (2000) 447.

[34] X. Lin, J. Jia, P. Hubberstey, M. Schröder, N. R. Champness, CrystEngComm 9 (2007) 438.

[35] M.-L. Liu, W. Shi, H.-B. Song, P. Cheng, D.-Z. Liao, S.-P. Yan, CrystEngComm 11 (2009) 102.

[36] M. Dincă, J. R. Long, Angew. Chem., Int. Ed. 47 (2008) 6766.

[37] A. D. Burrows, C. G. Frost, M. F. Mahon, M. Winsper, C. Richardson, J. P. Attafield, J. A. Rodgers, Dalton Trans. (2008) 6788.

[38] E. Pardo, R. Ruiz-García, J. Cano, X. Ottenwaelder, R. Lescouëzec, Y. Journaux, F. Lloret, M. Julve, Dalton Trans. (2008) 2780.

[39] Z.-G. Gu, Y.-F. Xu, X.-J. Yin, X.-H. Zhou, J.-L. Zuo, X.-Z. You, Dalton Trans. (2008) 5593.

[40] K. Drabent, Z. Ciunik, A. Ozarowski, Inorg. Chem. 47 (2008) 3358.

[41] A. Gavezzotti, Theoretical Aspects and Computer Modeling of the Molecular Solid State, John Wiely & Sons, Chichester, (1997).

[42] G. R. Desiraju, Angew. Chem., Int. Ed. Engl. 34 (1995) 2311.

[43] G. R. Desiraju, A. Gavezzotti, Acta Crystallogr., Sect. B 45 (1989) 473.

[44] D. E. Williams, Acta Crystallogr., Sect. A 52 (1996) 326.

[45] R. Robson, J. Chem. Soc., Dalton Trans. (2000) 3735.

[46] T. J. Prior, D. Bradshaw, S. J. Teat, M. J. Rosseinsky, Chem. Commun. (2003) 500.

[47] F. M. Tabellion, S. R. Seidel, A. M. Arif, P. J. Stang, J. Am. Chem, Soc. 123 (2001) 7740.

[48] X.-H. Bu, W. Chen, S.-L. Lu, R.-H. Zhang, D.-Z. Liao, M. Shionoya, F. Brisse, J. Ribas, Angew. Chem., Int. Ed. 40 (2001) 3201.

[49] M. Yoshizawa, M. Nagao, K. Umemoto, K. Biradha, M. Fujita, S. Sakamoto, K. Yamaguchi, Chem. Commun. (2003) 1808.

[50] G. Dong, P. Ke-liang, D. Chun-ying, H. Cheng, M. Qing-jin, Inorg. Chem. 41 (2002) 5978.

[51] X.-L. Wang, Y.-Q. Chen, G.-C. Liu, H.-Y. Lin, W.-Y. Zheng, J.-X. Zhang, J. Organomet. Chem. 694 (2009) 2263.

[52] J.-R. Li, X.-H. Bu, J. Jiao, W.-P. Du, X.-H. Xu, R.-H. Zhang, Dalton Trans. (2005) 464.

[53] S. Banfi, L. Carlucci, E. Caruso, G. Ciani, D. M. Proserpio, J. Chem. Soc., Dalton Trans. (2002) 2714.

[54] W.-J. Shi, C.-X. Ruan, Z. Li, M. Li, D. Li, CrystEngComm 10 (2008) 778.

[55] P.-P. Liu, A.-L. Cheng, Q. Yue, N. Liu, W.-W. Sun, E.-Q. Gao, CrystalGrowth&Design 8 (2008) 1668.

[56] Y. Liu, Y. Qi, Y.-H. Su, F.-H. Zhao, Y.-X. Che, J.-M. Zheng, CrystEngComm 12 (2010) 3283.

[57] F.-Y. Cui, K.-L. Huang, Y.-Q. Xu, Z.-G. Han, X. Liu, Y.-N. Chi, C.-W. Hu, CrystEngComm 11 (2009) 2757.

[58] J.-Q. Liu, Y.-N. Zhang, Y.-Y. Wang, J.-C. Jin, E. Kh. Lermontova, Q.-Z. Shi, Dalton Trans. (2009) 5365.

[59] R. P. Feazell, C. E. Carson, K. K. Klausmeyer, Inorg. Chem. 45 (2006) 2635.

[60] B.-C. Tzeng, H.-T. Yeh, T.-Y. Chang, G.-H. Lee, CrystalGrowth&Design 9 (2009) 2552.

[61] S.-C. Chen, Z.-H. Zhang, K.-L. Huang, Q. Chen, M.-Y. He, A.-J. Cui, C. Li, Q. Liu, M. Du, Crystal Growth&Design 8 (2008) 3437.

[62] J. Yang, G.-D. Li, J.-J. Cao, Q. Yue, G.-H. Li, J.-S. Chen, Chem. –Eur. J. 13 (2007) 3248.

[63] C.-J. Wang, H.-R. Ma, Y.-Y. Wang, P. Liu, L.-J. Zhou, Q.-Z. Shi, S.-M. Peng, Crystal Growth& Design 7 (2007) 1811.

[64] T. K. Prasad, M. V. Rajasekharan, Crystal Growth &Design 8 (2008) 1346.

[65] V. R. Pedireddi, S. Varughese, Inorg. Chem. 43 (2004) 450.

[66] B. Chen, F. R. Fronczek, A. W. Maverick, Chem. Commun. (2003) 2166.

[67] S. Lopez, S. W. Keller, Inorg. Chem. 38 (1999) 1883.

[68] S. Y. Lee, J. H. Jung, J. J. Vittal, S. S. Lee, Crystal Growth&Design 10 (2010) 1033.

[69] X.-M. Lin, H.-C. Fang, Z.-Y. Zhou, L. Chen, J.-W. Zhao, S.-Z. Zhu, Y.-P. Cai, CrystEngComm 11 (2009) 847.

[70] T. L. Hennigar, D. C. MacQuarrie, P. Losier, R. D. Rogers, M. J. Zaworotko, Angew. Chem., Int. Ed. 36 (1997) 972.

[71] M. A. Withersby, A. J. Blake, N. R. Champness, P. A. Cooke, P. Hubberstey, W.-S. Li, M. Schröder, Inorg. Chem. 38 (1999) 2259.

[72] N. P. Chatterton, D. M. L. Goodgame, D. A. Grachvogel, I. Hussain, A. J. P. White, D. J. Williams, Inorg. Chem. 40 (2001) 312.

[73] S. A. Baudron, M. W. Hosseini, Inorg. Chem. 45 (2006) 5260.

[74] X. Ribas, J. C. Dias, J. Morgado, K. Wurst, E. Molins, E. Ruiz, M. Almeida, J. Veciana, C. Rovira, Chem. Eur. J. 10 (2004) 1691.

[75] X. Ribas, J. Dias, J. Morgado, K. Wurst, M. Almeida, J. Veciana, C. Rovira, CrystEngComm 4 (2002) 564.

[76] X. Ribas, D. Maspoch, J. Dias, J. Morgado, M. Almeida, K. Wurst, G. Vaughan, J. Veciana, C. Rovira, CrystEngComm 6 (2004) 589.

[77] S. Takaishi, M. Hosoda, T. Kajiwara, H. Miyasaka, M. Yamashita, Y. Nakanishi, Y. Kitagawa, K. Yamaguchi, A. Kobayashi, H. Kitagawa, Inorg. Chem. 48 (2009) 9048.

[78] X. X-Ribas, J. C. Dias, J. Morgado, K. Wurst, I. C. Santos, M. Almeida, J. Vidal-Gancedo, J. Veciana, C. Rovira, Inorg. Chem. 43 (2004) 3631.

[79] L. N. Dawe, J. Miglioi, L. Turnbow, M. L. Taliaferro, W. W. Shum, J. D. Bagnato, L. N. Zakharov, A. L. Rheingold, A. M. Arif, M. Fourmigué, J. S. Miller, Inorg. Chem. 44 (2005) 7530.

[80] R. Bolligarla and S. K. Das, CrystEngCommun 12 (2010) 3409-3412

[81] Q. Changtao, W. Bing, X. Yin, L. Yonghua, J. Chem. Soc., Dalton. Trans. (1994) 2109.

[82] R. Daniel, E. C. James, A. F. Walter, L. R. Arnold, I. Christopher, A. G. Llia, Polyhedron 20 (2001) 2491.

[83] M. D.-V. José, M. M. José, C. Enrique, Inorg. Chem. Acta. 357 (2004) 611.

[84] J. Reglinski, M. Garner, I. D. Cassidy, P. A. Slavin, M. D. Spicer, D. R. Armstrong, J. Chem. Soc., Dalton Trans. (1999) 2119.

[85] J. L. Brusso, O. P. Clements, R. C. Haddon, M. E. Itkis, A. A. Leitch, R. T. Oakley, R. W. Reed, J. F. Richardson, J. Am. Chem. Soc. 126 (2004) 8256.

[86] Bruker. SADABS, SMART, SAINT and SHELXTL, 2000 (Bruker AXS Inc., Madison, Wisconsin, USA).

[87] G. M. Sheldrick, Acta Crystallogr. Sect. A 64 (2008) 112–122.

# Design, synthesis and characterization of new derivatives of quinoxaline-*o*-dithiol ligands: Their coordination complexes with transition metals

5 Chapter

**Abstract:-** We have designed and synthesized a new class of *N*-Heterocyclic quinoxaline-*o*-dithiol ligands and their mono- and bis-transition metal complexes. All the compounds **2a**–**i**, **3a**–**i**, **4a**–**i** and **5a**–**i** (see Scheme 5.1 and Tables 5.1–5.2 in the section of Results and Discussion below) have been characterized by IR, $^{1}H$, $^{13}C\{^{1}H\}$ NMR, mass spectroscopy, elemental analysis and the compounds **2d**, **2g** unambiguously characterized by X–ray crystallographic analysis. The present synthetic route offers us an excellent pathway to synthesize the derivatives of quinoxaline-*o*-dithiol ligands starting from the 3,4-diamino benzoic acid. The metal coordination complex of the ligand **5a** has been synthesized and characterized by single crystal X-ray analysis. This complex shows strong charge transfer (CT) band at 575 nm in its solid-state electronic absorption spectra. The electrochemical properties of complex **6** is performed by cyclic voltammetry, which shows a reversible one-electron-oxidative response at $E_{1/2}$ = +0.45 V *vs* Ag/AgCl ($\Delta E$= 0.07 V).

## 5.1. Introduction

The spontaneous self-organization of coordination compounds, through the combination of versatile polydentate organic ligands and transition metals can lead to supramolecular architectures. The metal directed self-assembly of supramolecular coordination compounds has attracted much interest during the past two decades [1] because it has been used to form different supramolecular architectures like helicates, boxes, squares, molecular containers and other structural motifs. Particularly, dithiolenes have attracted academic interest owing to the “non innocent” behavior of the dithiolate ligands in these complexes [2–10]. On the other hand, much effort has been dedicated toward practical applications for dithiolene complexes [11–14]. Most of the double- and triple-stranded helicates, that have been investigated so far, are made up from ligands containing N- and O-donors. Particularly helicates, containing oligopyrimidines and

dicatechols, have been studied intensively while other donor groups have received much less attention.

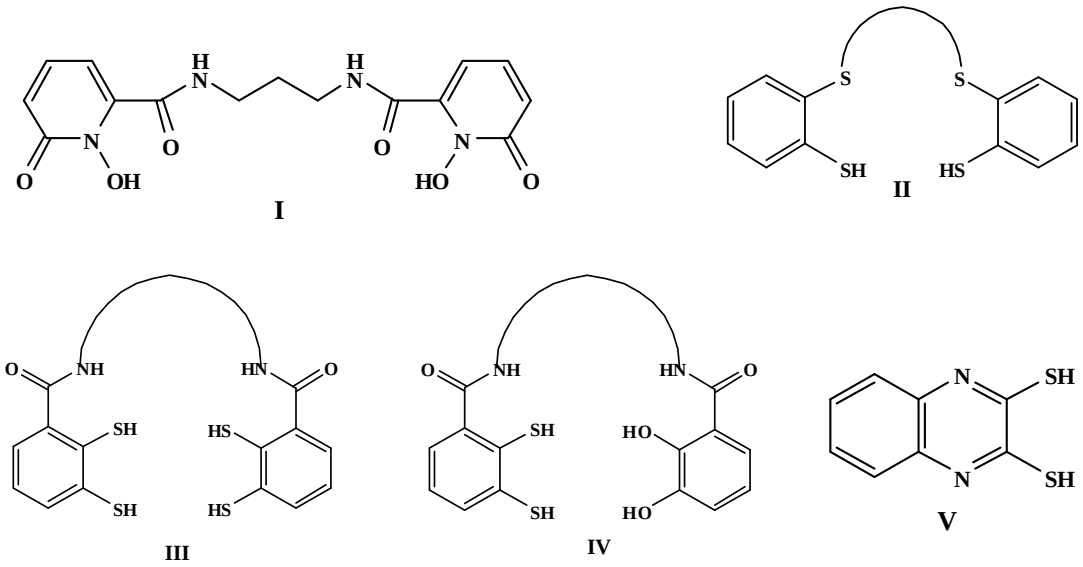


**Scheme 5.1.** Some reported bis and polydentate ligands.

Reymond and his co-workers isolated the first triple stranded helicates that contain exclusively oxygen donors for hydroxamato groups, such as, ligand **I** as shown in Scheme 5.1 [15–17]. In 1987, Lehn et al. reported the first structurally characterized metallo-helicate containing two tris(bipyridine) ligands and three $Cu^{I}$ ions [18–20]. Later, Raymond [21–23], Stack [24–25] and Albrecht [26–33] and their co-workers synthesized a series of dicatechol-ligands with different bridging groups that have been used for the preparation of dinuclear triple-stranded helicates.

Afterward, multidentate sulfur rich ligands of type **II** (see Scheme 5.1) have been used successfully in the preparation of model compounds for the active sites in nitrogenase [34–35] and for certain nickel enzymes [36]. Here two aromatic thiol units bridged via a thioether link which leads to a tetradentate ligand with two thiolate and two thioether sulfur donor atoms. Similar ligands with sulfur donors e.g., with benzene-*o*-dithiolate donor groups, reported by Hahn and co-workers in 1995, have been synthesized by *ortho* functionalization of benzene-*o*-dithiol that allows the preparation of first bis- and then tris(benzene-*o*-dithiol) ligands (e.g., ligand **III** in Scheme 5.1) [37–42]. In addition to symmetrical dithiol ligands, some unsymmetrical dithiol/dicatechols ligands have also been reported, such as ligand **IV (**see Scheme 5.1) [43–45].

Among such ligands, we are particularly interested in *N*-heterocyclic 1,2-ethylene-dithiol, such as, quinoxaline 2,3-dithiol (representation **V** in Scheme 5.1) bridged via amide bonds with different amines. Quinoxaline derivatives, which are known as 'benzopyrazine', have a synthetic advantage over other fused aromatic systems due to the existence of a high-yield synthetic route from diketone and diamine condensation. This class of ligands is useful to construct the building blocks in materials based coordination chemistry that includes non-helical dinuclear, dinuclear triple-stranded helicates or double stranded helical complexes with different metal ions. Moreover, quinoxaline derivatives have wide applications in dyes [46,47], efficient electron luminescent materials [48,49], organic semiconductors [50], chemically controllable switches [51], building blocks for the synthesis of anion receptors [52], cavitands [53] and dehydoannulenes [54]. In addition, quinoxaline ring moiety constitutes part of the chemical structures of various antibiotics such as Echinomycin, Levomycin and Actinoleutin that are known to inhibit growth of gram positive bacteria and are active against various transplantable tumors [46]. We present here the synthesis and characterization of a series of new *N*-heterocyclic mono- and bis (quinoxaline-*o*-dithiol) molecules that we intend to as use potential ligands for the formation of coordination complexes with transition metals. In this report, we have described three such nickel coordination complexes including single crystal structure of one of them.

## 5.2. Results and discussion

*5.2.1. Synthesis and characterization of mono- and bis quinoxaline-o-dithiol ligands*

Schemes 5.2 and 5.3 depict the preparation of the mono and bis(quinoxaline-*o*-dithiol) ligands **3a**–**i** and **5a**–**i**, respectively. The synthesis starts with 2,3-dichloroquinoxaline-6-carboxylic acid, which was prepared by condensation reaction of 3,4-diamino benzoic acid and oxalic acid in acidic medium followed by chlorination with $SOCl_2$ as described previously [55]. In the conversion of a carboxylic acid into an amide, 2,3-dichloroquinoxaline-6-carboxylic acid has been converted into the acid chloride [56] using thionyl chloride, followed by condensation with mono- or di-amine in the presence of triethylamine that affords the mono and bis(2,3-dichloro quinoxaline)-carboxamide derivatives **2a**–**i** and **4a**–**i**, respectively in yields 50–75%. Subsequently, for the preparation of quinoxaline-*o*-dithiols, the resulting 2,3-dichloroquinoxaline-carboxamide derivatives are treated with thiourea in absolute ethanol under

reflux condition followed by base hydrolysis. In order to prevent the breaking of amide bond, it is essential that the base hydrolysis

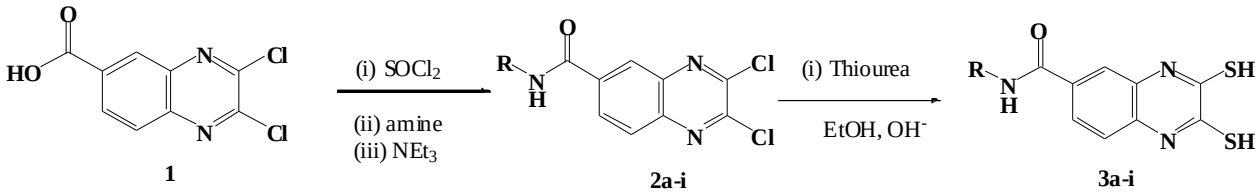


**Scheme 5.2.** Synthetic route for mono quinoxaline-*o*-dithiols

has to be done at low temperature (–10 ºC). Finally the acid hydrolysis affords dithiol ligands **3a**–**i** and **5a**–**i** as brown precipitate (see schemes 5.2 and 5.3). All the compounds **2a**–**i, 3a**–**i, 4a**–**i** and **5a**–**i** have been characterized by IR, mass, $^{1}H$, $^{13}C\{H\}$ NMR and elemental analysis. The molecular structures of compounds **2d** and **2g** were further confirmed by single crystal X-ray crystallographic analysis and the relevant thermal ellipsoidal plots are shown in Fig. 5.1. The crystallographic parameters, data collection and structure refinement of the compounds **2d** and **2g** are summarized in Tables 5.3, respectively. The crystal structure analyses show that the crystals of compounds **2d** and **2g** crystallize in monoclinic with space groups $P2_1/c$, and $Z' = 1$ for both compounds **2d** and **2g**; bonding dimensions within the molecules are unexceptional as shown in Fig. 5.1.

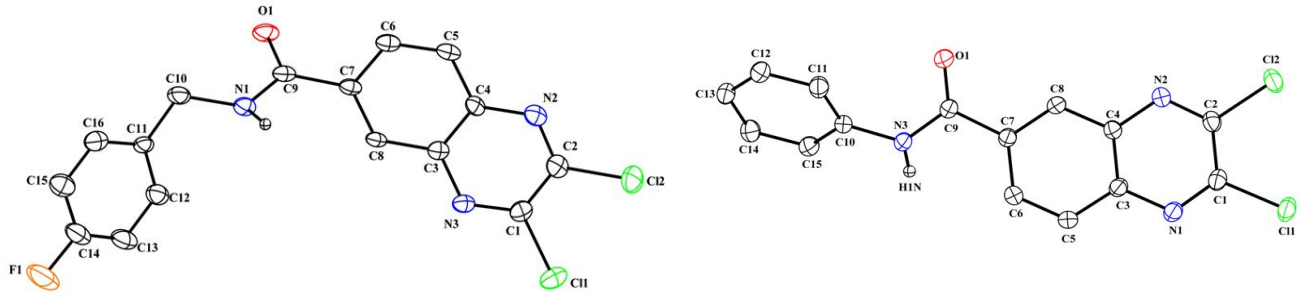


**(a)** **(b)**

**Fig. 5.1.** Thermal ellipsoidal plots of (a) compound **2d** and (b) compound **2g** with 20% probability. Hydrogen atoms are omitted for clarity

**Table 5.1.** Chloro and thiol products from Scheme 5.2

| S.No. | Chloro Product | Yield (%) | Thiol Product | Yield (%) |
|---|---|---|---|---|
| 1 | 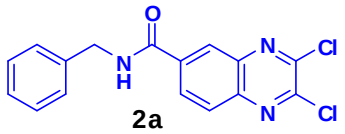 2a | 60.9 | 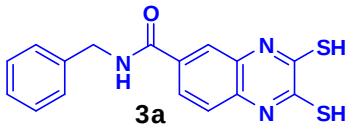 3a | 60.1 |
| 2 | 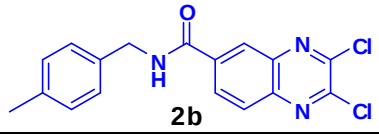 2b | 65.4 | 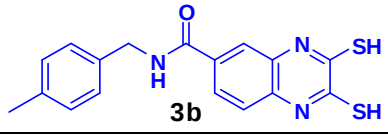 3b | 62.9 |
| 3 | 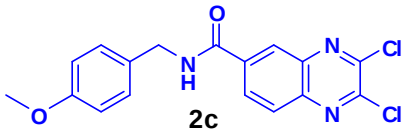 2c | 76.1 | 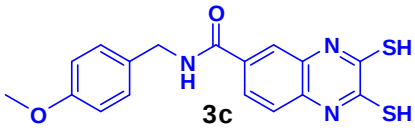 3c | 52.8 |
| 4 | 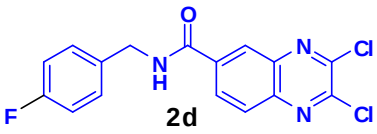 2d | 76.2 | 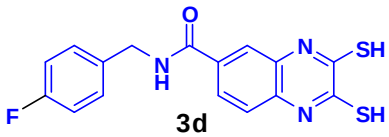 3d | 57.5 |
| 5 | 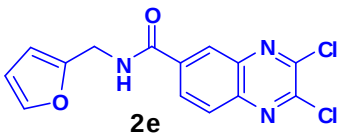 2e | 75.3 | 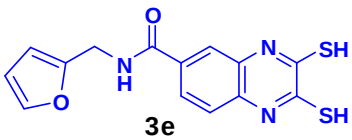 3e | 60.5 |
| 6 | 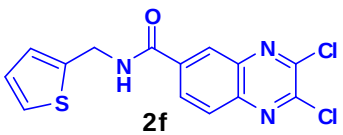 2f | 55.0 | 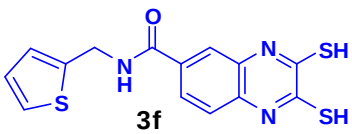 3f | 64.6 |
| 7 | 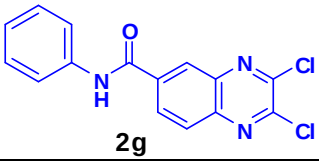 2g | 81.4 | 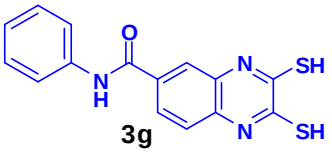 3g | 42.3 |
| 8 | 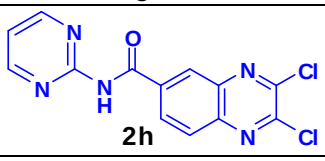 2h | 60.6 | 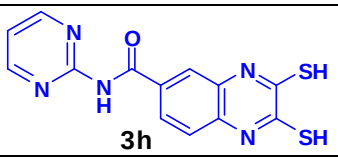 3h | 40.9 |
| 9 | 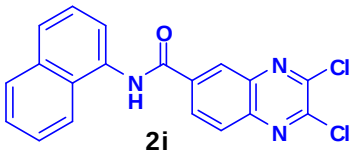 2i | 70.1 | 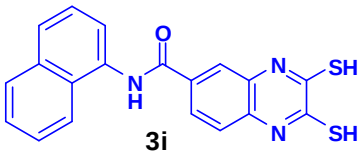 3i | 35.5 |

.

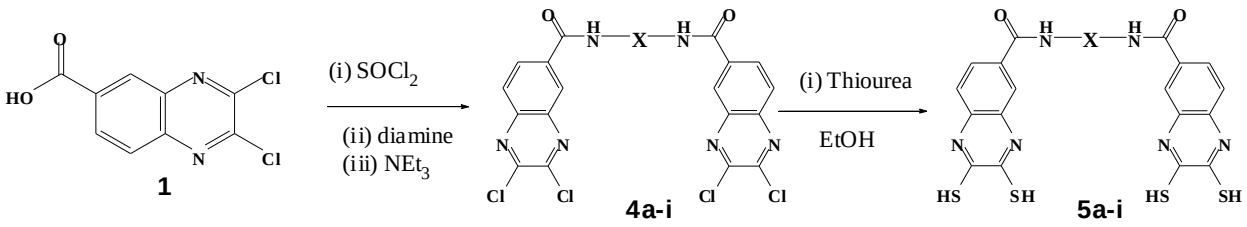


**Scheme 5.3.** Synthetic route for bis quinoxaline-*o*-dithiols

**Table 5.2**. Chloro and thiol products from Scheme 5.3

| S.no | Chloro product | Yield | Thiol product | Yield |
|---|---|---|---|---|
| 1 | 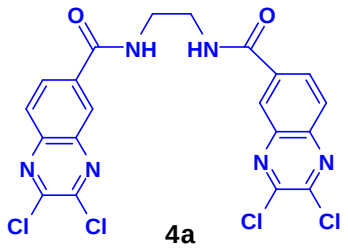 **4a** | 48.1 | 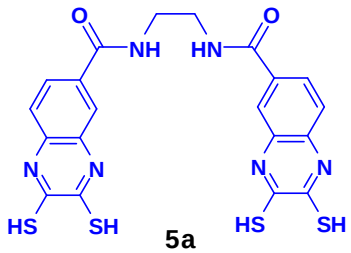 **5a** | 71.2 |
| 2 | 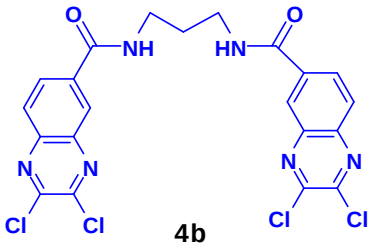 **4b** | 50.1 | 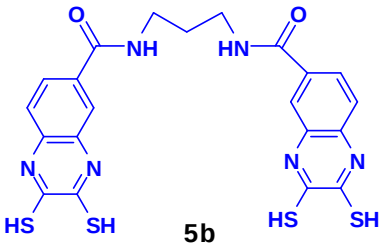 **5b** | 69.0 |
| 3 | 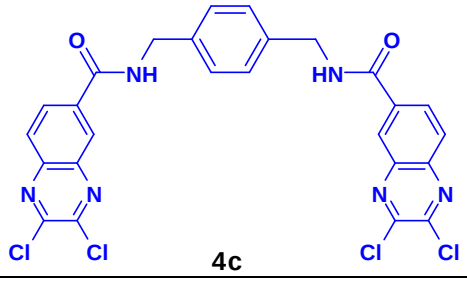 **4c** | 41.5 | 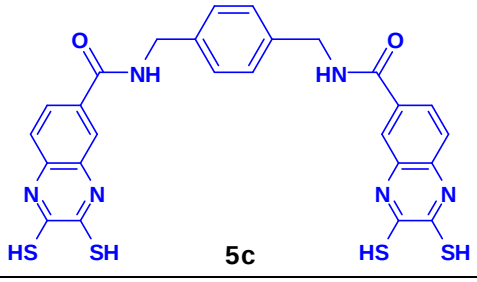 **5c** | 70.3 |
| 4 | 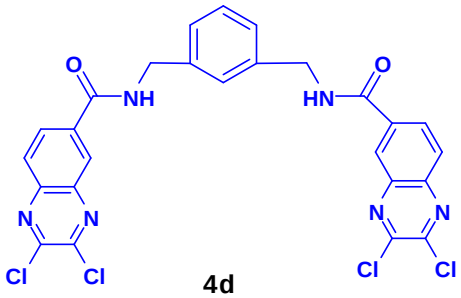 **4d** | 40.4 | 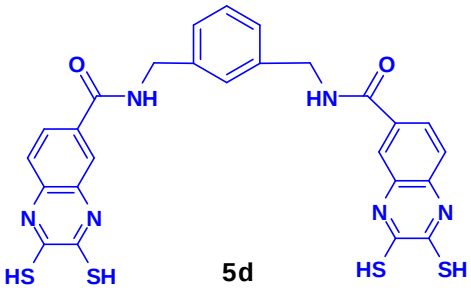 **5d** | 73.7 |

| | | | | |
|---|---|---|---|---|
| 5 | 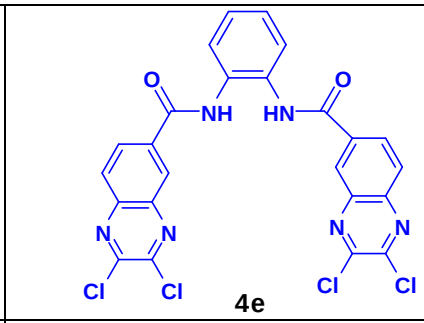 **4e** | 26.5 | 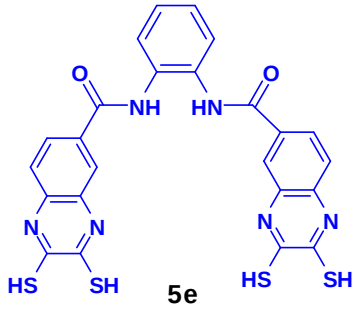 **5e** | 43.8 |
| 6 | 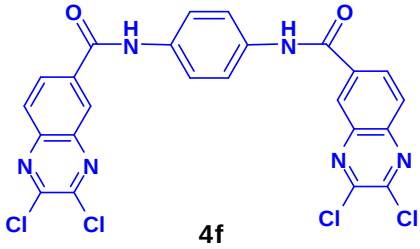 **4f** | 27.5 | 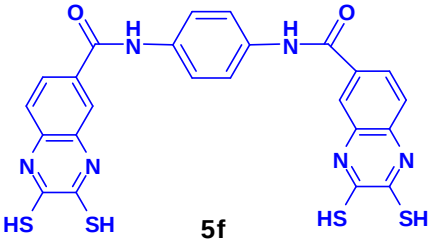 **5f** | 41.1 |
| 7 | 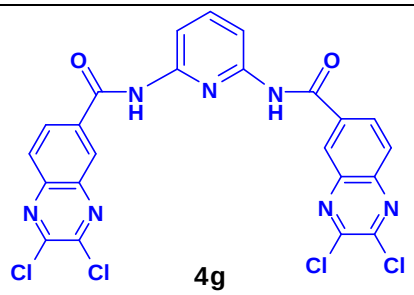 **4g** | 34.6 | 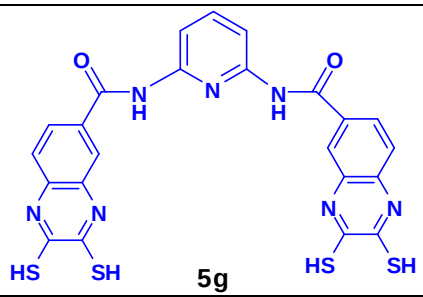 **5g** | 53.7 |
| 8 | 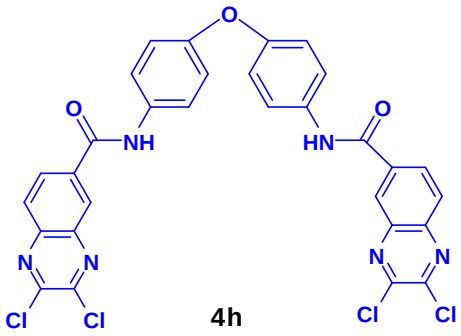 **4h** | 35.9 | 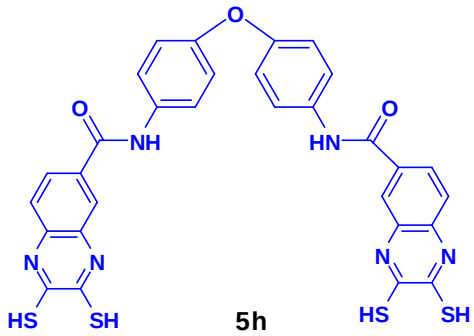 **5h** | 44.5 |
| 9 | 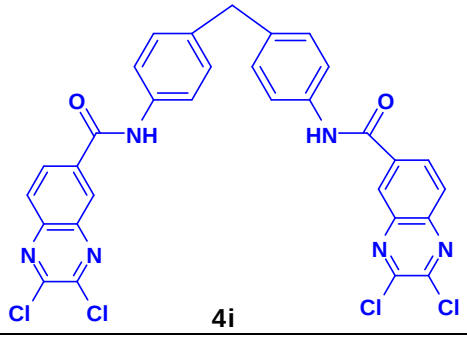 **4i** | 30.4 | 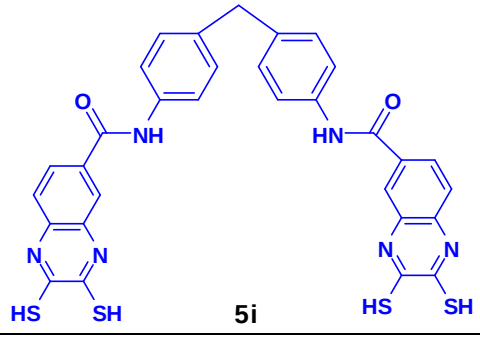 **5i** | 47.8 |

*5.2.2. Synthesis and characterization of metal complex **6***

Usually, dithiolato complexes are prepared by a simple metathesis reaction of highly reactive alkali metal dithiolates and metal halides by salt elimination. The use of alkali metal based dithiolates as well as ligand transfer reactions have been employed successfully to obtain dinuclear double stranded complexes with bis(dithiol) ligands [38,57,58].

We have synthesized a metal complex through a general common procedure, similar to previously described procedures [59] as shown in Scheme 5.4. The bis(dithiolate) tetra anions are generated, *in situ*, by the reaction of bis(dithiol) ligand 5a in a 1:1 stoichiometry in the presence of four equivalents of NaOH in methanol at −10 ºC. This is reacted with $NiCl_2{\cdot}6H_2O$ resulting in the formation of the respective nickel complex as violet color solution. After cation exchange with $Ph_4AsCl$ in methanol solution, complex $(Ph_4As)_4[Ni_2^{II}(\mathbf{5a})_2]$ (**6**) has been precipitated out as micro crystalline violet color solid.

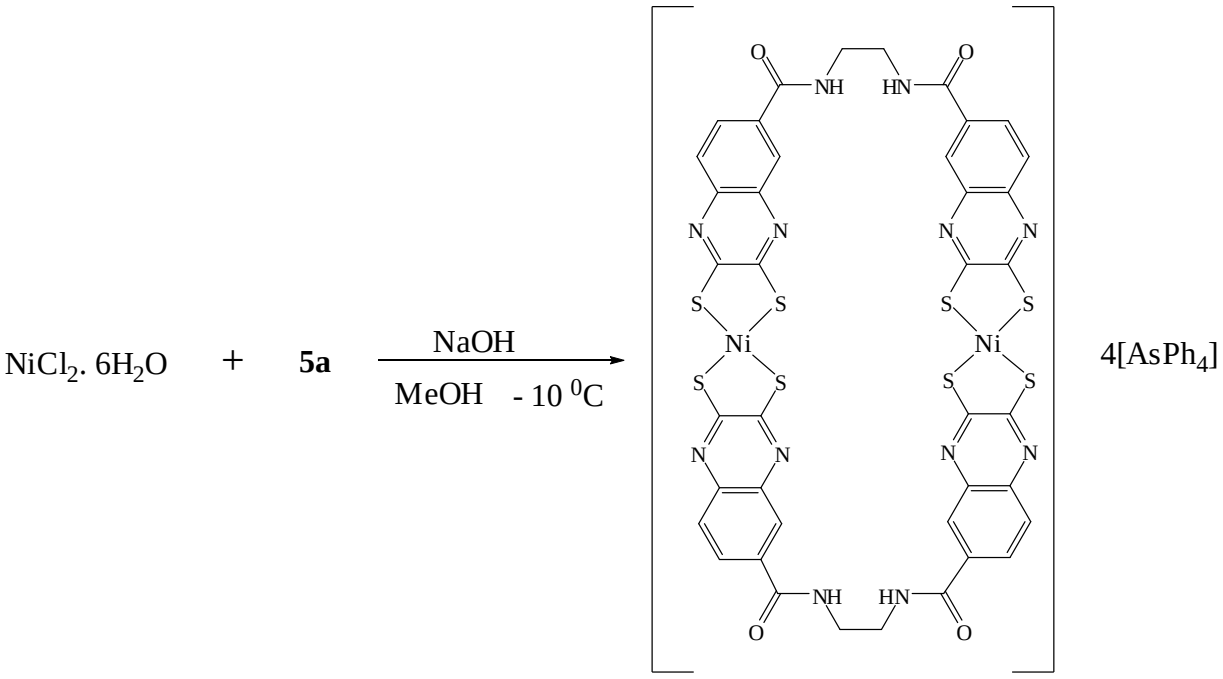


**Scheme 5.4.** Synthesis of complex $(PhAs)_4[Ni_2(\mathbf{5a})_2]$ (**6**).

The molecular structure of complex **6** has been determined by X-ray diffraction analysis. It is recrystallized from slow vapor diffusion of diethyl ether into saturated solution of the complex **6** in DMF. The molecular structure of the complex anion $[Ni_2^{II}(\mathbf{5a})_2]^{4-}$ in **6** is depicted

in Fig. 5.2. The crystal structure analyses show that the complex **6** crystallizes in triclinic system with space groups *P*-1. The complex anion shows overall square-planar coordination geometry around nickel. The structure analyses of this complex revealed the existence of discrete dinuclear bis(quinoxaline-*o*-dithiolato) nickelate complex anion with $[Ph_4As]^+$ cation. The complex anion contains two square-planar $[Ni(S_2C_8N_2H_3R)_2]$ units with the nickel center coordinated by two quinoxaline dithiolate units in a square-planar fashion. The average Ni–S bond lengths in the nickelate(II) complex is 2.175 Å. The structural parameters of the $[Ni(S_2C_8N_2H_3R)_2]$ moieties are unexceptional.

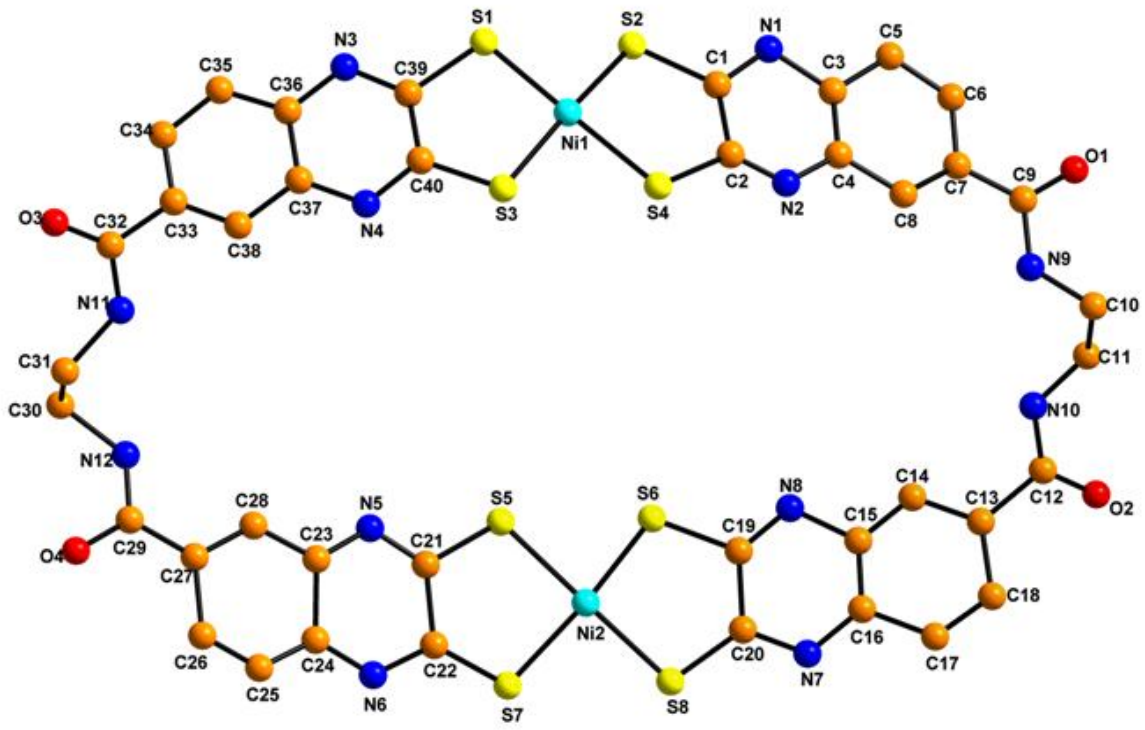


**Fig. 5.2.** Molecular structure of the nickelate anion $[Ni^{II}_2(\mathbf{5a})_2]^{4-}$ in the complex **6** (Hydrogen atoms, solvent molecules and cations have been omitted for clarity).

*5.2.3. Electronic absorption spectroscopy*:

UV/vis spectra of the nickel(II) complex **6** with ligand $\mathbf{5a}^{4-}$ is depicted in Fig. 5.3. The spectrum of Ni(II) complex shows the typical π–π* quinoxaline ring absorption of the ligand at ≈332 nm. An intense broad band is observed in the visible region centered at ~576 nm for complex **6**. These broad bands are due to the charge transfer (CT) transitions involving electronic

excitation from a HOMO which is a mixture of dithiolate ($\pi$) and metal ($d$) orbital character to a LUMO which is a $\pi^*$ orbital of the dithiolate, that are characteristics of metal(II) bis (dithiolene) complexes [60–62].

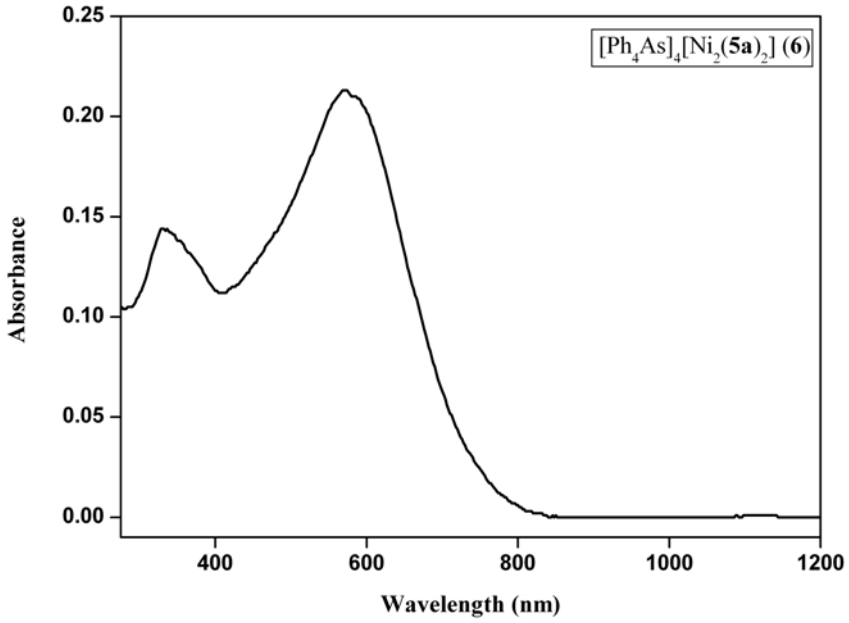


**Fig. 5.3**. Diffuse reflectance spectrum of the complex $[Ph_4As]_4[Ni_2(\mathbf{5a})_2]$ (**6**).

*5.2.4. Electrochemical studies*:

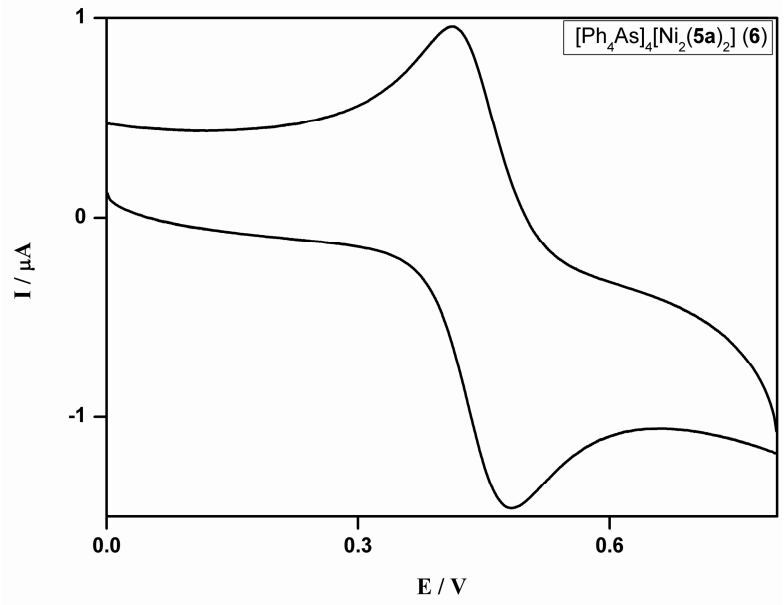


**Fig. 5.4.** Cyclic voltammogram of compound **6** and $[Ph_4As]_4[Ni_2(\mathbf{5a})_2]$ (**6**) in TBAP/DMF at a scan rate 100 mV $s^{-1}$.

The electrochemical property of complex **6** has been investigated by cyclic voltammetry (CV) studies in DMF (with 0.1 M *n*–$Bu_4NClO_4$ as supporting electrolyte, $v$ = 0.1 V/s) solution under an atmosphere of N2. It was initiated from the open circuit and scanned in the anodic direction as indicated in Fig. 5.4. As shown in Fig. 5.4, complex **6** undergoes a reversible oxidation ($\Delta E$= 0.07 V) at $E_{1/2}$ = +0.45 V *vs* Ag/AgCl, that corresponds to the $[Ni_2(\mathbf{5a})_2]^{2-}/[Ni_2(\mathbf{5a})_2]^{4-}$ redox couple in DMF, indicating that Ni(III) complex $[Ni_2(\mathbf{5a})_2]^{2-}$ is quite stable in the electrochemical scale.

*5.2.4.1. Comparison of Electrochemical Properties Between the $[Bu_4N]_2[Ni(6,7\text{-qdt})_2]$, $[Bu_4N]_2[Ni(qdt)_2]$ and $[Ph_4As]_4[Ni_2(5a)_2]$*

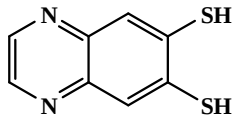


$H_2$6,7-qdt

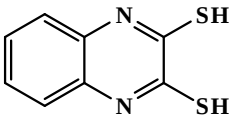


$H_2$qdt

The electrochemical studies indicate that the variation of electron withdrawing nature of the dithiolene moiety can tune the redox potentials of the concerned metal dithiolene complexes. Interestingly, complex $[Bu_4N]_2[Ni(6,7\text{-qdt})_2]$ (benzene ring attached dithiol) undergoes reversible oxidation at very low oxidation potential compared to the $[Ni(qdt)_2]^{2-}$ in MeOH solutions as shown in Fig. 5.5. It is known that the $E_{1/2}$ for the couple $[Ni(6,7\text{-qdt})_2]^{1-}/[Ni(6,7\text{-qdt})_2]^{2-}$ = +0.12 V *vs* Ag/AgCl ($\Delta E$= 74 mV) [63]. But the first oxidation for the complex $(Bu_4N)_2[Ni(qdt)_2]$ appears at $E_{1/2}$ = +0.41 V *vs* Ag/AgCl ($\Delta E$= 89 mV), that corresponds the $[Ni(qdt)_2]^{1-}/[Ni(qdt)_2]^{2-}$ redox couple in the electrochemical scale. In the present study, $[Ph_4As]_4[Ni_2(\mathbf{5a})_2]$ (**6**) shows redox wave at $E_{1/2}$ = +0.45 V *vs* Ag/AgCl ($\Delta E$= 71 mV) in DMF. The difference correlates well with the electronic structure of the dithiol moiety, which is directly attached to the metal center. This clearly indicates that oxidation of Ni from +2 to +3 is very easy in complex $[Bu_4N]_2[Ni(6,7\text{-qdt})_2]$ compared to the other complexes $(Bu_4N)_2[Ni(qdt)_2]$ and $[Ph_4As]_4[Ni_2(\mathbf{5a})_2]$ (**6**). It was mentioned that the $H_2$qdt system is difficult to oxidize than the carbocyclic-arene complex $H_2$6,7-qdt in keeping with greater electronegativity of nitrogen compared to carbon. This means that the ligand $\{6,7\text{-qdt}\}^{2-}$ is more electron releasing towards

the metal ion than the $\{qdt\}^{2-}$ ligand. Thus the location of the ring nitrogen atoms of $\{qdt\}^{2-}$ ligand can tune the redox potential of the concerned complex. In the case of complex **6** (present system), it is even more difficult to oxidize because it has an electron-withdrawing diamide bridge compare to $H_2$qdt and $H_2$6,7-qdt systems. Thus complex **6** shows a more positive oxidation potential.

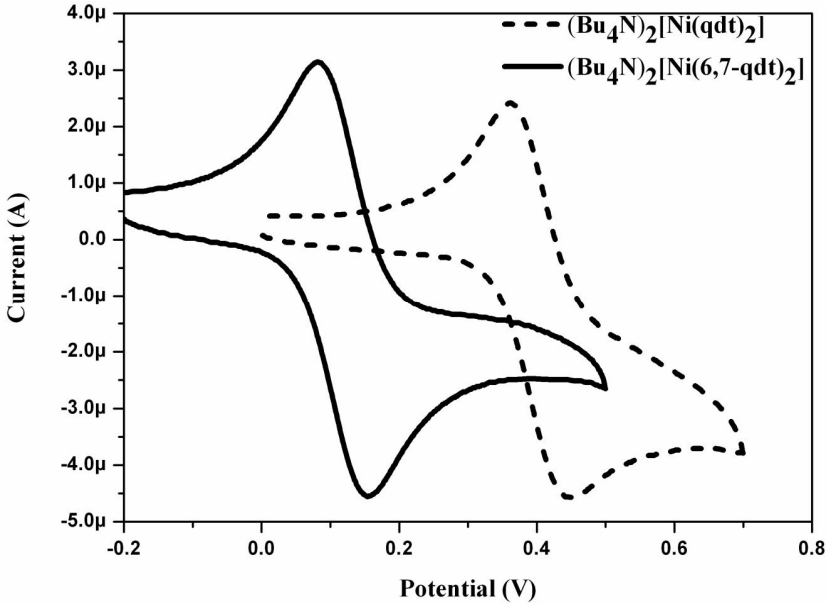


**Fig. 5.5.** Cyclic voltammograms of compounds $[Bu_4N]_2[Ni(6,7\text{-}qdt)_2]$ and $[Bu_4N]_2[Ni(qdt)_2]$ in TBAP/MeOH at a scan rate 50 mV $s^{-1}$.

## 5.3. EXPERIMENTAL SECTION

### *5.3.1. General procedures*

All the reactions were carried out using standard Schlenk and vacuum-line technique under an atmosphere of nitrogen. Dichloromethane was distilled from $CaH_2$, THF from sodium/benzophenone ketyl, and MeOH, EtOH from Mg powder under a $N_2$ atmosphere. 3,4-diamino benzoic acid was purchased from Aldrich and directly used without further purification. Micro analytical (C, H, N) data were obtained with a FLASH EA 1112 series CHNS Analyzer. The IR spectra (with KBr pellet) were recorded in the range of 400–4000 $cm^{-1}$ on a JASCO FT/IR-5300 spectrometer. Electronic spectra were obtained on a Cary 100 Bio UV–Visible spectrophotometer. $^1H$, $^{13}C$ and $^{31}P\{^1H\}$ NMR spectra were recorded on Bruker DRX–400

spectrometer using $Si(CH_3)_4$ (TMS) as an internal standard. Mass spectra were obtained on a BRUKER MAXIS type ESI TOF HRMS spectrometer. Solution mass spectra (LCMS) were obtained on a LCMS−2010A Shimadzu spectrometer. Melting points were measured in open capillary tubes and are uncorrected.

*5.3.2. Single crystal structure determination of compounds **2d, 2g** and **6***

Single crystals suitable for facile structural determination for the compound **2d** was measured on a three circle Bruker SMART APEX CCD, area detector system under [λ (Mo Kα) = 0.7103 Å], graphite monochromator X-ray beam, 2400 frames were recorded with an ω scan width of 0.3°, each for 8 s, crystal-detector distance 60 mm, collimator 0.5 mm. Data reduction performed by SAINTPLUS [64]. Empirical absorption corrections using equivalent reflections performed program SADABS [64]. Crystal data for compound **2g** and complex **6** was collected on Oxford, Gemini Diffractometer equipped with EOS CCD detector. Monochromatic Mo K*α* radiations (0.71073 Å) were used for the measurements. Absorption corrections using multi Ψ-scans were applied. The structures were solved by direct methods and least-square refinement on $F^2$ for all the compounds **2d**, **2g** and **6** by using SHELXS-97 [65]. All the non hydrogen atoms were refined anisotropically. Hydrogen atoms on the aromatic rings were introduced on calculated positions and included in the refinement riding on their respective parent atoms. The crystallographic parameters, data collection and structure refinement of the compounds **2d** and **2g** are summarized in Table 5.3.

*5.3.3. Electrochemical studies of Ni complex **6***

DMF (Finar, HPLC grade) used for performance of electrochemistry was dried with molecular sieve (4 Å) and then freshly distilled from $CaH_2$ under $N_2$. A solution of 0.1 M $[nBu_4N][ClO_4]$ (TBAP) (Across, electrochemical grade) in DMF was used as supporting electrolyte. A Cypress model CS-1090/CS-1087 electro analytical system was used for cyclic voltammetric experiments. The electrochemical experiments were measured in DMF containing $[Bu_4N][ClO_4]$ as a supporting electrolyte, using a conventional cell consisting of two platinum wires as working and counter electrodes, and a Ag/AgCl electrode as a reference. The potentials reported here are uncorrected for junction contributions. The potentials, reported here, are quoted against the ferrocene/ferrocenium ($Fc/Fc^+$) couple.

## 5.3.4. General procedure for derivatives of 2,3-chloro-Quinoxaline derivatives

**General Procedure I**

2,3-dichloroquinoxaline-6-carboxylic acid (**1**) (1.5 g, 6.19 mmol) was added to thionyl chloride (15 mL) and 2–3 drops of dry DMF was added as catalyst; the resulting reaction mixture was refluxed overnight. Excess thionyl chloride was removed by distillation at atmospheric pressure and then dried under reduced pressure. The resulting solid was dissolved in dry $CH_3CN$ (30 mL) followed by the slow addition of corresponding mono amine (1.29 g, 9.3 mmol) and dry triethylamine at 0 $^0$C. The reaction mixture was allowed to stir at room temperature for 1 h. under nitrogen atmosphere and the crude product was filtered and washed with hexane followed by diethyl ether 2-3 times to afford light brown solid as pure product. The same procedure was applied for all the compounds **2a–i**.

***N*-benzyl-2,3-dichloroquinoxaline-6-carboxamide (2a):**

The product **2a** was obtained as light brown solid and washed with hexane and diethyl ether as described in procedure I.

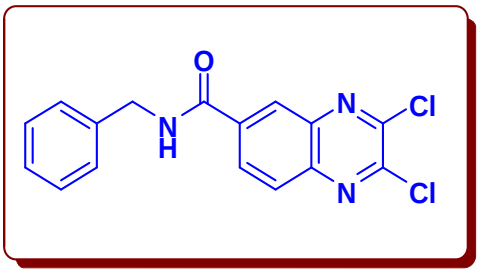


**Yield:** 60.9%

**Mp:** 230 ºC

**IR (KBr) $\nu_{max}$ cm$^{-1}$:** 3263(m), 2980(m), 1639(m), 1541(m), 1479(m), 1454(m), 1398(m), 1273(m), 1259(m), 1161(m), 1078(m), 1035(m), 997(m), 856(m), 742(m), 694(m)

**$^1$H NMR (400 MHz, DMSO-$d_6$):** $\delta$ 8.778 (s, 1H, NH), 8.383 (s, 1H, Ar–H), 8.110 (d, $J$ = 6.8 Hz, 1H, Ar–H), 7.733 (d, $J$ = 6.8 Hz, 1H, Ar–H) 7.077 (m, 5H, Ar–H), 4.349 (s, 2H, N–$CH_2$) ppm

**$^{13}$C NMR (100 MHz, DMSO-$d_6$):** $\delta$ 165.29, 146.13, 145.63, 141.35, 139.78, 138.67, 136.95, 130.25, 129.70, 128.24, 127.83, 127.56, 127.34, 126.92, 45.67 ppm

**ESI-MS (m/z):** 332.0352 $[M+1]^+$, 354.0175 $[M+Na]^+$

**Anal. Calcd. for $C_{16}H_{11}Cl_2N_3O$:** C, 57.85; H, 3.3377; N, 12.649%

**Found:** C, 57.80; H, 3.31; N, 12.54%

**2,3-dichloro-*N*-(4-methylbenzyl)quinoxaline-6-carboxamide (2b):**

The product **2b** was obtained as light brown solid and washed with hexane and diethyl ether as described in procedure I.

**Yield:** 65.42%

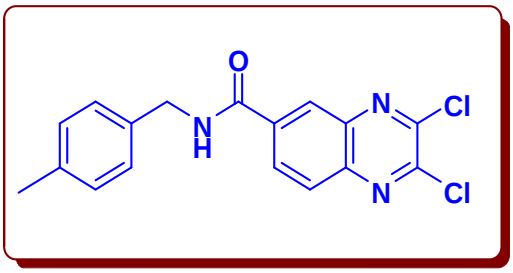


**Mp:** 235 ºC

**IR (KBr) $\nu_{max}$ $cm^{-1}$:** 3279(m), 2980(m), 1630(m), 1535(m), 1479(m), 1383(m), 1271(m), 1259(m), 1161(m), 1114(m), 1037(m), 997(m), 995(m), 893(m), 850(m), 808(m), 763(m), 684(m)

**$^1$H NMR (400 MHz, DMSO-$d_6$):** $\delta$ 9.524 (s, 1H, NH), 8.580 (s, 1H, Ar–H), 8.338 (d, $J$ = 1.6 Hz, 1H, Ar–H), 8.134 (d, $J$ = 8.8 Hz, 1H, Ar–H) 7.290 (t, $J$ = 7.6 Hz, 2H, Ar–H), 7.125 (t, $J$ = 7.2 Hz, 2H, Ar–H), 4.491 (s, 2H, N–$CH_2$), 2.229 (s, 3H, Ar–$CH_3$) ppm

**$^{13}$C NMR (100 MHz, DMSO-$d_6$):** $\delta$ 165.0, 146.5, 146.05, 141.59, 139.99, 138.181, 137.076, 136.69, 136.36, 130.51, 129.52, 129.32, 128.53, 127.82, 127.32, 45.73, 21.14

**ESI-MS (m/z):** 306.0517 $[M+1]^+$, 368.0338 $[M+Na]^+$

**Anal. Calcd. for $C_{17}H_{13}Cl_2N_3O$:** C, 58.98; H, 3.784; N, 12.137%

**Found:** C, 58.74; H, 3.69; N, 12.10%

**2,3-dichloro-*N*-(4-methoxybenzyl)quinoxaline-6-carboxamide (2c):**

The product **2c** was obtained as light brown solid and washed with hexane and diethyl ether as described in procedure I.

**Yield:** 76.1%

**Mp:** 228 ºC

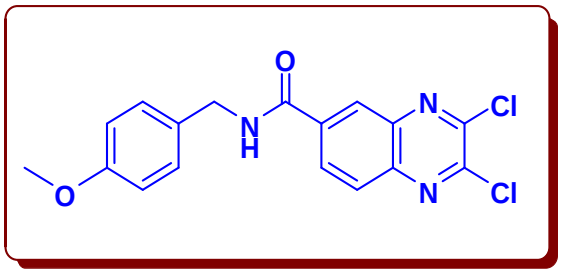

**IR (KBr) $\nu_{max}$ $cm^{-1}$:** 3288(m), 2978(m), 1631(m), 1533(m), 1512 (m), 1479(m), 1456(m), 1398(m), 1302(m), 1273(m), 1248(m), 1157(m), 1118(m), 1032(m), 997(m), 896(m), 854(m), 763(m), 700(m)

**$^1$H NMR (400 MHz, DMSO-$d_6$):** $\delta$ 9.534 (s, 1H, NH), 8.581 (s, 1H, Ar–H), 8.353 (d, $J$ = 7.6 Hz, 1H, Ar–H), 8.128 (d, $J$ = 8.4 Hz, 1H, Ar–H) 7.288 (t, $J$ = 7.2 Hz, 2H, Ar–H), 6.882 (t, $J$ = 7.6 Hz, 2H, Ar–H), 4.453 (s, 2H, N–$CH_2$), 3.712 (s, 3H, Ar–O$CH_3$) ppm

**$^{13}$C NMR (100 MHz, DMSO-$d_6$):** $\delta$ 164.90, 158.72, 146.53, 146.06, 141.57, 139.99, 137.10, 131.69, 130.52, 129.23, 128.50, 127.33, 114.15, 55.52, 45.70 ppm

**ESI-MS (m/z):** 362.0463 $[M+1]^+$, 384.0281 $[M+Na]^+$

**Anal. Calcd. for $C_{17}H_{13}Cl_2N_3O_2$:** C, 56.37; H, 3.62; N, 11.60%

**Found:** C, 56.28; H, 3.60; N 11.57%

**2,3-dichloro-*N*-(4-fluorobenzyl)quinoxaline-6-carboxamide (2d):**

The product **2d** was obtained as light brown solid and washed with hexane and diethyl ether as described in procedure I.

**Yield:** 76.23%

**Mp:** 234 ºC

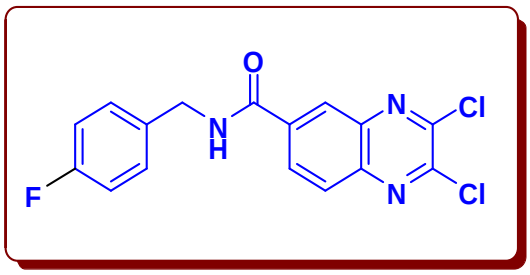

**IR (KBr) $\nu_{max}$ $cm^{-1}$:** 3269(m), 2980(m), 1637(s), 1610(m), 1539(m), 1512(m), 1481(m), 1398(m), 1273(m), 1224(m), 1159(m), 1120(m), 1037(m), 997(m), 896(m), 756(m), 640(m)

**$^1$H NMR (400 MHz, DMSO-$d_6$):** $\delta$ 9.660 (s, 1H, NH), 8.611 (s, 1H, Ar–H), 8.37 (d, *J* = 8.4 Hz, 1H, Ar–H), 8.148 (d, *J* = 8.8 Hz, 1H, Ar–H) 7.404 (t, *J* = 8.0 Hz, 2H, Ar–H), 7.152 (t, *J* = 8.4 Hz, 2H, Ar–H), 4.509 (s, 2H, N–$CH_2$) ppm

**$^{13}$C NMR (100 MHz, DMSO-$d_6$):** $\delta$ 165.08, 146.608, 146.126, 141.636, 140.006, 136.951, 135.962, 130.517, 129.903, 129.823, 128.564, 127.406, 115.608, 115.397, 45.707 ppm

**ESI-MS (m/z):** 350.0263 $[M+1]^+$, 372.0080 $[M+Na]^+$

**Anal. Calcd. for $C_{16}H_{10}Cl_2N_3OF$:** C, 54.88; H, 2.88; N, 11.99%

**Found:** C, 54.86; H, 2.83; N, 11.93%

**2,3-dichloro-*N*-(furan-2-ylmethyl)quinoxaline-6-carboxamide (2e):**

The product **2e** was obtained as light brown solid and washed with hexane and diethyl ether as described in procedure I.

**Yield:** 75.34%

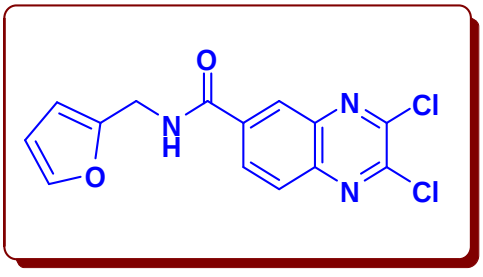

**Mp:** 229 ºC

**IR (KBr) $\nu_{max}$ $cm^{-1}$:** 3258(m), 2980(m), 1635(m), 1612(m), 1541(m),

1479(m), 1444(m), 1398(m), 1275(m), 1259(m), 1161(m), 1124(m), 1074(m), 1035(m), 999(m), 854(m), 740(m), 690(m)

**$^1$H NMR (400 MHz, DMSO-$d_6$):** $\delta$ 9.513 (s, 1H, NH), 8.581 (s, 1H, Ar–H), 8.346 (d, $J$ = 8.8 Hz, 1H, Ar–H), 8.148 (d, $J$ = 8.8 Hz, 1H, Ar–H) 7.590 (s, 1H, Ar–H), 6.403 (s, 1H, Ar–H), 6.325 (s, 1H, Ar–H), 4.437 (s, 2H, N–$CH_2$) ppm

**$^{13}$C NMR (100 MHz, DMSO-$d_6$):** $\delta$ 165.0, 152.45, 146.64, 146.14, 142.62, 141.65, 139.99, 136.80, 130.52, 128.58, 127.47, 110.99, 107.62, 45.7 ppm

**ESI-MS (m/z):** 322.0150 $[M+1]^+$, 343.9969 $[M+Na]^+$

**Anal. Calcd. for $C_{14}H_9Cl_2N_3O_2$:** C, 52.20; H, 2.81; N, 13.04%

**Found:** C, 52.15; H, 2.79; N, 13.03%

**2,3-dichloro-*N*-(thiophen-2-ylmethyl)quinoxaline-6-carboxamide (2f):**

The product **2f** was obtained as light brown solid and washed with hexane and diethyl ether as described in procedure I.

**Yield:** 55.01%

**Mp:** 235 ºC

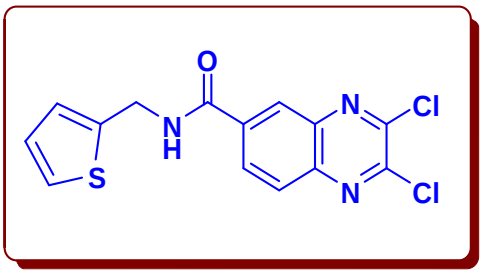


**IR (KBr) $\nu_{max}$ cm$^{-1}$:** 3261(m), 2980(m), 1637(m), 1612(m), 1531(m), 1479(m), 1442(m), 1398(m), 1296(m), 1273(m), 1159(m), 1078(m), 1035(m), 997(m), 858(m), 761(m), 698(m)

**$^1$H NMR (400 MHz, DMSO-$d_6$):** $\delta$ 9.691 (s, 1H, NH), 8.571 (s, 1H, Ar–H), 8.350 (d, $J$ = 6.8 Hz, 1H, Ar–H), 8.143 (d, $J$ = 8.4 Hz, 1H, Ar–H), 7.393 (d, $J$ = 5.2 Hz, 1H, Ar–H), 7.062 (d, $J$ = 3.2 Hz, 1H, Ar–H), 6.960 (s, 1H, Ar–H), 4.689 (s, 2H, N–$CH_2$) ppm

**$^{13}$C NMR (100 MHz, DMSO-$d_6$):** $\delta$ 164.91, 146.62, 146.13, 142.57, 141.65, 139.99, 136.79, 130.46, 128.59, 127.41, 127.16, 126.16, 125.58, 45.18 ppm

**ESI-MS (m/z):** 7.9916 $[M+1]^+$, 359.9735 $[M+Na]^+$

**Anal. Calcd. for $C_{14}H_9Cl_2N_3OS$:** C, 49.72; H, 2.6821; N, 12.4241%

**Found:** C, 49.70; H, 2.65; N, 12.40%

**2,3-dichloro-*N*-phenylquinoxaline-6-carboxamide (2g):**

The product **2g** was obtained as light brown solid and washed with hexane and diethyl ether as described in procedure I.

**Yield:** 81.4%

**Mp:** 240 ºC

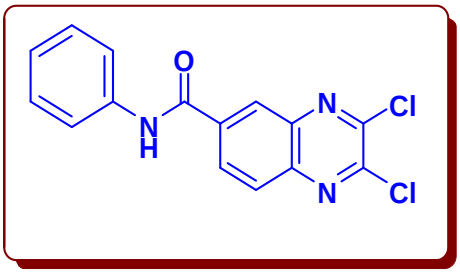


**IR (KBr) $\nu_{max}$ cm$^{-1}$:** 3326 (m), 2975(m), 1654(m), 1594(m), 1528(m), 1441(m), 1397(m), 1254(m), 1172(m), 1123(m), 1041(m), 991(m), 909(m), 843(m), 684(m), 591(m)

**$^1$H NMR (400 MHz, DMSO-$d_6$):** $\delta$ 10.746 (s, 1H, NH), 8.721 (s, 1H, Ar–H), 8.417 (d, $J$ = 8.4 Hz, 1H, Ar–H), 8.187 (d, $J$ = 8.4 Hz, 1H, Ar–H), 7.848 (d, $J$ = 8.4 Hz, 2H, Ar–H), 7.373 (t, $J$ = 8.0 Hz, 2H, Ar–H), 7.132 (t, $J$ = 7.6 Hz, 1H, Ar–H) ppm

**$^{13}$C NMR (100 MHz, DMSO-$d_6$):** $\delta$ 164.20, 146.50, 146.0, 141.57, 139.84, 138.52, 137.55, 130.63, 128.61, 128.06, 127.75, 124.35, 120.97 ppm

**ESI-MS (m/z):** 318.0201 $[M+1]^+$, 340.0019 $[M+Na]^+$

**Anal. Calcd. for $C_{15}H_9Cl_2N_3O$:** C, 56.63; H, 2.8512; N, 13.20

**Found:** C, 56.59; H, 2.849; N, 13.17%

**2,3-dichloro-*N*-(pyrimidin-2-yl)quinoxaline-6-carboxamide (2h):**

The product **2h** was obtained as light brown solid and washed with hexane and diethyl ether as described in procedure I.

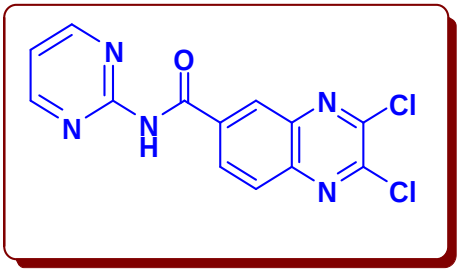

**Yield:** 60.65

**Mp:** 233 ºC

**IR (KBr) $\nu_{max}$ $cm^{-1}$:** 3391(m), 2947(m), 1698(m), 1583(m), 1517(m), 1435(m), 1331(m), 1265(m), 1128(m), 1035(m), 986(m), 838(m), 739(m), 635(m)

**$^1$H NMR (400 MHz, DMSO-$d_6$):** $\delta$ 11.446 (s, 1H, NH), 8.756 (st, *J* = 1.6 Hz, 2H, Ar–H), 8.636 (s, 1H, Ar–H), 8.350 (d, *J* = 6.8 Hz, 1H, Ar–H), 8.164 (d, *J* = 8.8 Hz, 1H, Ar–H), 7.293 (qt, *J* = 1.6 Hz, 1H, Ar–H) ppm

**$^{13}$C NMR (100 MHz, DMSO-$d_6$):** $\delta$ 164.68, 158.95, 158.39, 146.95, 146.27, 142.0, 139.83, 137.05, 131.01, 128.56, 118.16 ppm

**ESI-MS (m/z):** 320.0106 $[M+1]^+$, 341.9924 $[M+Na]^+$

**Anal. Calcd. for $C_{13}H_7Cl_2N_5O$:** C, 48.77; H, 2.2039; N, 21.87%

**Found:** C, 48.68; H, 2.197; N, 21.69%

**2,3-dichloro-*N*-(naphthalen-1-yl)quinoxaline-6-carboxamide (2i):**

The product **2i** was obtained as light brown solid and washed with hexane and diethyl ether as described in procedure I.

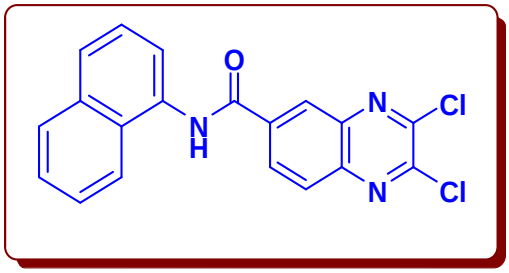

**Yield:** 70.1%

**Mp:** 231 ºC

**IR (KBr) $\nu_{max}$ $cm^{-1}$:** 2980(m),

1643(m), 1531(m), 1479(m), 1444(m), 1396(m), 1273(m), 1259(m), 1172(m), 1153(m), 1074(m), 1035(m), 997(m), 852(m), 794(m)

**$^1$H NMR (400 MHz, DMSO-$d_6$):** $\delta$ 10.946 (s, 1H, NH), 8.853 (s, 1H, Ar–H), 8.5145 (d, $J$ = 7.6 Hz, 1H, Ar–H), 8.235 (d, $J$ = 8.4 Hz, 1H, Ar–H), 8.027 (dd, $J_1$ = 7.6 Hz, $J_2$ = 7.6 Hz, 2H, Ar–H), 7.899 (d, $J$ = 7.6 Hz 1H, Ar–H), 7.668 (d, $J$ = 6.0 Hz 1H, Ar–H), 7.575 (br, 3H, Ar–H) ppm

**$^{13}$C NMR (100 MHz, DMSO-$d_6$):** $\delta$ 165.18, 146.80, 146.25, 141.82, 140.01, 137.20, 134.25, 133.89, 130.97, 129.57, 128.67, 128.58, 128.04, 127.08, 126.64, 126.59, 126.04, 124.50, 123.84 ppm

**ESI-MS (m/z):** 368.0357 $[M+1]^+$, 390.0178 $[M+Na]^+$

**Anal. Calcd. for $C_{19}H_{11}Cl_2N_3O$:** C, 61.98; H, 3.011; N, 11.41%

**Found:** C, 61.84; H, 2.97; N, 11.39%

## 5.3.5. General procedure for derivatives of Quinoxaline-2,3-dithiol derivatives

**General Procedure II**

3.0 mmol of derivatives of 2,3-dichloro quinoxaline carboxamide **2a–i** and 7.5 mmol of thiourea were suspended in 25–30 mL of absolute ethanol and this mixture was reflux for 3–4 h. The solution was concentrated to a small volume. The concentrated solution was diluted with 60 mL of water, cooled to −10 ºC and made alkaline by the addition of 6.0 mmol of NaOH, stirred until the clear solution was obtained. On acidifying with acetic acid, a brown color precipitate was formed which was separated by filtration, washed with water fallowed by diethyl ether and dried under vacuum. The same procedure was applied for all the compounds **3a-i**.

***N*-benzyl-2,3-dimercaptoquinoxaline-6-carboxamide (3a)**

The product **3a** was obtained as brown color precipitate and washed with water followed by diethyl ether as described in procedure II.

**Yield:** 60.1%

**IR (KBr) $\nu_{max}$ $cm^{-1}$:** 3381(w), 3128 (w), 1645(CO-NH)(s), 1604(m), 1487(m), 1412(m), 1358(m), 1311(m), 1236(m), 1141(m), 1005(m), 823(m), 725(m), 696(m), 650(m)

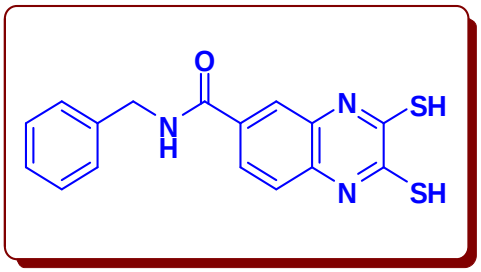


**$^1$H NMR (400 MHz, DMSO-$d_6$):** $\delta$ 9.050 (s, 1H, CO-NH), 7.874 (s, 1H, Ar–H), 7.675 (d, $J$ = 8.4 Hz, 1H, Ar–H), 7.348 (d, $J$ = 8.4 Hz, 1H, Ar–H), 7.310 (d, $J$ = 4.4 Hz, 4H, Ar–H), 7.227 (dd, $J_1$ = 4.0 Hz, $J_2$ = 4.8 Hz, 1H, Ar–H), 4.465 (s, 2H, HN–$CH_2$) ppm

**$^{13}$C NMR (100 MHz, DMSO-$d_6$):** $\delta$ 166.14 (CO-NH), 140.16, 130.50, 130.13, 128.74, 127.65, 127.18, 127.03, 123.44, 122.06, 120.51, 118.63, 117.77, 43.12 (HN–$CH_2$) ppm

**LC-MS (m/z):** 328.30 $[M+H]^+$

**Anal. Calcd. for $C_{16}H_{13}N_3OS_2$:** C, 58.69; H, 4.00; N, 12.83%

**Found:** C, 58.65; H, 3.97; N, 12.82%

**2,3-dimercapto-*N*-(4-methylbenzyl)quinoxaline-6-carboxamide (3b).**

The product **3b** was obtained as brown color precipitate and washed with water followed by diethyl ether as described in procedure II.

**Yield:** 62.9%

**IR (KBr) $\nu_{max}$ $cm^{-1}$:** 3281(w), 1641(CO-NH)(s), 1525(m),

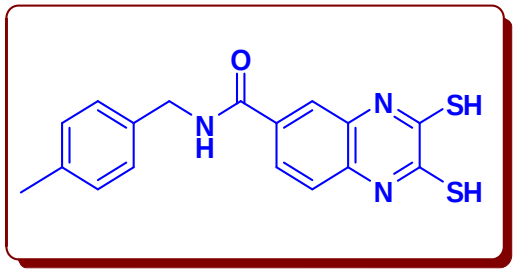

1359(m), 1302(m), 1140(m), 833(m), 698(m)

**$^1$H NMR (400 MHz, DMSO-$d_6$):** $\delta$ 9.175 (s, 1H, CO-NH), 7.892 (s, 1H, Ar–H), 7.7025 (d, *J* = 8.4 Hz, 1H, Ar–H), 7.496 (d, *J* = 8.4 Hz, 1H, Ar–H), 7.375 (d, *J* = 4.4 Hz, 2H, Ar–H), 6.995 (d, *J* = 4.4 Hz, 2H, Ar–H), 4.625 (s, 2H, HN–$CH_2$), 1.897 (s, 3H, Ar-$CH_3$) ppm

**$^{13}$C NMR (100 MHz, DMSO-$d_6$):** $\delta$ 165.58 (CO-NH), 143.27, 142.93, 131.26, 128.51, 127.10, 125.93, 125.75, 125.46, 125.24, 124.13, 115.98, 38.35 (HN–$CH_2$) ppm

**LC-MS (m/z):** 342.30 $[M+H]^+$ positive mode

**Anal. Calcd. for $C_{17}H_{15}N_3OS_2$:** C, 59.80; H, 4.43; N, 12.31%

**Found:** C, 59.79; H, 4.42; N, 12.29%

**2,3-dimercapto-*N*-(4-methoxybenzyl)quinoxaline-6-carboxamide (3c).**

The product **3c** was obtained as brown color precipitate and washed with water followed by diethyl ether as described in procedure II.

**Yield:** 52.8%

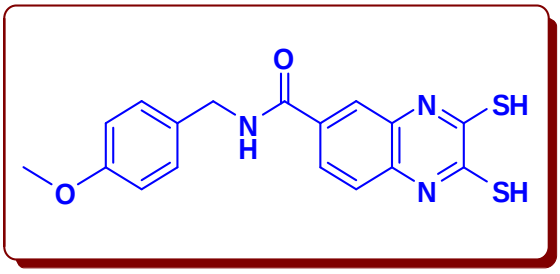


**IR (KBr) $\nu_{max}$ cm$^{-1}$:** 2955(w), 1641(CO-NH)(s), 1604(m), 1512(m), 1358(m), 1313(m), 1242(m), 1174(m), 1143(m), 1022(m), 910(m), 827(m), 750(m), 655(m)

**$^1$H NMR (400 MHz, DMSO-$d_6$):** $\delta$ 9.026 (s, 1H, CO-NH), 7.883 (s, 1H, Ar–H), 7.711 (d, *J* = 8.4 Hz, 1H, Ar–H), 7.385 (d, *J* = 6.8 Hz, 1H, Ar–H), 7.232

(d, *J* = 8.4 Hz, 2H, Ar–H), 6.872 (d, *J* = 8.4 Hz, 2H, Ar–H), 4.387 (s, 2H, HN–$\underline{CH_2}$), 3.708 (s, 3H, O–$\underline{CH_3}$) ppm

**$^{13}$C NMR (100 MHz, DMSO-$d_6$):** $\delta$ 165.57 ($\underline{CO}$-NH), 158.67, 131.97, 131.63, 130.38, 129.08, 128.41, 127.67, 124.15, 122.21, 116.03, 115.36, 114.15, 55.51(O–$\underline{CH_3}$), 42.66 (HN–$\underline{CH_2}$) ppm

**LC-MS (m/z):** 358.15 $[M+H]^+$ positive mode

**Anal. Calcd. for $C_{17}H_{15}N_3O_2S_2$:** C, 57.12; H, 4.23; N, 11.76%

**Found:** C, 57.09; H, 4.20; N, 11.75%

***N*-(4-fluorobenzyl)-2,3-dimercaptoquinoxaline-6-carboxamide (3d).**

The product **3d** was obtained as brown color precipitate and washed with water followed by diethyl ether as described in procedure II.

**Yield:** 57.56%

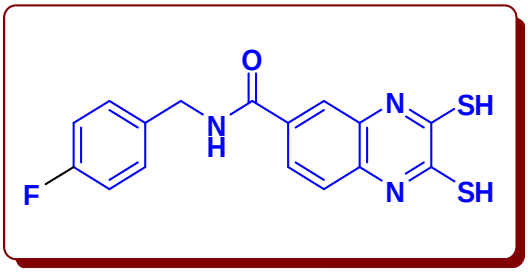


**IR (KBr) $\nu_{max}$ cm$^{-1}$:** 3256(w), 3076(w),2930 (m), 1639($\underline{CO}$-NH)(s), 1552(m), 1508(m), 1361(m), 1311(m), 1217(m), 1140(m), 1095(m), 1062(m), 877(m), 821(m), 727(m), 650(m)

**$^1$H NMR (400 MHz, DMSO-$d_6$):** $\delta$ 9.130 (s, 1H, CO-$\underline{NH}$), 7.901 (s, 1H, Ar–H), 7.746 (d, *J* = 8.4 Hz, 1H, Ar–H), 7.411 (d, *J* = 8.4 Hz, 1H, Ar–H), 7.351 (d, *J* = 8.4 Hz, 2H, Ar–H), 7.155 (d, J = 8.8 Hz, 2H, Ar–H), 4.442 (s, 2H, HN–$\underline{CH_2}$) ppm

**$^{13}$C NMR (100 MHz, DMSO-$d_6$):** $\delta$ 165.64 ($\underline{CO}$-NH), 154.51, 136.16, 131.58, 130.12, 129.74, 129.66, 128.15, 124.27, 122.24, 115.88, 115.58, 115.37, 46.06 (HN–$\underline{CH_2}$) ppm

**LC-MS (m/z):** 346.15 $[M+H]^+$ positive mode

**Anal. Calcd. for $C_{16}H_{12}FN_3OS_2$:** C, 55.63; H, 3.50; N, 5.50%

**Found:** C, 55.60; H, 3.48; N, 5.47%

**_N_-(furan-2-ylmethyl)-2,3-dimercaptoquinoxaline-6-carboxamide (3e).**

The product **3e** was obtained as brown color precipitate and washed with water and diethyl ether as described in procedure II.

**Yield:** 60.56%

**IR (KBr) $\nu_{max}$ $cm^{-1}$:** 3281(w), 1639(CO-NH)(s), 1531(m), 1358(m), 1302(m), 1141(m), 1012(m), 842(m), 738(m), 599(m)

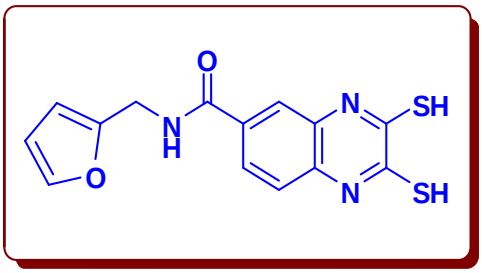


**$^1$H NMR (400 MHz, DMSO-$d_6$):** $\delta$ 9.343 (s, 1H, CO-NH), 8.447 (s, 1H, Ar–H), 8.207 (d, $J$ = 7.6 Hz, 1H, Ar–H), 8.018 (d, $J$ = 8.8 Hz, 1H, Ar–H), 7.596 (s, 1H), 7.577 (s, 2H), 4.525 (s, 2H, HN–$CH_2$) ppm

**$^{13}$C NMR (100 MHz, DMSO-$d_6$):** $\delta$ 165.19 (CO-NH), 152.70, 152.48, 142.53, 142.49, 141.27, 130.04, 128.44, 126.88, 110.99, 110.95, 107.43, 107.39, 36.64 (HN–$CH_2$) ppm

**LC-MS (m/z):** 318.15 $[M+H]^+$ positive mode

**Anal. Calcd. for $C_{14}H_{11}N_3O_2S_2$:** C, 52.98; H, 3.49; N, 13.24%

**Found:** C, 52.95; H, 3.48; N, 13.19%

**2,3-dimercapto-_N_-(thiophen-2-ylmethyl)quinoxaline-6-carboxamide (3f).**

The product **3f** was obtained as brown color precipitate and washed with water followed by diethyl ether as described in procedure II.

**Yield:** 64.61%

**IR (KBr) $\nu_{max}$ $cm^{-1}$:** 3412(m), 3117(w), 2970(m), 1647(CO-NH)(s), 1604(m), 1529(m), 1485(m), 1412(m), 1359(m), 1311(m), 1236(m), 812(m), 760(m), 655(m)

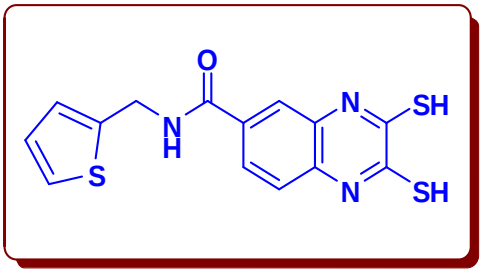


**$^1$H NMR (400 MHz, DMSO-$d_6$):** $\delta$ 9.048 (s, 1H, CO-NH), 7.899 (s, 1H, Ar–H), 7.738 (d, $J$ = 8.4 Hz, 1H, Ar–H), 7.408 (d, $J$ = 8.4 Hz, 1H, Ar–H), 7.199 (s, 1H), 7.183 (s, 1H), 7.124 (s, 1H), 4.416 (s, 2H, HN–$CH_2$) ppm

**$^{13}$C NMR (100 MHz, DMSO-$d_6$):** $\delta$ 165.60 (CO-NH), 137.94, 136.93, 136.28, 131.68, 130.24, 129.29, 128.27, 127.69, 126.03, 124.20, 115.97, 115.72, 42.95

**LC-MS (m/z):** 332.20 $[M–H]^+$ negative mode

**Anal. Calcd. for $C_{14}H_{11}N_3O_2S_3$:** C, 50.43; H, 3.33; N, 12.60%

**Found:** C, 50.39; H, 3.30; N, 12.58%

**2,3-dimercapto-*N*-phenylquinoxaline-6-carboxamide (3g).**

The product **3g** was obtained as brown color precipitate and washed with water and diethyl ether as described in procedure II.

**Yield:** 42.30%

**IR (KBr) $\nu_{max}$ $cm^{-1}$:** 3391(w), 3072(w), 2935(m), 1657(CO-NH)(s), 1601(m),1537(m),

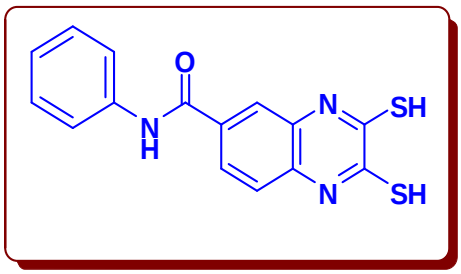

1491(m), 1442(m), 1361(m), 1317(m), 1246(m), 1141(m), 883(m), 819(m), 754(m), 686(m), 653(m), 603(m)

**$^1$H NMR (400 MHz, DMSO-$d_6$):** $\delta$ 10.342 (s, 1H, CO-NH), 7.927 (s, 1H, Ar–H), 7.829 (d, *J* = 8.4 Hz, 1H, Ar–H), 7.737 (d, *J* = 8.4 Hz, 1H, Ar–H), 7.469 (d, *J* = 8.4 Hz, 1H, Ar–H), 7.350 (t, *J* = 8.0 Hz, 2H, Ar–H), 7.101 (t, *J* = 6.8 Hz, 2H, Ar–H) ppm

**$^{13}$C NMR (100 MHz, DMSO-$d_6$):** $\delta$ 164.95 (CO-NH), 139.44, 132.18, 130.30, 129.14, 129.00, 128.14, 124.88, 124.30, 124.04, 120.84, 116.04, 115.65 ppm

**LC-MS (m/z):** 314.20 $[M+H]^+$ positive mode

**Anal. Calcd. for $C_{15}H_{11}N_3OS_2$:** C, 57.49; H, 3.54; N, 13.41%

**Found:** C, 57.44; H, 3.50; N, 13.38%

**2,3-dimercapto-*N*-(pyrimidin-2-yl)quinoxaline-6-carboxamide (3h).**

The product **3h** was obtained as brown color precipitate and washed with water and diethyl ether as described in procedure II.

**Yield:** 40.98%

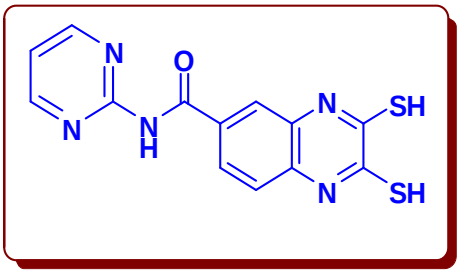


**IR (KBr) $\nu_{max}$ cm$^{-1}$:** 3391(w), 3072(w), 2935(m), 1657(CO-NH)(s), 1601(m),1537(m), 1491(m), 1442(m), 1361(m), 1317(m), 1246(m), 1141(m), 883(m), 819(m), 754(m), 686(m), 653(m), 603(m)

**$^1$H NMR (400 MHz, DMSO-$d_6$):** $\delta$ 10.752 (s, 1H, CO-NH), 8.227 (s, 1H, Ar–H), 8.029 (d, *J* = 8.4 Hz, 1H, Ar–H), 7.877 (d, *J* = 8.4 Hz, 1H, Ar–H), 7.802 (t, *J* = 7.6 Hz, 3H, Ar–H) ppm

**$^{13}$C NMR (100 MHz, DMSO-$d_6$):** $\delta$ 166.75 (CO-NH), 141.44, 134.18, 130.30, 129.00,128.74, 128.14, 124.88, 124.30, 123.04, 120.84 ppm

**LC-MS (m/z):** 316.02 $[M+H]^+$ positive mode

**Anal. Calcd. for $C_{13}H_9N_5OS_2$:** C, 49.51; H, 2.88; N, 22.21%

**Found:** C, 49.48; H, 2.85; N, 22.18%

**2,3-dimercapto-*N*-(naphthalen-1-yl)quinoxaline-6-carboxamide (3i).**

The product **3i** was obtained as brown color precipitate and washed with water followed by diethyl ether as described in procedure II.

**Yield:** 35.56%

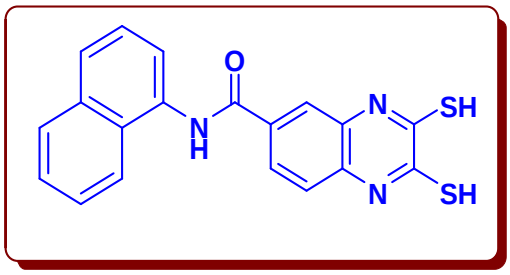


**IR (KBr) $\nu_{max}$ cm$^{-1}$:** 2930(w), 1643(CO-NH)(s), 1531(m), 1494(m), 1350(m), 1242(m), 1174(m), 1141(m), 1032(m), 792(m), 767(m), 605(m)

**$^1$H NMR (400 MHz, DMSO-$d_6$):** $\delta$ 10.655 (s, 1H, CO-NH), 8.525 (s, 1H, Ar–H), 8.176 (d, $J$ = 8.4 Hz, 1H, Ar–H), 8.067 (d, $J$ = 8.4 Hz, 1H, Ar–H), 7.969 (m, 5H), 7.868 (d, $J$ = 8.4 Hz, 2H, Ar–H) ppm

**$^{13}$C NMR (100 MHz, DMSO-$d_6$):** $\delta$ 165.46 (CO-NH), 134.23, 131.78, 130.30, 129.79, 129.48, 128.60, 128.48, 126.88, 126.58, 126.51, 126.49, 126.43, 126.03, 125.99, 125.03, 124.59, 124.14, 123.67 ppm

**LC-MS (m/z):** 364.40 $[M+H]^+$ positive mode

**Anal. Calcd. for $C_{19}H_{13}N_3OS_2$:** C, 62.79; H, 3.61; N, 11.56%

**Found:** C, 62.75; H, 3.59; N, 11.54%

## 5.3.6. General procedure for derivatives of Bis Quinoxaline-o-dichloro derivatives

**General procedure III**

2,3-dichloroquinoxaline-6-carboxylic acid (**1**) (1.5 g, 6.19 mmol) was added to thionyl chloride (15 mL) and 2–3 drops of dry DMF was added as a catalyst; subsequently, the reaction mixture was refluxed overnight. Excess thionyl chloride was removed by distillation at atmospheric pressure and then dried under reduced pressure. The resulting solid was dissolved in dry DCM (30 mL) followed by the slow addition of corresponding diamine (2.7 mmol) and dry triethylamine at 0 $^0$C. The reaction mixture was allowed to stir at room temperature for an hour under nitrogen atmosphere and the crude product was filtered and washed with hot methanol 2–3 times to yield light brown solid as a pure product. The same procedure was applied for all the compounds **4a-i**.

***N,N'*-(ethane-1,2-diyl)bis(2,3-dichloroquinoxaline-6-carboxamide) (4a).**

The product **4a** was obtained as light brown solid, washed with hot methanol 2–3 times as described in procedure III.

**Yield:** 48.1%

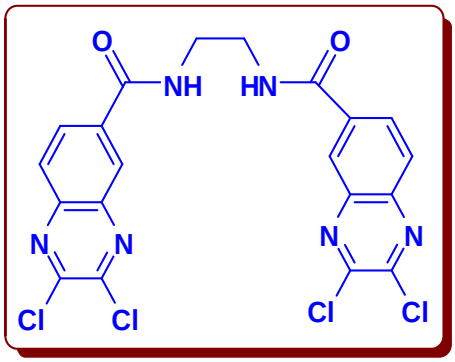


**IR (KBr) $\nu_{max}$ $cm^{-1}$:** 3281(s), 2932(m), 1641(CO-NH)(s), 1545(m), 1450(m), 1486(m), 1352(m), 1275(m), 1167(m), 1120(m), 999(m), 900(m), 846(m), 709(m), 642(m), 613(m)

**$^1$H NMR (400 MHz, DMSO-$d_6$):** $\delta$ 9.07 (s, 2H, NH), 8.533 (s, 2H, Ar-H), 8.30 (d, *J* = 8.0 Hz, 2H, Ar-H), 8.15 (d, *J* = 8.0 Hz, 2H, Ar-H) 3.56 (s, 4H, -$CH_2$) ppm

**$^{13}$C NMR (100 MHz, DMSO-$d_6$):** $\delta$ 167.11 (CO-NH), 147.21, 142.38, 139.93, 133.76, 131.33, 129.81, 125.97, 124.77, 40.41 ($CH_2$–NH) ppm

**LC-MS (m/z):** 510.75 $[M+H]^+$ positive mode

**Anal. Calcd. for $C_{20}H_{12}Cl_4N_6O_2$:** C, 47.09; H, 2.37; N, 16.47%

**Found:** C, 46.89; H, 2.361; N, 16.392%

***N,N'*-(propane-1,3-diyl)bis(2,3-dichloroquinoxaline-6-carboxamide) (4b).**

The product **4b** was obtained as light brown solid, washed with hot methanol 2–3 times as described in procedure III.

**Yield:** 50.18%

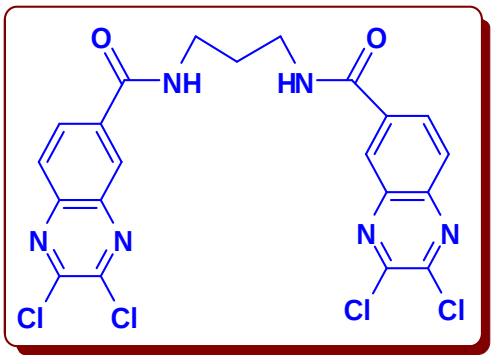


**IR (KBr) $\nu_{max}$ cm$^{-1}$:** 3352(st, N-H), 3057(s, Ar-H), 2953(m), 1645.3(CO-NH)(s), 1541.29(st, N-H), 1485.8(s), 1440.9(m), 1307.85(s), 1267.6(s), 1163.1(s), 1120.3(s), 1001(s)

**$^1$H NMR (400 MHz, DMSO-$d_6$):** $\delta$ 8.972 (s, 2H, NH), 8.505 (s, 2H, Ar-H), 8.298 (d, *J* = 8.4 Hz, 2H, Ar-H), 8.120 (d, *J* = 7.6 Hz, 2H, Ar-H), 3.332 (s, 4H, -$CH_2$), 1.885 (s, 2H, -$CH_2$) ppm

**$^{13}$C NMR (100 MHz, DMSO-$d_6$):** $\delta$ 165.09 (CO-NH), 146.49, 146.04, 141.51, 139.95, 137.28, 130.45, 128.47, 127.11, 46.00, 36.53 ppm

**LC-MS (m/z):** 525.30 $[M+H]^+$

**Anal. Calcd. for $C_{21}H_{14}Cl_4N_6O_2$:** C, 48.12; H, 2.69; N, 16.03%

**Found:** C, 48.05; H, 2.67; N, 16.0%.

***N,N'*-(1,4-phenylenebis(methylene))bis(2,3-dichloroquinoxaline-6-carboxamide) (4c)**

The product **4c** was obtained as light brown solid, washed with hot methanol 2–3 times as described in procedure III.

**Yield:** 41.57%

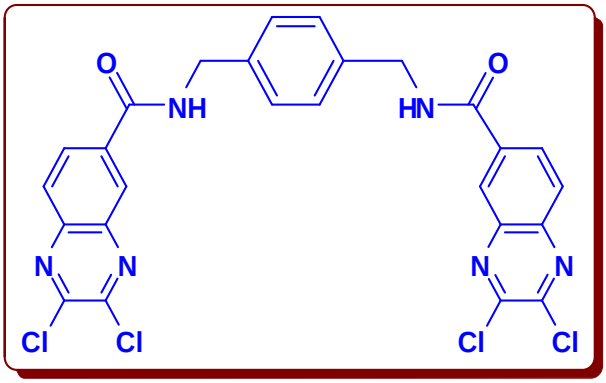


**IR (KBr) $\nu_{max}$ $cm^{-1}$:** 3238(br, N-H), 3040(s, Ar-H), 1634.8(CO-NH)(s), 1610(s), 1534.2 (st, N-H), 1484.8(s), 1309(s), 1276.6(s), 1156.1(s), 1112.3(s), 986.3(s), 893.27(s), 849.2(s)

**$^1$H NMR (400 MHz, DMSO-$d_6$):** $\delta$ 9.467 (s, 2H, NH), 8.568 (s, 2H, Ar-H), 8.334 (d, $J$ = 8.0 Hz, 2H, Ar-H), 8.147 (d, $J$ = 8.4 Hz, 2H, Ar-H), 7.338 (s, 4H, Ar-H), 4.525 (s, 4H, -$CH_2$) ppm

**$^{13}$C NMR (100 MHz, DMSO-$d_6$):** $\delta$ 165.12 (CO–NH), 146.50, 145.98, 141.42, 139.88, 139.79, 136.98, 130.42, 128.80, 128.40, 127.13, 126.20, 125.66 (Ar-C), 43.16 ($CH_2$–NH) ppm

**LC-MS (m/z):** 585.00 $[M–H]^+$ positive mode

**Anal. Calcd. for $C_{26}H_{16}Cl_4N_6O_2$:** C, 53.27; H, 2.75; N, 14.33%

**Found:** C, 53.16; H, 2.70; N, 14.32%.

**_N,N'_-(1,3-phenylenebis(methylene))bis(2,3-dichloroquinoxaline-6-carboxamide) (4d).**

The product **4d** was obtained as light brown solid, washed with hot methanol 2–3 times as described in procedure III.

**Yield:** 40.47%

**IR (KBr) $\nu_{max}$ $cm^{-1}$:** 3364(st, N-H), 3040(s, Ar-H), 1643.8(CO-NH)(s), 1616(s), 1534.2 (st, N-H), 1484.8(s), 1430(s), 1320.5(s), 1271.6(s), 1172.1(s), 1123.3(s), 1002.7(s), 896.27(s)

**$^1$H NMR (400 MHz, DMSO-$d_6$):** 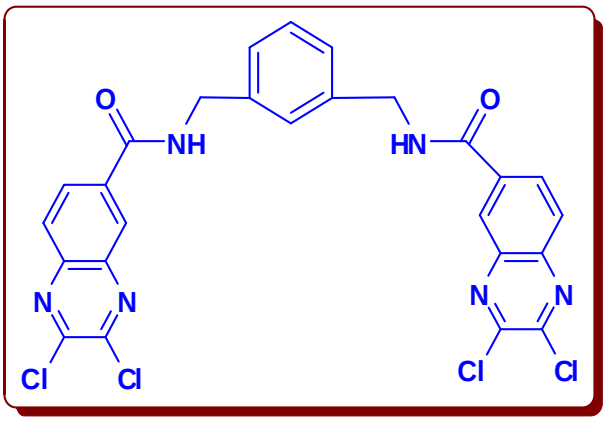

$\delta$ 9.460 (s, 2H, NH), 8.446 (s, 2H, Ar-H), 8.257 (d, $J$ = 8.8 Hz, 2H, Ar-H), 8.027 (d, $J$ = 8.4 Hz, 2H, Ar-H), 7.315 (d, $J$ = 8.0 Hz, 2H, Ar-H), 7.245 (d, $J$ = 8.0 Hz, 2H, Ar-H), 4.542 (s, 4H, -$CH_2$) ppm

**$^{13}$C NMR (100 MHz, DMSO-$d_6$):** $\delta$ 165.12 (CO–NH), 146.50, 145.98, 141.42, 139.88, 139.79, 136.98, 130.42, 128.80, 128.40, 127.13, 126.20, 125.66 (Ar-C), 43.16 ($CH_2$–NH) ppm

**LC-MS (m/z):** 587.01 $[M+H]^+$ positive mode

**Anal. Calcd. for $C_{26}H_{16}Cl_4N_6O_2$:** C, 53.27; H, 2.75; N, 14.33%

**Found:** C, 53.16; H, 2.70; N, 14.32%

***N,N'*-(1,2-phenylene)bis(2,3-dichloroquinoxaline-6-carboxamide) (4e).**

The product **4e** was obtained as light brown solid, washed with hot methanol 2–3 times as described in procedure III.

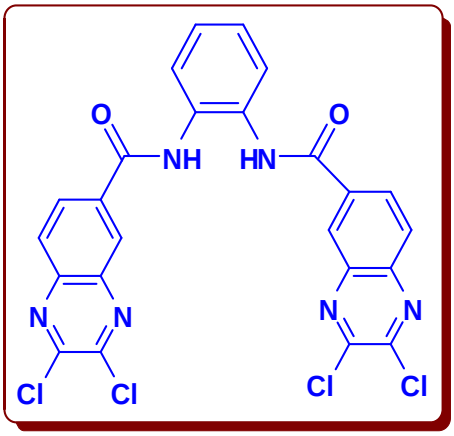


**Yield:** 26.59%

**IR (KBr) $\nu_{max}$ $cm^{-1}$:** 3279(br, N-H), 3055(s, Ar-H), 1645.4 (CO-NH)(s), 1547.2 (st, N-H), 1402.8(s), 1319(s), 1271.6(s), 1236.1(s), 1155.3(s), 1122(s), 1001(s), 883(s), 846(s), 819.2(s)

**$^1$H NMR (400 MHz, DMSO-$d_6$):** $\delta$ 9.192 (s, 2H, NH), 8.710 (s, 2H, Ar-H), 8.548 (d, $J$ = 8.8 Hz, 2H, Ar-H), 8.251 (d, $J$ = 8.8 Hz, 2H, Ar-H), 8.081 (d, $J$ = 8.8 Hz, 2H, Ar-H), 7.455 (d, $J$ = 8.8 Hz, 2H, Ar-H) ppm

**$^{13}$C NMR (100 MHz, DMSO-$d_6$):** $\delta$ 166.52 (CO–NH), 148.50, 145.89, 141.82, 139.18, 139.79, 136.98, 130.42, 128.80, 128.40, 127.13, 126.20 (Ar-C) ppm

**LC-MS (m/z):** 559.00 $[M+H]^+$ positive mode

**Anal. Calcd. for $C_{24}H_{12}Cl_4N_6O_2$:** C, 51.64; H, 2.17; N, 15.06%

**Found:** C, 51.42; H, 2.12; N, 15.01%

***N,N'*-(1,4-phenylene)bis(2,3-dichloroquinoxaline-6-carboxamide) (4f).**

The product **4f** was obtained as light brown solid, washed with hot methanol 2–3 times as described in procedure III.

**Yield:** 27.5%

**IR (KBr) $\nu_{max}$ $cm^{-1}$:** 3279(br, N-H), 3055(s, Ar-H), 1645.4(CO-NH)(s), 1547.2 (st, N-H), 1402.8(s), 1319(s), 1271.6(s), 1236.1(s), 1155.3(s), 1122(s), 1001(s), 883(s), 846(s), 819.2(s)

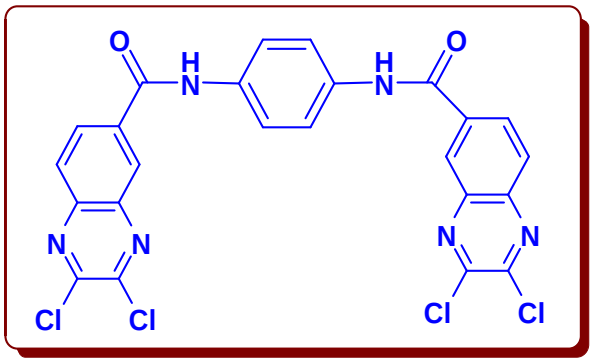

**$^1$H NMR (400 MHz, DMSO-$d_6$):** $\delta$ 10.67 (s, 2H, NH), 8.71 (s, 2H, Ar-H), 8.42 (d, $J$ = 8.0 Hz, 2H, Ar-H), 8.22 (d, $J$ = 8.0 Hz, 2H, Ar-H), 7.84 (s, 4H, Ar-H) ppm

**$^{13}$C NMR (100 MHz, DMSO-$d_6$):** $\delta$ 166.03 (CO–NH), 148.50, 146.28, 140.42, 139.88, 139.79, 136.98, 131.42, 128.80, 128.40, 127.59 (Ar-C) ppm

**LC-MS (m/z):** 559.00 $[M+H]^+$ positive mode

**Anal. Calcd. for $C_{24}H_{12}Cl_4N_6O_2$:** C, 51.64; H, 2.17; N, 15.06%

**Found:** C, 51.42; H, 2.12; N, 15.01%

***N,N'*-(pyridine-2,6-diyl)bis(2,3-dichloroquinoxaline-6-carboxamide) (4g).**

The product **4g** was obtained as light brown solid, washed with hot methanol 2–3 times as described in procedure III.

**Yield:** 34.6%

**IR (KBr) $\nu_{max}$ $cm^{-1}$:** 3418(br, N-H), 1693.6(CO-NH)(s), 1587.2(st, N-H), 1506(s),

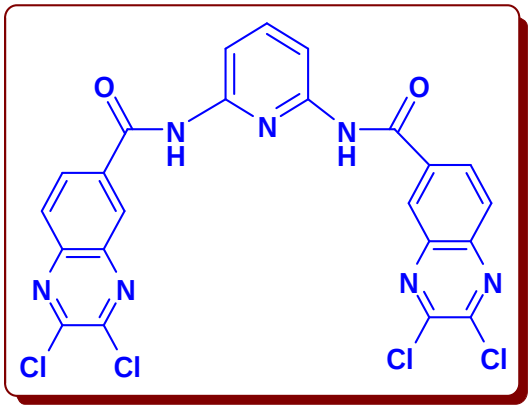

1450.8(s), 1311(s), 1263.6(s), 1151.1(s), 1001(s), 875(s), 846(s), 796.2(s)

**$^{1}$H NMR (400 MHz, DMSO-$d_6$):** $\delta$ 11.016 (s, 2H, NH), 8.690 (s, 2H, Ar-H), 8.397 (d, *J* = 8.4 Hz, 2H, Ar-H), 8.183 (d, *J* = 8.0 Hz, 2H, Ar-H), 7.930 (t, *J* = 6.4 Hz, 3H, Ar-H) ppm

**$^{13}$C NMR (100 MHz, DMSO-$d_6$):** $\delta$ 166.97 (CO–NH), 148.34, 145.69, 142.52, 139.98, 139.02, 135.98, 130.72, 128.92, 128.40, 127.13 (Ar-C) ppm

**LC-MS (m/z):** 557.39 $[M–H]^+$ positive mode

**Anal. Calcd. for $C_{23}H_{11}Cl_4N_7O_2$:** C, 49.40; H, 1.98; N, 17.53%

**Found:** C, 49.25; H, 1.84; N, 17.05%

***N,N'*-(4,4'-oxybis(4,1-phenylene))bis(2,3-dichloroquinoxaline-6-carboxamide) (4h).**

The product **4h** was obtained as light brown solid, washed with hot methanol 2–3 times as described in procedure III.

**Yield:** 35.97%

**IR (KBr) $\nu_{max}$ cm$^{-1}$:** 3277(br, N-H), 3057(s, Ar-H), 1645.4(CO-NH)(s), 1601(st, N-H), 1527(br), 1504(m), 1406.8(s), 1350(s), 1325(s), 1271.6(s), 1271(s), 1157.3(s), 1128(s), 1001(s), 850(s), 823(s)

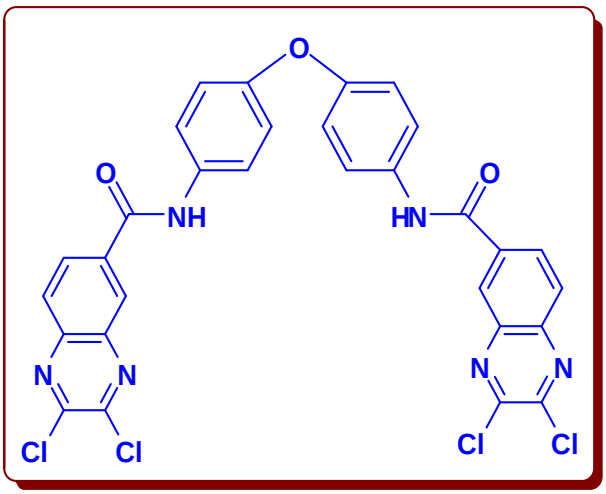

**$^1$H NMR (400 MHz, DMSO-$d_6$):** δ 10.649 (s, 2H, NH), 8.681 (s, 2H, Ar-H), 8.388 (d, *J* = 8.8 Hz, 2H, Ar-H), 8.200 (d, *J* = 8.8 Hz, 2H, Ar-H), 7.831 (d, *J* = 9.2 Hz, 4H, Ar-H), 7.062 (d, *J* = 8.8 Hz, 4H, Ar-H) ppm

**$^{13}$C NMR (100 MHz, DMSO-$d_6$):** δ 166.12 (CO–NH), 147.74, 146.29, 142.42, 139.88, 139.79, 136.98, 130.42, 128.80, 128.49, 127.53, 126.40, 125.82 (Ar-C) ppm

**LC-MS (m/z):** 650.25 $[M+H]^+$ positive mode

**Anal. Calcd. for $C_{30}H_{16}Cl_4N_6O_3$:** C, 55.41; H, 2.48; N, 12.92%

**Found:** C, 55.37; H, 2.29; N, 12.86%

***N,N'*-(4,4'-methylenebis(4,1-phenylene))bis(2,3-dichloroquinoxaline-6-carboxamide) (4i).**

The product **4i** was obtained as light brown solid, washed with hot methanol 2–3 times as described in procedure III.

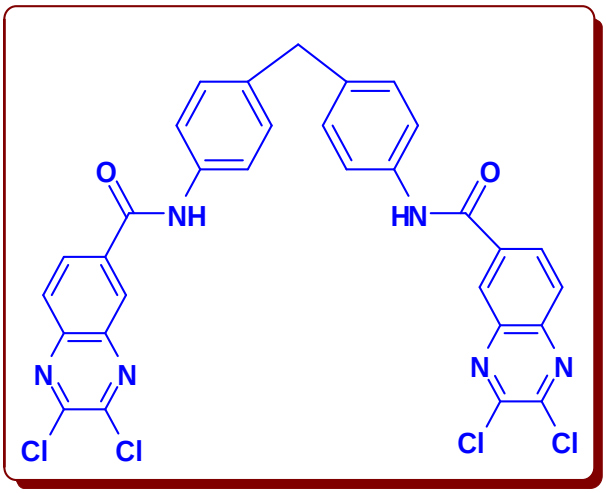


**Yield:** 30.4%

**IR (KBr) $\nu_{max}$ cm$^{-1}$:** 3300(br, N-H), 3038(s, Ar-H), 1649.4(CO-NH)(s), 1597.2 (st, N-H), 1529(br), 1408.8(s), 1321(s), 1273.6(s), 1155.3(s), 1124(s), 1001(s), 883(s), 846(s), 815.2(s)

**$^1$H NMR (400 MHz, DMSO-$d_6$):** δ 10.571 (s, 2H, NH), 8.665 (s, 2H, Ar-H), 8.304 (d, *J* = 8.4 Hz, 2H, Ar-H), 8.184 (d, *J* = 8.4 Hz, 2H, Ar-H), 7.736 (d, *J* = 8.4 Hz, 4H, Ar-H), 7.242 (d, *J* = 8.0 Hz, 4H, Ar-H), 3.923 (s, 2H) ppm

**$^{13}$C NMR (100 MHz, DMSO-$d_6$):** $\delta$ 167.12 (CO–NH), 148.74, 146.29, 142.42, 139.88, 139.79, 136.98, 130.42, 128.80, 128.40, 127.13, 126.20, 125.66 (Ar-C), 47.16 ($CH_2$–NH) ppm

**LC-MS (m/z):** 648.70 $[M+H]^+$ positive mode

**Anal. Calcd. for $C_{31}H_{18}Cl_4N_6O_2$:** C, 57.47; H, 2.80; N, 12.96%

**Found:** C, 57.35; H, 2.76; N, 12.89%

## 5.3.7. General procedure for derivatives of Bis Quinoxaline-o-dithiol derivatives

**General procedure IV**

2.0 mmol of derivatives of bis(2,3-dichloro quinoxaline)-carboxamide **4a-I** and 8.0 mmol of thiourea were suspended in 25–30 mL of absolute ethanol and this mixture was reflux for 3–4 h. The solution was concentrated to a small volume. The concentrated solution was diluted with 60 mL of water, cooled to –10 ºC and made alkaline by the addition of 6.0 mmol of NaOH. It was then stirred until the clear solution was obtained. On acidifying with acetic acid, a brown color precipitate was formed which was separated by filtration, washed with water fallowed by diethyl ether and dried under vacuum. The same procedure was applied for all the compounds **5a-i**.

***N,N'*-(ethane-1,2-diyl)bis(2,3-dimercaptoquinoxaline-6-carboxamide) (5a).**

The product **5a** was obtained as brown color precipitate and washed with water followed by diethyl ether as described in procedure IV.

**Yield:** 71.2%

**IR (KBr) $\nu_{max}$ cm$^{-1}$:** 3381(w), 1643(CO-NH)(m), 1612(w) 1547(m), 1410(m), 1138(m), 1242(m), 1174(m), 1141(m), 1032(m), 792(m), 767(m), 611(m)

**$^1$H NMR (400 MHz, DMSO-$d_6$):** $\delta$ 8.591 (s, 2H, NH), 7.834 (s, 2H, Ar-H), 7.576 (d, $J$ = 8.0 Hz, 2H, Ar-H), 7.325 (d, $J$ = 8.4 Hz, 2H, Ar-H), 3.430 (s, 4H) ppm

**$^{13}$C NMR (100 MHz, DMSO-$d_6$):** $\delta$ 166.65 (CO–NH), 143, 139.19, 136.77, 129.89, 128.75, 125.99, 125.01, 122.91, 63.16 ($CH_2$–NH) ppm

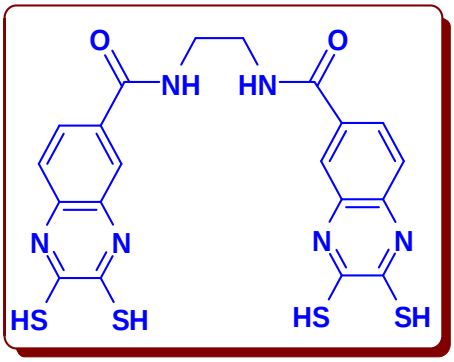


**LC-MS (m/z):** 502.45 $[M+H]^+$ positive mode

**Anal. Calcd. for $C_{20}H_{16}N_6O_2S_4$:** C, 47.98; H, 3.22; N, 16.79%

**Found:** C, 47.54; H, 3.18; N, 16.51%

***N,N'*-(propane-1,3-diyl)bis(2,3-dimercaptoquinoxaline-6-carboxamide) (5b).**

The product **5b** was obtained as brown color precipitate and washed with water followed by diethyl ether as described in procedure IV.

**Yield:** 69.0%

**IR (KBr) $\nu_{max}$ cm$^{-1}$:** 3381(st, N-H), 1647.8(CO-NH)(s), 1601(s), 1533.2 (st, N-H), 1483.8(s), 1412(s), 1358(s), 1313(s), 1232.5(s), 1140.6(s), 906(s), 827.54(s), 746.3(m), 457(w)

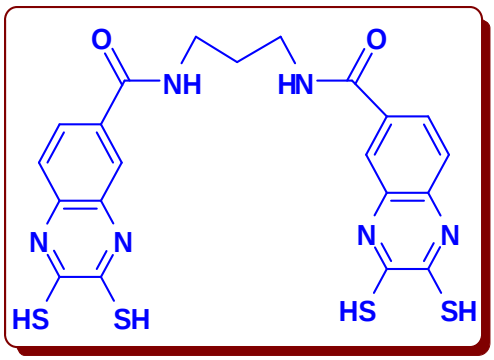


**$^1$H NMR (400 MHz, DMSO-$d_6$):** $\delta$ 8.578 (s, 2H, NH), 7.863 (s, 2H, Ar-H), 7.673 (d, $J$ = 8.4 Hz, 2H, Ar-H), 7.380 (d, $J$ = 8.4 Hz, 2H, Ar-H), 3.330 (s, 4H), 1.893 (s, 2H) ppm

**$^{13}$C NMR (100 MHz, DMSO-$d_6$):** $\delta$ 165.69 (CO–NH), 136.23, 131.84, 130.18, 128.34, 127.34, 126.12, 124.12, 115.85, 37.65 ($CH_2$–NH), 29.66 ppm

**LC-MS (m/z):** 515.35 $[M+H]^+$ positive mode

**Anal. Calcd. for $C_{21}H_{18}N_6O_2S_4$:** C, 49.01; H, 3.53; N, 16.33%

**Found:** C, 48.89; H, 3.46; N, 16.16%.

***N,N'*-(1,4-phenylenebis(methylene))bis(2,3-dimercaptoquinoxaline-6-carboxamide) (5c).**

The product **5c** was obtained as brown color precipitate and washed with water followed by diethyl ether as described in procedure IV.

**Yield:** 70.3%

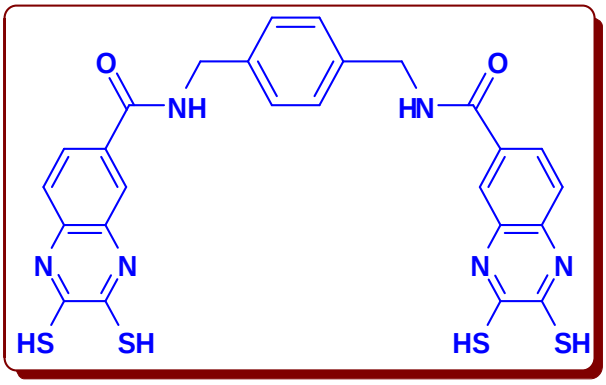


**IR (KBr) $\nu_{max}$ $cm^{-1}$:** 3391(st, N-H), 3180(s), 1647.8(CO-NH)(s), 1604(s), 1541.2 (st, N-H), 1417.8(s), 1361(s), 1305(s), 1230.6(s), 1138(s), 895.4(s), 827.5(s), 752.3(m), 646.2(w)

**$^1$H NMR (400 MHz, DMSO-$d_6$):** $\delta$ 8.956 (s, 2H, NH), 7.821 (s, 2H, Ar-H), 7.586 (d, $J$ = 8.6 Hz, 2H, Ar-H), 7.273 (d, $J$ = 8.0 Hz, 2H, Ar-H), 7.159 (br, 4H, Ar-H), 4.435 (s, 4H) ppm

**$^{13}$C NMR (100 MHz, DMSO-$d_6$):** $\delta$ 166.49 (CO–NH), 155.39, 139.60, 138.72, 134.28, 133.04, 131.62, 127.68, 123.10, 119.38, 113.53, 108.39, 43.0 ($CH_2$–NH) ppm

**LC-MS (m/z):** 576. 20 $[M+H]^+$ positive mode

**Anal. Calcd. for $C_{26}H_{20}N_6O_2S_4$:** C, 54.15; H, 3.50; N, 14.57%

**Found:** C, 53.99; H, 3.32; N, 14.41%

**_N,N'_-(1,3-phenylenebis(methylene))bis(2,3-dimercaptoquinoxaline-6-carboxamide) (5d).**

The product **5d** was obtained as brown color precipitate and washed with water followed by diethyl ether as described in procedure IV.

**Yield:** 73.7%

**IR (KBr) $\nu_{max}$ $cm^{-1}$:** 3379(st, N-H), 3175(s), 1643.8(CO-NH)(s), 1604(s), 1541.2 (st, N-H), 14179.8(s), 1413(s), 1365(s), 1307(s), 1141.6(s), 827.54(s), 729.3(m), 478(w)

**$^1$H NMR (400 MHz, DMSO-$d_6$):** $\delta$ 9.749 (s, 2H, NH), 8.607 (s, 2H, Ar-H), 8.354 (d, $J$ = 7.6 Hz, 2H, Ar-H), 8.058 (d, $J$ = 8.0 Hz, 2H, Ar-H), 7.973 (s, 4H, Ar-H), 5.227 (s, 4H) ppm

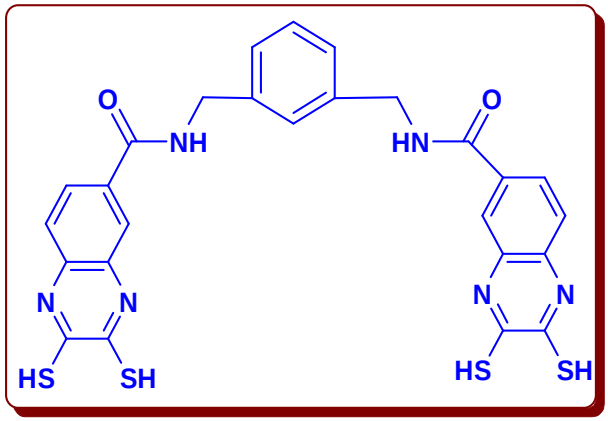


**$^{13}$C NMR (100 MHz, DMSO-$d_6$):** $\delta$ 166.30 (CO–NH), 140.64, 140.27, 140.15, 136.75, 133.87, 131.57, 128.73, 126.75, 126.63, 126.16, 123.22, 118.52, 43.15 ($CH_2$–NH) ppm

**LC-MS (m/z):** 576. 20 $[M+H]^+$ positive mode

**Anal. Calcd. for $C_{26}H_{20}N_6O_2S_4$:** C, 54.15; H, 3.50; N, 14.57%

**Found:** C, 53.99; H, 3.32; N, 14.41%

**_N,N'_-(1,2-phenylene)bis(2,3-dimercaptoquinoxaline-6-carboxamide) (5e).**

The product **5e** was obtained as brown color precipitate and washed with water followed by diethyl ether as described in procedure IV.

**Yield:** 43.8%

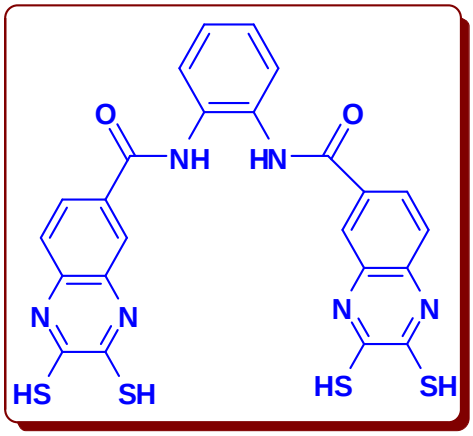


**IR (KBr) $\nu_{max}$ $cm^{-1}$:** 3192(w), 1641(CO-NH)(m), 1599(w) 1547(m), 1533(m), 1444(m), 1356(m), 1311(m), 1138(m), 754(m), 609(m)

**$^{1}$H NMR (400 MHz, DMSO-$d_6$):** $\delta$ 9.035 (s, 2H, NH), 8.326 (s, 2H, Ar-H), 8.190 (d, $J$ = 7.6 Hz, 2H, Ar-H), 7.942 (d, $J$ = 7.6 Hz, 2H, Ar-H), 7.504 (br, $J$ = 8.4 Hz, 4H, Ar-H) ppm

**$^{13}$C NMR (100 MHz, DMSO-$d_6$):** $\delta$ 166.01 (CO–NH), 154.19, 139.20, 138.12, 134.57, 133.01, 131.52, 127.68, 125.68 123.10, 119.38, 113.53, 108.39 (Ar–C) ppm

**LC-MS (m/z):** 548.65 $[M+H]^+$ positive mode

**Anal. Calcd. for $C_{24}H_{16}N_6O_2S_4$:** C, 52.54; H, 2.94; N, 15.32%

**Found:** C, 52.10; H, 2.74; N, 15.19%

***N,N'*-(1,4-phenylene)bis(2,3-dimercaptoquinoxaline-6-carboxamide) (5f).**

The product **5f** was obtained as brown color precipitate and washed with water followed by diethyl ether as described in procedure IV.

**Yield:** 41.1%

**IR (KBr) $\nu_{max}$ $cm^{-1}$:** 3420(br, N-H), 1647.4(CO-NH)(s), 1612.6(s), 1556(br, N-H), 1516(s), 1402.8(s), 1358(s), 1315.6(s), 1138(s), 823(s), 520.8(s)

**$^1$H NMR (400 MHz, DMSO-$d_6$):** $\delta$ 8.956 (s, 2H, NH), 7.821 (s, 2H, Ar-H), 7.586 (d, $J$ = 8.6 Hz, 2H, Ar-H), 7.273 (d, $J$ = 8.0 Hz, 2H, Ar-H), 7.159 (br, 4H, Ar-H) ppm

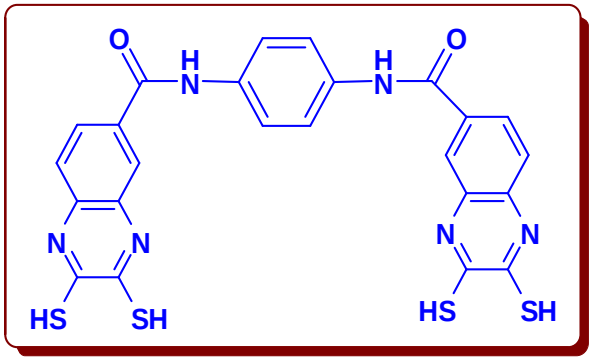

**$^{13}$C NMR (100 MHz, DMSO-$d_6$):** $\delta$ 166.34 (CO–NH), 153.19, 138.90, 138.32, 135.57, 132.01, 131.72, 127.08, 124.68 123.41, 119.38 (Ar–C) ppm

**LC-MS (m/z):** 548.65 $[M+H]^+$ positive mode

**Anal. Calcd. for $C_{24}H_{16}N_6O_2S_4$:** C, 52.54; H, 2.94; N, 15.32%

**Found:** C, 52.32; H, 2.82; N, 15.23%

***N,N'*-(pyridine-2,6-diyl)bis(2,3-dimercaptoquinoxaline-6-carboxamide) (5g).**

The product **5g** was obtained as brown color precipitate and washed with water followed by diethyl ether as described in procedure IV.

**Yield:** 53.7%

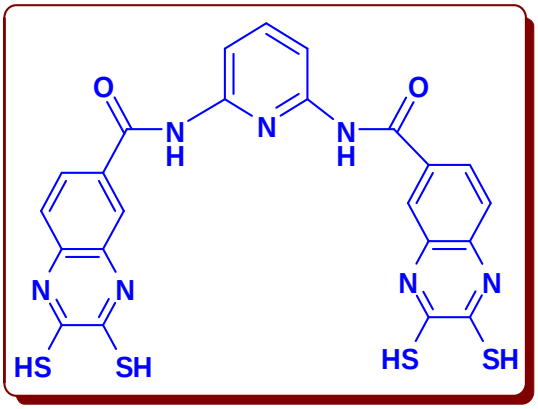

**IR (KBr) $\nu_{max}$ cm$^{-1}$:** 3418(br, N-H), 1685.6(CO-NH)(s), 1578.2(st, N-H), 1512(s), 1448.8(s), 1301(s), 1236.6(s), 1164(s), 1001(s), 875(s), 846(s), 796.2(s)

**$^{1}$H NMR (400 MHz, DMSO-$d_6$):** $\delta$ 10.016 (s, 2H, NH), 8.790 (s, 2H, Ar-H), 8.097 (d, *J* = 8.4 Hz, 2H, Ar-H), 7.803 (d, *J* = 8.0 Hz, 2H, Ar-H), 7.730 (t, *J* = 6.8 Hz, 3H, Ar-H) ppm

**$^{13}$C NMR (100 MHz, DMSO-$d_6$):** $\delta$ 164.97 (CO–NH), 148.43, 146.59, 143.82, 139.98, 138.42, 135.98, 130.27, 128.22, 128.10, 127.43 (Ar-C) ppm

**LC-MS (m/z):** 550.12 $[M+H]^+$ positive mode

**Anal. Calcd. for $C_{23}H_{15}S_4N_7O_2$:** C, 50.26; H, 2.75; N, 17.84%

**Found:** C, 49.96; H, 2.54; N, 17.71%

***N,N'*-(4,4'-oxybis(4,1-phenylene))bis(2,3-dimercaptoquinoxaline-6-carboxamide) (5h).**

The product **5h** was obtained as brown color precipitate and washed with water followed by diethyl ether as described in procedure IV.

**Yield:** 44.52%

**IR (KBr) $\nu_{max}$ cm$^{-1}$:** 3391(st, N-H), 3279(s, Ar-H), 1643.8(CO-NH)(s), 1616(s), 1534.2 (st, N-H), 1498.8(s), 1410(s), 1228.5(s), 1136.6(s), 1020, 827.54(s), 642.3(m), 516(w)

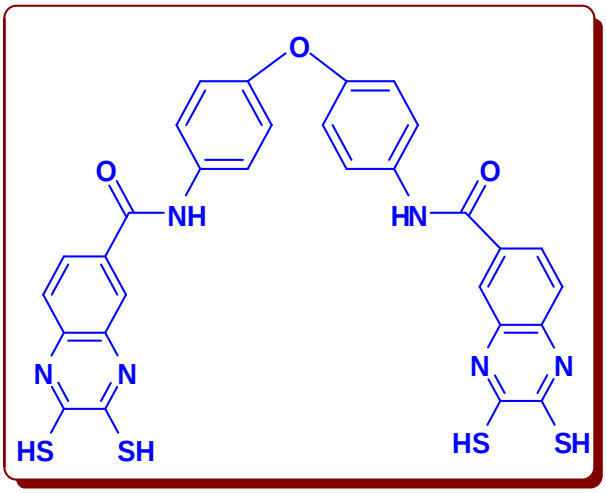


**$^{1}$H NMR (400 MHz, DMSO-$d_6$):** $\delta$ 10.240 (s, 2H, NH), 7.915 (s, 2H, Ar-H), 7.664 (d, *J* = 8.4 Hz, 2H, Ar-H), 7.343 (d, *J* = 8.4 Hz, 2H, Ar-H), 7.207 (s, 4H, Ar-H), 7.027 (s, 4H, Ar-H) ppm

**$^{13}$C NMR (100 MHz, DMSO-$d_6$):** $\delta$ 165.90 (CO–NH), 140.45, 140.01, 139.55, 138.95, 135.17, 132.23, 128.13, 126.92, 126.63, 126.71, 123.22, 118.52 ppm

**LC-MS (m/z):** 641.10 $[M+H]^+$ positive mode

**Anal. Calcd. for $C_{30}H_{20}N_6O_3S_4$:** C, 56.23; H, 3.15; N, 13.12%

**Found:** C, 56.14; H, 2.98; N, 13.04%

***N*,N'-(4,4'-methylenebis(4,1-phenylene))bis(2,3-dimercaptoquinoxaline-6-carboxamide) (5i).**

The product **5i** was obtained as brown color precipitate and washed with water followed by diethyl ether as described in procedure IV.

**Yield:** 47.8%

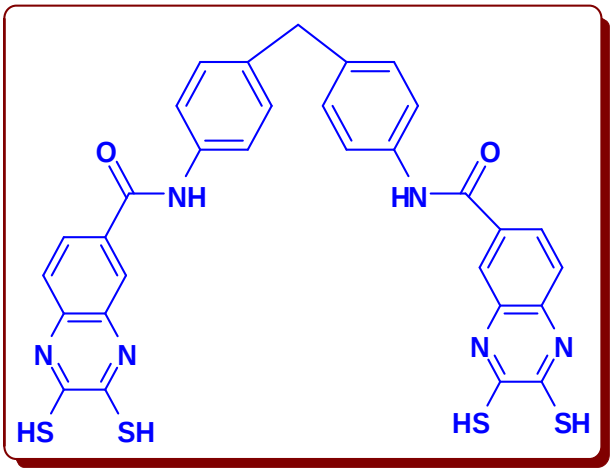


**IR (KBr) $\nu_{max}$ cm$^{-1}$:** 3398(st, N-H), 1643.8(CO-NH)(s), 1601(s), 1531.2(st, N-H), 1408.8(s), 1319(s), 1246.5(s), 1140.6(s), 771.54(s), 609.5(w)

**$^1$H NMR (400 MHz, DMSO-$d_6$):** $\delta$ 10.204 (s, 2H, NH), 7.931 (s, 2H, Ar-H), 7.701 (d, $J$ = 6.8 Hz, 2H, Ar-H), 7.380 (d, $J$ = 6.8 Hz, 2H, Ar-H), 7.207 (br, 8H, Ar-H), 3.895 (s, 2H, $CH_2$) ppm

**$^{13}$C NMR (100 MHz, DMSO-$d_6$):** $\delta$ 166.09 (CO–NH), 140.35, 140.73, 140.55, 138.95, 133.17, 132.37, 128.73, 126.12, 126.63, 126.71, 123.22, 118.52, 48.45 ($CH_2$–NH) ppm

**LC-MS (m/z):** 639.10 $[M+H]^+$ positive mode

**Anal. Calcd. for $C_{31}H_{22}N_6O_2S_4$:** C, 58.29; H, 3.47; N, 13.16%

**Found:** C, 57.93; H, 3.41; N, 12.96%

### 5.3.8 General Procedure for the Synthesis of $[Ph_4As]_4[Ni_2(5a)_2]$ (6)

Ligand **5a** tetraanion is generated, *in situ*, by treatment of **5a** (0.10 g, 0.199 mmol) with NaOH (0.032 g, 0.8 mmol) in MeOH (10mL) at temperature –10 ºC. To the resulting clear red solution, $NiCl_2 \cdot 6H_2O$ (0.047 g, 0.199 mmol) was added; the resulting dark blue solution was stirred for 15–20 min. Dark blue micro crystals were precipitated by adding tetraphenyl arsonium(V) chloride hydrate (0.167 g, 0.399 mmol); the micro crystals were filtered, washed with water followed by diethyl ether, and dried at room temperature. It was recrystallized from DMF solution by vapor diffusion with diethyl ether. Yield: 0.256 g (50.1% based on Ni). IR (KBR pellet) ($\upsilon/cm^{-1}$): 3429 (br, N-H), 2926(w), 1637(CO-NH)(s), 1521(s, N-H), 1473(m), 1439(m), 1365(m), 1305(m), 1263(m), 1163(m), 1120(m), 1081(m), 995(m), 833(m), 740(m), 686(m), 615(m), 464(m).

Crystallographic data for complex **6**: $As_4C_{70}H_{58}N_{14}Ni_2O_6S_8$, $M$ = 1864.51 g $mol^{-1}$, $T$ = 298(2) K, Triclinic, space group *P-1*, $a$ = 11.267(2) Å, $b$ = 18.405(4) Å, $c$ = 18.823(4) Å, $V$ = 3553.7(12) $Å^3$, $Z$ = 2, $Dc$ = 2.536mg $m^{-3}$, $F$ (*000*) = 2574, crystal size = 0.30 × 0.20 × 0.10 $mm^3$, 32456 reflections were measured with 14519 unique reflections ($R_{int}$ = 0.0835), of which 14519 ($I > 2\sigma(I)$) were used for the structure solution. Final $R_1$ ($wR_2$) = 0.1445 (0.3759), 775 parameters. The final Fourier difference synthesis showed minimum and maximum peaks of -1.721 and +2.042e.$Å^{-3}$ respectively

**Table 5.3.** Crystal data and structural refinement table for compounds **2d** and **2g**

| | **2d** | **2g** |
|---|---|---|
| Formula | $C_{16}H_{10}Cl_2FN_3O$ | $C_{15}H_9Cl_2N_3O$ |
| FW | 350.17 | 318.15 |
| Crystal system | Monoclinic | Monoclinic |
| Space group | $P2_1/c$ | $P2_1/c$ |
| a/Å | 4.820(10) | 5.268(4) |
| b/Å | 12.030(2) | 31.295(2) |
| c/Å | 31.236(6) | 8.127(6) |
| α [°] | 90.00 | 90.00 |
| β [°] | 93.56(3) | 90.89(10) |
| γ [°] | 90.00 | 90.00 |
| Z | 4 | 4 |
| $\rho_{cal}$/ Mg $m^{-3}$ | 1.286 | 1.577 |
| Goodness-of-fit on $F^2$ | 0.941 | 1.104 |
| $R_1(F^2_0)$ [ $I > 2\sigma(I)$] | 0.0678 | 0.0399 |
| $wR_2$ ($F^2_0$) [ $I > 2\sigma(I)$] | 0.1448 | 0.1012 |
| $R_1(F^2_0)$ (all data) | 0.1126 | 0.0437 |
| $wR_2$ ($F^2_0$) (all data) | 0.1753 | 0.1036 |
| Largest diff. peak and hole [e.$Å^{-3}$] | 0.272 and -0.228 | 0.258 and -0.293 |

## 5.4. Conclusion

In conclusion, we have prepared series of new directional ligands with a quinoxaline-*o*-dithiolate (S–S) donor set. Out of these newly synthesized bidentate (**3a–i**) and tetradentate ligands (**5a–i**), **5a** was preferentially metalated by $Ni^{II}$ at the quinoxaline-*o*-dithiolato donor function to form a double stranded *N*-Heterocyclic non-helical macro cyclic dinuclear square-planar complex. Diffused reflectance spectra of this compound shows a broad band in the visible region which is

due to the charge transfer (CT) transitions involving electronic excitation from a HOMO which is a mixture of dithiolate ($\pi$) and metal ($d$) orbital character to a LUMO which is a $\pi^*$ orbital of the dithiolate, that are characteristics of metal(II) bis(dithiolene) complexes.

Cyclic voltammetry (CV) studies reveal that complex **6** undergoes reversible oxidation ($\Delta E$= 0.07 V) at $E_{1/2}$ = +0.45 V *vs* Ag/AgCl, that corresponds the $[Ni_2(\mathbf{5a})_2]^{2-}/[Ni_2(\mathbf{5a})_2]^{4-}$ redox couple in DMF. We also have described the comparison studies of electrochemical properties between the present nickel complex $[Ph_4As]_4[Ni_2(\mathbf{5a})_2]$ (**6**) with Ni complexes containing $H_2$6,7-qdt and $H_2$qdt systems. The oxidation potential of the present system has more positive than $H_2$6,7-qdt and $H_2$qdt systems. The electrochemical properties (the first oxidation potentials) of the complexes are dependent on the electron donating/withdrawing nature of the attached to the dithiolene core moiety. From these results, we conclude that the dithiloene ligand must be participating to a large extent in electron transfer process.

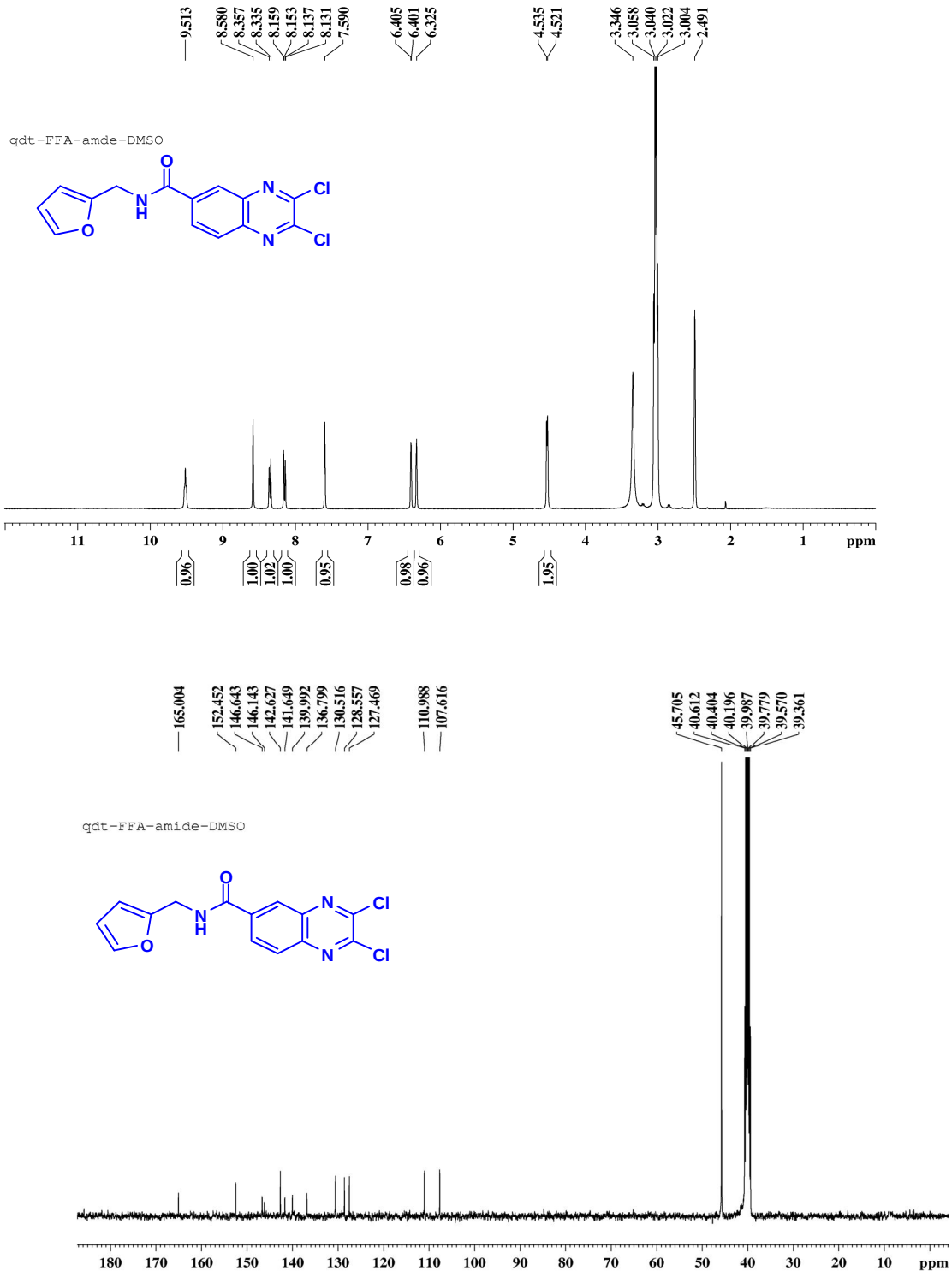


**Fig. 5.6.** $^{1}H$ and $^{13}C$ NMR spectra of compound **2e**

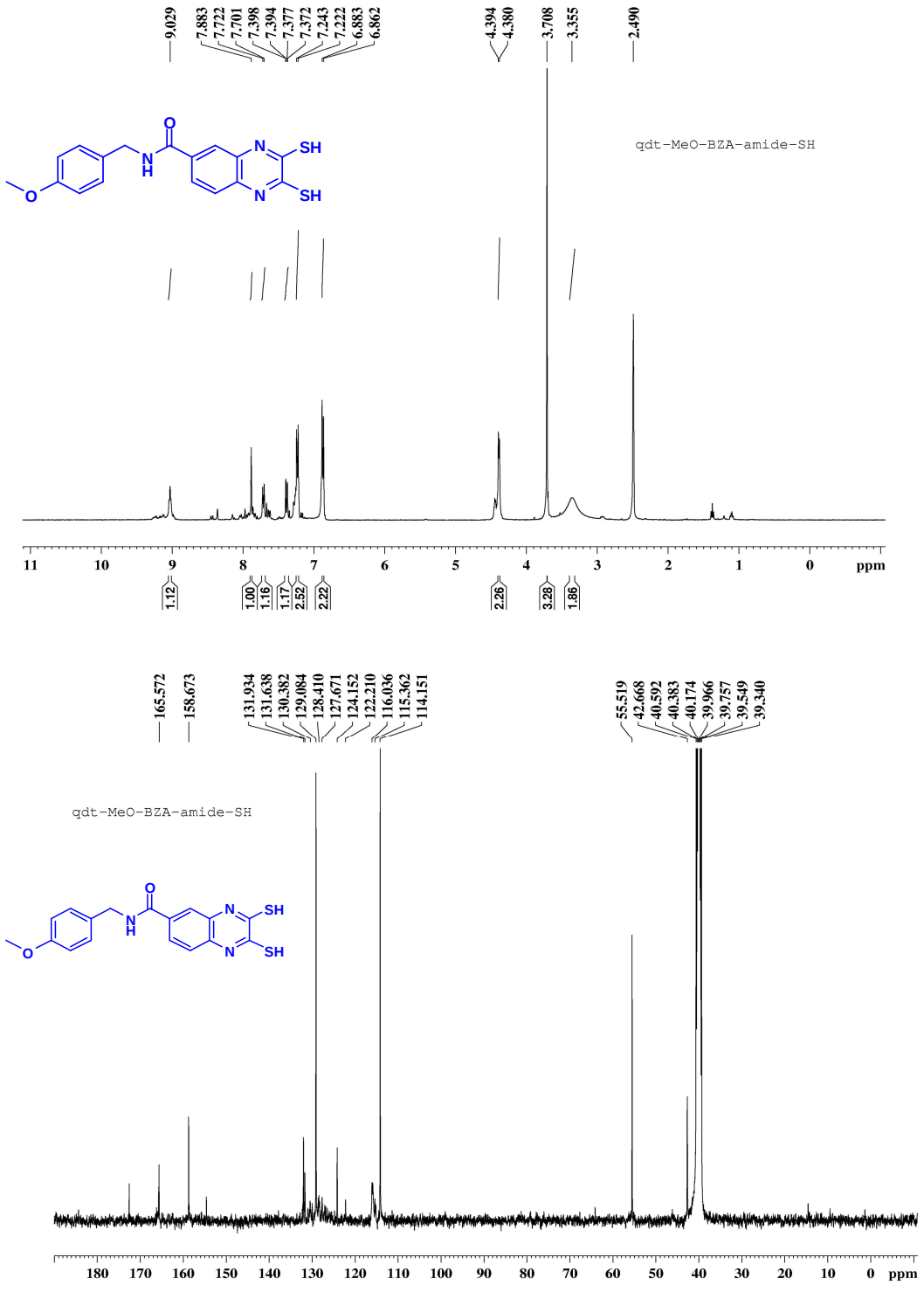


**Fig. 5.7.** $^{1}H$ and $^{13}C$ NMR spectra of compound **3c**

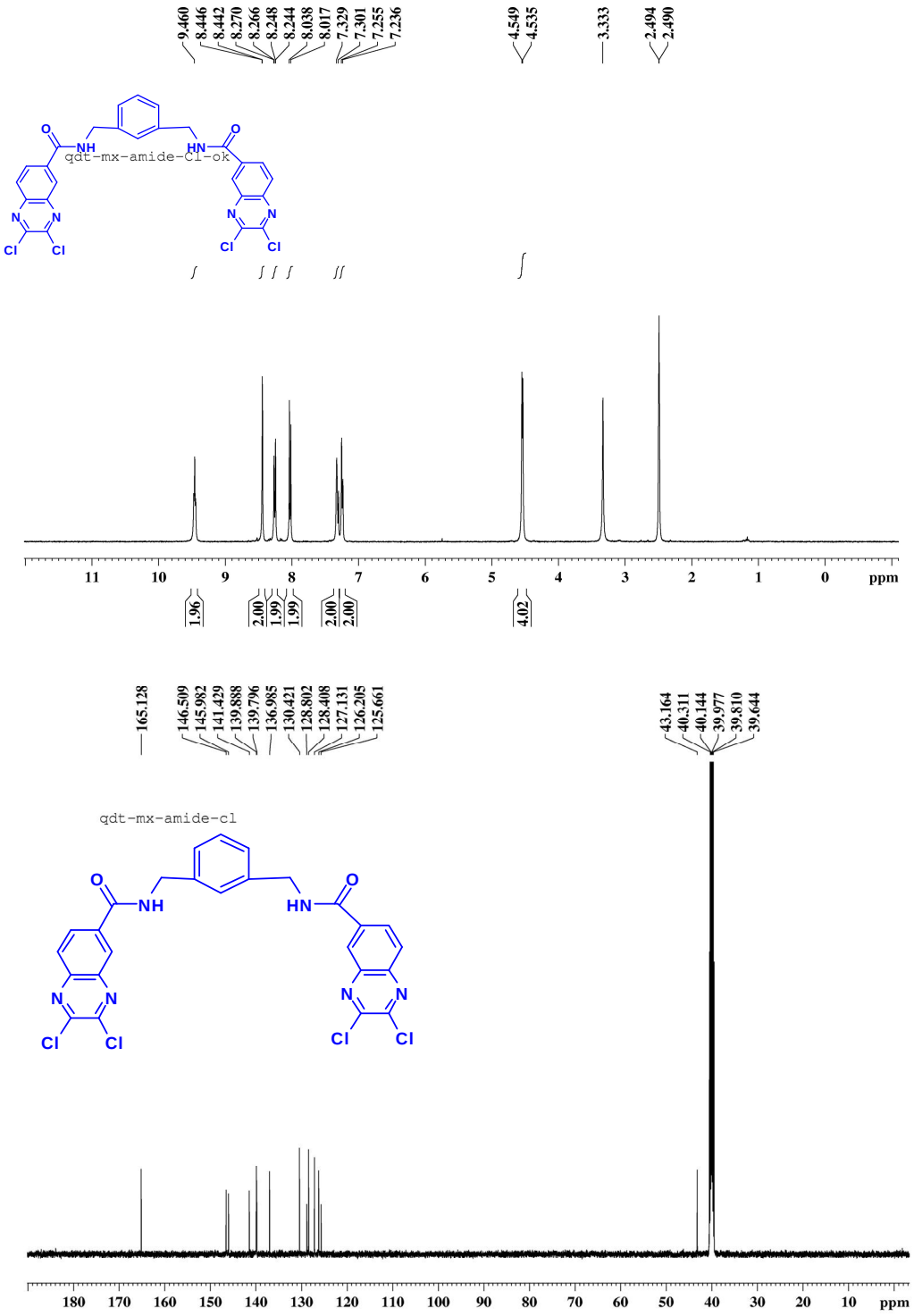


**Fig. 5.8.** $^{1}H$ and $^{13}C$ NMR spectra of compound **4d**

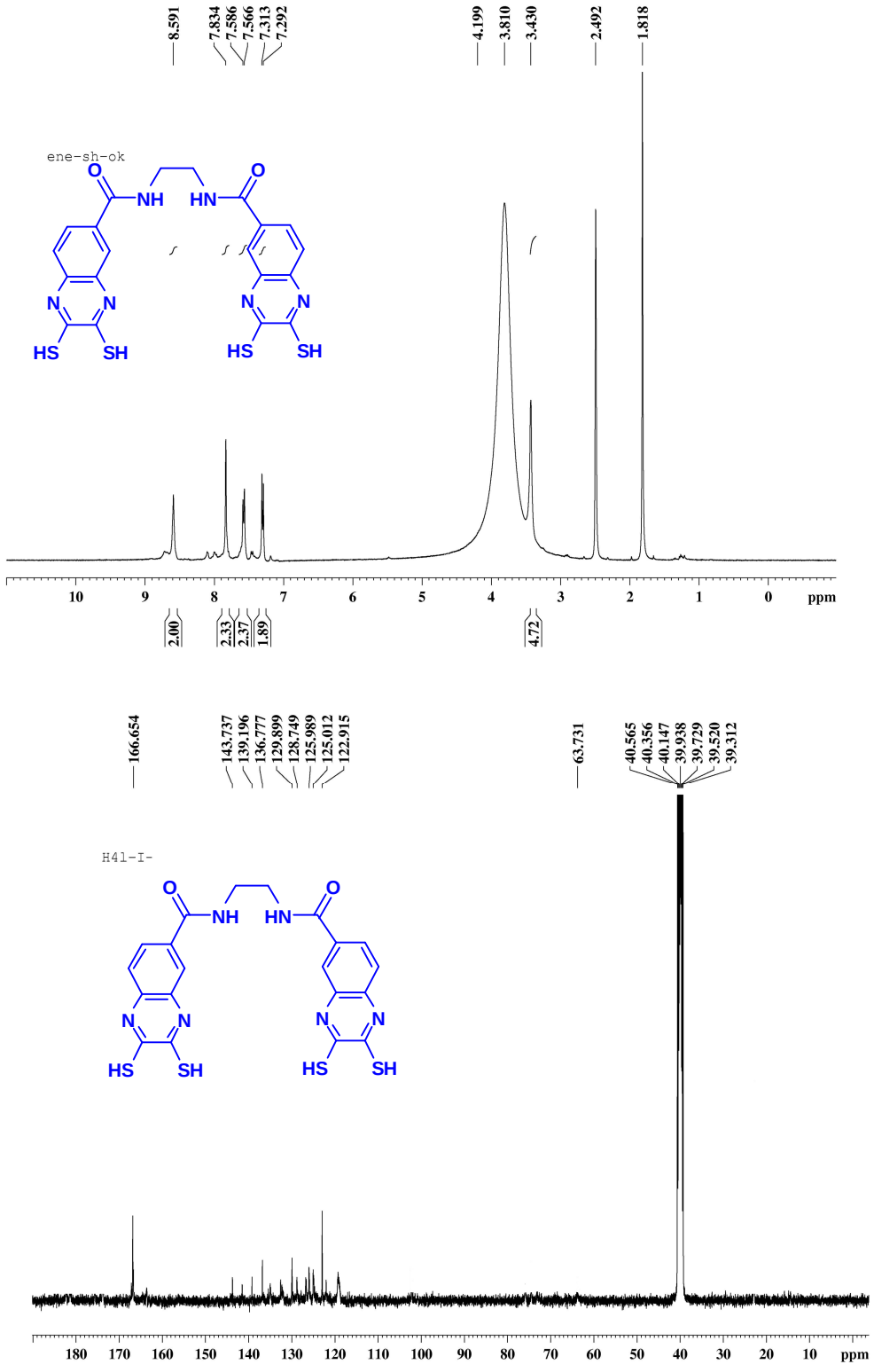


**Fig. 5.9.** $^{1}H$ and $^{13}C$ NMR spectra of compound **5a**

## 5.5. References


[1] J.-M. Lehn, Supramolecular Chemistry: Concepts and Perspectives VCH, Weinheim, (1995)

[2] J. A. McCleverty, Prog. Inorg. Chem. 10 (1968) 49.

[3] G. N. Schrauzer, Acc. Chem. Res. 2 (1969) 72.

[4] R. Eisenberg, Prog. Inorg. Chem. 12 (1970) 295.

[5] R. P. Burns, C. A. McAuliffe, Adv. Inorg. Chem. Radiochem. 22 (1979) 303.

[6] C. J. Mahadevan, Crystallogr. Spectrosc. Res. 16 (1986) 347.

[7] E. I. Stiefel, R. Eisenberg, R. C. Rosenberg, H. B. Gray, J. Am. Chem. Soc. 88 (1966) 2956.

[8] A. Davison, N. Edelstein, R. H. Holm, A. H. Maki, Inorg. Chem. 2 (1963) 1227.

[9] For EPR studies see: A. H. Maki, N. Edelstein, A. Davison, R. H. Holm, J. Am. Chem. Soc. 86 (1964) 4580.

[10] R. Kirmse, J. Stach, W. Dietzsch, G. Steimecke, E. Hoyer, Inorg. Chem. 19 (1980) 2679.

[11] For a review see: U. T. Mueller-Westerhoff, B. Vance, Comprehensive Coordination Chemistry; Pergamon Press: Oxford, U.K., 2 (1987) 595.

[12] Dithiolene dyes with strong near-IR absorption: U. T. Mueller-Westerhoff, B. Vance, D. I. Yoon, Tetrahedron 47 (1991) 909.

[13] S. Oliver, C. Winter, Adv. Mater. 4 (1992) 119.

[14] Building blocks in conducting and superconducting salts: P. Cassoux, L. Valade, H. Kobayashi, A. Kobayashi, R. A. Clark, A. E. Underhill, Coord. Chem. Rev. 110 (1991) 115.

[15] C. J. Carrano, K. N. Raymond, J. Am. Chem. Soc. 100 (1978) 5371−5374.

[16] C. J. Carrano, S. R. Cooper, K. N. Raymond, J. Am. Chem. Soc. 101 (1979) 599−604.

[17] R. C. Scarrow, D. L. White, K. N. Raymond, J. Am. Chem. Soc. 107 (1985) 6540−6546.

[18] J.-M. Lehn, A. Rigault, J. Siegel, J. Harrowfield, B. Chevrier, D. Moras, Proc. Natl. Acad. Sci. USA 84 (1987) 2565–2569.

[19] R. Krämer, J.-M. Lehn, A. Marquis-Rigault, Proc. Natl. Acad. Sci. USA 90 (1993) 5394–5398.

[20] B. Hasenknopf, J.-M. Lehn, G. Baum, D. Fenske, Proc. Natl. Acad. Sci. USA 93 (1996) 1397–1400.

[21] B. Kersting, M. Meyer, R. E. Powers, K. N. Raymond, J. Am. Chem. Soc. 118 (1996) 7221–7222.

[22] D. L. Caulder, K. N. Raymond, Angew. Chem. 109 (1997) 1508–1510.

[23] M. Meyer, B. Kersting, R. E. Powers, K. N. Raymond, Inorg. Chem. 36 (1997) 5179–5191.

[24] E. J. Enemark, T. D. P. Stack, Inorg. Chem. 35 (1996) 2719–2720.

[25] E. J. Enemark, T. D. P. Stack, Angew. Chem. Int. Ed. Engl. 34 (1995) 996–998.

[26] M. Albrecht, S. Kotila, Angew. Chem. Int. Ed. Engl. 34 (1995) 2134–2137

[27] M. Albrecht, S. Kotila, Chem. Commun. (1996) 2309–2310.

[28] M. Albrecht, S. Kotila, Angew. Chem. Int. Ed. Engl. 35 (1996) 1208–1210.

[29] M. Albrecht, M. Schneider, H. Röttele, Angew. Chem. 111 (1999) 512–515.

[30] M. Albrecht, M. Schneider, R. Fröhlich, New J. Chem. 22 (1998) 753–754.

[31] M. Albrecht, Chem. –Eur. J. 6 (2000) 3485–3489.

[32] M. Albrecht, M. Schneider, Eur. J. Inorg. Chem. (2002) 1301–1306.

[33] M. Albrecht, I. Janser, H. Houjou, R. Fröhlich, Chem. –Eur. J. 10 (2004) 2839–2850.

[34] D. Sellmann, W. Soglowek, F. Knoch, M. Moll, Angew. Chem., Int. Ed. Engl. 28 (1989) 1271.

[35] D. Sellmann, W. Soglowek, F. Knoch, G. Ritter, J. Dengler, Inorg. Chem. 31 (1992) 3711.

[36] D. Sellmann, S. Fünfgelder, G. Pöhlmann, F. Knoch, M. Moll, Inorg. Chem. 29 (1990) 4772.

[37] F. E. Hahn, W. W. Seidel, Angew. Chem. Int. Ed. Engl. 34 (1995) 2700–2703.

[38] H. V. Huynh, C. Schulze Isfort, W. W. Seidel, T. Lügger, R. Fröhlich, O. Kataeva, F. E. Hahn, Chem. –Eur. J. 8 (2002) 1327–1335.

[39] H. V. Huynh, W. W. Seidel, T. Lügger, R. Fröhlich, B. Wibbeling, F. E. Hahn, Z. Naturforsch. B 57 (2002) 1401–1408.

[40] F. E. Hahn, T. Kreickmann, T. Pape, Dalton Trans. (2006) 769–771.

[41] F. E. Hahn, T. Kreickmann, T. Pape, Eur. J. Inorg. Chem. (2006) 535–539*;*

[42] T. Kreickmann, C. Diedrich, T. Pape, H. V. Huynh, S. Grimme, F. E. Hahn, J. Am. Chem. Soc. 128 (2006) 11808–11819.

[43] F. E. Hahn, C. Schulze Isfort, T. Pape, Angew. Chem. Int. Ed. 43 (2004) 4807–4810.

[44] C. Schulze Isfort, T. Kreickmann, T. Pape, R. Fröhlich, F. E. Hahn, Chem. –Eur. J. 13 (2007) 2344–2357.

[45] F. E. Hahn, M. Offermann, T. Pape, R. Fröhlich, Angew. Chem. 120 (2008) 6899–6902.

[46] A. Kumar, S. Kumar, A. Saxena, A. De, S. Mozumdar, Catal. Commun. (2008) 778.

[47] J. Y. Jaung, Dyes and Pigments 71 (2006) 45.

[48] G. Sakata, K. Makino, Y. Karasawa, Heterocycles, 27 (1988) 2481.

[49] K. R. J. Thomas, M. Velusamy, J. T. Lin, C. H. Chuen, Y. T. Tao, Chem. Mater. 17 (2005) 1860.

[50] S. Dailey, W. J. Feast, R. J. Peace, I. C. Sage, S. Till, E.L. Wood, J. Mater. Chem. 11 (2001) 2238.

[51] M. J. Crossley, L. A. Johnston, Chem. Commun. (2002) 1122.

[52] T. Kazunobu, O. Ryusuke, M. Tomohiro, Chem. Commun. (2002) 212.

[53] J. L. Sessler, H. Maeda, T. Mizuno, V. M. Lynch, H. Furuta, J. Am. Chem, Soc. 124 (2002) 13474.

[54] O. Sascha, F. Rudiger, Synlett (2004) 1509.

[55] D. S. M. Fabio, M. S. Aline, V. Juliano, D. S. Bernardo, P. P. Jacks, S. Bruno, S. G. Norberto, N. Ademir, Tetrahedron 64 (2008) 5410–5415

[56] Y. Hin-Lap, Z. Jingyu, M. Hong, T. Yanging, M. Neil, Tucker and K.-Y. Alex. Jen, J. Am. Chem. Soc. 128 (2006) 13042–13043.

[57] T. Kreickmann , F. E. Hahn , Chem. Commun. (2007) 1111 –1120.

[58] W. W. Seidel , F. E. Hahn , Bioinorg. Chem. Appl. 3 (2005) 69 –80.

[59] R. Bolligarla, G. Durgaprasad, S. K. Das, Inorg. Chem. Commun. 12 (2009) 355–358.

[60] S. D. Cummings, R. Eisenberg, Inorg. Chem. 34 (1995) 2007–2014.

[61] S. D. Cummings, R. Eisenberg, Inorg. Chem. 34 (1995) 3396–3403.

[62] S. I. Shupack, E. Billig, R. J. H. Clark,; R. Williams, H. B. Gray, J. Am. Chem. Soc. 86 (1964) 4594.

[63] R. Bolligarla, G. Durgaprasad S. K. Das, Inorg. Chem. Commun. 14 (2011) 809–813.

[64] Bruker. *SADABS, SMART, SAINT* and *SHELXTL*, 2000 (Bruker AXS Inc., Madison, Wisconsin, USA).

[65] G. M. Sheldrick, Acta Crystallogr. Sect. A 64 (2008) 112–122.

# Future Scope of the Present Thesis

**Towards the biological importance**

Dihydrogen ($H_2$) gas has the potential to be an unlimited source of clean energy, if simple and efficient methods of production and utilization can be developed. Recent research has significantly advanced our understanding the nature's most efficient catalysts, the [FeFe]-hydrogenases for hydrogen production, that catalyses the reductive generation of hydrogen. Ott and his co-workers have reported high efficient Photoelectrochemical hydrogen generation catalyst by mimicking the enzyme active site. Thus, we are interested to prepare such efficient catalyst for hydrogen generation by using 1,2-enedithiolate ligands: work in this direction is going on presently in our laboratory.

**Towards the Solid-State Function Materials**

The design and syntheses of coordination polymers or metal-organic frameworks (MOFs), that involve attentive selection of organic ligands with suitable functional groups and metal ions, have attracted considerable attention because such solid-functional materials have potential to be used as gas storage, nonlinear optical, conducting and magnetic materials. In the fourth chapter of the present thesis, we have described the alkali metal ion based coordination polymers of Metal(III) dithiolene complex anion $[M^{III}(diph\text{-}6,7\text{-}qdt)_2]^{1-}$ [M = Cu(III), Au(III)], where simple variation of the coordination solvents results in the variation of the structural diversities and dimensionalities. In this aspect, we would like to prepare electro-conductive coordination polymers with transition metals, such as, Cu, Co and Ni by using different new *N*-heterocyclic-*o*-dithiol ligands, e.g., 6,7-quinoxaline-dithiol, 2,3-quinoxaline dithiol and 2,3-pyrazine dithiol.

Very recently, two electro-conductive coordination polymers $Cu[Cu(pdt)_2]$ and $Cu[Ni(pdt)_2]$ have been reported, and these show relatively high electrical conductivity at room temperature with high porosity based on pyrazine bis(dithiolate) building blocks (Fig. 1). In addition, the conductivity of $Cu[Ni(pdt)_2]$ has been enhanced through partial oxidation of its framework. The increasing in counducvity is due to oxidative doping and the resulting framework is a p-type semicounductor. Metal-organic framewoks of these dithiolene based compounds exhibit reletively high elctrical conductvity. In this way, our newly synthesized alkali metal ion based coordination polymers containing alkali cations can be exchanged by transition metal ions such

as Cu(I) ions to get good porous conducting materials and the work is going on presently in this direction in our laboratory.

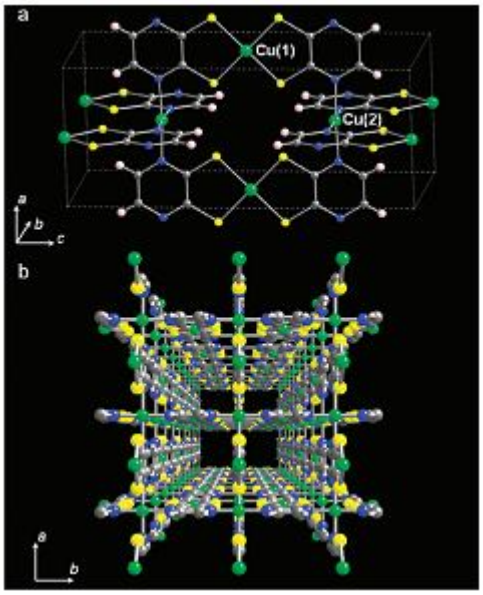


**Fig. 1.** (a) Crystal structure in Cu[Cu(pdt)2]. (b) Perspective view of the crystal structure of $Cu[Cu(pdt)_2]$. Color code: green, Cu; yellow, S; gray, C; blue, N; pink, H.

## Towards the Metallosupramolecular Chemistry with Bis(quinoxaline-*o*-dithiol) Ligands

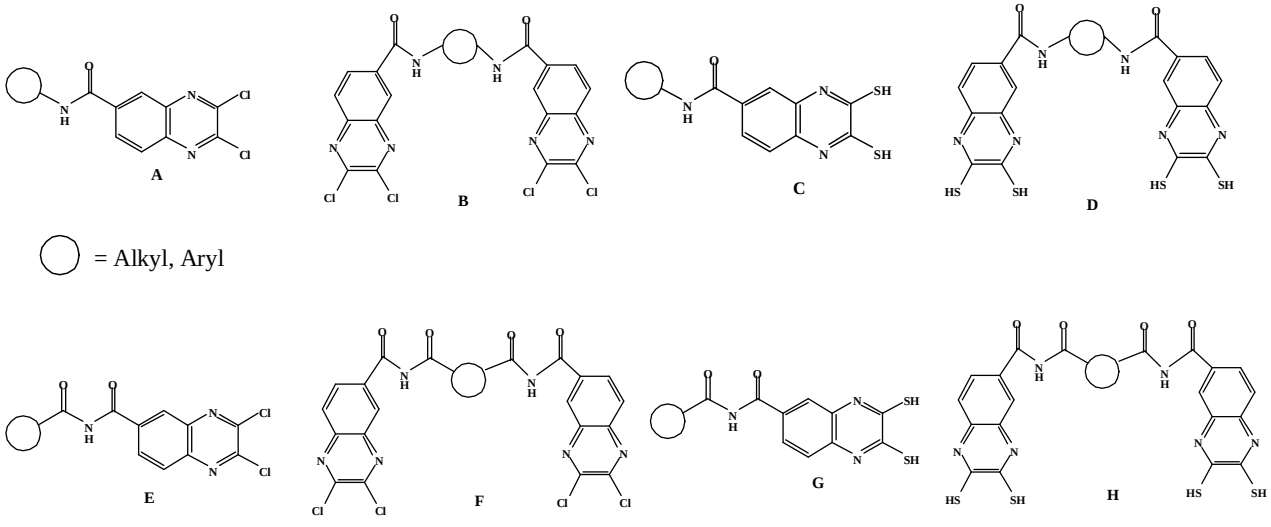


**Scheme1.** Chloro- and thiol-derivatives of quinoxaline molecules.

The recognition and sensing of anions using fluorescent based sensors has become an active research area within the field of supramolecular chemistry. In the fifth chapter of the present

thesis, we have designed and synthesized new mono- and bis Chloro derivatives of quinoxaline molecules **A** and **B** and we would like to prepare ligands such as **E** and **F** as shown in Scheme 1**.** These types of fluorescent molecules can acts as sensors for sensing different kinds of anions such as fluoride, acetate, sulphate and perchlorates and also useful in bio-imaging with organic fluorescent molecules for visualization of cellular structure, membranes, macromolecules and ions. It is well-known that quinoxalines are strong electron-accepting materials in organicphotovoltaic cells (OPVs) due to their high electron affinity originated from the two symmetric unsaturated nitrogen atoms. In addition, the introduction of internal diimine units to the aromatic ring system allows electronic alterations to impart highly electrophilic characteristics to the ring. As a consequence, benzopyrazines find increasing use in light-emitting and electrontransporting materials for the manufacture of highly efficient OLEDs.

In the fifth chapter of the present thesis, we have described a new method for the *ortho*-functionalization of quinoxaline-*o*-dithiol that led to the preparation of the first mono and bis(quinoxaline-*o*-dithiol) ligands such as **C** and **D** (Scheme 1), respectively and now the preparation and characterization of ligands such as **G** and **H** (as shown in Scheme 1) are under progressing in our laboratory**.** Our research in the field of ene-dithiolates drives us to incorporate the quinoxaline-*o*-dithiolato binding unit into larger polydentate ligands: these can be used for the generation of metallosupramolecular assemblies. These new ligands offer an opportunity for the preparation of new coordination complexes. This might lead to interesting dithiolene complexes of transition metals of varying geometry that can be useful in their redox chemistry.

One dinuclear nickel complex has been described with bis(quinoxaline-*o*-dithiol) ligand. By using these ligands, we would like to synthesize dinuclear double stranded or triple stranded helical complexes with a titanium(IV) ion, as well as their coordination chemistry with metallocene fragments.

# List of Publications

**1.** 1,2-Ene Dithiolate Bridged Diiron Carbonyl-Phosphine and -Phosphite Complexes in Relevance to the Active Site of [FeFe]-hydrogenases**:** Synthesis, Characterization and Electrocatalysis.

**Gummadi Durgaprasad** and Samar K. Das* *J. Organomet. Chem.* **2012** (In Press)

**2.** Synthesis, Crystal Structure and Electrocatalysis of 1,2-ene Dithiolate Bridged Diiron Carbonyl, Phosphine and Phosphite Complexes in Relevance to the Active Site of [FeFe]-hydrogenases

**Gummadi Durgaprasad**, Ramababu Bolligarla, and Samar K. Das*, *J. Organomet. Chem.* **2012**, *706-707*, 37–45

**3.** Synthesis, structural characterization and electrochemical studies of $[Fe_2(\mu\text{-L})(CO)_6]$ and $[Fe_2(\mu\text{-L})(CO)_5(PPh_3)]$ ($L^{2-}$ = pyrazine-2,3-dithiolate, quinoxaline-2,3-dithiolate and pyrido[2,3-*b*]pyrazine-2,3-dithiolate): towards modeling the active site of [FeFe]-Hydrogenase

**Gummadi Durgaprasad**, Ramababu Bolligarla, and Samar K. Das*, *J. Organomet. Chem.* **2011**, *696*, 3097–3105.

**4.** Design, Synthesis and Characterization of New *N*-Heterocyclic Mono- and Bis (quinoxaline-*o*-dithiol) Ligands

**Gummadi Durgaprasad** and Samar K. Das* *communicated.*

**5.** Influence of Coordinated Crystallizing Solvents and bulkiness of ligands in Tuning the Structural Diversity and Dimensionality of Alkali Metal Based Coordination Polymers of Metal Bis(Dithiolene) Complexes

**Gummadi Durgaprasad** and Samar K. Das* *manuscript under preparation*

**6.** Synthesis, Molecular Structure and Supramolecular Chemistry of a New Nickel-Quinoxaline Dithiolate System $[Bu_4N]_2[Ni(6,7\text{-qdt})_2]$ ($6,7\text{-Qdt}^{2-}$ = Quinoxaline-6,7-dithiolate) and Comparison of its Electronic and Electrochemical Properties with those of $[Bu_4N]_2[Ni(qdt)_2]$ ($Qdt^{2-}$ = Quinoxaline-2,3-dithiolate)

Ramababu Bolligarla, **Gummadi Durgaprasad** and Samar K. Das*, *Inorg. Chem. Commun.* **2011**, *14*, 809–813.

**7.** 6,7,6',7'-Tetraphenyl-[2,2']bi[1,3-dithia-5,8-diaza-cyclopenta[*b*]napthalenylidene]

Ramababu Bolligarla, **Gummadi Durgaprasad** and Samar K. Das*, *Acta Cryst. E* **2011**, E*67*, 2231–2232.

**8.** Ion-pair charge transfer complex with near-IR absorption: Synthesis, crystal structure and properties of $[Hb]_2[Cu(mnt)_2]$ (Hb = 1-(4-((1H-imidazol-1-yl)methyl)benzyl)-1H-imidazol-3-ium))

Ravada Kishore, Bharat Kumar Tripuramallu, **Gummadi Durgaprasad** and Samar K. Das* *J. Mol. Str*. **2011**, *990*, 37–43.

**9.** Acid-Base Behavior of a Simple Metal Bis(Dithiolate) System: Synthesis, Crystal Structure and Spectroscopy of $[Bu_4N]_2[M^{II}(ppdt)_2]$ (M = Ni, Pt; $ppdt^{2-}$ = pyrido[2,3-*b*]pyrazine-2,3-dithiolate)

Ramababu Bolligarla, Ravada Kishore, **Gummadi Durgaprasad** and Samar K. Das*, *Inorg. Chim. Acta* **2010**, *363*, 3063–3069.

**10.** A Nitrogen Rich Ni(II)-Dithiolate System Exhibiting Acid-Base Behavior: Synthesis, Supramolecular Structure and Spectroscopy of $[Bu_4N]_2[Ni^{II}(ppdt)_2]$ ($ppdt^{2-}$ = pyrido[2,3-b]pyrazine-2,3-dithiolate)

Ramababu Bolligarla, **Gummadi Durgaprasad** and Samar K. Das*, *Inorg. Chem. Commun.* **2009**, *12*, 355-358.

## Poster and Oral Presentations

1. **Gummadi Durgaprasad** and Samar K. Das*, Synthesis, structural characterization and electrochemical studies of $[Fe_2(\mu\text{-}L)(CO)_6]$ and $[Fe_2(\mu\text{-}L)(CO)_5(PPh_3)]$ (L = pyrazine-2,3-dithiolate, quinoxaline-2,3-dithiolate and pyrido[2,3-*b*]pyrazine-2,3-dithiolate): towards modeling the active site of [FeFe]-Hydrogenase, Poster presentation at "**XII-MTIC-2007** (**Modern Trends in Inorganic Chemistry**)" and held in December-**2007**, Indian Institute of Technology Madras, Chennai, India.

2. **Gummadi Durgaprasad** and Samar K. Das*, Synthesis, structural characterization and electrochemical studies of $[Fe_2(\mu\text{-}L)(CO)_6]$ and $[Fe_2(\mu\text{-}L)(CO)_5(PPh_3)]$ (L = pyrazine-2,3-

dithiolate, quinoxaline-2,3-dithiolate and pyrido[2,3-*b*]pyrazine-2,3-dithiolate): towards modeling the active site of [FeFe]-Hydrogenase, Poster presentation at ***"Chemfest-2008 (in-house)"*** which was held in School of Chemistry, University of Hyderabad, Hyderabad, India on March, **2008.**

3. **Gummadi Durgaprasad**, Gummadi Durgaprasad, and Samar K. Das*, Synthesis, Crystal Structure and Electrocatalysis of 1,2-ene Dithiolate Bridged Diiron Carbonyl, Phosphine and Phosphite Complexes in Relevance to the Active Site of [FeFe]-hydrogenases, Poster presentation at ***"Chemfest-2010 (in-house)"*** which was held in School of Chemistry, University of Hyderabad, Hyderabad, India on March, **2010.**

4. **Gummadi Durgaprasad** and Samar K. Das*, Synthesis, Crystal Structure and $e^-$-withdrawing effect of different *N*-heterocyclic dithiols and $e^-$-donating effect of different Phosphine and Phosphite ligands on diiron carbonyl complex: towards the active site of [FeFe]-hydrogenase, Oral and Poster presentation at ***"Chemfest-2011(in-house)"*** which was held in School of Chemistry, University of Hyderabad, Hyderabad, India on January, **2011.**